THE UNIVERSITY *of* EDINBURGH

Mechanism of anti-influenza virus activity of Maillard reaction products derived from *Isatidis* roots

by

Lijing Ke

A thesis submitted to The University of Edinburgh for the degree of

Doctor of Philosophy

The University of Edinburgh

2010

ABSTRACT

The cyto-protective compositions and effects of antiviral Maillard reaction products (MRPs) derived from roots of *Isatis indigotica F.* were examined using biochemical and biophysical methods. The Maillard reaction was identified as the main source of compounds with anti-viral activity, an observation which has led to the proposal of a new class of active compounds that protect cells from influenza virus infection.

In the roots, arginine and glucose were revealed to be the predominant reactants for the Maillard reaction. Significant anti-influenza virus effects were demonstrated in the RIE MRPs derived from the roots (RIE refers to the '*radix Isatidis* extracts'), and in Arg-Glc MRPs which are synthesised with arginine and glucose. Arg-Glc MRPs were confirmed as suitable models for the study of the antiviral effects of the root extracts. Furthermore, RIE MRPs and Arg-Glc MRPs were found to bind to the plasma membranes of erythrocytes and MDCK cells, and altered their properties. A novel antiviral mechanism was proposed: that MRPs achieve their cyto-protective effects by binding to the cell membrane rather than by direct action on viral particles.

To validate the proposed mechanism, the interaction between MRPs and membrane lipids was investigated by biophysical experiments with phospholipids bilayers. Arg-Glc MRPs affected the rigidity of lipid packing in monolayers and bilayers, while RIE MRPs enhanced the fluidity. Both types of MRPs inserted into the hydrophobic core of bilayers, to differing extents, and induced the stabilisation or destabilisation of bilayers in a concentration-dependent manner. At certain concentrations, MRPs prevented the lamellar structure of bilayers from being destabilised by a viral fusion peptide, improved the lipid order and thereby inhibited cell-virus membrane fusion. The mechanism of the anti-influenza virus activity of RIE was therefore correlated to the interaction between MRPs and phospholipid bilayers, an integral component of the plasma membrane.

ACKNOWLEDGEMENTS

This research has been done with support and resources of Royal (Dick) School of Veterinary Studies at The University of Edinburgh, and the Insitute of Biotechnology at Fuzhou University, China.

Data collection and scientific assistance was provided at the Institute Laue Langevin (ILL) Grenoble, France; the Berlin Neutron Scattering Center (BENSC) at the Helmholtz-Zentrum Berlin for Materials and Energy (HZB), Berlin, Germany; Elettra Synchrotron Light source, Trieste, Italy; and National Synchrotron Radiation Research Center (NSRRC), Taiwan.

I would like to specifically mention the instrument scientists at the sources as they provided invaluable assistance in data collection and in answering my questions.

Bruno Deme (D16, ILL)

Thomas Hauβ (V1, BENSC)

Michael Rappolt (SAXS, Elettra)

Ming-Tao Lee (LXD, NSRRC)

I would like to thank the people at Fuzhou Institute of Biotechnology, specifically:

Prof Pingfan Rao, who was joint-supervising my study and research by providing enormous advice on many scientific aspects and sharing inspirational ideas. Without him, I probably would never discover the beauty of science and taste the bitterness of becoming a scientist. I could only hope there would be one day a young folk would have a full-hearted thank to me, as I had to him.

Dr Jianwu Zhou, a true brother who was always there to share the excitements and toughness of academic life whenever I was in Fuzhou or heading off for experiments somewhere in Europe. Prof Shutao Liu, Mr Xiaochao Chen, Mr Guanzhen Gao, Ms Huiqin Wang, Mr Wei Lu, for their great support and the assistance in data collection.

I would also like to thank my fellow colleagues in our laboratory at The University of Edinburgh:

Dr Mojtaba Hadian – Our ‘Borat’ Brother from Iran, his hi-jinks and adventures kept us all entertained and made sure things were light-hearted and relaxed in the lab.

Mr Farid Sa’adedin – A close collaborator over the last few years, Farid has been invaluable at distracting me from my PhD work by travelling around the globe together. So if my PhD is penalised for being late, the blame is entirely on him.

My supervisors at the Royal (Dick) School of Veterinary Studies:

Second Supervisor: Dr Alastair McDonald

Without Alastair I would not be in this position of doing a PhD at The University of Edinburgh. His experience of living in Fuzhou resulted in close links formed between the laboratory in Fuzhou and Edinburgh, and allowed me to become a PhD student at the Royal Dick. His guidance and help at Edinburgh University with regards to my thesis has been gratefully appreciated.

Primary Supervisor: Prof Jeremy Bradshaw

Jeremy has been a constant source of support and guidance during my time as a PhD student. Whether it was in Edinburgh, Grenoble, Berlin, Taiwan and Fuzhou, Jeremy has always been there to provide feedback and encouragement. I thank him for all the effort he has made, the time he has sacrificed for me in establishing my research, especially with the experience at the Large Scale Structure facilities; it has been invaluable knowledge in advancing my scientific career. For that and more, I will always be in his debt.

I would have to thank my Family: Mr & Mrs Ke the Papa and Mama, Lingyan Pan my wife and my sister and her family, for their continuous support through these years. Back at home, I am always very lucky to be taken care of so well and have nothing to worry about except my research when I was at home. If there is anything I could give them to return the favour, that it would only be finishing lab work half hour earlier and having a nice and chilled evening with my family.

DECLARATION

I declare that this thesis has been composed by myself, and that the work described herein is a presentation of my original research work. Wherever contributions of others are involved, every effort is made to indicate this clearly, with due reference to the literature, and acknowledgement of collaborative research and discussions.

The work was done under the guidance of Professor Jeremy P. Bradshaw at the University of Edinburgh, United Kingdom, has not been submitted for any other degree except as specified. The candidate has not been registered for a degree at any other institution throughout his period of registration at the University of Edinburgh.

Candidate: Lijing Ke
Date: 12th July 2010

ABBREVIATIONS

A	lateral area/lipid
aa	amino acid
Arg	arginine
Arg-Glc MRPs	Maillard reaction products of *L*-arginine and *D*-glucose.
Arg+Glc	solution of arginine and glucose at equal molar
BSA	bovine serum albumin
BAPNA	*N*-benzoyl-*DL*-arginine-*p*-nitroanilide
C	cells, i.e. MDCK cells
CC_{50}	50% cytotoxic concentration
cDNA	complementary DNA
CPE	cytopathic effect
d	lamellar d-spacing
d_W	steric water layer thickness
d_C	hydrocarbon chain length
d_H	headgroup thickness
d-Arg	deuterated arginine, *L*-Arginine-2,3,3,4,4,5,5-*d*7
d-Arg-Glc MRPs	MRPs of *d*7-*L*-arginine and *D*-glucose
DMEM	Dulbecco's Modified Eagle's Medium
DMPC	dimyristoyl-phosphatidylcholine

DMSO	dimethyl sulfoxide
DOPC	dioleoyl-phosphatidylcholine
DOPG	dioleoyl-phosphatidylglycerol
DSC	differential scanning calorimetry
DTT	dithiothreitol
EC_{50}	50% efficient concentration
ESI	electrospray ionization
F(q)	bilayer form factor
G	correction factor
Glc	glucose
GP	general polarization
GRITIP	glycated *radix Isatidis* trypsin inhibitor protein
H	horizontal
HA	haemagglutinin of influenza viruses
HI	haemagglutination inhibition
H_{II}	inverted hexagonal phase of phospholipids
HPLC	high performance liquid chromatography
IA	Influenza A FM1 (H1N1, mouse-adapted) virus
IB	influenza B/Shanghai/93-1(C3C2, 1:320 9/2/99)
IEF	isoelectric focusing
I_{HV}	fluorescence intensity at vertical position excited by horizontally polarised light

I_{HH}	fluorescence intensity at horizontal position excited by horizontally polarised light
I_0	excitation and emission polarisers in parallel position
I_{90}	excitation and emission polarisers in perpendicular position
I_{m3m}	primitive cubic phase
I(q)	scattered intensity
kDa	kilo-dalton
L_α	biologically relevant liquid crystalline phase of phospholipids
L_β	gel phase of phospholipids
LC	liquid chromatography
LC-MS	liquid chromatography-mass spectroscopy
LDH	Lactate Dehydrogenase
LXD	lamellar x-ray diffraction
MALDI	matrix-assisted laser desorption/ionisation
MC540	Merocyanine 540
MCE	boiling water extract of pulps of *Momordica charantia Linn.*
MDCK	Madin-Darby canine kidney
MeDOPE	*N*-methyl-dioleoyl-phosphatidylethanolamine
MLVs	multilamellar versicles (liposome)
MRPs	Maillard reaction products
MS	mass spectroscopy
MTT	3-[4,5-dimethylthiazol-2-yl]-2,5-diphenyl-tetrazolium bromide

O.D.	optical density
PAS	periodic acid-Schiff
PBS	phosphate-buffered saline
PC	phosphatidylcholine
PE	phosphatidylethanolamine
PFU	plaque forming units
pI	isoelectric point
PVDF	polyvinylidene difluorid
q, s	scattering vector: $q = 2\pi s = 4\pi \sin\theta / \lambda$
Q_{II}	inverted cubic phase of phospholipids
r	anisotropy
RH	relative humidity
7-d RIE	RIE extracted from roots incubated at 60°C, 85% rh for 7 d
RIE	*radix Isatidis* extract, boiling water extract of the roots
RITIP	*radix Isatidis* trypsin inhibitor protein
RPLC	reversed phase liquid chromatography
SAXS	small angle x-ray scattering
SDS-PAGE	Sodium dodecyl sulphate polyacrylamide gel electrophoresis
SEM	Scanning Electron Microscopy
SIV	simian immunodeficiency virus
SP-P1	the 1st peak fraction separated with SP650M ion-exchange HPLC
SP-P2	the 2nd peak fraction separated with SP650M ion-exchange HPLC

SPW-P1	the 1st peak fraction separated with SP-5PW ion-exchange HPLC
SPW-P2	the 2nd peak fraction separated with SP-5PW ion-exchange HPLC
S(q)	structure factor
SUVs	small unilamellar versicles (liposome)
T	temperature
t	time
T_H	temperature of lamellar-inverted hexagonal phase transition
T_Q	initiating temperature of lamellar-to-inverted cubic phase transition
T_M	initiating temperature of L_β-to-L_α transition
TC_0	0% toxic concentration
TC_{50}	50% toxic concentration
TCM	traditional Chinese medicine
TEMED	Polymerisation promoter
TIU	trypsin inhibitor units
v	vertical
$\rho(z)$	electron density
ΔH_f	heat consumption of phase transition per mole lipid

Table of Contents

CHAPTER 1

INTRODUCTION

Historically, herbal medicine forms an integral part of traditional Chinese medicine. It has featured in a number of evidence-base scientific studies, thereby giving it credibility as an alternative to conventional medicine. Commonly recognised as a black coloured and bitterly flavoured soup, Chinese herbal medicine has been embraced by patients who have experienced its efficacy. Simultaneously it has been challenged by physicians and scientists for the 'blackness' of how it works. Using the extract of *radix Isatidis* as an example of antiviral herbal medicine, this study seeks to shed light on this "blackness", and to illuminate the molecular mechanism of its effective components, Maillard Reaction Products (MRPs), which are typically dark chocolate brown in colour.

A number of antiviral agents, either chemically synthesised or purified from natural sources, have been developed against various pathogenic viruses, e.g. influenza viruses. Most of these agents tend to rely upon specific interactions between the drug molecule and a viral protein/polysaccharide. The inhibitors, oseltamivir and amantadine, are two examples, and used in the treatments for seasonal flu. The specific molecular recognition between the drugs and viral compositions has the advantages of high efficiency and low side effects, as well as two drawbacks. Firstly, those drugs have very narrow spectra of activity and, secondly, viruses may develop resistance against them (in the case of amatadine, resistance involved a single amino acid replacement in the M2 protein).

Within Chinese culture, preparations of natural materials have been used for centuries as a treatment or prophylaxis against viruses. *Radix Isatidis* extract (RIE) has long been employed as an antiviral drug in traditional Chinese medicine, and is currently licensed in China for use as an anti-influenza agent. Unlike vaccines or neuraminidase inhibitors, RIE's antiviral effects appear to involve binding to the plasma membrane surface of respiratory epithelial cells, to protect them from infection by blocking viral attachment. This may explain RIE's broad spectrum of antiviral activities, which may not depend on ligand-receptor recognition.

Much of this work focuses on the properties of the Maillard Reaction Products, which comprise the principal components of many Traditional Chinese Medicines (TCMs). The MRPs are a product of the preparation procedures, which typically involve hot-water extractions from sun-dried medicinal plants. My approach to this project was to characterise the molecular mechanism of MRPs as a mixture from natural resources or from an artificial synthesis system, while simultaneously trying to identify the single effective molecules of MRPs.

1.1. TRADITIONAL CHINESE MEDICINE AND HERBAL MEDICINE

1.1.1. What is a traditional Chinese medicine?

What is a traditional Chinese medicine (TCM)? If we use Google, various answers to this question can be found, from a number of different perspectives. One definition, from the website of Nature Publishing Group (Nature 2010) is as follows:

> "TCM is 'a system of treatment that emphasises the proper balance or disturbances … (which) consists of a group of techniques and methods, including acupuncture, herbal medicine, oriental massage and qigong (a form of energy therapy)."

Some of these techniques and methods, i.e. acupuncture and herbal medicine, have been intensively studied in a wide range of medical research settings (Tang, 2006). Although it is still arguable whether all the therapeutic claims can be justified, it is becoming clear that certain TCMs have proven pharmaceutical activity. There is increasing number of evidences from laboratory and clinical studies to support claims such as the pain-reducing effects of acupuncture (Fireman *et al.* 2001), the effectiveness of artemisinin (discovered in the leaves of *Artemisia annua*, a TCM herb) in treating of multi-drug resistant strains of *Falciparum malaria* (Price *et al.*, 1999) (PRICE, 1996), and now the effectiveness of RIE for antiviral applications (Chen, Wu, *et al.*, 2006) (Jin, Ren, Meng, & Li, 2007).

1.1.2. Chinese herbal medicine

In TCM, herbal medicines have traditional importance and have been studied systematically. They are used in more than four fifths of treatments employing Chinese medicines (Bensk, Clavey, Erich, Andrew, & Bensky, 2004). What makes the herbal medicines of TCM such a unique tonic among the herbal medicines popularly used in different parts of the world? The answer seems to reside in the processing of medicinal plants, in terms of sun-drying and hot water extraction.

Ancient practitioners of TCM established a comprehensive system of preparing and practicing herbal medicines based on their clinical experience and understanding of the human body. This herbal system has two arms. One is a proper way of preparing the herbs

that goes much further than preservation and may be recognized as an ancient Chinese version of herbal pharmacy. Another is the prescriptions or formulas of sets of herbs grouped for certain disorders or diseases. These usually involve several kinds of herbs (4 to 14 kinds depends on the type and seriousness of the targeted disease). The herbs in the prescription are chosen and dosed with the guidance (Bensk, Clavey, Erich, Andrew, & Bensky, 2004), which combines the written Chinese medicine theory and the doctor's clinical diagnosis. Both aspects are crucial for TCM's therapeutic effects and comprise the unique characters of TCM compared to herbal medicines from other parts of world. However, the processing of fresh plants into a medicinal formulation, typically and traditionally a soup, is undoubtedly a major factor, irrespective of whether it is a single herb, like *Banlangen*, or a TCM prescription containing a dozen types of herbs.

1.1.3. General properties of Chinese herbal medicine: processing and components

Leaves, roots, stems and seeds of medicinal plants are the major ingredients of Chinese herbal medicine (Chinese Pharmacopoeia Commission 2005). However, instead of being applied freshly, most of these materials need to be sundried or boiled before being given to patients. Two steps of heating, sun-drying and boiling in water, endow Chinese herbal medicine decoctions with a common characteristic of a dark brownish colour, regardless of what herbs have been incorporated into the formulas or prescriptions. The dramatic colour change indicates the occurrence of a major chemical interaction among the native components of herbs.

In terms of quantity of chemicals involved in this interaction, the Maillard reaction is the dominant chemical reaction during this heating process, whose products, MRPs, are the major compounds contributing to the dark colour (for details of the Maillard reaction, see Section 1.3.). Moreover, my previous studies indicate that MRPs are very possibly the effective components of herbal TCM (see Section 1.3.5.).

1.2. RADIX ISATIDIS AND ITS MEDICINAL APPLICATIONS

1.2.1. General introduction of the plant.

Radix Isatidis, *Banlangen* in Chinese, is the dried roots of the plant *Isatis indigotica Fort.* or *Isatis tinctoria L.* (Fam. *Brassicaceae*), is a widely-used antiviral TCM. As an officially approved medicinal material (Chinese Pharmacopoeia Commission 2005), 'Ban-Lan-Gen' and its hot water extracts have been widely used to prevent and treat several types of viral infection, including influenza, epidemic hepatitis and epidemic encephalitis B (Price *et al.* 1999). They have even served as major herbal tonics during the outbreaks of Severe Acute Respiratory Syndrome (SARS) in China, Hong Kong and Taiwan (Lin & Tsai 2005). Regardless of the different subtypes of haemagglutinin and neuraminidase of viruses and their constant mutations, RIE was found to be clinically effective against various subtypes and strains of influenza viruses (Wang *et al.* 2006) (Liu, Li & Jiang 2008). This indicates that RIE probably targets a common substance of the virus and is therefore generally effective over different subtypes of flu viruses.

1.2.2. Medicinal history of *Banlangen*

Banlangen is cultivated in various regions across China, mainly in Anhui, Hebei and Jiangsu provinces in northern China. The earliest record of *Banlangen* as a medicine is in a Chinese medical classic, 'Qian Jin Fang', written in C.E. 652 by the famous physician Simiao Sun*. Apart from viral infection diseases, *Banlangen* is also employed in the treatment of bacterial infections such as erysipelas, toxic heat, and pneumonia (Niebuhr 1970)(Yeung 1985)(Duke & Ayensu 1985)(Bown 1995). It is effective against various types of bacteria, including haemolytic *streptococcus* (Kong *et al.* 2008a), *E. coli* (Kong *et al.* 2008b), *C. diphtheriae* and *Salmonella enteritidis* (Zhao *et al.* 2006). Claiming the multifunctional therapeutic benefits, *Banlangen* has becomes a suitable candidate for the application of evidence-based

* Simiao Sun is also called Saint Sun as a compliment to his enormous contribution to the advancment of Chinese medicine in his time. His book, Qian Jin Fang (Prescriptions Worth A Thousand Gold), is one of the most important and dominant books in the history of Chinese medicine.

pharmaceutical studies of Chinese herbal medicines. Its phytochemical composition and identified effective components are discussed later in this chapter (see section 1.2.3. below).

1.2.3. Phytochemistry of the roots

A wide range of chemicals has been extracted and identified from the roots of *Isatis indigotica F.*. These range from a dye called indigo, which can also be extracted from another plant in the same family, namely 'dyer's woad', to the most common substance in plants, saccharides. The major components of the plant's chemical composition are total saccharides (67.0%), reducing sugar (14.2%), protein (13.6%) and free amino acids (4.2%) (see Section 7. For details). A single amino acid, arginine, accounts for up to 3.6% dry weight of fresh roots or 3.12% in sundried roots; it is the most abundant of the 17 kinds of amino acids determined in *radix Isatidis*. Furthermore, approximately 85% of the free amino acids is arginine, which is equal to 39.5% of total amino acids in fresh roots, and 38.1% sun-dried roots. The extraordinarily high content of arginine in sundried *radix Isatidis* has also been reported by several independent studies (Xiang 2007) (Dong & Liu 2001) (Zou, Hong & Koh 2005), and was presumed to be the major effective components of Ban-lan-gen. For this reason, arginine has been designated by the Chinese Pharmacopoeia Committee, as a major characteristic with which to identify the authenticity of *Radix isatidis* material (Chinese Pharmacopoeia Commission 2005). The high levels of amino acids, proteins and reducing sugars in *radix Isatidis* could easily react with each other during heat processing, and could generate a large amount of MRPs.

1.2.4. Recognized active components of the roots

To date, fresh plant tissues have been the major materials used in studies to identify the effective components of *Banlangen*. Various extracted compounds have been examined for their antiviral activity, including glycosides, peptides, lectins polysaccharides and alkaloids (Li, Yan, *et al.* 2009) (Hu & Zheng 2003) (Xu *et al.* 2005) (Nagai *et al.* 1998). In 2005, a 'fingerprint' of the root and its extracts was constructed by analysing these compounds with high performance liquid chromatograph (Li, Ma, *et al.* 2009) (Lin *et al.* 2005). However, none of these particular compounds showed any promising impact on either cell protection or direct virus disinfection. Compounds known to have mild inhibitory effects on viruses,

such as polypeptides, glycosides and alkaloids, were either presenting at a very low concentration, or were insufficiently soluble in aqueous solution to be delivered by oral administration. In contrast, most herbal medicines in TCM are served as broth, which is a mixture of aqueous solution and colloid suspension (Hou *et al.* 2004). It should be noted that any aqueous insoluble chemical could hardly be the principal component of a clinically effective herbal TCM, regardless of how potent it might be observed in the pharmacological studies *in vitro*.

As one of the major components of RIE, MRPs are readily dissolved in water and may be administered orally. As described later in this chapter, the anti-influenza virus activity of MRPs from RIE has been demonstrated by *in vitro* studies, but the mechanism of the antiviral action remains unknown.

1.3. THE MAILLARD REACTION AND ITS PRODUCTS

1.3.1. Chemistry of the Maillard reaction

The Maillard reaction is named after the French chemist Louis Maillard who first described it in 1912 (Maillard 1912). It is a non-enzymatic browning chemistry reaction between amino acids (or peptides, or proteins) and a reducing sugar, usually requiring heat. In 1953, the first coherent diagram of this reaction was laid out by Hodge (Fig 1.1) (Hodge 1953). As a major chemical change which occurs during food processing and physiological aging, MRPs have been associated with a number of functions and bioactivities. MRPs production has been linked to flavouring, food colouring, modification of proteins and lipids with non-enzymatic glycosylation, and the formation of antioxidant or mutagenic compounds.

As shown in Fig 1.1, the Maillard reaction could be described briefly as follows. The reaction initiated from a reducing sugar and amino group (i.e. from amino acids or aminophospholipid) forms an unstable Schiff base. The Amadori rearrangement product (ARP) is formed slowly from the Schiff base by an intramolecular process namely Amadori rearrangement. The ARP will then degrade in a pH-dependent manner into three groups of possible products:

Reductones (pH>7),

Fission products (pH>7),

Schiff's base of hydroxymethylfurfural (pH≤7).

Some reactive carbonyl and dicarbonyl compounds could form in the 'fission' pathway (Figure 1.1). From reductones or fission products, with the participation of sugar, Strecker aldehydes of amino acids and aminoketones are formed. Onwards, the reaction could then take either one of two possible directions, depending on whether or not there is an intervention of amino compounds. In the presence of amino compounds, the brown nitrogenous polymers and copolymers, melanoidins are the end products, while aldol condensation and nitrogen-free polymers result in the absence of amino compounds. Lastly, at the earlier step of glycation, carbonyl fission products could also be formed from N-substituted glycosylamine with the mediation of free radicals. This fragmentation of saccharide is now known as the Namiki pathway (Hayashi & Namiki 1980).

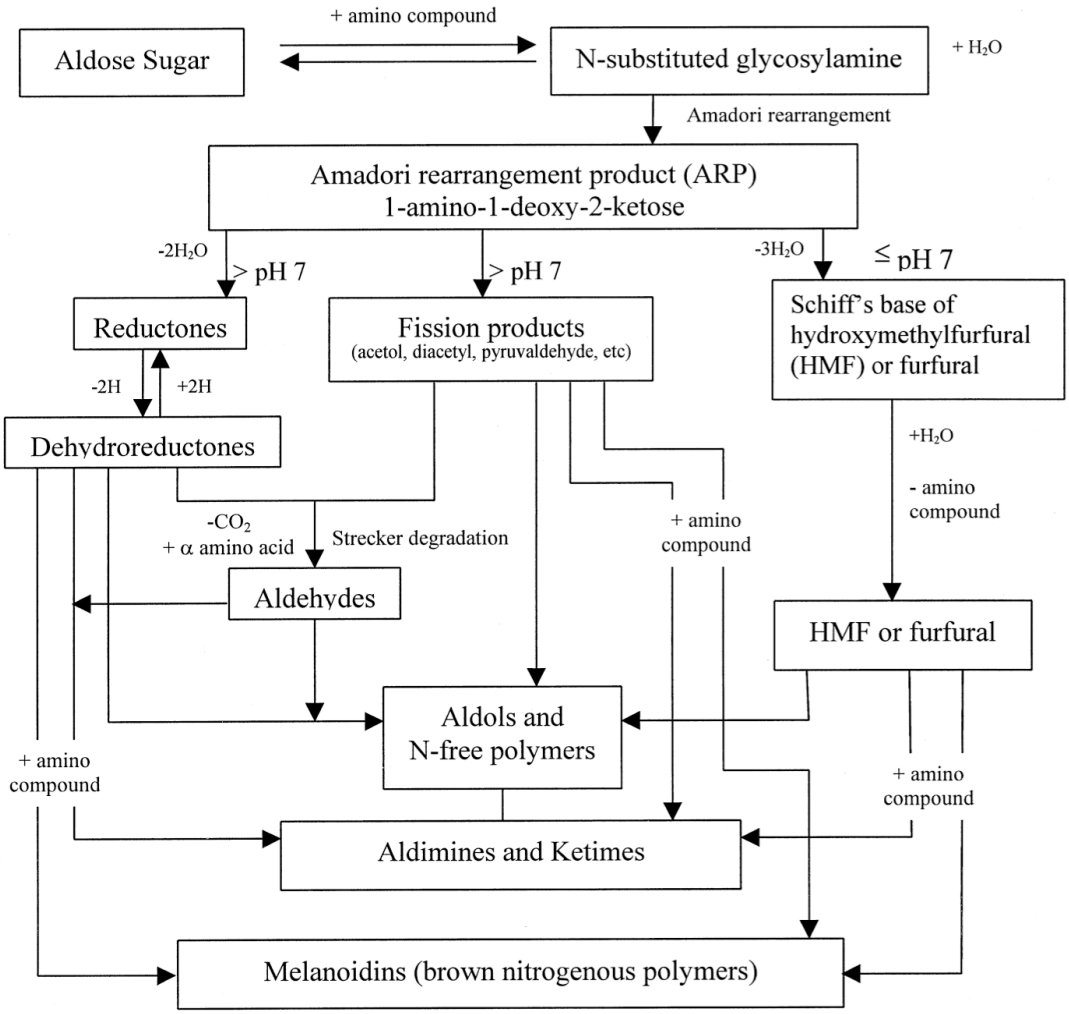

Figure 1.1 The Maillard reaction scheme modified from Hodge's (Martins, Jongen & Boekel 2001).

A detailed example of the formation of an Amadori product is given in Fig 1.2. The free amino group of a protein reacts with the aldehyde of glucose to form a carbinolamine. Carbinolamine dehydrates to a Schiff base, which subsequently undergoes a slow molecular rearrangement to form the Amadori product. It is important to note that the Amadori product exists as a mixture of several cyclic isoforms, although only a single isoform is shown here in the diagram.

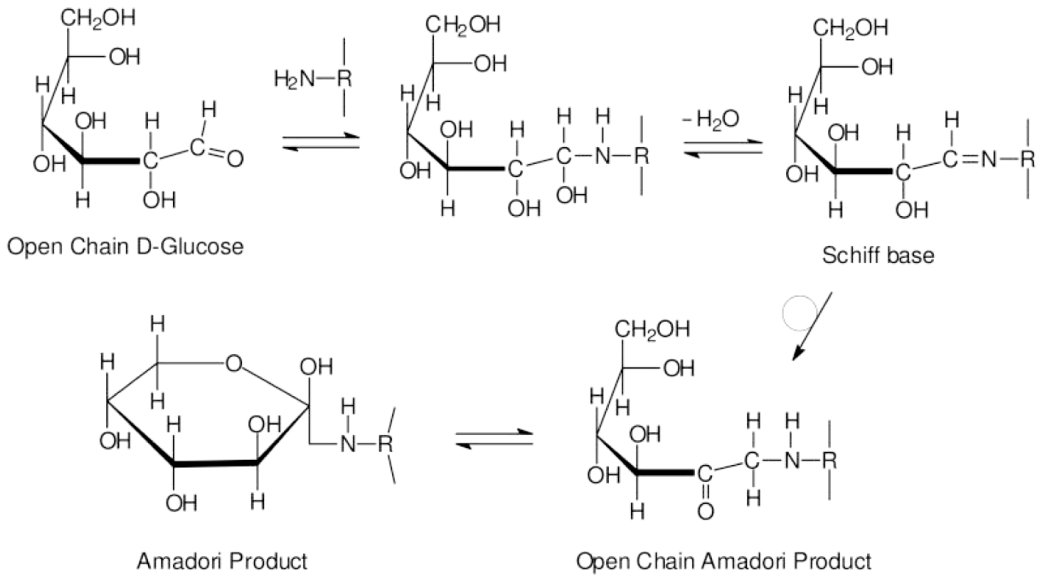

Figure 1.2 Amadori product formed between glucose and amino group of protein (Zhang *et al.* 2009)

Somewhere between the Amadori product and melanoidins, intermediate glycation products (IGPs) and advanced glycation end-products (AGEs) are formed by subsequent oxidative decomposition of the Amadori product and the reaction between tissue proteins and reactive carbonyl/dicarbonyl compounds. IGPs includes a wide range of reactive carbonyl and dicarbonyl compounds, such as glyoxal, methylglyoxal, glycolaldehyde, 3-deoxyglucosone, 1-deoxyglucosone, 4,5-dioxopentose, and 5,6-dioxohexose (Fig 1.3).

AGEs forms at a relatively late stage of the Maillard reaction. They appear in a wide range of tissues and foods, and are highly correlated with the physiological and pathological influence of MRPs *in vivo* (Nguyen 2006). A group of AGEs compounds that have been extensively studied in glycation-related diseases and aging are listed here for reference (Fig 1.4), including N ε -(carboxymethyl)lysine (CML), N ε -(carboxylethyl)lysine (CEL), S-(carboxymethyl)cysteine (CMC), pyrraline, 3-deoxyglucosone-derived imidazolium crosslink (DOGDIC), pentosidine, glucosepane, glyoxal lysine dimer (GOLD), crosslines, and fluorolink (Qibin Zhang, 2009).

However, this is not the end of story. The Maillard reaction is much more complicated than what has been implied by the Hodge diagram (Fig 1.1) (Martins, Jongen & Boekel 2001). Not only reducing sugars, but also other carbohydrates, lipids, ascorbic acid, could participate in the reaction with their degradation products. For example, two IGPs, glyoxal

and methylglyoxal, could also be produced by peroxidation of lipids, instead of Amadori product decomposition (Lederer & Klaiber 1999). In addition, the Maillard reaction and lipid peroxidation may both include a whole network of complex reactions. They are intimately interrelated and produce products that influence each other. AGEs and advanced lipoxidation end products (ALEs) are also the very common intermediates and products. The similarity and interaction between these two pathways increase the complexity of the Maillard reaction chemistry, and lead to the suggestion that they should be included in one general carbonyl pathway (HidalgoI & Zamora 2006).

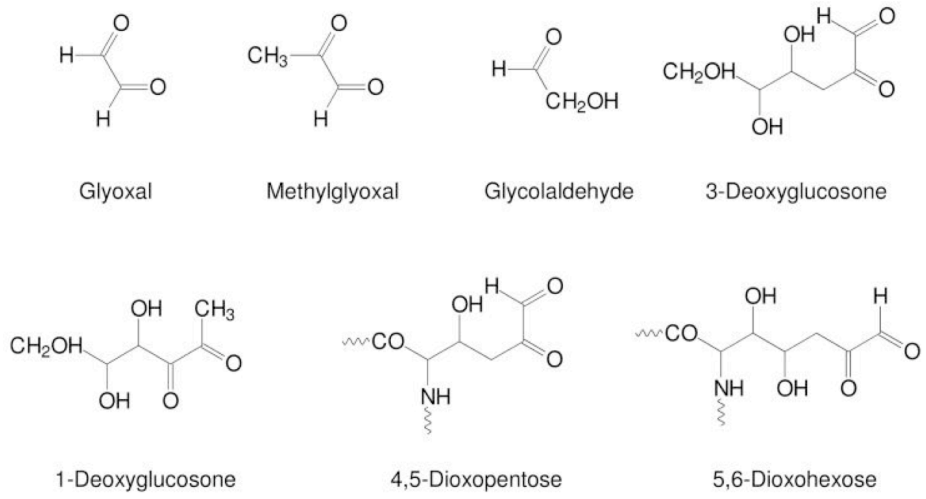

Figure 1.3 Representative intermediate glycation products (Zhang *et al*. 2009).

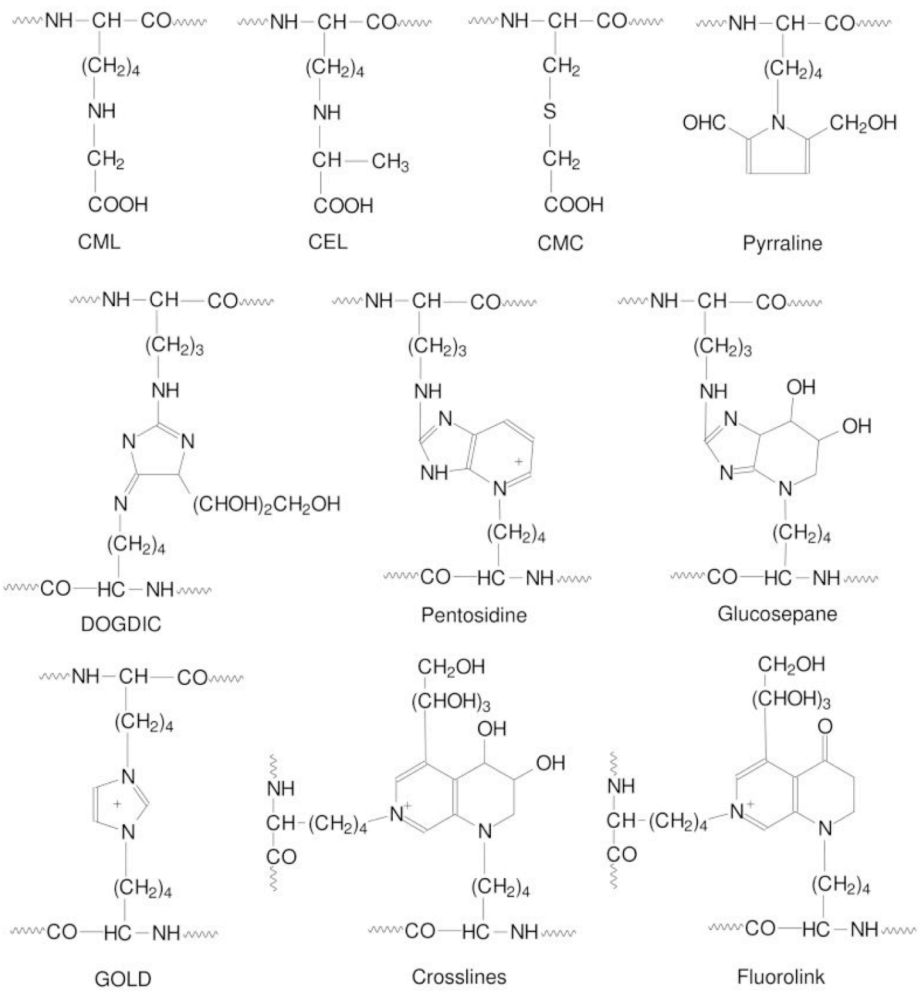

Figure 1.4 Representative advanced glycation end-products (Zhang *et al*. 2009).

1.3.2. Biological functions and effects of MRPs

It is well known that the Maillard reaction products (MRPs) have important influence on functional macromolecules, living cells, tissues and the most normal substances, our daily foods. The haemoglobin of erythrocytes may be glycated. The reaction also affects the oxidative stability and shelf life of many foods, such as milk (Hansen & Hemphill 1984), pasta (Anese *et al.* 1999), cereals (Lingnert & Lundgren 1980) and meat (Bedinghaus & Ockerman 1995). Two aspects of MRPs' biological effects, antioxidant or free radical scavenging activity and physiological influence, are described here due to their close relevance to the subject of this study.

1.3.2.1. Antioxidant effects of MRPs

In 1954, the antioxidant capacity of MRPs was investigated for the first time, by Franzke and Iwainsky (Franzke & Iwainsky 1954). Some fractions with potent antioxidant activities were separated and compared to the conventional antioxidants commonly used in food (Lingnert & Hall 1986).

By increasing reaction time or temperature, the colour of MRPs darkens while their antioxidant activities become correspondingly stronger at the beginning but dropped down afterwards (2 h in the glucose-glycine model system) (Yoshimura *et al.* 1997). But in other model systems, the browning of MRPs solution generally corresponds to the increase in antioxidant activities (Benjakul, Lertittikul & Bauer 2005) (Antony *et al.* 2000). However, this may not be 'related to the free-radical scavenging activity of the MRPs at prolonged heating conditions' (Morales & Jiménez-Pérez 2001). The antioxidant activity of MRPs is unstable and easy to be lost during separation (Lingnert & Waller 1983). The relationship between colour and antioxidant capacity was also demonstrated by the fact that decolourisation of MRPs diminished their antioxidant properties. This indicates that brown-coloured compounds make a major contribution to the antioxidant activity (Yen & Hsieh 1995). Interestingly, the reducing activity of MRPs decreases, corresponding to the increase in heating time, which indicates a mechanism unrelated to a conventional oxidative-reducing balance. It is generally believed that MRPs form in certain intermediate stage of the reaction have the highest antioxidant or free radical scavenging activities (Morales & Jiménez-Pérez 2001) (Yoshimura *et al.* 1997).

It has postulated that the major mechanism of the antioxidant action of MRPs relies on their ability to trap positively charged metabolites, scavenging oxygen radicals or chelating metal, particularly iron, to form inactive complexes (Yoshimura *et al.* 1997). However, this hypothesis remains unproven and the compounds responsible for the antioxidant effects have yet to be identified.

1.3.2.2. Physiological effects of MRPs

According to the majority of experimental data to date, MRPs are commonly considered as a risk to health, particularly in terms of AGEs generated under physiological condition *in vivo* (Vlassara *et al.* 2007). AGEs have been suggested to play an important role in the

development of chronic complications of diabetes (Wautier & Guillausseau 2001). As chemicals indicating decay of function proteins, MRPs have been blamed for the generation of a mutagenic agent, acrylamide (Byrne, Mottram & Martens 2002), and increasing the risk of aging and disease like Diabetes (Chuyen 2006), which would result in vascular complications and loss of sight (Jakuš & Rietbrock 2004) (Lee, Simpson & Ortwerth 1999). However, evidences have been raised against the dietary AGEs being a risk to human health (Ames 2007). Some beneficial properties of MRPs, have been documented which includes anti-oxidative activity and desmutagenic effects (Chuyen 1998) (Yen & Hsieh 1994) (Yoshimura *et al.* 1997).

Both positive and negative influences of MRPs on cell reproduction have been reported (Rufián-Henares & Morales 2006) (Kundinger 2004) (Harris & Tan 1999) (Einarsson, Snygg & Eriksson 1983). MRPs from amino acids and glucose showed significant impacts on the growth of the microorganisms (Harris & Tan 1999). This impact varies according to which amino acid was used. MRPs derived from reaction of arginine, glycine and histidine with glucose, promoted the growth of *S. aureus* and *S. enteritidis*, while MRPs of cysteine and glucose inhibited the growth of both germs. Furthermore, heating to a higher temperature or for a longer incubation time, strengthened the inhibitory effect of Cys-Glc MRPs. It has been demonstrated that there is a direct link between antimicrobial ability, the intensity of the browning, the pH at the end of synthesis and the reducing capacity of MRPs (Harris & Tan 1999).

With the approach of aging or disease, MRPs formed by carbohydrate or lipid-derived intermediates with proteins, lead to the formation of advanced glycation and lipoxidation end-products (AGE/ALEs) (Thorpe & Baynes 2003). AGEs, which are widely recognised as risk markers in aging and diseases, showed angiogenic effects on cultured endothelial cells (from the vein of human umbilical cord) at the concentrations ranged from 0.5 to 50 μg/mL, showing no change on cell proliferation rates (Tezuka *et al.* 1993).

However, the therapeutic benefits of MRPs have not been reported in any published studies. In the previous studies, MRPs derived from some herbal Chinese medicines showed the ability to protect different types of mammal cells from chemical toxin or pathogen, by a common mechanism. More details of this are given in the next section.

1.3.3. MRPs and herbal TCM

As described in Section 1.1.3, the Maillard reaction occurs widely during the preparation of herbal TCM. MRPs predominate, therefore, in the composition of the herbal soup, and very possibly contribute the effective components responsible for TCM's multi-target therapeutic effects.

However, MRPs have rarely been the subject of research carried out upon TCM or phytochemicals. A relevant report appeared in the chemical composition studies (Li *et al.* 1999) (Cao, Zheng & Xu 2001) (Suzuki *et al.* 2004) on the Arginyl-fructosyl-glucose from red ginseng (*Panax ginseng C.A.Meyer* or *P.schinseng Nees*) (Cho *et al.* 2008), but no therapeutic effect of MRPs was declared (Yoo *et al.* 1999). The nearly complete neglect of MRPs in TCM studies may be due to the complexity of the chemical nature of MRPs (Martins & Boekel 2005), and thus the extreme difficulty in their separation and isolation. This difficulty has been amplified by the combination of herbs used in TCM. If it is not possible to characterise unambiguously the compounds from a simple Maillard reaction between amino acid and monosaccharide, how much more difficult would it be to predict the chemical fingerprint of MRPs in a four-herb-composite TCM formula?

1.3.3.1. MRPs and the roots extracts

In a study of RIE, it was shown that it inhibited the attachment of influenza A virus to the host cells (Chen *et al.* 2006). During the preparation, a high content of amino acids, proteins, sugar and MRPs were produced and accounted for approximately 30% of the dry weight of the preparation. Arginine is the most abundant single Maillard reactant in the roots, while glucose and sucrose are the most abundant monosaccharide and disaccharide in the roots. Sucrose accounts for up to 87% of the mono and disaccharides produced, and may hydrolysise to form glucose and fructose at low pH and high temperature. MRPs formed from arginine and glucose therefore become a potential representative of the whole family of MRPs in RIE (as described later in Section 4.2.2).

1.3.3.2. MRPs and Momordica charantia L. extracts

The Maillard reaction may occur in other medicinal plants. Bitter melon (*Momordica charantia Linn.*), serves as a daily vegetable to people in many regions of southern and

eastern Asia, and is widely used in China as an anti-diabetic agent. It is also known as a contraceptive and antiviral agent. Like RIE, the preparation of *Momordica charantia* extracts (MCE) includes sun-drying and extraction with boiling water.

In contrast to its fresh counterparts, sundried *Momordica charantia L.* pulps have a smaller proportion of soluble protein, total saccharides and reducing sugars, which indicates the occurrence of Maillard reaction. Glucose, fructose and maltose have been identified from fresh *Momordica charantia L.* pulps. Among them, fructose and glucose equally dominate the monosaccharides content of the vegetable pulps.

Just like as in the roots, arginine and glucose are the predominant components of the free amino acids and reducing sugars. Arginine accounts for 32.4% of the total amino acids and 59.3% of the free amino acids in the fresh pulps of *Momordica charantia*. Two continuous heat-processing steps were performed for preparing the MCE: sundried at 20~30°C for days and boiling at 100°C for several hours. The arginine content of sun-dried pulps and MCE decreased from 1.44% (w/w, fresh pulps) to 0.47% (sun-dried) and 0.24% (boiled) subsequently.

As shown in Fig 1.5, MRPs from MCE administered orally reversed the progress of cellular damage (Fig 1.5a) induced by the autoimmune response in genetic Type 2 diabetic rats, and restored the healthy population of pancreatic islet β-cells (Fig 1.5b) at three dosages. The cellular-protective or repairing effects was so effective, that antioxidant activity alone could not fully explain the mechanism of this action. A series of experiments were conducted to determine the mechanism of MRPs on the β-cells, in addition to being a potent antioxidant. Cells achieved the better recovery from oxygen free radical damage with MRPs treatment prior to the damage than after the damage (Fig 1.6). Oxygen free radicals damage may destabilise the cell membrane by oxidising the membrane lipids, thereby destabilising the integrity of membrane. Theoretically, pore formation would occur from the membrane destabilisation and allow a macromolecule, such as green fluorescence protein (GFP), to pass through the cell membrane freely and appear in the cellular plasma. Pre-treatment using MRPs of MCE stopped this abnormal cross-membrane transportation, by preventing the formation of free radicals induced pores on cell membrane (Fig 1.7). Combining this with data from diabetic rats, MRPs of MCE show a clear cellular membrane protective activity against free radials. It could be argued that the strong free radical scavenging capacity of MRPs may also assist its cellular protective action. This capacity, however, requires a relatively high concentration of MRPs, which is unrealistic in both *in vivo* and *in vitro*

studies, and should not have resulted in different outcomes depending on whether the MRPs treatment was applied before or after the free radical interference. If they do protect the membrane and stop the entry of GFP, it may be assumed that the MRPs act on the matrix of the cell membrane, lipid bilayers, rather than any other components.

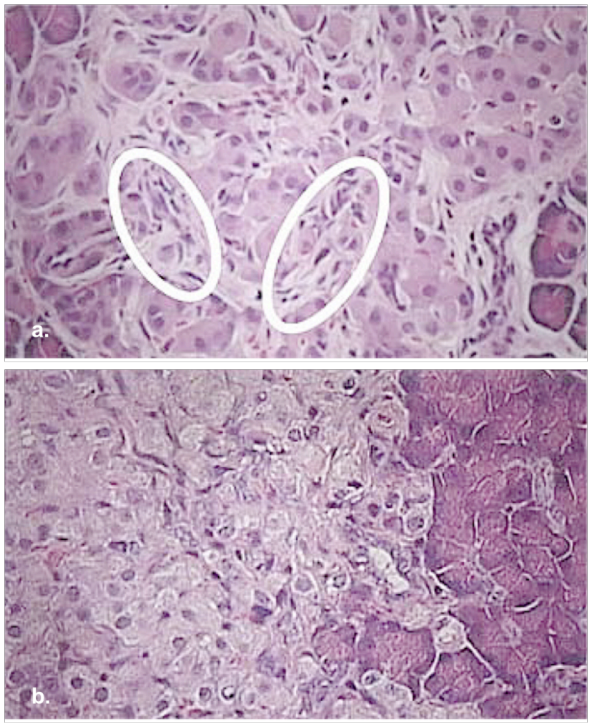

Figure 1.5 Optical microscopy (HE stains) image of pancreas islet tissue slices of GK/Crj genetically modified Type 2 diabetic rats.

a. Pathological pancreas islet tissue, shows deformed and dysfunctional β-cells. **b.** MCE administrated pancreas islet tissue, shows reduced foam cells, vitreous depositions and hypertrophic islets, increase insulin secretion (figures are quoted from unpublished data by Prof.Guangzeng Xi in Xi'an 4th Military Medical University, P.R.China).

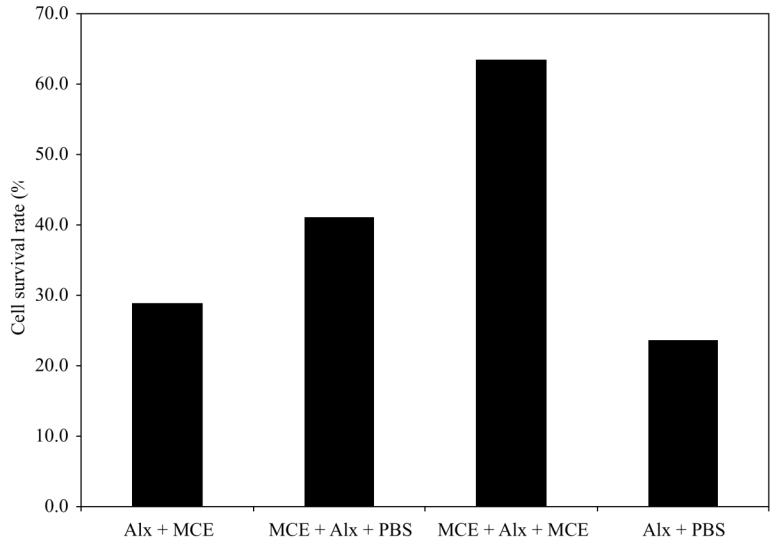

Figure 1.6 Protection or repairing effects on alloxan damaged β-cells *in vitro* by MCE MRPs.

Alx stands for alloxan (1 mM, 1 h). PBS, phosphate sodium buffer (pH7.2, for cell culture use). MCE stands for MCE MRPs (2 mg/mL, 1 h) in the diagram. The cell survival rates were 28.8%, 41.0%, 63.4% and 23.5% for the 'repairing group', 'protecting group', 'repairing plus protecting group' and the negative control ('alloxan damaged' group), respectively (Xiang *et al.* 2007).

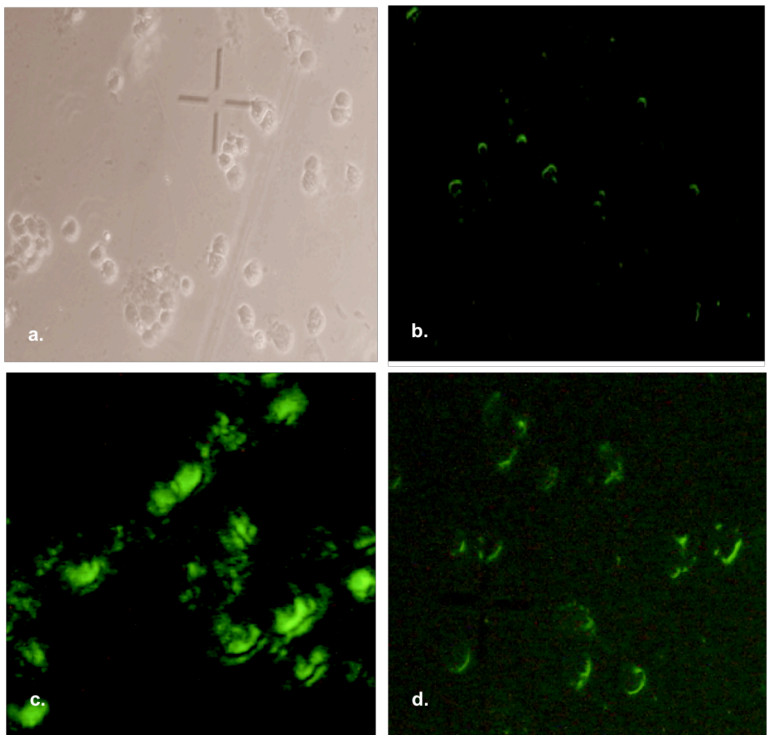

Figure 1.7 Fluorescent microscopy studies of MCE MRPs protecting HIT-T15 β-cells from alloxan damage.

a. Normal β-cells in white light: ×100.

b. Normal β-cells in fluorescence: ×100. No green fluorescent light was observed.

c. Alloxan damaged cells + GFP (Green Fluorescent Protein): ×400. The plasma of damaged cells was lighted up by GFP.

d. MCE protected cells + alloxan + GFP: ×400. Only weak green fluorescence was investigated on the surface of the cells; the damage caused by alloxan was effectively avoided.

(data not published, quoted from a joint work conducted by Lijing Ke and Xiaonan Huang)

1.3.4. Cytoprotective effects of MRPs on erythrocytes

Haemagglutination is mediated by the binding of viral envelope glycoprotein haemagglutinin (HA) to cellular plasma membrane receptors, sialic acid residues of glycolipids (Rogers *et al.* 1985) (Wiley & Skehel 1987) (Kobasa *et al.* 2004). As previously reported (Chen *et al.* 2006), RIE MRPs inhibited the haemagglutination induced by influenza A viruses which indicates blocking the association of HA with its receptor. This is consistent with the results from antiviral studies on MDCK cells (described in section 1.4.1), and supports the assumption that RIE inhibits the viruses' attachment to cell membrane. Furthermore, MRPs of arginine and glucose inhibited the attachment of influenza virus to erythrocytes in the same manner as MRPs from RIE, indicating it is possible to use the MRPs between a single amino acid and a reducing sugar in order to diminish the complexity of MRPs derived from plant tissues.

1.3.5. Effects of RIE on the surface charge of cell membrane

Every cell carries an electric charge, according to its membrane composition. The surface charge of the plasma membrane varies according to different species of cells and their physiological status (Gallin, Durocher & Kaplan 1975) (Miller *et al.* 1998) (Briandet *et al.* 1999). Capillary electrophoresis (CE) is a sophisticated analytical technique that is capable of separating and identifying compounds and particles in a highly complicated system, based on their charge-mass ratio. Theoretically, if bioactive molecules, such as MRPs from RIE, bind to the plasma membranes of cells, the surface charge potential of the membrane is likely to change as a response to the binding. In the previous studies, CE provides a useful method for characterising and quantifying erythrocytes or other cells (Lu *et al.* 2003), and has been used successfully to identify the potential changes on the erythrocyte membranes caused by treatment with RIE or virus binding (Chen *et al.* 2006). RIE prolonged the electrophoretic retention time of normal erythrocytes by 60 s (~15%), which reveals a dramatic change in the membrane charge. This result indirectly illuminates the existence of components of RIE, i.e. MRPs, upon the cell membrane surface. However, it remains unclear whether the MRPs may affect the morphological and physiological properties of cell membrane, or the virus-induced membrane fusion process.

1.4. INFLUENZA VIRUS AND ANTI-INFLUENZA VIRUS AGENTS

1.4.1. General background to the viruses

Influenza viruses are enveloped RNA viruses belonging to the *Orthomyxoviridae* family. Influenza pandemics present a major threat to human and animal health as recently witnessed by the outbreaks of influenza virus A: H5N1 (avian flu) in 2005 and A: H1N1 (swine flu) in 2009.

Three sub-viral components form the major part of each influenza virion: an outermost envelope, an intermediate layer of matrix protein M1 and a helical viral ribonucleocapsid core in the centre (Nayak *et al.* 2009). The transmembrane proteins haemagglutinin (HA), neuraminidase (NA) and M2 are embedded in the lipid bilayer of viral envelope (Fig 1.9).

There are three types of influenza viruses: A, B and C. Humans can be infected with any of the three types. Generally, influenza types A or B viruses cause epidemics of human flu almost every winter. Among these 3 types of virus, only influenza A viruses are further classified by subtypes based on the two main surface glycoproteins of the virus membrane, haemagglutinin (HA) and neuraminidase (NA). There are 16 known HA subtypes and 9 known NA subtypes, which make 144 known combinations of HA and NA possible. However, only a few influenza A subtypes are currently in circulation among people, mostly H1N1 and H3N2. Influenza A subtypes and B viruses may be further characterised into strains. One subtype of influenza A could have several strains due to the 'antigenic drift', which refers to small and gradual changes of HA and NA that occur through point mutations in the genes of two main surface proteins. Influenza C viruses have a mild influence on human and do not cause epidemics or pandemics (CDC 2005).

As a result influenza A subtypes H1N1 and H3N2 were used in this study, as they represent the general characters of pathogenic seasonal flu viruses.

1.4.2. Composition of the membrane lipids of influenza A virus

Influenza viruses share some common classes of phospholipids with the plasma membranes of their eukaryotic host cells, regardless of subtypes and strains. Five classes of phospholipids have been identified as the main composition of membrane lipids in influenza A virus (H0N1, WSN strain). They are sphingomyelin (SPH), phosphatidyl choline (PC),

phosphatidyl inositol (PI), phosphatidyl serine (PS) and phosphatidyl ethanolamine (PE). The proportion of each class, analysed by gel thin-layer chromatography, is 26.4±2.6% (SM), 17.8±4.5% (PC), 20.5±0.5% (PI+PS) and 35.8±2.2% (PE), respectively (Lenard *et al.* 1976). A comparative study of influenza A and B viruses revealed that the classes of phospholipids in both types of virions were in close similarity, although some unique differences were also reported in the fatty acid composition of individual phospholipids of the viruses (Blough 1971).

It is well known that influenza viruses leave their host cells by budding from the plasma membrane. They obtain their membrane envelopes in this process (Fig 1.10). Moreover, Rodriguez Boulan and Sabatini (Boulan & Sabatini 1978) have shown that influenza viruses (fowl plaque virus, FPV) budded from the apical domain of cell membrane whereas another enveloped virus, vesicular stomatitis virus (VSV), budded from the opposite side of the cell, from the basolateral membrane domain. The phospholipid compositions of these two viruses varied significantly, which reflects the substantial difference in the composition of the apical and basolateral membrane domains of MDCK cells (Meer & Simons 1982).

Lipid rafts are lipid microdomains enriched in sphingolipids and cholesterol. The viral envelope is not composed of the homogeneous lipids but a mosaic mixture of lipid microdomains which contain raft-associated proteins and non-raft-associated proteins. Lipid rafts have been shown to play critical roles in several aspects of viral life cycle, including viral fusion and entry, or viral assembly and budding process (Nayak, Hui & Barman 2004) (Nayak & Reichl 2004). The most common lipids found in lipid rafts of human cells contain PC or PE. Among the transmembrane proteins of viruses, HA and NA associate with the lipid rafts whereas M2 does not (Nayak *et al.* 2009).

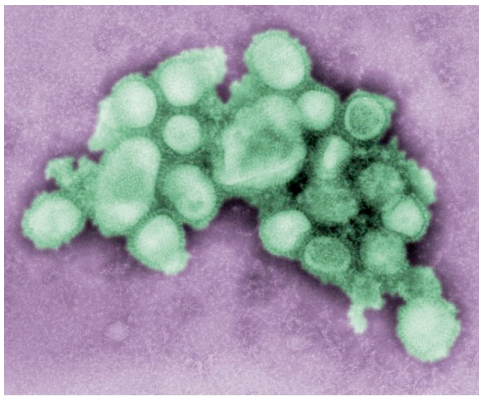

Figure 1.8

This preliminary negative-stained transmission electron micrograph (TEM) depicts some of the ultrastructural morphology of the A/CA/4/09 swine flu virus.

Picture from CDC website (CDC 2005)

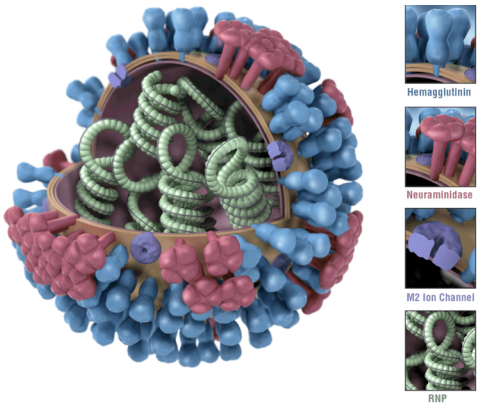

Figure 1.9

A 3D graphical representation of the biology and structure of a generic influenza virus (not specific to the 2009 H1N1 virus).

Picture from CDC website (CDC 2005)

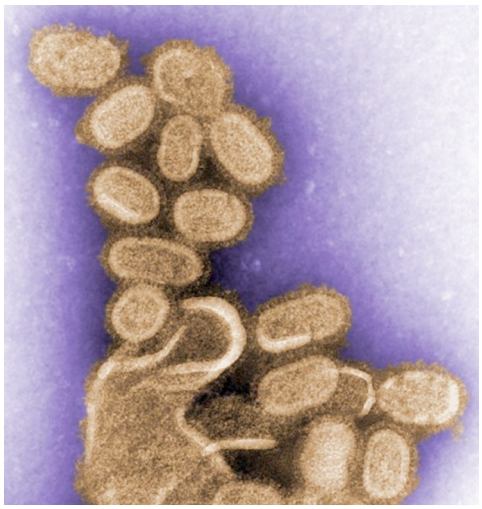

Figure 1.10

This negative stained transmission electron micrograph (TEM) shows recreated 1918 influenza virions that were collected from supernatants of 1918-infected Madin-Darby Canine Kidney (MDCK) cells cultures 18 hours after infection.

Picture from CDC website (CDC 2005)

1.4.3. Recognized anti-influenza virus agents and their mechanisms

As an enveloped virus, the infectious cycle of influenza virus typically involves four steps: binding, fusion or entry, replication and budding. Together these provide several opportunities for antiviral activity to inhibit the viral replication. For example, some antibodies inhibit the attachment of viruses to cells (Ugolini *et al.* 1997) (Reading & Dimmock 2007) (Klasse & Sattentau 2002). Peptidylchloroalkylketone inhibitors prevent the fusion event by inhibiting cleavage of the precursor of HA (Tashiro & Rott 1996); the approved drugs amantadine and rimantadine prevent viral particles from uncoating prior to their release into the cytoplasm by blocking the M2 ion channel (Pinto & Lamb 2007) (Ilyushina *et al.* 2007) (Duff 1992). Neuraminidase inhibitor, Oseltamivir for instance, competes with sialic acid, blocking activity of viral neuraminidase, to prevent the virus from being released from infected cells by membrane budding (Gubareva, Webster & Hayden 2002) (Moscona 2005). However, all of these drugs rely on their interference with membrane proteins like M2 protein (ion channel) and HA, or polysaccharides incorporating sialic acid. These sophisticated mechanisms, which are highly dependent on structural recognition, are undoubtedly very efficient, but share a common weakness: it is not difficult for viruses to develop resistance to these drugs by simple genetic mutations.

Amantadine and Oseltamivir (trade name 'Tamiflu') are two leading anti-influenza virus agents in the frontline of the battle against seasonal flu. Although they have been very successful in controlling influenza A and B virus epidemics, there have been warnings that the rapidly growing number of novel virus strains with resistance to these drugs might out-weight their efficacy in the next flu pandemic. According to the US Centre for Disease Control, all H3N2 viruses and 2009 H1N1 flu viruses have shown resistance to adamantine, which is no longer recommended for treatment of flu. Some comments have also been made about Oseltamivir, for which a higher dosage and longer duration of treatment have been recommended. Great efforts have been made to develop new antiviral compounds, based on different mechanisms, to offer high-efficiency, low-resistance treatments for constantly mutative seasonal flu. MRPs derived from TCM, more specifically from *radix Isatidis*, and their interaction with lipid bilayers, might provide a new direction in the treatment of influenza.

1.5. HYPOTHESIS AND AIMS OF THIS STUDY

1.5.1. Hypothesis

Since we have seen the important role MRPs might play in TCM, and the unusual mechanism for protecting cell membranes, a conventional study is carried out here to determine the interaction between MRPs and bilayers of membrane lipids, to identify the active compounds and to elucidate the underlying molecular mechanism. Due to the complex nature of the Maillard reaction, the MRPs involved in this study must be simplified and modeled to cancel out any unnecessary background. One of the solutions is to limit the reactants to a typical amino acid and reducing monosaccharide, i.e. arginine and glucose, and carefully control the conditions of reaction to ensure the reproducibility of Arg-Glc MRPs in various experiments.

The active MRP molecules from RIE may initiate their action on the target cells by specific binding to the plasma membrane. The binding may occur on a basis of structure recognition or interaction between secondary bonds of MRPs and membrane components, with a minor influence on the conventional signalling pathway on cell plasma membrane. MRPs act rather like a "firewall" blocking attachment of the virus, and preventing infection of the cells. The amphiphilic characteristics of their structures may explain their affinity for cell membranes. Possible target molecules on the cell membrane may include: 1) lipids which form the bilayer of the plasma membrane; 2) the native proteins and polysaccharides on the cell membrane; 3) the MRPs derived from lipids, proteins and polysaccharides on the cell membrane.

Due to the fact that lipids, particularly phospholipids, form the 'backbone' of membrane and being intensively studied, the lipid bilayer was placed on the top of the list for this study.

1.5.2. Aims

This study aims to characterise the antiviral mechanism of MRPs derived from RIE by providing answers for the subjects listed below: 1) elucidate the binding of MRPs to phospholipids bilayers; 2) effects of MRPs on phospholipids bilayers; 3) influence of MRPs on virus-induced membrane fusion; 4) anti-influenza virus mechanism of MRPs.

CHAPTER 2

MATERIALS AND METHODS

2.1. MATERIALS

2.1.1. MRPs of *radix Isatidis* Extracts (RIE)

2.1.1.1. Species and growth of the plant

The raw material, *radix Isatidis* (Bei Ban-Lan-Gen), belongs to the *Cruciferae* family. It is the roots of a tetraploid strain of *Isatis indigotica Fortune*, which is grown under the conditions of Good Agricultural Practice (GAP), in Ruanqiao Town, Taihe County, Fuyang City, Anhui Province. The plant grow for 4 months (approximately equal to 2~3 times harvest of their leaves), between each June and October, before the harvest in October ~ November every year. The collected whole plants were identified as *Isatis indigotica Fort.* by Prof. Chengzi Yang from Fujian Traditional Chinese Medicine College.

2.1.1.2. Raw materials processing and preparation of RIE MRPs

The fresh roots were harvested and sun-dried in Fuyang City, Anhui Province, P.R. China. The sun-drying was performed under the conditions shown below: 20~25°C (day), 5~10°C (night), 2 ~ 4 weeks depending on the local climate. The yield of sun-drying is 1 kg sun-dried roots from about 2.5 kg fresh roots.

To prepare RIE MRPs, 1400 g sun-dried roots were extracted twice with boiling water at 100°C, for 2 h and 1 h, respectively. The solution was filtered and vacuum concentrated at 50°C until the relative density reached 1.20. After the stock was precipitated by 60% ethanol at 4°C, the suspension was vacuum concentrated at 50°C to produce the RIE MRPs as brown powder.

2.1.2. MRPs of *Momordica charantia L.* Extracts (MCE)

Fresh fruits of bitter gourd (*Momordica charantia Linn.*) and sliced sun-dried pulps were purchased from the Exemplary Bitter Gourd Planting Farm (Huxian County, Shanxi Province, P.R.China). The boiling water (100°C) extracts of the pulps were vacuum concentrated at 70°C to produce the brown powder of MCE MRPs.

2.1.3. MRPs of arginine and glucose

1 mmol of *L*-arginine (non-animal source, Sigma) and 1 mmol *D*-glucose were mixed thoroughly, and incubated in a humid atmosphere over a saturated solution of potassium bromide (80% RH) at 40°C. After a 7-day incubation, the reaction products were dissolved in 5 mL deionised water to obtain Arg-Glc MRPs.

The deuterated Arg-Glc MRPs (DAG) was prepared with 1 mmol of *L*-Arginine-2,3,3,4,4,5,5-*d*7 (C/D/N ISOTOPES Inc.) and 1 mmol *D*-+-glucose in H_2O following the same procedure as described above.

2.1.4. Influenza viruses

Influenza strains A/Beijing/95-262(H1N1/C_2E_3, 1:640 8/2/99) and B/Shanghai/93-1(C_3C_2, 1:320 9/2/99) were purchased from the National Influenza Center of China. Influenza A virus FM1 (H1N1, mouse-adapted strain) was generously provided by Fujian Centre of Disease Control (Fuzhou, Fujian, P.R.China). All viruses were cultured in the allantoic cavity of 11-day-old chick embryos at 33°C for 48 h. Isolated virus stocks were stored in aliquots of phosphate buffered saline at -80°C.

2.1.5. MDCK cells

Madin-Darby canine kidney (MDCK) cells were purchased from the China Center for Type Culture Collection. Continuous MDCK cells were grown in Dulbecco's Modified Eagle's Medium (DMEM) containing 10% calf serum, penicillin G (100 mg/L), streptomycin (80 mg/L), and sodium bicarbonate (3.7 g/L), at 37°C in a humidified incubator containing 5% CO_2 (Thermo Forma Series II Water Jacketed CO_2 Incubator, Model 3111, USA) (All supplements were purchased from GIBCO, Invitrogen Corporation).

2.1.6. Liquid Chromatographic Materials

Table 2.1 HPLC columns used in the protein separation and purification

LC columns	Size (mm)	Manufactory
Toyopearl SP-650M strong cation ion-exchange chromatography	16.0×250	TOSOH, Japan
Oligo-R3 C18 RPLC	4.6×250	PerSeptive Biosystems, USA
TSK-GEL G3000SWXL size-exclusion chromatography	7.8×300	TOSOH, Japan
POROS 20 Micron HP2 hydrophobic chromatography	3.0×150	PerSeptive Biosystems, USA

2.1.7. Low osmotic media

Sodium ehloride was dissolved in de-ionised water to make 0.9% saline and filtered with 0.22 μm, and diluted to 0.1%, 0.2%, 0.3%, 0.45% to make low osmotic pressure solution.

The reagents and chemicals used in this study are purchased from Sigma-Aldrich, unless specified elsewhere.

2.2. METHODS

2.2.1. Biochemistry studies

2.2.1.1. Extraction of proteins

100 g roots were frozen in liquid nitrogen, before smashed by high speed pulverizer (800 rpm). 300 mL extraction buffer (pH 7.2, 0.01 mol/L PB + 0.1 mol/L NaCl) was added and stirred at 4°C for 12 h. The supernatant was separated by centrifugation at 12000 rpm for 20 min, at 4°C (Hitachi, Japan).

2.2.1.2. Protein concentration determination

The total protein content was determined by Kjeldahl assay (Cataldo, Schrader, & Youngs, 1974), Folin-Phenol assay (Lowry, Rosebrough, Farr, & Randall, 1951) and Bradford assay (Bradford, 1976).

Kjeldahl determines the amount of nitrogen in protein. A protein index of 6.25 was used in this study. In Folin-Phenol Assay, bovine serum albumin (BSA) was used as the protein standards (Table 2.2). The protein concentration was calculated with Eq 2.1. In Bradford assay, BSA was also used as the protein standard. The protein concentration was calculated with Eq 2.2.

Reagents of Folin-Phenol assay (Lowry, Rosebrough, Farr, & Randall, 1951)

Reagent A, 10 g Na_2CO_3, 2g NaOH and 0.25 g $KNaC_4H_4O_6 \cdot 4H_2O$, dissolved in 500 mL H_2O. Reagent B, 0.5 g $CuSO_4 \cdot 5H_2O$ dissolved in 100 mL H_2O.

Reagent C, alkaline copper solution. Mix 50 mL of Reagent A with 1 mL of Reagent B. Discard after 1 d.

Reagent D, diluted Folin reagent. Titrate Folin-Ciocalteu phenol reagent (stored in the dark, 4°C) with NaOH to a phenolphthalein end-point. On the basis of this titration, dilute the Folin reagent (about 2-fold) to make it 1 N in acid.

Reagents of Bradford assay assay (Bradford, 1976)

Coomassie Brilliant Blue G-250 (100 mg) was dissolved in 50 mL 95% ethanol. To this solution 100 mL 85% (w/v) phosphoric acid was added. The resulting solution was diluted to

a final volume of 1 litre. Final concentrations in the reagent were 0.01% (w/v) Coomassie Brilliant Blue G-250, 4.7% (w/v) ethanol, and 8.5% (w/v) phosphoric acid.

Table 2.2 The BSA working standard for Folin-Phenol assay

Reagents	Tube number					
	1	**2**	**3**	**4**	**5**	**6**
BSA solution (mL)	0	0.2	0.4	0.6	0.8	1.0
H_2O (mL)	1.0	0.8	0.6	0.4	0.2	0
BSA content (μg)	0	50	100	150	200	250
Reagent C (mL)	5	5	5	5	5	5
Reagent C (mL)	0.5	0.5	0.5	0.5	0.5	0.5

$$Protein\ concentration\ (mg/mL) = 420.99 \times A_{650nm} - 7.68,\ R^2 = 0.9943$$

Equation 2.1

$$Protein\ concentration\ (mg/mL) = 1159.60 \times A_{595nm} - 41.544\ ,\ R^2 = 0.9933$$

Equation 2.2

(The standard curves are not shown, but available on request)

2.2.1.3. Saccharides concentration determination

The saccharides concentration in the roots was determined with the anthrone sulfuric acid assay (Dische, 1967). Four milliliters of anthrone (2 mg/mL) was added to 1 mL of D-glucose solution of 100, 200, 300, 400, 600, 800 μg/mL (cooled on ice, 5 min), produced on heating (100°C, 10 min) a cyan colour (λ_{max}= 620 nm). The absorbance was measured after cooling for 10 min in water bath. The reducing sugar concentration of sample was measured by 1 mL solution of each sample. The same volume of distilled water was used as control.

Fresh roots were frozen by liquid nitrogen, then smashed by a high-speed pulveriser (800 rpm). 10 g of smashed roots was extracted with 30 mL deionised water for 12 h. The monosaccharide and small molecular weight fraction were removed by dialysis. Then the

extraction was hydrolyzed with 3.0 M sulfuric acid for 25 min at 60°C, and neutralised with NaOH. The hydrolysates were diluted to 250 mL, and then measured with anthrone sulfuric acid assay. The equation below (Eq 2.3) was obtained from the standard curve Fig 2.1 and Table 2.3.

$$Saccharides\ concentration\ (mg/mL) = 8.7842 \times A_{620nm} - 0.0115,\ R^2 = 0.9992$$

Equation 2.3

Table 2.3 Standard curve of glucose concentration.

Number	**1**	**2**	**3**	**4**	**5**	**6**
Concentration (mg/mL)	0.01	0.02	0.04	0.06	0.08	0.1
	0.076	0.167	0.340	0.517	0.697	0.853
A620nm	0.065	0.150	0.331	0.509	0.717	0.879
		0.141	0.326	0.519	0.706	0.847
Average A620nm	0.0705	0.158	0.332	0.515	0.707	0.860

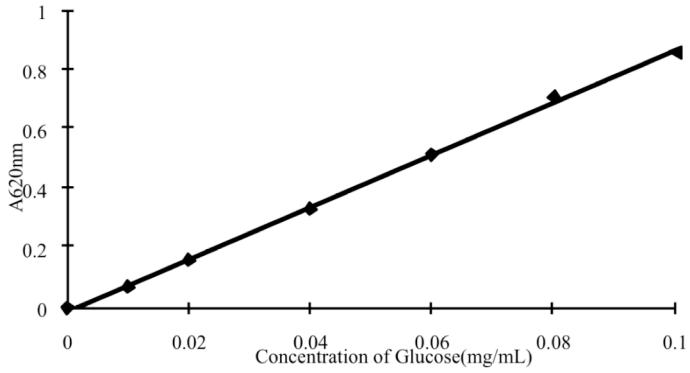

Figure 2.1 Standard curve of glucose concentration measured by the anthrone sulphuric acid assay.

2.2.1.4. Amino acids analysis

The fresh and sun-dried *Isatis* roots were weighted and frozen in liquid nitrogen then smashed by a high-speed pulveriser (800 rpm).

Total amino acids

30 mg smashed sample and 3 mL HCl (6 mol/L) were sealed in a vacuumed glass tube, and hydrolyzed at 130°C for 6 h. When the sample had been completely hydrolyzed, opened the tube after cooling down, and diluted with distilled water to 25 mL. 5 mL of this diluted solution was evaporated to dryness, and the substance was dissolved and diluted in 0.02 mol/L HCl, centrifuged at 14,000 g for 20 min, then the suspension was subjected to amino acid analysis (Hitachi L-8800 automatic amino acid analyser).

Free amino acids

1 g of smashed fresh roots, sun-dried roots and heat-dried roots (40°C) were each suspended in 30 mL of 0.02 mol/L HCl, and sonicated for 1 h. Each mixture was centrifuged (14,000 g, 20 min), and the suspension was subjected to amino acid analysis.

2.2.1.5. Monosaccharides and disaccharides analysis

Reducing sugars were identified by HPLC method (Karlsson, Winge, & Sandberg, 2005) modified to fulfill the requirement of measuring sugars from fresh plants. A TSK-gel Amide-80 column (250 mm × 4.6 mm I.D., 5 μm, 80 Å, Tosho, Japan) was used for separation at 60°C. The flow rate was 1.0 mL/min and injection volumes were 10 μL. The mobile phase was a mixture of acetonitrile, ethyl acetate and deionised water (60:25:15, v/v). The sugars were detected by an evaporative light scattering detector (Sedere Inc., USA), coupled in-line after a UV detector. Nitrogen was used as the ELSD nebuliser gas (3.5 bar), at 40°C, with the gain set to 8. The standard curve was obtained from a mixture of the rhamnose, xylose, arabinose, *D*-fructose, mannose, *D*-glucose, *D*-galactose, sucrose and maltose (0.4, 0.8, 1.0, 1.2, 1.6, 2.0 mM of each), with a log-log linear curve fit (Excel, Microsoft). All samples were dissolved in mobile phase solution and applied to the chromatography column.

2.2.1.6. Protein gel electrophoresis

Sodium dodecyl sulphate polyacrylamide gel electrophoresis (SDS-PAGE), is a protein separation technique widely used in biochemistry and molecular biology according to its electrophoretic mobility. Proteins may have different mobility due to the differences in their molecular weight and their secondary, tertiary or quaternary structures. As an anionic detergent, SDS binds to the proteins and coats them with uniform negative charges, which reduces them to their primary structure. Therefore, the samples in SDS-PAGE have identical charge per unit mass, which results in the fractionation of different compositions by their size (in terms of molecular weight).

SDS-PAGE electrophoresis was performed by Laemmli protocol (Laemmli, 1970), which generally includes 1) preparing the polyacrylamide gel and assembling the gel devices, 2) coating the protein samples by mixing samples with SDS sample buffer and boiling for 10 min, 3) loading the samples and running the electrophoresis with the 'running buffer', 4) fixing the gel with ethanol and glacial acetic acid solution, and staining the separated proteins with Coomassie Brilliant Blue.

The proteins can be dissociated by boiling in the presence of SDS and a reducing agent, i.e. dithiothreitol (DTT) or 2-mercaptoethanol (β-mercaptoethanol), then are electrophoresed through 12.5% polyacrylamide at 120 V. The use of reducing agents brakes down the disulfide linkages of proteins and further denatures the proteins, which thereby breaks up the oligomeric subunits of protein structure. This method is known as reducing SDS-PAGE, which is most commonly used. Non-reducing SDS-PAGE can be used when the natural structure of protein is crucial for the analysis. By comparing the results from these two types of SDS-PAGE, the number of disulphide linkages can be revealed.

Table 2.4 Buffers and chemicals for SDS-PAGE

Reagents	Compositions	Storage
Buffer A (30% Gel)	Acrylamide 29.2 g N,N'-Methylenebisacrylamide 0.8 g dissolved in deionised water 100 mL	4°C
Buffer B (resolving buffer)	1.5 M TRIS-HCl buffer (pH 8.8) TRIS 18.2 g SDS 0.4 g HCl 2 mL dissolved in deionised water 100 mL	4°C
Buffer C（stacking buffer）	0.5M TRIS-HCl buffer (pH 8.8) TRIS 6.1 g SDS 0.4 g HCl 4.2 mL dissolved in deionised water 100 mL	4°C
Polymerisation initiator	Ammonium persulphate 0.2g dissolved in deionised water 1 mL	Room temperature
Polymerisation promoter	TEMED	4°C
Anode/cathode buffer	25mM TRIS, 0.01 M GLY, 0.1‰SDS TRIS 3 g GLY 14.4 g SDS 1 g dissolved in deionised water 1000 mL	4°C
Fixing buffer	Ethanol 500 mL Glacial acetic acid 100 mL deionised Wate 400 mL	Room temperature
Staining buffer	Coomassie Brilliant Blue R250 500 mg Methanol 225 mL Acetic acid 50 mL deionised water 225 mL	Room temperature
Bleaching buffer	95% ethanol 250 mL Glacial acetic acid 80 mL dissolved in deionised water 1000 mL	Room temperature

Table 2.5 The preparation of stacking gel and resolving gel

Gel buffer	Resolving gel (10%)	Resolving gel (12.5%)	Stacking gel (4%)
Buffer A	6.0 mL	7.5 mL	0.8 mL
Buffer B	4.5 mL	4.5 mL	/
Buffer C	/	/	1.5 mL
Deionised water	7.5 mL	6.0 mL	3.7 mL
Polymerisation initiator	50 µL	50 µL	30 µL
Polymerisation promoter	12 µL	12 µL	6 µL

Periodic acid-Schiff (PAS) Staining

PAS staining was used to identify the glycoproteins or glycated proteins in the extracts of the roots (Glossmann & Neville, 1971). In glycoproteins, two types of carbohydrate-peptide linkage have been identified, the N- and the O- linkage. In glycation, either exogenous or endogenous, glucose or fructose is often found to bond to the proteins by the Maillard reaction. Periodic acid can selectively oxidise the glucose residues to form aldehydes, which react with the Schiff reagent and results in a magenta colour.

Reagents and protocol:

1. Fixing solution: trichloroacetic acid 50 mL in 450 mL water, 10% (v/v), 60 min.
2. Washing solution: deionised water, 1 min each time, twice.
3. Oxidising solution: 1% (w/v) periodic acid in water, stores in dark at 4°C, 60 min.
4. Washing solution: deionised water, 15 min each time, twice.
5. Schiff reagent: basic fuchsin 1.0 g in 200 mL water, sodium metabisulphite 3.2 g in 200 mL water, HCl 4.2 mL, stirring overnight at 4°C, mixes with the activated carbon 2.0 g and vortex for 1 min. Samples were stained for 60 min.
5. Washing solution: deionised water, 1 min.
6. Reducing solution: 0.25% (w/v) sodium metabisulphite, 3.5% (w/v) acetic acid in 500 mL water, at 4°C overnight.
7. Washing solution: deionised water.

Calculation of molecular weight

The migration distance and gel length were measured to calculate the relative mobility R_f for each protein, with Eq 2.4. The molecular weight (Log) was plotted as a function of R_f for standards and extrapolate size of unknown.

R_f = *distance migrated* / *gel length* **Equation 2.4**

2.2.1.7. Isoelectric focusing (IEF)

IEF is an electrophoretic technique for separating proteins based on their pIs in an electric field through a medium (i.e. a gel), which has a pH gradient. Proteins carry positive, negative or zero net charge depending on the pH of their solution, and thereby migrate different distance in the gel according to their net charge (Righetti, 1983) (Righetti, Bossi, & Gelfi, 1998). The pI of a protein can be determined with IEF.

IEF was performed according to the instruction manual of AE6541 apparatus (ATTO Co., Japan). Briefly, a gel made of agarose, sorbitol and urea was prepared with a pH gradient of 3.5 to 10.0 (A-C310, ATTO Co., Japan), stored at 4°C and used within 3 months. After treated with reducing sample buffer, the protein samples were applied for electrophoresis under 300 V for 150 min. The gel was then stained with Coomassie Brilliant Blue R250 according to the SDS-PAGE staining method (see Section 2.2.1.6) (Reisner, 1975). The full length of gel and the migration distance of protein to the cathode were measured for the calculation of pI. The standard pH curve was drawn by measuring the pH of every 5 mm fraction of a blank gel (no sample loaded), which was identical to the experimental gel except the loaded samples. 10 mM KCl was used for extracting the buffer salts from the blank gel.

2.2.1.8. Purification of protein by HPLC

High Performance Liquid Chromatography (HPLC) was used as the main method of protein purification. HPLC includes utilising different types of stationary phase (i.e. the hydrophobic saturated carbon chains), the mobile phases and analytes through the column, and a detector (typically a UV/VIS detector or a Refractive Index (RI) detector) that provides a

characteristic retention time for the analytes like proteins, peptides and sugars. By changing the type of detectors, different characteristics of analytes can be addressed, i.e. the fluorescence, light scattering. The retention time of analytes varies depending on several apparatuses of the chromatography system, including the strength of their interactions with the stationary phase, the ratio and/or composition of mobile solvents used, the flow rate of the mobile phase and the size (diameter, length) of the column, which is densely packed with the stationary phase. The high density of packing and small particle size of the chromatographic resin used in HPLC allows a high efficiency on separation of compositions in a highly complicated mixture with a shorter column compared to the ordinary column chromatography (Scopes, 1994).

Cation-exchange liquid chromatography and reversed phase liquid chromatography were the major methods of protein separation. Toyopearl SP-650M strong cation-exchange resin was used for isolation of RITIP proteins from the fresh roots, while Toyopearl SP-5PW cation-exchange resin was used for isolation of GRITIP proteins from sun-dried roots. The proteins were purified with C18 chromatographic column (Oligo-R3). The purity was checked with a size-exclusion HPLC column (TSK-Gel G3000SWXL).

For separations using the strong cation-exchange column (16 mm×100 mm, SP-650M, Toyopearl, Japan). The flow rate was 1 mL/min. The citric acid-sodium citrate buffer (0.02 M, pH3.0) was used as mobile phase. A salt gradient of 0.5~1.0 M NaCl was used to elute the compounds bound to the stationary phase. The detector wavelength was 280 nm. A fraction collector was used to collect the separated protein fraction at a rate of 5 mL/tube.

For separations using the reverse phase LC column (4.6 mm×250 mm, POROS Oligo-R3 C18, ABI, USA), the flow rate was 1 mL/min. The mobile phase was 0.1% TFA water solution. An acetonitrile gradient (0~55%) was used to elute the proteins from the stationary phase. The detector wavelength was 280 nm. The isolated fractions were collected manually.

For separation of glycated proteins, 5 mL of roots extracts was loaded to a cation-exchange column (4.6 mm × 250 mm, SP-5PW, Toyopearl, Japan) with a mobile phase containing 0.02M citrates buffer (pH4.0) at the flow rate of 1 mL/min. The elution gradient was 0~1 M NaCl during 60 min.

2.2.1.9. Amino acids sequencing of protein

The amino acid sequences of purified proteins were determined with Edman degradation. Edman degradation, developed by Pehr Edman (Edman, 1950), is a method of sequencing amino acids in a protein/peptide. In this method, the amino acid at the N-terminal of sequence is labelled with phenyl isothiocyanate under alkaline conditions and cleaved off one by one as a thiazolinone derivative under acidic conditions, while the peptide bonds between other amino acids were not affected. The thiazolinone amino acid forms a stable derivative, phenylthiohydantoin (PTH)- amino acid, which can be characterised by HPLC. This procedure can then be repeated to identify the next amino acid. This cycle can accurately repeated up to 30 times (means 30 amino acids) with 98% efficiency for each amino acid. A beauty of the Edman degradation is that only a small amount of peptide (10 - 100 picomole) was required for the sequencing procedure. There is also a major drawback of this method: it cannot sequence more than 50 to 60 amino acid residues (Niall 1973). It is because the efficiency of Edman degradation is not 100%, meaning that the cleavage step may not occur every time. Therefore, to obtain the full-length sequence of protein/peptide, the large proteins/peptides can be cleaved into smaller peptides before proceeding with the Edman degradation.

After being applied for SDS-PAGE electrophoresis, the protein bands were transferred to polyvinylidene difluorid (PVDF) membrane with the transfer buffer (as shown in Table 2.5) and stained in 0.1% Coomassie Brilliant Blue R250 in 50% methanol for 1-2 minutes. The protein blots were destained with several changes of 10% acetic acid in 50% methanol until the bands became visualized (usually about 5 minutes). The blot was washed twice with deionised H_2O then dried with air.

Table 2.6 Preparation of transfer buffer

Chemicals	Amount
Gly	9 g
Tris	1.93 g
SDS	1 g
20% methanol	200 mL

2.2.1.10. Molecular cloning

The genes of the purified proteins were cloned from fresh tissue of the roots, following the protocol below: Primer design → Isolation of mRNA → First strand cDNA synthesis → 3'-RACE (Rapid Amplification Of cDNA Ends) PCR → 5'-RACE PCR → Agarose gel electrophoresis → Purification PCR products from a PCR reaction or a gel → Cloning of purified DNA into plasmid vectors → Transformation of E. coli → M13 amplification of insert from E. coli → Automated DNA sequencing was carried out (Generay Biotech Inc., Shanghai, China) → Bioinformatics analysis.

Raw sequence data from replicates were read by Chromas (Version 1.45) software and then edited. Translations of nucleic acid data (in all six frames) were conducted using the Translate tool on ExPASy Molecular Biology Server (http://ca.expasy.org/tools/dna.html). The correct reading frame was manipulated by using the Vector NTI (Version 9.0) software. Sequences were compared to EMBL and GENBANK nucleic acid databases using the FASTA and BLAST programs using default values. Wu-blast 2 programs were used to compare sequences with those contained in nucleotide and protein databases (SwissProt, Release 53 and EMBL Release 90) by aligning the query sequences with previously characterised genes.

2.2.1.11. Mass spectroscopy

Mass spectrometry is widely used for the characterisation of proteins, either in their pure form or in a mixture. Proteins need to be ionised before detected by the mass monitor. There are two primary methods for the ionisation of whole proteins: electrospray ionisation (ESI) and matrix-assisted laser desorption/ionisation (MALDI) (Link *et al.* 1999) (Fenn *et al.* 1989) (Loo, Udseth & Smith 1989). Two approaches are used for characterising proteins. Firstly, known as the "top-down" strategy, the intact proteins are ionised and introduced to a mass analyser. Secondly, proteins are enzymatically hydrolysed into smaller peptides by a protease (i.e. trypsin). Subsequently these peptides are loaded into the mass spectrometer and identified by peptide mass fingerprinting. Hence, the second approach (also known as the "bottom-up" proteomics strategy) is able to identify the peptides and infer the existence of proteins. In this study, the molecular weight of the protein was determined by ESI-mass spectroscopy.

Two methods are widely used to fractionate proteins and/or the peptides from their enzymatic digestion. The whole proteins could be analysed with two-dimensional gel electrophoresis, while HPLC is used to separate and characterise peptides after the enzymatic digestion (Perkins *et al.* 1999). In my studies, the later method was used for analysing the glycation sites on the proteins.

2.2.1.12. LC-MS analysis of enzymatic protein hydrolysates

The analysis was performed with LC/MSD Trap XCT (Agilent, USA). RPLC was performed by using a C18 column (Phenomenex, Gemini C18, 250 mm × 4.6 mm, 5 μm) and the elution gradient of 0~100% CH_3CN, containing 0.1% TFA. The elution volume was 60 mL at a flow rate of 1 mL/min. The UV detector wavelength was 214 nm. The LC fractions were ionised and immediately analysed by an electronspray ionisation mass spectrometer immediately. This was performed in cationic mode, 2000 m/z, spray air pressure 40 psi, nitrogen drying flow rate 12 L/min, drying temperature 350°C, capillary voltage 3.5 kV, with a ion scanning over the range from m/z 50 to 2200.

Table 2.7 Gradient (B%)

Time	B%	Flow Rate (ml/min)
0	0	1.0
10	0	1.0
70	100	1.0
80	100	1.0

2.2.1.14. Glycation sites analysis

Genes of purified native proteins from the roots were cloned and the cDNA sequences were obtained. Simulated hydrolysis was performed with cDNA sequences by a software package called Peptidemap (http://prowl.rockefeller.edu/prowl/peptidemap.html). The peptide sequences from the simulation were manually paired with peptide fragments from the pepsin hydrolysis and mass spectroscopy. The glycation sites, together with the types of glycation, were identified by overlapping the peptide fragments obtained from enzymatic hydrolysis simulation and mass spectrum (Moreno *et al*. 2008).

2.2.2. Bioactivity characterisation

2.2.2.1. Cytotoxicity assay

Cytotoxicity of sample was evaluated on MDCK cells with the published assay (Schmidtke *et al.*, 2001). MDCK cells (2×10^4 cells per well) were plated at in 96-well flat-bottomed microtitre plates, and incubated for 2 d at 37°C in a 5% CO_2 humidified incubator. After removal of the medium, 200 μL of medium with serial concentrations of samples were added. The cells were then incubated at 37°C for 72 h. Six duplicates were use for each sample concentration. 200 μL/well of medium was used as control.

After the incubation, the supernatant was removed with pipette and the cells were washed with 300 μL sodium chloride saline for three times to remove dead cells. The cells were then fixed and stained with 50 μL of crystal violet (0.03%, w/v) in 20% methanol solution for 10 mins. After washing with 300 μL of water for further 6 times, the stained cell monolayers were treated with 100 μL lysis buffer (0.898 g of sodium citrate and 1.25 mL of 1 N HCl in 98.05 mL 47.5% ethanol) for 20 mins to elute the crystal violet. Finally, the absorbance of each well was measured by an ELISA reader (DG5031, Beijing) at 630 nm. Cell viability was evaluated by the percentage of the mean absorbance of each dilution to that of the background control:

$$Cell\ survival\ rate = (mean\ O.D._{sample} / mean\ O.D._{control}) \times 100\% \quad \textbf{Equation 2.5}$$

The 50% cytotoxic concentration (CC_{50}) was calculated by plotting cell survival rates at dose response curve, using EXCEL.

2.2.2.2. Infection of virus to MDCK cells

Following established protocols (Levi, Beeor-tzahar & Amon 1995) (Sladowski *et al.* 1993), MDCK cells (10^5 cells/well) were plated in 96-well plates 24 h prior to virus infection. The medium was then replaced by 100 μL DMEM viral suspension containing approximate 50 PFU (plaque forming units) influenza viruses, with or without serial concentrations of antiviral agents. As the control, 100 μl/well DMEM and sample solution were added to 6 wells. The mixture of cells and viruses was incubated for 60 min at 33°C in a 5% CO_2 humidified incubator, to allow viruses' attaching to cells. The supernatant was then carefully removed. The cells were washed with PBS for 3 times, before the culture medium was

added. The infected cultures were incubated at the same conditions as above for 3 d. The monolayer of cells was then washed with PBS to remove dead cells and the cell viability was determined by MTT assay.

2.2.2.3. Colourimetric MTT assay

The cell proliferation was determined with MTT assay as reported (Loosdrecht *et al.* 1994). In this method, the yellow tetrazolium salt (MTT) is reduced to form insoluble purple formazan crystals by the metabolically active cells. The formazan crystals are dissolved in DMSO and applied for the absorbance quantification using spectrophotometre. The linear relationship between cell number and absorbance varies between different types of cells. It has to be established for each type of cells to enable an accurate and reliable quantification of the proliferation rates. Among the applications for the method are drug sensitivity/ resistance, cytotoxicity, response to growth stimulators, and cell activation/replication.

Briefly, by the end of the cell incubation, 100 µL of MTT (3-[4,5-Dimethylthiazol-2-yl]-2,5-diphenyltetrazolium bromide) solution (1 mg/mL in PBS, stored in dark at 2-8°C) was added to each well after the culture media was removed, and incubated at 37°C for 4 h. The MTT solution was then replaced by 150 µL DMSO. After thoroughly dissolving and mixing, the absorbance of each well was measured with an ELISA reader (DG5031) at 570 nm. The cell proliferation rate was calculated with Eq 2.6.

$$\textit{Cell proliferation rate (\%)} = [(\textit{mean O.D.}_{sample} - \textit{mean O.D.}_{control})/ \textit{mean O.D.}_{control}] \times 100$$

Equation 2.6

2.2.2.4. Growth of influenza viruses

The viruses were grown in embryonated eggs to maintain their titres. The 10-day-old embryonated and pathogen-free eggs were purchased from local breeding farm. The eggs were placed in front of a light source one by one, in order to locate the allantoic cavity just next to the air sac, as shown in Fig 2.2. The location was marked with a marker pen.

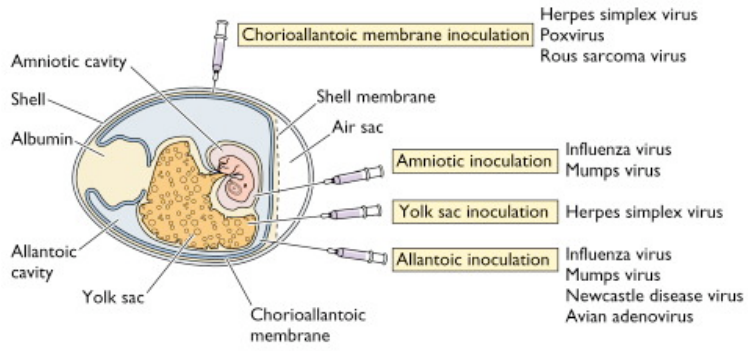

Figure 2.2 Allantoic inoculation of influenza viruses (Racaniello 2009).

The egg was sterilised with 75% ethonal solution before a hole (10×6 mm) was drilled at the top of the air sac. A small amount of virus inoculum (0.2 mL) was injected through the hole, which was sealed with a sterilised medical tape. Three eggs were used for each strain of viruses. The eggs were then incubated at 33°C for 3 d before harvest. A daily check on the viability of embryos was performed to abandon the embryos died within 24 h of inoculation.

Before harvest, eggs were stored at 4°C overnight. The top part of egg was sterilised with 75% ethanol solution. The shell of air sac and the membrane of allantoic cavity were removed with a medical tweezers. The allantoic fluid was sucked out with 10 mL Pasteur pipettes. Next, the fluid was centrifuged at 3000 rpm for 5 min to remove blood and cells. Haemagglutination was performed immediately to determine the HA titre of viruses (as described in Section 2.2.2.5 below). The HA titre of influenza A viruses H1N1/PR8 was 1024, when that of H3N2 was 128.

2.2.2.5. Determination of anti-influenza virus activities of MRPs

The antiviral effects of RIE MRPs, Arg-Glc MRPs and their purified components are investigated *in vitro* on H1N1 and H3N2 influenza viruses. This study was carried out in cooperating with Guangzhou Respiration Diseases Institute, China.

The inhibitory effects of the MRPs on influenza virus were evaluated by the following methods: haemagglutination inhibition, influenza virus titration, MTT assay, plaque reduction assay. The details of these methods are given in the corresponding sections of this chapter.

2.2.2.6. Haemagglutination Inhibition test (Micro-HI)

Haemagglutinin (HA) on the influenza virus membrane can recognise and bind to its receptor, sialic acids, on the plasma membrane of erythrocytes, and subsequently induce the haemagglutination. By observing the degrees of haemagglutination, the inhibitory activity of MRPs on the HA-receptor binding was determined (Potter & Oxford 1979) (Arenas *et al.* 1990).

Fresh chick blood was collected using heparin as anticoagulants. The red blood cells were washed with normal saline for 3 times and collected by centrifuge at 1000 rpm for 10 min. The cells were re-suspended and diluted with normal saline (0.9% NaCl) to make an 1% (v/v) suspension, stored at 4°C before each test. The antiviral medicines, ribavirin (50 mg/mL) and amatadine (1 mg/mL) were used as control. Influenza A viruses H1N1/PR8 and H3N2 were used in the tests. The suspensions of these two viruses were diluted with normal saline by 256 times and 32 times, respectively, to obtain working virus suspension (HA titre=4) for HA inhibition tests.

Two-fold dilutions of samples were prepared by mixing 50 μL sample with 50 μL normal saline. The virus suspension (HA titre=4, 50 μL) was mixed with each dilution of samples, and stored at 4°C for 45 min. 50 μL 1% chicken red blood cells were then added and stirred, stored at 4°C for 30 min. A morphological observation was performed with a normal laboratory microscope. The results were presented as 4+, 3+, 2+, 1+, ±, -.

2.2.2.7. Plaque reduction assays

The assay was performed according to previously reported protocol (Gaush & Smith 1968) (Burleson, Chambers & Wiedbrauk 1992) with some modifications. Briefly, MDCK cells were allowed to growth in 6-well plates for 2 days till the cells become confluent. After the culture medium was removed, cells were infected by 1 mL of the influenza viruses (50 PFU) in DMEM medium with or without antiviral agents. After incubation for 1 h at 33°C, the infection medium was replaced by 2 mL of medium containing 0.4% agarose. The normal cells were used as control in all tests. All of the cells were incubated for 72 h at 33°C and then stained overnight by 0.1% neutral red and 0.4% agarose in medium. 0.25% trypsin was included to improve the infection activity of the virus. Plaques were counted and the percentages of plaque inhibition were calculated with Eq 2.7.

Plaque inhibition rate (%) = [(*control -sample*)/ *control*] × *100*

Equation 2.7

2.2.2.8. Scanning Electron Microscopy (SEM)

The scanning electron microscope (SEM) scans the sample with a high-energy electron beam to generate a image of sample surface. It reveals the information about the sample regarding surface topography, composition and electrical conductivity, etc. This image is so precise that the disordering of HA spikes on the surface of viruses can be seen when the pH of their circumstance becomes acidic (Ruigrok *et al.* 1986) (Wharton *et al.* 1995). In the infection of influenza virus, the viral particles may be found on the surface of the host cells (i.e. MDCK cells in this study), either when the viruses are penetrating into or budding from the cells. These particles can be observed with SEM.

MDCK cells were grown to confluence on polyethyleneimine-coated cover slips (10 mm diameter) in 24-well plastic tissue culture plates (16 mm well diameter). The administration of RIE (15 mg/mL) was carried out as described in Section 3.2.1.5 in order to observe the drug's influence on different aspects of viral infection. Two incubating conditions were used in order to control the process of infection. To investigate the inhibitory effects of RIE on the viral cytopathic impacts, the cells were incubated with viruses at 33°C for 1 h, then the free viruses were removed and cells were incubated in 200 μL medium for further 6 h. To investigate RIE's effects on virus binding, the cells were incubated with viruses at 4 °C for 1 h and then the free viruses were removed.

After being washed with PBS buffer for 3 times, the cells were fixed with 2.5% glutaraldehyde-2.0% paraformaldehyde in 0.1 M cacodylate buffer (pH 7.4) for 1 h at room temperature, and post-fixed with 1% OsO_4 in the same buffer for 45 min, followed by thoroughly washing and dehydrating in ethanol, being treated with isoamyl acetate and dried to a critical point with HCP-2. The cells were mounted on stubs, coated with gold and observed with a scanning electron microscope (SEM; JSM5310/LV, JEOL).

2.2.2.9. Trypsin inhibition: BNPNA-based assay

Trypsin inhibitory activities of RITIP1/2/3 were assayed by a BNPNA-based assay *(Baker et al.* 2009) (Smith *et al.* 1980) (McManus 1995). *N*-benzoyl-*DL*-arginine-*p*-nitroanilide (BAPNA) was purchased from Maikun Chemical Inc. (Shanghai, China). For control, 2 mL sample solution was mixted with 5 mL BAPNA solution (0.4 mg/mL in 0.1 M Tris-$CaCl_2$

buffer, pH 8.2) and incubated at 37°C for 10 min. 2 mL of trypsin solution (20 μg/mL, in 1 mM HCl) from porcine pancreas (Amersco Inc., OH, USA) and 1 mL acetic acid was added into the sample and BAPNA mixed solution. For the measurement of sample activity, the sample solution was mixed with trypsin at certain proportion. The pre-heated BAPNA (37°C, 5 mL) was added and incubated at 37°C for 10 min. The acetic acid was added (1 mL) immediately to terminate the hydrolysis. Trypsin activity was monitored at 410 nm with a spectrophotometer (Model 752, Shanghai). The trypsin activity unit was defined as 1 unit per 0.01 absorbance intensity. The inhibitory activity was presented as trypsin inhibitor units (TIU). The inhibition rate was calculated with Eq 2.8.

Inhibition rate (%) = TIU/trypsin activity units×100 **Equation 2.8**

2.2.2.10. Enhancement of Arg-Glc MRPs on mechanical strength of cell membrane

Incubation of Arg-Glc MRPs with erythrocytes

Erythrocytes were separated from 10 mL blood (healthy female volunteer), in which EDTA was added to prevent haemaaggregation, by centrifuged at 350 g for 5 min. Cells were rinsed by 0.9% saline for 3 times and then diluted to 1% (by volume) suspension. The cells were sedimented from 1 mL 1% suspension by centrifuge, and then mixed with various concentration of Arg-Glc MRPs or arg+glc solution. The mixture of cells and sample was incubated at 37°C for 2 h, being stirred up every 15 min. The cells were sedimented again to remove the supernatant, and washed with saline for 3 times until resuspended in low osmotic pressure solution at 37°C for 1 h. The LDH activity and haemoglobin content of supernatant were determined.

Lactate Dehydrogenase (LDH) Assay

LDH assays performed here is to assess LDH released into the media as a marker of dead cells. The supernatant of erythrocytes was tested for the LDH activity by following the referenced protocol (Wu *et al.* 1992) (Watanabe 1995).

2.2.3. Membrane biophysical studies

2.2.3.1. Langmuir balance

Lipid monolayers were assembled using a Langmuir film balance (NIMA Technology, Coventry, UK) to measure the area per lipid molecule at constant surface pressure or surface tension change when the area of lipid monolayers was reduced gradually. 24 μg of lipid was used to form the monolayer. The surface pressure was set to 20 mN/m. The barrier speed was set to 200 cm^2/min. In experiments with MRPs, until the formation of lipid monolayer, RIE-MRPs were dissolved in pH7.4, 0.1 mol/L PB and transferred to the subphase by pipetting the solution underneath the trough barrier, to provide a final subphase concentration of 300 μM. The barrier movement was programmed to maintain the initial surface pressure, and we recorded any changes in surface area.

2.2.3.2. Neutron diffraction

Neutrons are particles bound to the atomic nucleus of almost all atoms. Free neutrons produced by a nuclear reactor, or spallation source, can exhibit wave phenomena like diffraction. Diffraction occurs when waves encounter obstacles of a comparable size to their wavelength. By slowing down a neutron beam emanating from a reactor, the wavelength of the beam can be adjusted to about one Ångström, so that they can be used to conduct a diffraction experiment. For a sample with the regular structure, i.e. the lamellar bilayers in a multibialayer stack, the scattering would occur at well-defined angles (θ) according to Bragg's law (Bragg 1913).

Sample Preparation

Lipids were purchased from Avanti Polar Lipids or Sigma. 20 mg samples were dissolved in chloroform and deposit onto quartz microscope slides by a nitrogen-propelled artist's airbrush. The slides were then placed in a vacuum over for 2 h in order to remove all traces of the solvent. Samples were hydrated in a humid atmosphere with water contained 8.06% or 25% ^2H_2O. The samples were protected from light whenever possible in order to reduce the chance of lipid peroxidation.

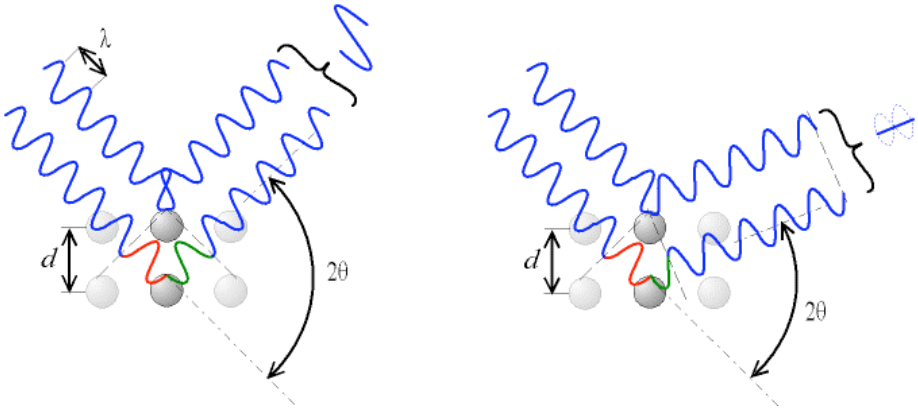

Figure 2.3 Constructive and destructive wave interference.

According to the angle of deviation (2θ), the resulting phase shift causes constructive (left) or destructive (right) interference (Wikipedia 2010). The interference is constructive when the phase shift is a multiple of 2π, which can be used to re-construct the lipid packing in the bilayers.

Constructive interference on the phospholipid bilayers can be expressed by Bragg's law (Yeagle 1993). The lattice spacing of a multibilayer stack can be calculated from Eq 2.9.

$$n\lambda = 2d \times Sin\theta \qquad \textbf{Equation 2.9}$$

where n is an integer, λ is the wavelength of the incident beam (i.e. neutron, X-ray), d is the lattice spacing between the planes of bilayers, and θ is the angle between the incident ray and the scattering planes.

Data collection

Neutron-diffraction measurements were carried out on the D16 membrane diffractometer at the Institut Laue et Langevin, Grenoble, France, or the V1 membrane diffractometer at the BENSC, Helmholtz Zentrum Berlin, Germany. Humidity control was achieved by changing the temperature of the sample can (at the ILL) or changing the saturated salts solutions in the sample can (at BENSC). At the ILL, the difference between the ambient temperature in the sample can and the temperature of water slots at the bottom of the sample can was adjusted individually with water baths.

Each sample was quickly transferred straight from a humid tube into the sample can. After a minimum 6 h equilibration, a series of continuous θ-2θ scans were initiated (from θ= 1.5° to 20.0° for DOPC, 1.8° to 16.0° for DMPC). The samples were run at 298 ~ 303 K for DOPC, and at 310K for DMPC.

Data analysis

The two-dimensional array of detector counts for each frame of data was corrected for variations in pixel response. The complete set of frames from each scan were then collapsed into a linear spectrum and combined to generate a pseudo θ-2θ scan. All the analysis at this stage were carried out by the software LAMP on D16 or CARESS on V1. The background around each peak was fitted and subtracted using PeakFit (Systat Software Inc., USA) or Igor Pro (Version 6.0, WaveMetrics Inc., Oregon, USA). Gaussian distributions were then fitted to the Bragg reflections and the angular position, width and area of each peak recorded. Absorption and Lorentz corrections were applied and the square-root of the intensities taken to produce the structure factor amplitudes.

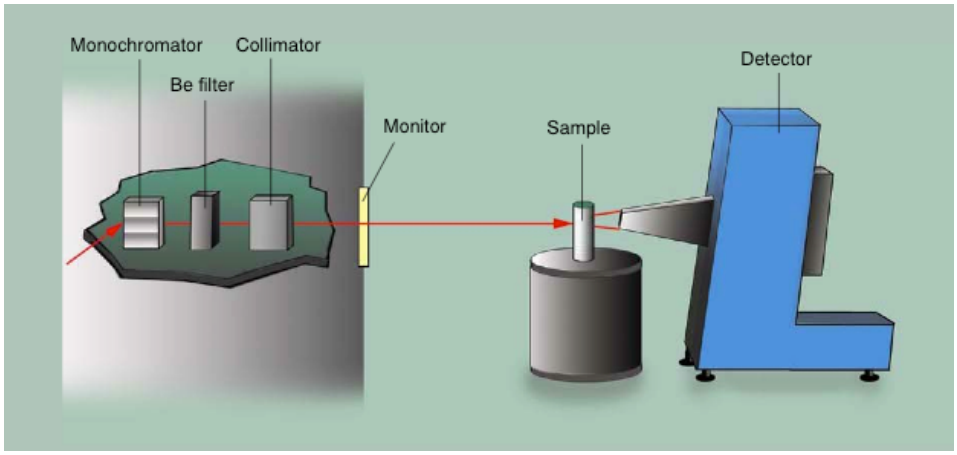

Figure 2.4 Schematic representation of the V1 neutron membrane diffractometer.

Picture from BENSC website (Hauss 2010).

2.2.3.3. Differential Scanning Calorimetry

Dry the lipid

The concentration of DMPC and DOPE-Me were 100 mM, including various MRPs concentrations ranging from 100:0 to 100:100 by molar ratio. Lipids were dissolved in 500 µL chloroform and vortexed with certain amount of MRPs aqueous solution thoroughly. The suspension of lipids and MRPs were then sonicated for several minutes until the mixture become translucent. The chloroform and water was evaporated under nitrogen immediately and left in vacuum for at least 2 h to remove the traces of solvent.

Rehydration

The dried lipids and MRPs were rehydrated with buffer (pH 7.4, 20 mM PIPES + 1 mM EDTA + 150 mM Sodium Chloride + 0.3 mM Sodium Azide) at 40°C. A cycle of vortex-sonicating-liquid nitrogen freezing-thawing of rehydrated lipid suspension was repeated for 6 times to improve the alignment of lipid packaging in MLVs.

Measurement

The suspension was then sealed with a press in an aluminium pan. The weight of pan was recorded before and after sealing, which allows the amount of lipids in the pan to be calculated by its weight accurately. A Pyris 1 differential scanning calorimeter (Perkin Elmer, US) was employed, at a scan rate of 40 °C/min. 30 μL of sample was sealed in a pan which could hold a maximum volume of 50 μL. Heating scans were performed in a range of -30°C to 85°C (Epand *et al.* 2005), but varied between different lipids. The transition temperature (initial temperature) and delta Hf was measured and calculated by Pyris data analysis software (Version 7.0.0.0110, 2004, Perkin Elmer Inc.), which recognizes transition peak with Gaussian distribution and does a automatic calculation of initial temperature and ΔH_f, according to the thermal consumption of MLVs and the weight of lipids in the chamber.

2.2.3.4. Laurdan fluorescence spectroscopy

Multilamellar vesicles (MLVs) and small unilamellar vesicles (SUVs) were prepared. 5 mol% of Laurdan were added into lipids (at a concentration of 50 μ M). After equilibration at 37°C for 1 h, measurements were carried out by a FLUOROMAX-3 spectrofluoro-photometer (JOBIN YVON, Horiba, Japan). The generalised polarisation (*GP*) of excitation at 350 nm was calculated by Eq 2.10, where I_g and I_{lc} are the steady-state emission intensities at 440 nm and 490 nm, respectively (Ashley *et al.* 2006) (Parasassi *et al.* 1990).

$$GP = (I_g - I_{lc})/(I_g + I_{lc}) \qquad \textbf{Equation 2.10}$$

2.2.3.5. Merocyanine 540 anistropic fluorescence spectroscopy

Steady-state MC540 anisotropy measurements were obtained by a fluorometer (Xe-900, Edinburgh Analytical Instrument) equipped with polarisers. The slit of laser light was set at 2 mm, the excitation slits was 2 mm and the emission slits was set at 5-6 mm in order to

receive enough counts for calculation. MLVs of DMPC and DOPC were prepared as described previously. Lipids and MC540 were dried by nitrogen stream in the tube and put in vacuum overnight to remove trace of solvent, then was re-hydrated and diluted to proper concentration right before applying to fluorometer. MRPs was added into the system after re-hydration. Sample should be avoided from lights during the preparation. The measurement was carried out at 37°C. Each sample was calibrated in the cuvette for 5 min to reach the temperature. The intensity at both 90° and 0° was used for calculating *G* value and *r*, by the formula as below.

$G = I_{HV}/I_{HH}$, H: horizontal, 90°; V: vertical, 0° **Equation 2.11**

$r = (I_0 - GI_{90})/(I_0 + 2GI_{90})$ **Equation 2.12**

2.2.3.6. X-Ray diffraction

Two methods, small angle X-ray scattering (SAXS) and lamellar X-ray diffraction (LXD), were employed to investigate the effects of MRPs and/or SIV fusion peptide on the phase transition and structural transforming of lipid bilayers. In SAXS, the elastic scattering of X-rays (wavelength 1~2 Å) on a homogeneous sample is monitored at very low angles, typically ranged from 0.1° to 10°. SAXS is capable of analysing the structure of macromolecules with a size between 50 and 250 Å. It may be applied to study the structure of phospholipid multilayers. The resulting scattering profiles contain structural information including the shape and size of lipids, characteristic distances of lipid leaflets, thickness of the water layer, and other data (Glatter & Kratky 1982). In contrast to neutron diffraction, SAXS provides a way of observing the real-state structure and phase behavior of lipids in liposome dispersion.

LXD has been successfully used to measure the size of the hydrophobic region of DLPC bilayers (Hung & Chen 2003), and peptide-induced pore formation (Chen, Lee & Huang 2003). It differs from SAXS. Instead of controlling the phase transition by adjusting the temperature, the humidity was adjusted to induce the transition. This provides steady-state structural information of lipid bilayers under various levels of hydration.

The details of SAXS and LXD measurements are given in Section 8.2.

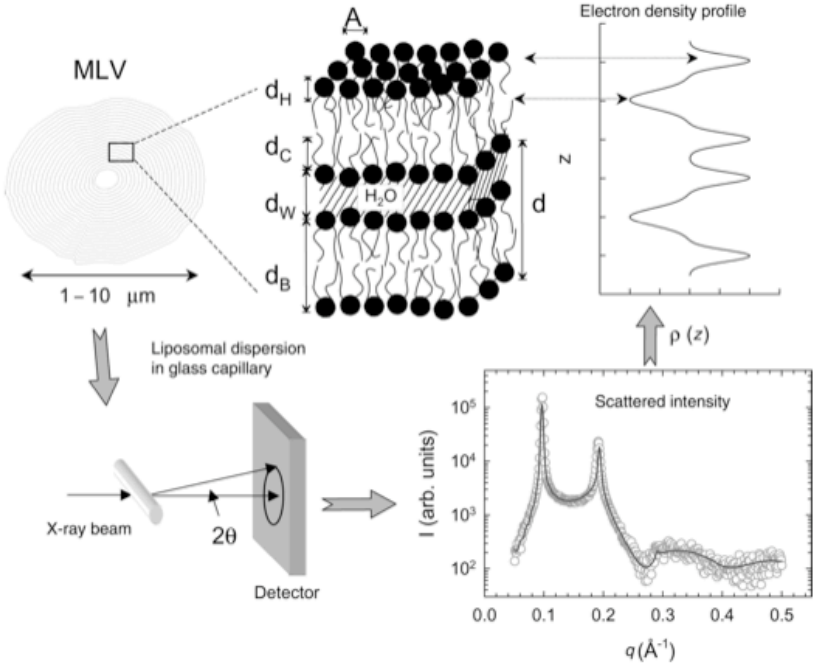

Figure 2.5 Principle of the SAXS experiments on lipid bilayers.

The liposomal dispersion (MLVs) is exposed to X-rays and the scattering intensity is recorded as a function of the scattering vector. The structural information was obtained through the electron density profiles by analysing the diffraction pattern (Rappolt & Pabst 2008).

2.2.4. Data analysis and statistics

Results will be generally derived from at least three independent experiments. Means ± S.D. will be calculated and groups of data will be compared using Student's t test. Statistical significance and high significance will be set at $P < 0.05$ and $P < 0.01$, respectively. The percentage will be compared using X^2 test.

CHAPTER 3

THE INHIBITORY EFFECTS OF RIE MRPS ON INFLUENZA VIRUS INFECTION: *IN VITRO* STUDIES

3.1. AIMS OF THIS CHAPTER

As an officially approved Chinese herbal medicine by the State Food and Drug Administration of China, the aqueous extracts of *Isatis indigotica Fort.* have been used to treat various viral infections and diseases, particularly seasonal flu. Its anti-influenza virus effects have been the subjects of pharmacological studies *in vitro* and *in vivo* (Jin *et al.* 2007) (Liu, Li & Jiang 2008) (Wang *et al.* 2009) (Li *et al.* 2009). However, due to the complexity of its chemical composition and the numerous chemical changes that occur during the heating process involved in its production, little is known about the mechanism of its antiviral activity nor the effective components.

Among the studies reported so far, different strategies have been employed to investigate the actions of the roots on influenza virus infection. For example, Hu *et al.* measured the lectin activity of the roots and its capacity to inhibit haemagglutination (Hu & Zheng 2003). Li *et al.* tested the direct effects of the herb on infectivity of influenza A by culturing the viruses in chick embryos in the presence of herbal extracts (Li *et al.* 2009). However, the results were not conclusive about the *in vivo* antiviral mechanism of the roots preparations.

Two questions have to be addressed. Firstly, what is the major target of the action of RIE, the host cells or viral particles? The infectious cycle involves a serial of interactions, reactions and key stages, which have been targeted by some well-known antiviral agents (Fig 3.1). For instance, Tamiflu targets the repackaging and release of viral particles from their host cells (Moscona 2005), and has become a major antiviral drug against the worldwide threats of H5N1 avian flu and H1N1 swine flu. Amantadine is another option of fighting against seasonal flu epidemic. It targets two stages (Whittaker 2001), the un-coating of the genetic material and the synthesis of viral proteins (Schmidtke & Bauer 2006). Apart from basing on a number of biochemical pathways, the antiviral drugs act either on cells or on viruses. Before understanding the molecular mechanism of RIE's antiviral actions, we have to distinguish the target at the cell-virus level.

Secondly, what is the impact of the heating process on the efficacy of RIE? In another words, are the chemical reactions that occur during the preparation of the herbal decoction important to the medicinal function of RIE? The fresh roots contain hundreds of active compounds. The sun-dried roots and their boiling water extracts may contain even more due to the heating process of preparation. Before trying to isolate the major effective

components, it is necessary to determine which category of compounds has the stronger antiviral activity, native or modified compounds.

In this chapter, these two questions are addressed by testing the cell viability of Madin-Darby canine kidney (MDCK) cells infected with different subtypes of influenza virus, by studying the inhibition of haemagglutination by herbal extracts, and by looking at the inhibitory effects on viral replication. The MDCK cell study should be able to identify the main target of RIE activity as either cells or virusal particles by comparing RIE's efficacy when it is applied at different stage of virus infectious life cycle. Three kinds of extracts were prepared respectively from fresh roots, sun-dried roots and 7-day incubated roots and examined for their antiviral activities, in order to determine the impacts of the heating process on RIE's therapeutic functions.

3.2. THE ANTI-INFLUENZA VIRUS EFFECT OF RIE ON MDCK CELLS AND ITS HYPOTHESIZED MECHANISM

In earlier work (Wu 2005) (Chen *et al.* 2006), RIE was demonstrated to prevent influenza A virus induced haemagglutination. Furthermore, capillary electrophoresis of erythrocytes revealed remarkable changes in the electrical charge of erythrocyte membranes (Lu *et al.* 2003) and implied that RIE's anti-haemagglutination is possibly due to interaction with erythrocytes rather than influenza virus. However, this conclusion cannot be extrapolated to RIE's antiviral action because inhibition of haemagglutination is not fully equivalent to antiviral activity. The influence of RIE treatments on viral infection was investigated with MDCK cells by MTT assays, plaque reduction assays and scanning electron microscopy. The target of RIE's antiviral action was identified, and the results are reported here.

3.2.1. Materials and Methods

3.2.1.1. Preparation of RIE

RIE was prepared as described in Section 2.1.1.

3.2.1.2. Viruses

Influenza viruses used in this study were cultured as described in Section 2.1.4.

3.2.1.3. Cytotoxicity measurement

Madin-Darby canine kidney (MDCK) cells were cultured as described in Section 2.1.5. Cytotoxicity of RIE was measured as described in Section 2.2.2.1.

3.2.1.4. Antiviral effects of RIE in vitro

MDCK cells were infected by viruses as described in Section 2.2.2.2.

Two methods were employed to evaluate the antiviral activity of RIE *in vitro*: 1) increases in the survival rates of MDCK cells determined by MTT assay; 2) plaque reduction assay. The EC_{50} values were calculated by Reed-Muench method (Reed & Muench 1938).

1) Cell protection rate measured by colourimetric MTT assay

After virus infection with or without prior RIE administration (1 h at 33°C), the cell monolayer was washed by PBS, and cultured in medium for 3 d. 100 μL of MTT (3-[4,5-dimethylthiazol-2-yl]-2,5-diphenyltetrazolium bromide) solution (1 mg/mL in PBS) was added to each well and incubated for 4 h, and then replaced by 150 μL isopropanol. After thorough dissolving, the absorbance of each well was measured by an ELISA reader (DG5031) at 540 nm. The normal MDCK cells and viruses infected cells were used as controls. Five duplicates were used for each group. The cell protection rate was calculated by means of absorbance with Eq 3.1.

$$Cells\ protection\ rate\ (\%) = (O.D._{VR} - O.D._{V}) / (O.D._{R} - O.D._{V}) \times 100\% \qquad \textbf{Equation 3.1}$$

$O.D._{VR}$ = Virus and RIE; $O.D._{V}$ = Virus only; $O.D._{R}$ = RIE only

2) Plaque reduction assay

The assay was performed as described in Section 2.2.2.4. RIE was hired as antiviral agent.

3.2.1.5. Comparison of RIE inhibitory effects on viral infection at different timing of viral replication cycle

The infectious cycle of an enveloped virus primarily involves four phases: binding to a receptor on the membrane, membrane fusion or entry, replication and assembly, and budding (Fig 3.1). However, the methods mentioned above are not able to identify in which phase the antiviral agent acts. In order to distinguish at which phase of virus infection is affected, RIE was introduced to cells or viruses at three different time points corresponding to phases of virus infection. Cells were allocated to three groups, as described below, in order to observe the effects of RIE at each time point. The EC_{50} of RIE (50 mg/mL) was used for both of influenza virus A (H1N1) and B. RIE was incubated with cells or viruses for 3 h. Virus infection was performed as described in Section 2.2.2.2. The cell viability was determined by MTT assay after 3 day's culture, using normal cells and infected cells as control.

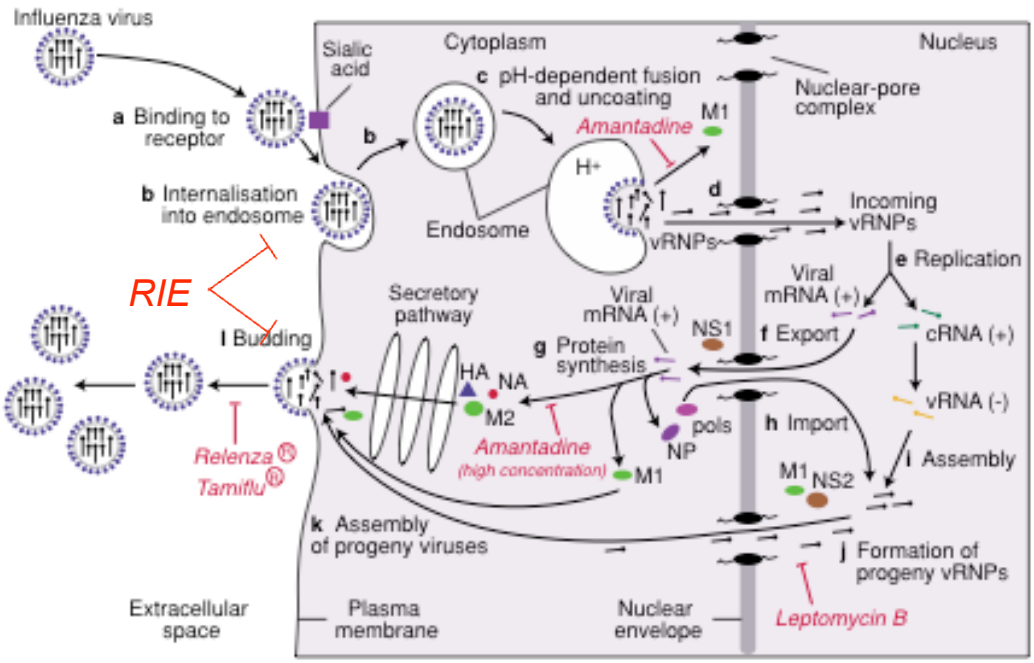

Figure 3.1 Schematic representation of replication cycle of an influenza virus and the possible targets of RIE.

Adapted from Whittaker's diagram (Whittaker 2001).

1) Protection group (C+RIE+IA or C+RIE+IB in Fig. 3.4A)*

Cells were incubated with RIE for 3 h at 33°C in cell incubator, prior to exposure to viruses (50 PFU) at 33°C for 1 h. After incubating with RIE, cells were washed twice with PBS buffer to remove free RIE. Cell culture medium was then added.

2) Repair group (C+IA+RIE and C+IB+RIE in Fig. 3.4B)*

Cells were incubated with virus at 33°C for 1 h, to allow viral infection to occur. The cells were then washed twice with PBS buffer to remove any free viruses in the supernatant, before incubating with RIE for 3 h at 33°C. The cells were washed twice with PBS buffer again to remove the free RIE, then cell culture medium was added.

3) Direct action group (IA+RIE+C and IA+RIE+C in Fig. 3.4C)*

* 'IA' refers to Influenza A FM1 (H1N1, mouse-adapted) virus, 'IB' refers to influenza B/Shanghai/93-1(C3C2, 1:320 9/2/99), 'C' refers to MDCK cells.

The viruses were incubated with RIE at 33°C for 3 h to allow any direct action of RIE to occur. After that, the mixture was centrifuged at 100,000 g for 90 min at 4°C. The sedimented virus was suspended again with PBS buffer and introduced to cells at 33°C for 1 h to allow the occurring of viral infection. The suspension was thoroughly removed, then the cells were washed twice with PBS and the culture medium was added.

3.2.1.6. Scanning electron microscopy

MDCK cells were grown to confluence on polyethyleneimine-coated cover slips (10 mm diameter) in 24-well plastic tissue culture plates (16 mm well diameter). The administration of RIE (15 mg/mL) was carried out as described in Section 3.2.1.5. in order to observe the drug's influence on different aspects of viral infection, two incubating conditions were used in order to control the process of infection. To investigate the inhibitory effects of RIE on the viral cytopathic impacts, the cells were incubated with viruses at 33°C for 1 h, then the free viruses were removed and cells were incubated in 200 µL medium for further 6 h. To investigate RIE's effects on virus binding, the cells were incubated with viruses at 4°C for 1 h and then the free viruses were removed.

After being washed with PBS buffer for 3 times, the cells were fixed with 2.5% glutaraldehyde-2.0% paraformaldehyde in 0.1 M cacodylate buffer (pH 7.4) for 1 h at room temperature, and post-fixed with 1% OsO_4 in the same buffer for 45 min, followed by thoroughly washing and dehydrating in ethanol, being treated with isoamyl acetate and dried to a critical point with HCP-2. The cells were mounted on stubs, coated with gold and observed with a scanning electron microscope (SEM; JSM5310/LV, JEOL).

3.2.2. Results

3.2.2.1. Cytotoxicity results

In order to evaluate the potential cytotoxic effects of RIE on cells, MDCK cells were incubated with RIE for 72 h before the cell survival rate was measured with MTT assay. As shown in Fig 3.2, at low concentrations of RIE, ranging from 1 mg/mL to 10 mg/mL, the cell survival rates were not significantly different to that of normal cells. The lowest cell survival rate of all assayed RIE concentrations was 53% (at 100 mg/mL). There is a significant

decrease in the cell survival rates when the concentration of RIE rises from 40 to 100 mg/mL. Therefore, the 50% cytotoxic concentration in MDCK cells was higher than the maximum assayed concentration (100 mg/mL) of RIE. These results indicate that RIE has a low cytotoxicity to MDCK cells, when no cytotoxicity was observed at concentration lower than 10 mg/mL.

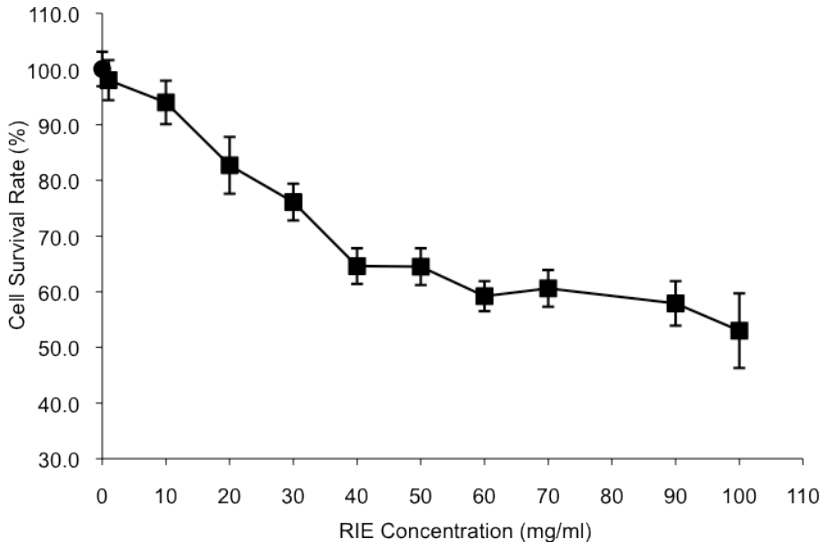

Figure 3.2 Cytotoxic effect of RIE on the MDCK cells.

The cells incubated with RIE at the serial concentration were marked as (■). The control group was marked as (●). n=6; RIE=1 mg/mL, P>0.05; RIE=10 mg/mL, P<0.05; others, P<0.01.

3.2.2.2. In vitro antiviral activity of RIE

Is RIE effective on a single strain of influenza viruses or on different types of viruses? To answer this question, the protective effects of RIE on two different strains of influenza A viruses and one strain of influenza B virus were evaluated and compared, in terms of cell protection rate and plaque inhibition rate. RIE inhibited all three influenza virus strains. As shown in Fig 3.3A and B, the EC_{50} values of RIE's protection effects on MDCK cells against infection of viruses are 12.6 mg/mL for influenza A FM1, 17.6 mg/mL for influenza A H1N1 and 47.1 mg/mL for influenza B, measured by MTT assay. Influenza B viruses requested the highest concentration of RIE.

Similar results were achieved by plaque reduction assay. The EC_{50} values were 13.6 mg/mL, 19.0 mg/mL and 50.1 mg/mL, for influenza A FM1, H1N1 and influenza B viruses,

respectively. Generally, the two influenza A viruses appeared more sensitive to the inhibition of RIE than did the influenza B virus. But there is no significant difference on the inhibitory effects of RIE in the mechanism studies shown below (Fig 3.4). The different impacts of RIE on influenza A and B viruses warrants further study. Since the EC_{50} of influenza B virus was around 50 mg/mL, the following mechanism studies of the RIE's antiviral effects on both of influenza virus A and B were conducted at this concentration. Moreover, in this test, the incubation of 100 mg/mL RIE with cells and influenza A virus together for 1 h at 33°C raise the cells survival rate up to 91%. This result indicates the short time exposure of cells to RIE conducts much less cyto-toxicity than the 72 h incubation employed in the cytotoxicity tests. Therefore, RIE at 50 mg/mL should not be a threat to cells' viability.

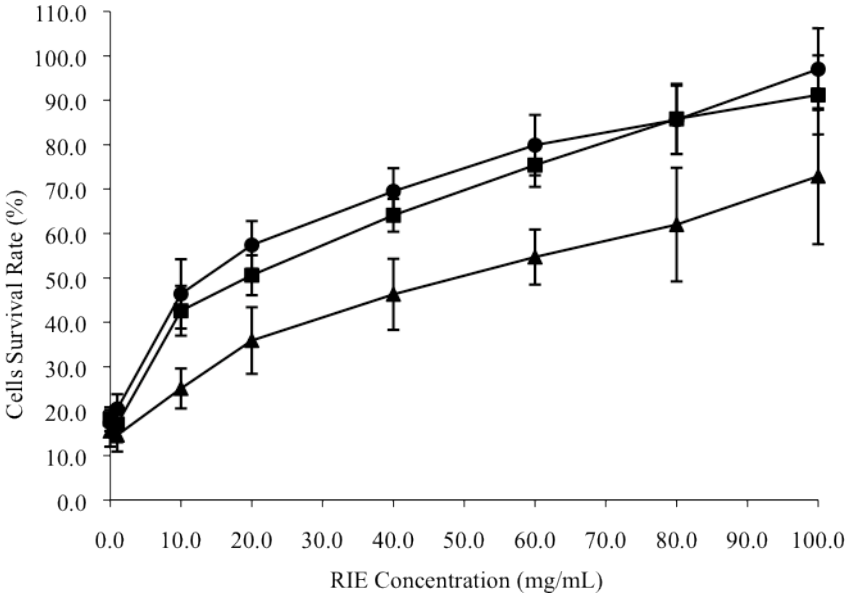

A. Effects of RIE pre-treatment on the cell survival rate, measured by MTT assay.

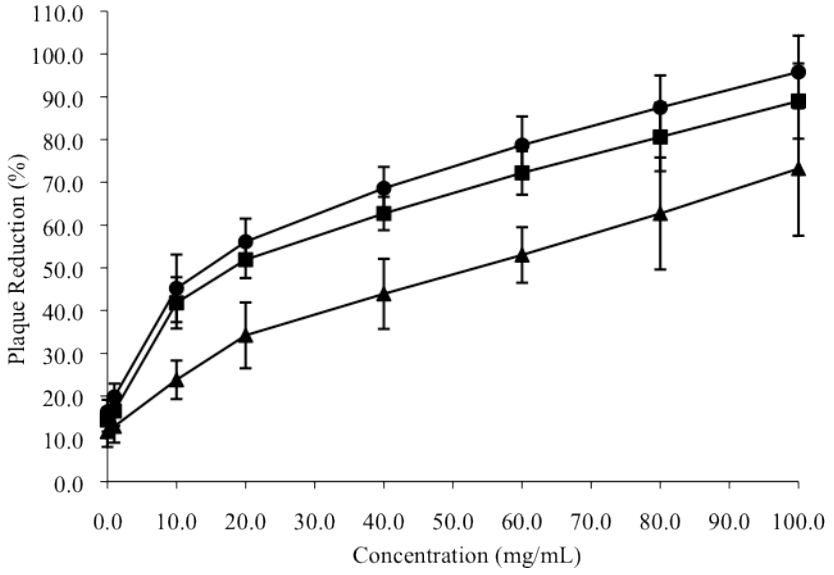

B. Inhibitory effects of RIE pre-treatment on plaque formation measured by the plaque reduction assay.

Figure 3.3 Anti-influenza virus effects of RIE on MDCK cells.

Three strains of influenza virus were used in the experiments: influenza A FM1 (H1N1, mouse-adapted) virus (●) and influenza A/Beijing/95-262(H1N1/C2E3, 1:640 8/2/99) (■) (n=6. RIE=1.0 mg/mL, P>0.05; others, P<0.01); influenza virus B/Shanghai/93-1(C_3C_2, 1:320 9/2/99) (▲) (n=6. RIE=1.0 mg/mL, P>0.05; RIE=10 mg/mL and 20 mg/mL, P<0.05; others, P<0.01)

3.2.2.3. *In vitro anti-viral mechanism studies on RIE: cell viability study*

The infectious cycle of an enveloped virus primarily involves four steps: binding, fusion or entry, replication and budding, which together provide several opportunities for viral inhibition. Antiviral agents act on either host cells or viruses to achieve the inhibitory effects on viral infectious cycle. For example, some antibodies inhibit the attachment of viruses to cells (Ugolini *et al.* 1997) (Reading & Dimmock 2007) (Klasse & Sattentau 2002). Peptidylchloroalkylketone inhibitors prevent the fusion event by inhibiting cleavage of the precursor of HA (Tashiro & Rott 1996); as shown in Fig 3.1, the approved drugs amantadine and rimantadine can stop viral particles releasing into the cytoplasm by inhibiting the uncoating of viral particles (Pinto & Lamb 2007) (Ilyushina *et al.* 2007) (Duff 1992); neuraminidase inhibitor, i.e. Tamiflu, prevents the budding of progeny virus from the cell membrane (Gubareva, Webster & Hayden 2002) (Moscona 2005).

To understand the molecular mechanism of RIE's antiviral activity, the targets of RIE's action have to be firstly narrowed down to either cells or viruses. MRPs are possibly the major composition of RIE, like in a big population of traditional Chinese herbal medicines. Another TCM herbal tonic, namely MCE, has shown its cyto-protective effects on pancreatic islet cells (Xiang *et al.* 2007). It has been revealed that MRPs forms a significant amount of components of MCE (Ke *et al.* 2010). Sharing MRPs as a mutual composition with MCE, RIE is assumed to have cyto-protective effects on virus host cells. To illuminate the assumption, RIE was applied to cells or viruses according to three different phases of viral replication cycle, as described in Section 3.2.1.5.

It is important to notice that the efficacy of RIE depends on when it was introduced to cells and viruses, as shown in Fig 3.4. In contrast with virus-infected cells, only the 'protection group' achieved a significant improvement on cell survival rates among the three groups. When RIE was introduced to cells after virus binding to cells (referred to as 'repair group', shown in Fig 3.4B), the cell survival rates were only 29 ± 2% in influenza A and 41 ± 8% in influenza B, and were not significantly different from controls of viruses infected cells. However, the same figures were almost doubled if RIE was introduced to cells prior to the viruses' appearance (referred to as 'protection group', shown in Fig 3.4A). The cell survival rates were 63 ± 6% to influenza A viruses and 65 ± 14% to influenza B viruses, respectively ($P< 0.01$). It is about two third of cells remained uninfected in both types of influenza viruses, which is a remarkable protection effect. At the same time, much fewer virus particles appeared on the surface of RIE pre-treated cells than on the cells without RIE

treatment (counted by SEM, see Section 3.2.2.4). There was no direct action of RIE on both strains of viruses, because direct incubating RIE and viruses together didn't neutralise the infectivity of viruses. Corresponding with cell survival rates, the virus titres in suspensions measured by the haemagglutination assay, only decreased in the 'protection group' of cells (data not shown, but available on request).

3.2.2.4. In vitro anti-viral mechanism studies on RIE: morphological study

The cytopathic effect (CPE) of MDCK cells was observed by scanning electron microscopy (SEM). As shown in Fig 3.5, CPE appeared in the influenza virus infected MDCK cells (Fig 3.5B) and the cells of 'repair group' and 'direct action group' (Fig 3.5C&D). In contrast, there is no CPE observed in the cells from the 'protection group', in which cells were incubated with RIE (15 mg/mL) prior to virus infection (Fig. 3.5A). This is consistent with RIE's protection effects, as described in the last section, on cell viability against virus infection, investigating with MTT assay.

In addition, the cells were incubated with the same amount of virus at 4°C for 1 h. The suspending viruses were then removed by a thorough washing with PBS. The electronic micrographs were taken immediately (Fig 3.5E&F). At this time point and temperature, viruses had been associated to cell membrane, but not yet internalised (Matlin *et al.*, 1981). Numerous virus particles (arrows) bound to the MDCK cell plasma membrane in the absence of RIE (Fig 3.5F). On the contrary, attached virus particles were rarely observed on the MDCK cells protected by RIE MRPs (Fig 3.5E).

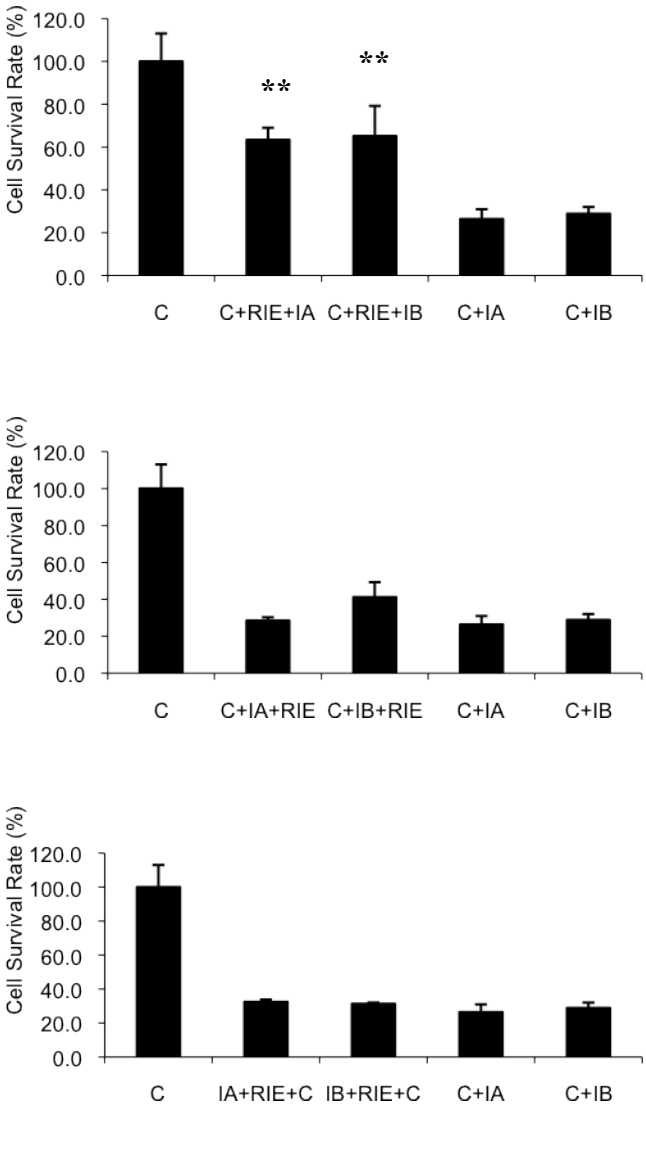

Figure 3.4 *In vitro* protective effects of RIE on MDCK cells against influenza viruses.

Influenza A H1N1 (mouse-adapted) virus was used in IA, while influenza B/Shanghai/93-1(C_3C_2, 1:320 9/2/99) was used in IB. 50 mg/mL of RIE was used in all of the groups. Normal MDCK cells (C) and cells infected by viruses (C+IA, C+IB) were used as controls. Both of the IA, and IB groups included C+RIE+V (Fig. 3a), C+V+RIE (Fig. 3b) and V+RIE+C (Fig. 3c). $n \geq 4$, "**", $P < 0.01$; others, $P > 0.05$.

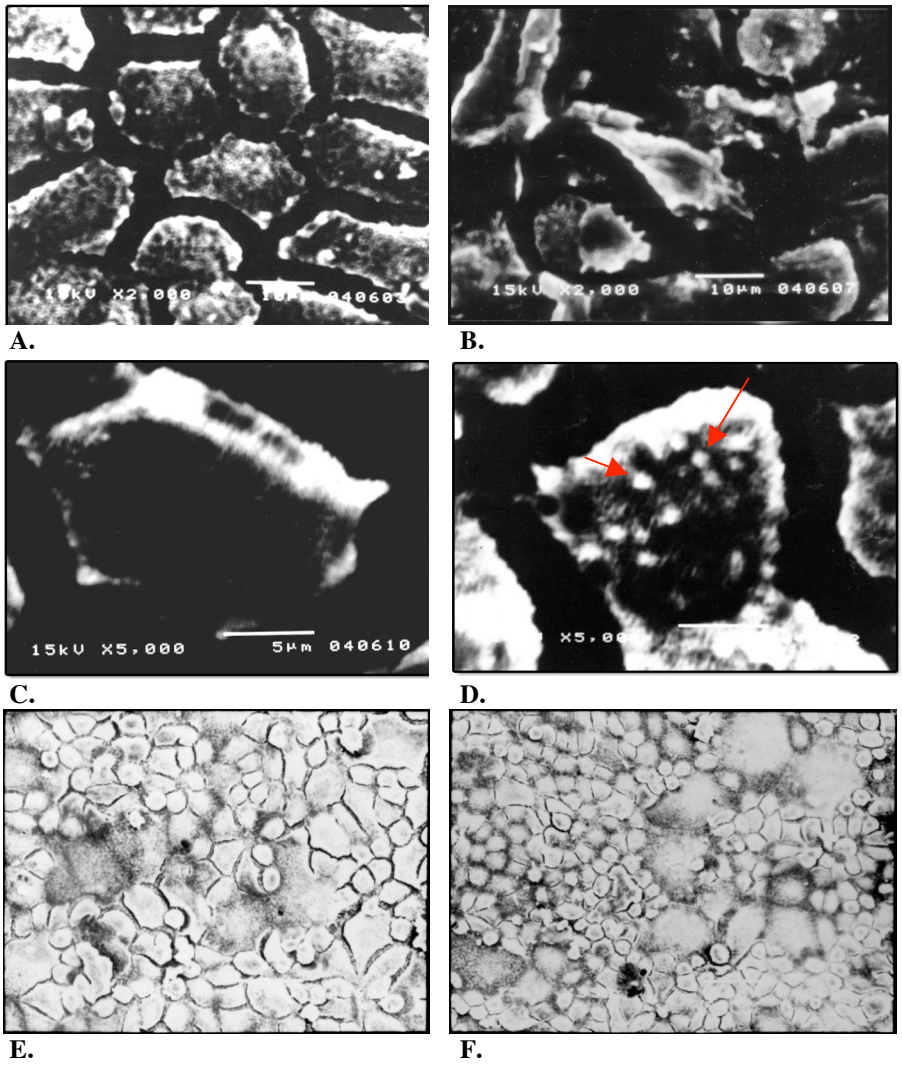

Figure 3.5 Scanning electron micrographs of MDCK cells infected with 50 PFU influenza A H1N1 (mouse-adapted) virus (IA) in the time point-depended RIE administration experiments.

A: 'Protection group', cell grown at 33°C, magnified ×2000;
B: 'Virus infected Control', the virus infected cells, grown at 33°C, magnified ×2000;
C: 'Repair group', cells grown at 33°C, magnified ×5000;
D: 'Direct action group', cells grown at 33°C, magnified ×5000;
E: 'Protection group', cells were incubated with viruses at 4°C, magnified ×350;
F: 'Virus bound cells', cells were incubated with viruses at 4°C, magnified ×350;
Arrows: virus particles binding to the microvilli and other parts of plasma membrane. (These photos were scanned by a Flat Scanner, Acer S2W 3300U, using Adobe Photoshop 6.0)

3.2.3. Conclusions and Discussions

RIE and its MRPs are effective *in vitro* in inhibiting viral infections caused by two subtypes of viruses, influenza A (H1N1) viruses and influenza B viruses, on Madin-Darby Canine Kidney (MDCK) cells. RIE promoted the proliferation of both normal and virus infected cells, reduced plaque formation and blocked virus entry across the membrane. A very low cytotoxicity of RIE was observed on MDCK cells (CC_{50} > 100 mg/mL).

As described in 3.2.2.3, three assumptions are drawn from the results.

Firstly, as RIE failed to prevent viral infection by direct actions on viruses and neutralising them, RIE is assumed to act on MDCK cells rather than influenza viruses.

Secondly, RIE can bind to cell plasma membrane or enter cell plasma and affect the early events of viral infection, such as binding and fusion of membrane, uncoating of virus particles in cytoplasm. As any free RIE was thoroughly washed off after incubation with cells in all three groups, only those RIE who bound to the cell plasma membrane or internalised into the cell plasma would contribute to the rise of cell survival rates. Furthermore, because of the stronger effects of 'protection group' than 'repair group', it is crucial for RIE to participate cell-virus interaction in an early stage, particular prior to the presence of viruses.

Thirdly, RIE probably binds to, and acts on, the cell's plasma membrane. This is because, if internalisation of RIE made an equal contribution to its inhibitory effects, the RIE treatment after virus infection ('repair group') should have resulted more positively than it did. This assumption is supported by the inhibitory effects of RIE on haemagglutination induced by influenza A viruses (Chen *et al.* 2006), in the same manner with results from MDCK cells. Haemagglutination is a result of the binding of viral envelope glycoprotein haemagglutinin (HA) to its plasma membrane receptors, sialic acid residues of glycolipids (Thompson, Barclay & Zambon 2004) (Cox & Subbarao 1999). Since direct treatment of RIE to virus did not decrease the infectivity and haemagglutination of virus, it is more confident to assume that cell plasma membrane, instead of the membrane of virus, is the target of RIE.

Hence, the inhibitory effects of RIE on viral infection may be confined to the binding and fusion stage of infection. RIE may mainly work on the plasma membrane of MDCK cells to inhibit the binding and fusion process of virus. This assumption is supported by SEM studies assayed, in which very few virus particles were seen to bind to the RIE incubated MDCK

cells. There are two kinds of possible binding sites for RIE on the plasma membrane, membrane lipids or membrane glycoproteins. However, due to its high EC_{50} value and extraordinarily low cytotoxicity, RIE is assumed to act on cell membrane not through the ligand-receptor pattern. Membrane lipids are therefore most possibly the binding sites for RIE.

The EC_{50} of RIE ranges from 12.6 to 50.1 mg/mL, which seems too high to be an efficient antiviral agent. However, two factors have to be taken into account.

Firstly, the evaluation assay of EC_{50} employed in this study was not optimal method, due to the cell protection model of RIE. Pre-treatment of cells with RIE is obligated to achieve the maximum protection effects. However, during EC_{50} evaluation, RIE was introduced to cells with the virus together instead of prior to virus incubation. The EC_{50} of RIE obtained by this method is undervalued.

Secondly, as a mixture, RIE contains hundreds of compounds, within which the proportion of the effective ingredients is expected to be low. The EC_{50} of the effective compositions will not be determined accurately until the compositions are purified.

Both of these two factors may diminish the efficacy of RIE and consequently requires a high effective concentration. A new method, in accordance with RIE's virus binding inhibitor property, should be established for further studies to appropriately quantified inhibitory effects of RIE on virus infection.

Based on the observation above, effective components in RIE, which are responsible for the anti-haemagglutination and anti-influenza effects, could be classified into two categories: native compounds from the fresh plant and modified compounds formed in the processing of plant material. The native compounds may include various active molecules like lectin or neuraminidase inhibitors, and are generally unstable to heat processing. Even if there is potent antiviral capacity among these native compositions, it is hard to believe they will survive through the boiling water extraction involved in the preparation of RIE. Taking lectin as an example, although the fresh roots contained lectin (Hu & Zheng 2003), which may inhibit haemagglutination, it would hardly remain active after the boiling water extraction. Furthermore, the fact that RIE's EC_{50} on influenza virus A H1N1 is less than 20.0 mg/mL while the effective concentration of isolated lectin on the same type of virus is 45.3 mg/mL, indicates the lectin can not the effective antiviral component, at least not the major

one. Since the native compounds of roots cannot explain antiviral effects of RIE, it is worthwhile to study the modified compounds and their bioactivities.

3.3. DIFFERENCES IN THE CYTOTOXICITIES AND ANTIVIRAL ACTIVITIES OF FRESH ROOTS, SUN-DRIED ROOTS AND RIE

The previous section has shown that RIE inhibits influenza viruses by binding to cells and blocking the early events of influenza virus infectious cycle. However, as described in Section 1.2.4, none of compositions from fresh roots shows promising antiviral activities. Does RIE become effective only because it is a highly concentrated preparation of native compounds from the roots, or, because of the major chemical changes that occured in the heat extraction procedure?

To answer this question, the cytotoxicity and anti-influenza virus tests were conducted on three preparations of the roots: the cold water (4°C) extracts of fresh roots; the cold water extracts of sun-dried roots; and the 7-d RIE, a boiling water extracts of 7-day incubated sun-dried roots. The samples represent three typical intermediates of RIE preparation, and help to track the gradual evolution of chemical species and biological activities of the roots.

3.3.1. Materials and Methods

3.3.1.1. Preparation of fresh roots extracts

Fresh roots extracts were obtained by cold aqueous extraction at 4°C, eliminating the occurrence of Maillard reaction. The fresh roots were crushed into powder with a food grinder. 35 g of powder was suspended in 105 mL PBS buffer (0.01 mol/L, pH 7.2, Na_2HPO_4-NaH_2PO_4; 0.1 M NaCl), stirring overnight at 4°C. The supernatant (72 mL) was collected by centrifuging at 21,400 g for 15 min, and stored at -20°C before use.

3.3.1.2. Preparation of Sun-dried roots extracts

Sun-dried roots extracts were obtained by cold aqueous extraction at 4°C, eliminating the occurrence of Maillard reaction. The sun-dried roots were crushed into powder with a food grinder. 35 g of powder was suspended in 105 mL PBS buffer (0.01 mol/L, pH 7.2, Na_2HPO_4-NaH_2PO_4; 0.1 M NaCl), stirring overnight at 4°C. The supernatant (52 mL) was collected by centrifuging at 21,400 g for 15 min, and stored at -20°C before use.

3.3.1.3. Preparation of 7-d RIE

7-d RIE was prepared as described here. 50 g of sun-dried roots was incubated at 60°C, 85% rh, for 7 days. The roots were then boiled in 400 mL pure water in a beaker for 2 h. The supernatant was collected by filtering with cotton gauze. The solid residues were boiled in 400 mL pure water for 1 h. The supernatant was collected and combined with the previous supernatant, and then applied to centrifuge at 21,400 g, 15 min. The supernatant of centrifuge was collected and then diluted with pure water to 155 mL. Extracts were stored at -20°C before use.

3.3.1.4. Ribavirin

The antiviral drug, Ribavirin, was used as a control. Ribavirin was purchased from Henan Topfond Pharmaceutical Co., Ltd. and used without further purification.

3.3.1.5. Cytotoxicity measurement

Madin-Darby canine kidney (MDCK) cells were cultured as described in Section 2.1.5.

Cytotoxicity of RIE was measured as described in Section 2.2.2.1. Each of the RIE sample was diluted into a serial of concentrations for evaluation (1:3, 1:9, 1:27,…). TC_0 and TC_{50} were calculated accordingly by Reed-Muench method.

3.3.1.6 Haemagglutination inhibition test

The haemagglutination inhibition was conducted as described in Section 2.2.2.6.

The HA titre of influenza A viruses H1N1/PR8 was 1024, when that of H3N2 was 128. This suspension of these two viruses was diluted with normal saline by 256 times and 32 times, respectively, to obtain working virus suspension (HA titre=4) for HA inhibition tests. Fresh chick blood was collected and made into 1% (v/v) suspension, stored at 4°C.

Two-fold dilutions of the samples were prepared by mixing 50 μL sample solution with 50 μL normal saline. The virus suspension (HA titre=4, 50 μL) was mixed with each dilution of samples, and stored at 4°C for 45 min. 50 μL 1% chicken red blood cells were then added and stirred, stored at 4°C for 30 min. Morphological observation was performed with a normal laboratory microscope. The results were presented as 4+, 3+, 2+, 1+, ±, –.

4+: 100% of erythrocytes agglutinated.

3+: 75% of erythrocytes agglutinated.

2+: 50% of erythrocytes agglutinated.

1+: 25% of erythrocytes agglutinated.

±: slightly agglutinated, less than 25% of erythrocytes.

−: No visible agglutination.

3.3.1.7. Plaque reduction assays

Plaque reduction measurement was performed as described in Section 2.2.2.7, with some modifications. MDCK cells were grown in 12-well plates, 2.5×10^5 cells per well. The experiments were conducted on confluent MDCK cell monolayers after 48 h. After removal of culture media, cell monolayers were wash with PBS to clean up bovine albumin from the media. Cells were then inoculated with 200 μL of 50 plaque forming units (pfu) virus suspension in test medium. Virus adsorption was carried out at 35°C, 5% CO_2, for 2 h. The infectious medium was removed and the cell monolayers were overlaid with 1.5 mL DMEM medium containing 0.4% agar and serial concentrations of samples. Each concentration and control had in 3 duplicates. After agar aggregated, cells were incubated at 37°C, 5% CO_2 for 48-72 h. Plates were checked everyday for viral pathological changes. When the untreated virus control reach 4+, the testing medium was removed and cells were fixed with 10% formalin solution for 30 min. Plates were then stained with crystal violet solution to count the number of plaques. The plaque forming units of each concentration were calculated with Eq 3.2.

plaque forming units (pfu/mL) = (mean plaque number of each well) / (pfu of virus inoculation) × (dilution times) **Equation 3.2**

3.3.2. Results

3.3.2.1. Impacts of heat processing on the cytotoxicity of the roots

The cytotoxicities of three preparations of the roots were compared to evaluate the impacts of heat processing, meaning sun-drying (25°C - 40°C), incubating in humid circumstance and boiling (100°C), on the toxicity of RIE upon MDCK cells. As shown in Fig 3.6 and

Table 3.1, the cold water extracts of sun-dried roots and the boiling water extracts of 7-day incubated roots (namely 7-d RIE) present much lower toxicities than the cold water extracts of fresh roots and the control drug Ribavirin. TC_0 of sun-dried roots extracts was 22 mg/mL, while TC_{50} of which was 35.5 mg/mL. 7-d RIE achieved the highest numbers on these two figures, which are 31.5 mg/mL and 62.5 mg/mL, indicating a lowest toxicity among the three roots samples. TC_0 and TC_{50} of fresh roots extracts were 0.8 mg/mL and 2.4 mg/mL, respectively. Sun-drying made the major contribution to decrease of cytotoxicity by lowering the TC_0 and TC_{50} by 15-25 times. On top of sun-drying, incubation at 60°C and boiling water extraction decreased the cytotoxicity even more, by 25-40 times comparing to that of fresh roots extracts.

Ribavirin is a conventional antiviral drug, with an efficacy against a wide range of RNA and DNA viruses. TC_0 of ribavirin conducted here was 1.6 mg/mL, which is consistent with previous report (Crance *et al.* 2003). Sun-dried roots extracts and 7-d RIE are less toxic than the Ribavirin, while the fresh roots extracts is more toxic than Ribavirin. However, it has to be born in mind that the concentrations of three samples were calculatedfrom the dry weight of roots, which contains a large portion of insoluble compositions. The concentrations of effective soluble compositions are less than the numbers represent as dry weight. In case of 7-d RIE, 100 mg dry weight of roots is equal to 25.8 mg of soluble compositions.

The results above imply that heat processing modifies ingredients in the roots and results in a much lower toxicity upon cells. The decrease on toxicity is correlative with strength of heating, including temperature and length of heating time. Furthermore, since Maillard reaction popularly occurred in the heat processing, as a major outcome, the formation of MRPs may contribute to the weakening of toxicity.

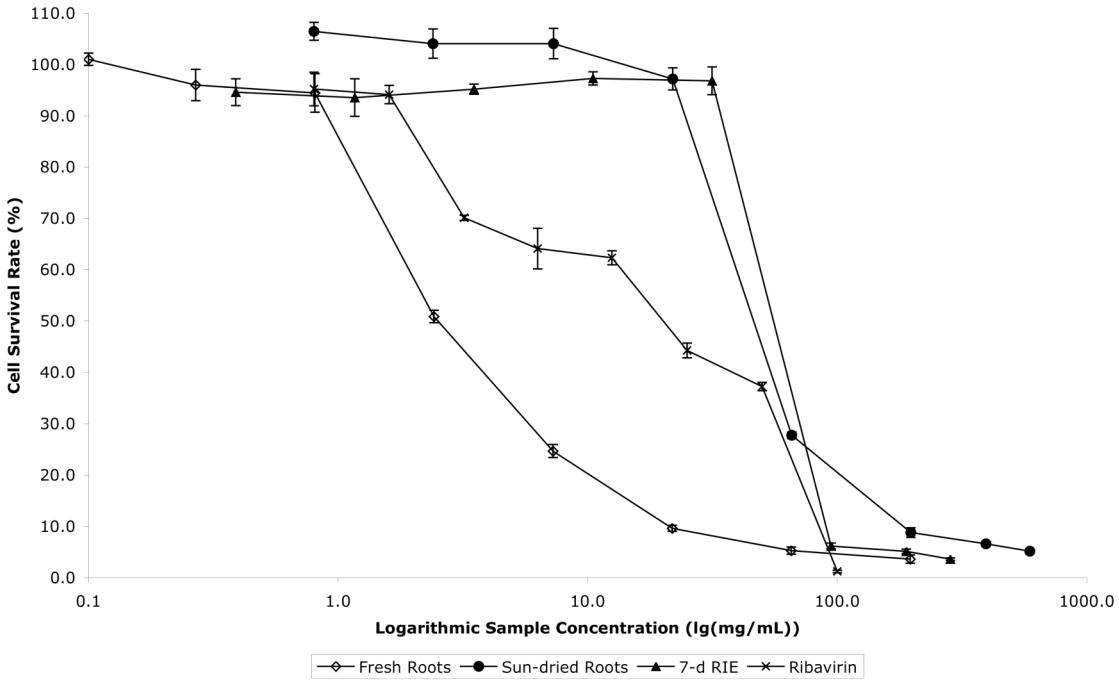

Figure 3.6 Mean dose-response curve of cytotoxicity determined with fresh roots extracts, sun-dried roots extracts and 7-d RIE by MTT assays on MDCK cells. (n=8, P<0.01)

Table 3.1 The cytotoxicity of three types of the roots extracts

	TC_0 (dry weight mg/mL)	TC_{50}（dry weight mg/mL）
Fresh roots extracts	0.8	2.4
Sun-dried roots extracts	22.0	35.5
7-d RIE	31.5	62.5
Ribavirin	1.6	17.9

3.3.2.2. Impacts of heat processing on the cytoprotective effects of the roots

The capacities of fresh roots extracts, sun-dried roots extracts and 7-d RIE on preventing influenza A viruses induced cell death were examined on MDCK cells by MTT assay, and present as 'cell protection rate' in Fig 3.7. The concentrations of these samples were chosen on the basis of their TC_0 values. The concentration gradient was started at a maximum value, at which no cytotoxicity was observed, and continued by diluting 2 times each for 7 concentrations.

As a control, ribavirin significantly protected cells from viral infection at most of the assayed concentrations. No cytoprotective effects were observed on this antiviral drug at concentrations lower than 0.03 mg/mL. The efficacy of Ribavirin proved the method is suitable for evaluating cell protective activity of the roots samples.

In contrast to RIE's enhancement of cell viability, the cold-water extracts of fresh roots induced an even more severe cell death in cooperating with viruses, than by viruses alone. Certain compounds from the raw roots must have promoted the infection of virus and caused cell death. The sun-dried roots extracts did not help much on improving the cell viability against viruses. However, at 20 mg/mL, a concentration very close to its TC_0, the extracts slightly increased the cell survival rate. Being constant with results from cytotoxicity tests, 7-d RIE had been helpful for cells to survive through viral infection. At concentrations higher than 4 mg/mL, 7-d RIE protected cells from virus-induced death, and reserved up to 40% more cells at 32 mg/mL. The protection rates dropped along dilutions of the sample, indicating a concentration-dependent cyto-protective activity.

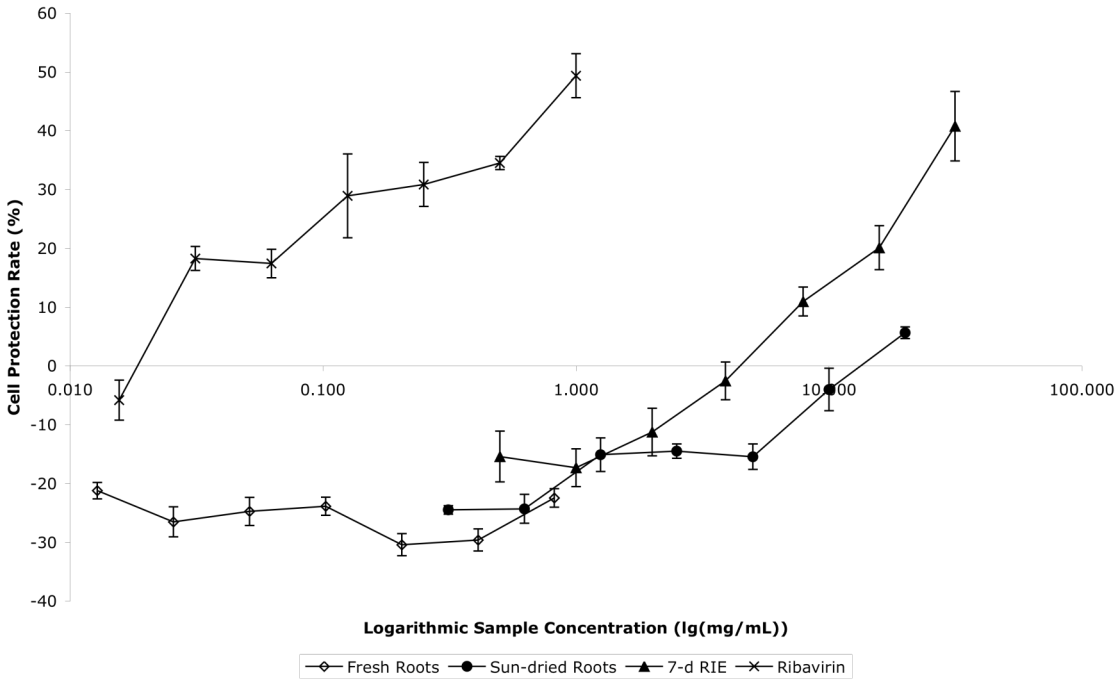

Figure 3.7 Mean dose-response curve determined with fresh roots extracts, sun-dried roots extracts, 7-d RIE and ribavirin by MTT assays in MDCK cell monolayers infected with influenza A viruses (H1N1). (n=4, P<0.01)

3.3.2.3. Impacts of heat processing on the haemagglutination inhibitory activities of the roots

The conventional antiviral drugs studied, including ribavirin and amantadine, nearly conducted any inhibition on haemagglutinin of H1N1 and H3N2, except amantadine on H3N2 viruses induced haemagglutination at concentrations greater than 125 μg/mL. It is a very high concentration for amantadine. The maximum concentration of this drug was only 25 μg/mL on a resistance study over 12 influenza A virus strains (Schmidtke & Bauer 2006).

In general, haemagglutination inhibition was observed in all three aqueous extracts of the roots, upon two influenza A virus strains, while HI titre was increased corresponding to progress of heat processing. 7-d RIE presented the strongest HI titre 128 (as shown in Table 3.2) on H1N1 viruses, which was more than 8 times higher than that of fresh roots extracts. The minimum effective concentration of 7-d RIE was 2.2 mg/mL (dry weight of roots). Sun-dried roots extracts lied in between the fresh roots and 7-d RIE. However, 7-d RIE possessed a much weaker inhibition on H3N2 viruses induced haemagglutination at a HI titre of 16.

Table 3.2 Inhibition of haemagglutination induced by influenza A virus (H1N1)

Dilutions / Samples	2	2^2	2^3	2^4	2^5	2^6	2^7	2^8	2^9	HI Titre
Fresh roots extracts	–	–	–	1+	3+	4+	4+	4+	4+	14
Sun-dried roots extracts	–	–	–	–	1+	2+	4+	4+	4+	28
7-d RIE	–	–	–	–	–	–	–	4+	4+	128
Ribavirin	–	4+	4+	4+	4+	4+	4+	4+	4+	2
Amantadine	1+	2+	4+	4+	4+	4+	4+	4+	4+	< 4

Table 3.3 Inhibition of haemagglutination induced by Influenza A virus (H3N2)

Dilutions / Samples	2	2^2	2^3	2^4	2^5	2^6	2^7	2^8	2^9	HI Titre
Fresh roots extracts	—	—	1+	4+	4+	4+	4+	4+	4+	7
Sun-dried roots extracts	—	—	—	1+	4+	4+	4+	4+	4+	14
7-d RIE	—	—	—	—	4+	4+	4+	4+	4+	16
Ribavirin	1+	4+	4+	4+	4+	4+	4+	4+	4+	<2
Amantadine	—	—	—	4+	4+	4+	4+	4+	4+	8

3.3.2.4. Impacts of heat processing on plaque-reduction activities of the roots

The cold-water extracts of fresh roots did not reduce the formation of plaque. In contrast, they increased the number of plaque, indicating a promotion on virus infection. At 0.4 mg/mL, fresh roots extracts increased the formation of plaque by 80%.

Sun-dried roots extracts achieved the better inhibitory effects than fresh roots by significantly reducing the formation of plaque at concentrations higher than 1.25 mg/mL, in

a dose-responsible manner. The greatest inhibition was achieved at the maximum tested concentration of 20 mg/mL.

7-d RIE completely inhibited the formation of plaque at all assayed concentrations, which were ranged from 1.0 mg/mL to 31.5 mg/mL. The soluble ingredients of 7-d RIE were weighed as freeze-dried powder. It was about 25 mg of the soluble compositions per 100 mg dry weight of roots. Therefore, the tested minimum effective concentration of 7-d RIE is 1.0 mg/mL (dry weight of roots), equal to 0.25 mg/mL soluble ingredients. And it is reasonable to anticipate that 7-d RIE would be effective in inhibiting haemagglutination at a concentration lower than the minimum concentration tested here.

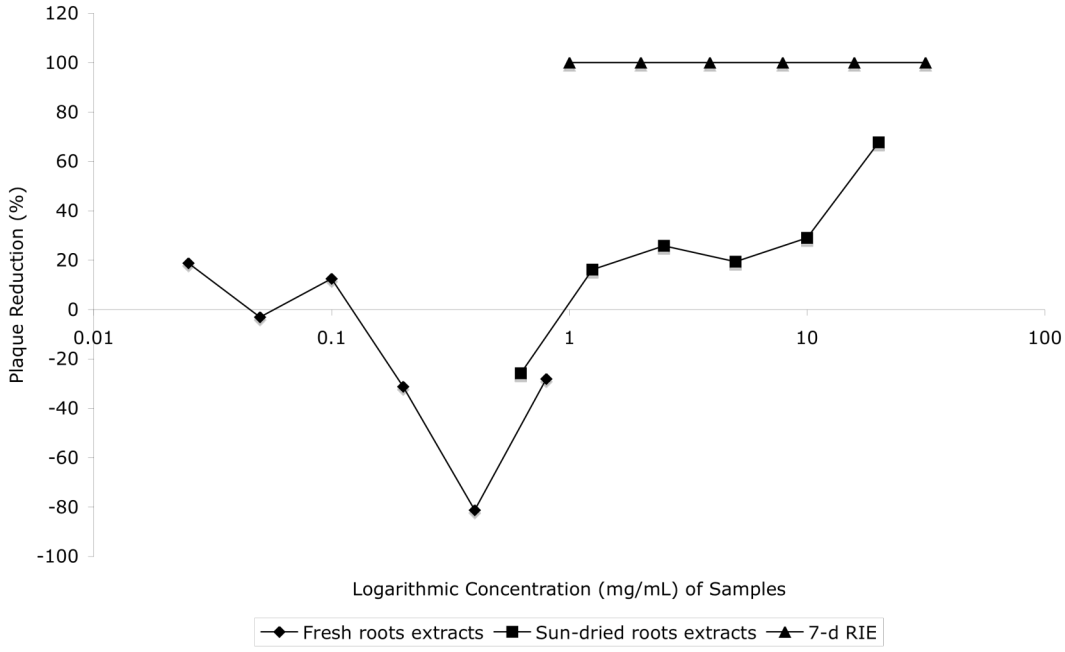

Figure 3.8 Dose-response curve determined with fresh roots extracts, sun-dried roots extracts, 7-d RIE by Plaque reduction assays in MDCK cell monolayers infected with influenza A viruses (H1N1) (*n*=3).

Concentrations of samples: (1) Fresh roots extracts: 0.8, 0.4, 0.2, 0.1, 0.05, 0.025 mg/mL; (2) Sun-dried roots extracts: 20, 10, 5, 2.5, 1.25, 0.625 mg/mL; (3) 7-d RIE: 31.5, 15.8, 7.9, 3.9, 2.0, 1.0 mg/mL.

3.3.3. Conclusions and Discussions

By using the same amount (dry weight) of raw materials, complexity of the native chemical composition from the fresh roots extracts, the sun-dried roots extracts and the boiling water extracts was cancelled out. By comparing the influences of three samples on cell proliferation, it was discovered that the heating process reduced the cytotoxicity of native plants while increased the antiviral cytoprotective effects of aqueous extracts of the roots.

The extracts of sun-dried roots conducted a stronger cytoprotective effect and a lower cytotoxicity than that of fresh roots, although both extracts were prepared with cold-water extraction to minimize the speed of chemical reactions between compositions of roots. 7-d RIE has the highest degree of heat-dependant reaction, and also possessed the highest cytoprotective effect and lowest cytotoxicity.

Chemical reactions and their products should be responsible for these progresses in physiological impacts of these water extracts of the roots. As described in Section 1.3.1, Maillard reaction generally occurred in many heat process like preparation of the roots decoction. This reaction, controlled by parameters like temperature, reactants and time, has dominant impacts on heat-induced chemical reactions in plants. Its products, MRPs, are consequently the important candidates of effective compositions, which are correlative to the new physiological properties generated during the preparation of sun-dried roots and boiling water extracts.

Two subtypes of influenza A viruses showed different susceptibility to amantadine. It is consistent with earlier report on amantadine resistance among 3 subtypes of porcine influenza A viruses. 9 out of 12 viruses studied, including H1N1, H1N2 and H3N2, are resistant to amantadine, examined by plaque reduction assays (Schmidtke & Bauer 2006). Furthermore, except M2 protein, haemagglutinin (H7) has been suggested to play a role in amantadine resistance of H7N7 viruses (Ilyushina *et al.* 2007). H1N1 viruses are more susceptible to 7-d RIE than H3N2, measured by haemagglutination inhibition assay. The susceptibilities of different subtypes viruses to either amantadine or 7-d RIE are therefore correlated to the types of HA.

As described in Section 3.2, RIE inhibits viral absorption and infection on MDCK cells, on H1N1 and H3N2 influenza A viruses and influenza B virus. It is in an agreement with RIE's haemagglutination inhibition activities on the H1N1 and H3N2 viruses. These results imply

that RIE is possibly effective to a range of influenza viruses regardless the genetic differences among their HA and NA proteins.

Furthermore, haemagglutination inhibitory effects of RIE support the hypothesis drawn in Section 3.2.2.3, that RIE acts on the host cell plasma membrane to conduct its antiviral activity. It is because HA on the membrane of virus interacts with sialic acid receptors on the cell plasma membrane to induce the haemagglutination. RIE has to interfere the interaction between HA and its cellular receptor, in order to inhibit the agglutination.

3.4. HYPOTHESIS

A hypothesis was drawn from the above observations and conclusions for this study. RIE acts on the cellular plasma membrane to conduct its inhibitory effects on influenza virus infection. The heating process during preparation of RIE generates and enhances the antiviral effects. Maillard reaction dominates the heat-incorporated chemical reactions in the roots, and conducts a significant improvement on cell membrane interactive capacity of RIE with its products, MRPs. Further studies were carried out accordingly with the aim of confirming the hypothesis.

CHAPTER 4

PURIFICATION AND CHARACTERISATION OF ACTIVE MRPS-RELATED COMPONENTS

4.1. AIMS OF THIS CHAPTER

In the last chapter, the target of RIE's anti-influenza virus activity has been addressed to the host cell, while the impacts of the heating process on the efficacy of RIE and its active components have been intensively studied. In this chapter, the major compositions of the roots, including proteins, saccharides and their derivates, are investigated, with the aim of identifying the major ingredients responsible for RIE's antiviral effects.

As discussed previously, the heating process has been shown to play an important role in regulating the anti-influenza virus activity of RIE. The Maillard reaction is the dominant reaction during the heat processing. In order to occur, the Maillard reaction requires the participation of corresponding reactants. To gain further understanding of the antiviral ingredients of RIE, it is necessary to isolate and characterise the components of the roots that participate in the Maillard reaction. These components could typically include amino acids, reducing sugars, proteins and peptides. The relative content of each of these components will be analysed, the pure molecules will be isolated and characterised, and their biological activities will be examined accordingly. An appropriate representative of the MRPs of RIE will be chosen for the later biophysical studies.

4.2. BIOCHEMISTRY OF THE ROOTS

4.2.1. Materials and Methods

4.2.1.1. Protein concentration

As described in Section 2.2.1.2, the protein concentration was determined by Kjeldahl assay (Cataldo, Schrader & Youngs 1974), Folin-Phenol assay (Lowry *et al.* 1951) and Bradford assay (Bradford 1976). The protein concentration was calculated with Eq 2.1 and Eq 2.2.

4.2.1.2. Determination of carbohydrates content

The starch content of the fresh roots was measured by the anthrone sulphuric acid assays as described in Section 2.2.1.3.

4.2.1.3. Amino acids analysis

The amino acids composition was analysed with an automatic amino acid analyser (Hitachi L-8800, Japan) using a standard ion-exchange HPLC protocol based on the reported methods (Hamilton, Bogue & Anderson 1960) (Hill *et al.* 1979). The samples were prepared as described in Section 2.2.1.4. The HPLC measures were conducted by Ms. Aiping Qian at Fujian Academy of Agricultural Sciences.

4.2.1.4. SDS-PAGE of proteins

SDS-PAGE electrophoresis was performed by the Laemmli protocol (Laemmli 1970). The proteins were dissociated with SDS and β-mercaptoethanol and electrophoresed through 12.5% polyacrylamide at 120 V.

4.2.1.5. Isoelectrofocusing

IEF was performed as described in Section 2.2.1.7.

4.2.1.6. Periodic acid-Schiff (PAS) Staining

Periodic acid-Schiff (PAS) staining was used to identify the glycoproteins (Glossmann & Neville 1971).

4.2.1.7. Identification of reducing sugars

As described in Sectioni 2.2.1.5, an HPLC method (Karlsson, Winge & Sandberg 2005) with a TSK-gel Amide-80 colum (TOSHO, Japan) was applied. The sugars were detected by an evaporative light scattering detector (SEDERE Inc., USA).

4.2.1.8. Purification of the representative proteins and MRPs molecules

As described in Section 2.2.1.8, HPLC was used as the main method of purification. Cation-exchange liquid chromatography and reversed phase liquid chromatography were the major methods of protein separation. Toyopearl SP-650M strong cation ion-exchange resin was used for isolation of RITIP proteins from fresh roots, while Toyopearl SP-5PW cation-exchange resin was used to isolate GRITIP proteins from sun-dried roots. The proteins were purified with a C18 chromatographic column (Oligo-R3). The purity was examined with a size-exclusion HPLC column (TSK-Gel G3000SWXL). The chromatographic columns used in this study were summarised in Section 2.1.6.

4.2.1.9. Preparation of Arg-Glc MRPs

1 mmol of *L*-arginine (non-animal source, Sigma) and 1 mmol *D*-glucose (Sigma) were mixed thoroughly and incubated in a humid atmosphere over a saturated solution of potassium bromide (80% RH) at 40°C. After 7-days of incubation, the Arg-Glc MRPs was dissolved in 5000 μL deionised water.

4.2.1.10. Enzymatic hydrolysis of proteins from the roots

Hydrolysis of proteins from the roots was conducted by the published method (Corzo-Martínez *et al.* 2010) with a few modifications. The conditions of enzymatic hydrolysis was optimised by adjust concentration of enzyme, time of hydrolysis, pH and temperature.

Pepsin in powder form (Sigma P7000, 1:10000, 542 U/mg, from porcine stomach mucosa) was dissolved in 0.1 M KCl-HCl buffer (pH 2) to make a 1.92% (w/v) solution. The purified proteins from the roots were dissolved in 0.1 M KCl-HCl buffer (pH 2.0) to make 1 mg/mL solution. Pepsin solution was added to protein solution at a volume ratio of 1:20, before incubation at 37°C for 3 h. At the end of incubation, the solution was heated to 100°C for 10 min to deactivate the enzyme. The hydrolysates were then applied to RPLC and mass spectroscopy for analysing the peptide fragments.

4.2.1.11. LC-MS analysis of protein hydrolysates

The analysis was performed with LC/MSD Trap XCT (Agilent, USA). RPLC was performed by using a C18 column (Phenomenex, Gemini C18, 250 mm × 4.6 mm, 5 μm) and the elution gradient of 0~100% CH_3CN, containing 0.1% TFA. The elution volume was 60 mL at a flow rate of 1 mL/min. The UV detector wavelength was 214 nm. The LC fractions were ionised and immediately analysed by an electronspray ionization mass spectrometer immediately. This was performed in cationic mode, 2000 m/z, spray air pressure 40 psi, nitrogen drying flow rate 12 L/min, drying temperature 350°C, capillary voltage 3.5 kV, with a ion scanning over the range from m/z 50 to 2200.

4.2.1.12. Glycation sites analysis

Genes of purified native proteins from the roots were cloned and the cDNA sequences were obtained. Simulated hydrolysis was performed with cDNA sequences by a software package called Peptidemap (http://prowl.rockefeller.edu/prowl/peptidemap.html). The peptide sequences from the simulation were manually paired with peptide fragments from the pepsin hydrolysis and mass spectroscopy. The glycation sites, together with the types of glycation, were identified by overlapping the peptide fragments obtained from enzymatic hydrolysis simulation and mass spectroscopy.

4.2.2. Results

4.2.2.1. Protein and saccharide content

Tables 4.1 and 4.2 showed the protein and carbohydrate content of the roots, and that of the pulps of *Momordica charantia Linn.* The soluble protein content of the roots was measured with three methods (Kjeldahl assay, Folin-Phenol assay and Bradford assay) described in Section 4.2.1.1. Sun-drying slightly reduced the protein content of the roots, and allowed a remarkably higher proportion to be extracted with water (Table 4.1). This is consistent with the ability of the Maillard reaction to increase the solubility and heat stability of proteins (Pan *et al.* 2005) (Watanabe, Sato & Kato 1980). Similar to the protein, the total saccharides contents were almost the same in fresh and sun-dried roots. However, a larger proportion of the saccharide in sun-dried roots is reducing sugars (Table 4.2), while Maillard reaction supposed to consume a number of reducing sugars during the sun-dry process. There are two

possible explanations for this unexpected high proportion: the influence of MRPs on the anthrone sulphuric acid assay, which gave a fake reading; or hydrolysis of polysaccharides by endogenious enzymes from the roots.

In contrast to the roots, the sun-dried pulps (of *Momordica charantia Linn.*) has smaller proportions of soluble proteins, total saccharides and reducing sugars, which indicates that the Maillard reaction has been more extensive. The reducing sugars account for a much higher proportion of saccharides in the pulps compared to the roots; over 50% in the former compared to only 14% in the latter. The high content of water in the pulps allows the Maillard reaction to occur more readily, and resulting in a lower concentration of reducing sugar.

Similar to the protein, total saccharide content was almost the same in fresh as in sun-dried roots, while reducing sugar content was raised by 10% in sun-dried roots (Table 4.2). The unexpected rise of reducing sugars in sun-dried roots may probably be attributed to two reasons: broke-down of polysaccharides caused by sun-drying; or the influence of MRPs on the anthrone sulphuric acid assay.

Table 4.1 Protein contents of fresh and sun-dried plants

	Total Protein Content (%, w/w) [1]	Soluble Proteins (mg/mL) [2]
Fresh *roots*	13.6	2.6
Sun-dried *roots*	11.4	10.6
Fresh pulps	15.3	4.2
Sun-dried pulps	NA	2.6

1. Total protein contents of the roots and the pulps were determined by Kjeldahl assay. 2. The soluble protein contents were determined by the Lowry method. BSA was used as the protein standard. The protein concentration was calculated with Eq 2.1.

Table 4.2 Carbohydrate contents of fresh and sun-dried plants.

	Total Saccharides (%, w/w)	Reducing Sugar (%, w/w)
Fresh *roots*	67.0	14.2
Sun-dried *roots*	65.0	25.7
Fresh pulps	8.8	4.7
Sun-dried pulps	6.8	1.9

Carbohydrate content of the roots and the pulps, determined by anthrone sulphuric acid assay (Dische 1967). D-glucose solutions of 100, 200, 300, 400, 600, 800 μg/mL were used to determine the

standard curve. The absorbance at λ= 620 nm was measured to determine the reducing sugar concentration of samples. The same volume of distilled water was used as control.

4.2.2.2. Amino acids Analysis

As shown in Table 4.3, of the 17 different amino acids detected in the roots, 5 are particularly abundant: aspartic acid, glutamic acid, lysine, arginine and proline. The content of arginine is remarkably high, at 3.59% of dry weight of fresh roots and 3.12% of sun-dried roots. In fresh roots, 39.49% of total amino acid is arginine. Within the arginine, about 85.51% of it is free amino acid.

The total amino acid content dropped from 9.09% to 8.18% after sun-drying. The amount of free amino acids decreased successively from 4.21% through to 3.87%, 1.69% and 1.16%, according to the strength of heating process, by means of sundry at 20~30°C, baking dry at 40°C and boiling at 100°C. Among the individual amino acids, arginine contributed the most dramatic decrease after the heating process, from fresh 3.07% (fresh) to boiled 0.67% (boiled).

As shown in Table 4.4, arginine is the most abundant amino acid in the fresh *Momordica charantia* pulps, which was 32.4% of their total amino acids and 59.3% of their free amino acids. The figures for their sun-dried counterparts were 33.8% and 51.8%, respectively. Arginine decreased progressively from 1.44% (w/w) to 0.47% and 0.24%, again according to the strength of heating process, by means of sun-drying at 20~30°C and boiling at 100°C.

As an alkaline amino acid, arginine is an active reactant in the Maillard reaction. Due to the particularly high proportion of this amino acid, arginine is presumed to make a major contribution to the formation of MRPs in RIE and MCE. This was why it was chosen for preparing the Arg-Glc MRPs used in this study as a simplified model to simulate the chemical compositions and biological functions of RIE MRPs and MCE MRPs.

The free amino acid of the roots decreased successively from 4.21% through to 3.87%, 1.69% and 1.16%, correlating with the strength of heating process, by means of sundry at 20~30°C, baking dry at 40°C and boiling at 100°C. Among individual amino acids, arginine accounted for the most dramatic decrease, from the fresh 3.07% to the boiled 0.67%. As an alkaline amino acid, arginine is one of the most active reactants in Maillard reaction. With its

extraordinary high content, arginine has been presumed to be one major source of RIE MRPs and MCE MRPs.

Table 4.3 Amino acid content of the fresh and sun-dried roots. *

Amino Acids	Total amino acids		Free amino acids			
	Fresh	Sun-dried	Fresh	Sun-dried	Baked	Boiled
Aspartic acid	0.65	0.57	0.08	0.07	0.04	0.03
Threonine	0.38	0.35	0.18	0.09	0.09	0.06
Serine	0.29	0.26	0.05	0.06	0.03	0.02
Glutamic acid	0.88	0.73	0.05	0.02	0.01	0.01
Glycine	0.26	0.26	0.01	0.01	0.00	0.00
Alanine	0.29	0.31	0.07	0.11	0.04	0.02
Cystine	0.03	0.02	0.01	0.02	0.00	0.00
Valine	0.38	0.38	0.07	0.10	0.05	0.03
Methionine	0.00	0.03	0.00	0.01	0.00	0.00
Isoleucine	0.24	0.23	0.03	0.04	0.02	0.01
Leucine	0.38	0.37	0.03	0.07	0.03	0.02
Tyrosine	0.12	0.12	0.01	0.02	0.01	0.00
Phenylalanine	0.24	0.22	0.02	0.05	0.03	0.01
Lysine	0.56	0.47	0.13	0.16	0.08	0.04
Tryptophan	—	—	—	—	—	—
Histidine	0.26	0.22	0.11	0.09	0.05	0.03
Arginine	**3.59**	**3.12**	**3.07**	**2.65**	**1.02**	**0.76**
Proline	0.53	0.51	0.29	0.31	0.17	0.10
Total	9.09	8.18	4.21	3.87	1.69	1.16

Table 4.4 Amino acid content of the fresh and sun-dried pulps.∗

Amino Acids	Total amino acids (%, w/w)			Free amino acids (%, w/w)	
	Fresh	**Sun-dried**	**Boiling**	**Fresh**	**Sun-dried**
Aspartic acid	0.31	0.10	0.32	0.07	0.02
Threonine	0.20	0.08	0.10	0.00	0.04
Serine	0.17	0.04	0.13	0.05	0.01
Glutamic acid	0.68	0.23	0.61	0.00	0.02
Glycine	0.13	0.05	0.18	0.01	0.00
Alanine	0.14	0.07	0.19	0.04	0.02
Cystine	0.05	0.01	0.03	0.00	0.01
Valine	0.19	0.06	0.11	0.09	0.03
Methionine	0.03	0.02	0.02	0.02	0.02
Isoleucine	0.12	0.03	0.08	0.05	0.01
Leucine	0.18	0.04	0.10	0.06	0.02
Tyrosine	0.13	0.03	0.05	0.05	0.01
Phenylalanine	0.19	0.05	0.09	0.12	0.03
Lysine	0.19	0.05	0.03	0.06	0.01
Tryptophan	–	–	–	–	–
Histidine	0.18	0.03	0.03	0.14	0.01
Arginine	**1.44**	**0.47**	**0.24**	**1.12**	**0.29**
Proline	0.12	0.04	0.05	0.02	0.01
Total	4.44	1.39	2.36	1.89	0.56

∗ Total amino acid and free amino acid contents of the *Isatidis* roots or the pulps of *Momordica charantia Linn.* were expressed as a percentage of the dry weight of pulps (%, w/w).

4.2.2.3. Analysis of monosaccharide and disaccharide

As shown in Figure 4.1, xylose, fructose, glucose, sucrose and maltose have been identified from fresh roots tissue, while glucose, fructose and maltose were identified from fresh *Momordica charantia L.* pulps by the same method. In both plants, glucose was the major monosaccharide (>40% of monosaccharides in the roots), while sucrose was the most dominant sugar in the roots. Fructose and glucose were almost equally rich in pulps of *Momordica charantia Linn*. Sucrose accounted for 65.9% of total monosaccharides and disaccharides of the roots, of which glucose accounted for 9.9%. Sucrose may be partially hydrolysed during the boiling water extraction, especially at acidic condition, to produce the equal molar amount of glucose and frutose. In summary, glucose is expected to make a major contribution to the formation of MRPs in both herbs.

4.2.2.4. Starch content determination

The starch content of fresh roots was determined with two dilutions of its cold-water extracts and gained a mean values of 31.1±1.0% (w/w). The hydrolysates of starch might also have contributed to the generation of MRPs during RIE's sun-drying and boiling processes.

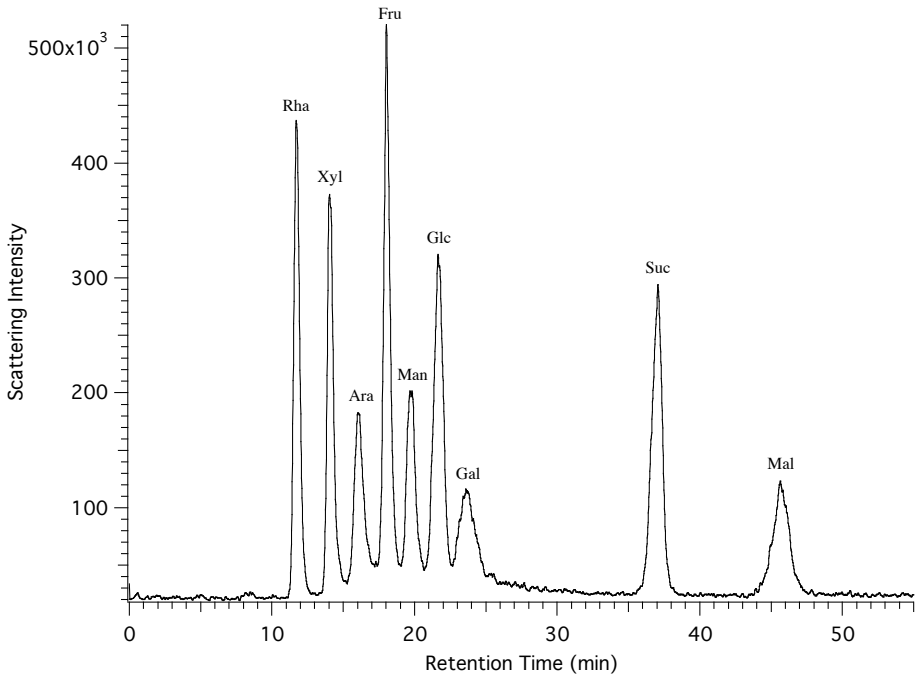

A

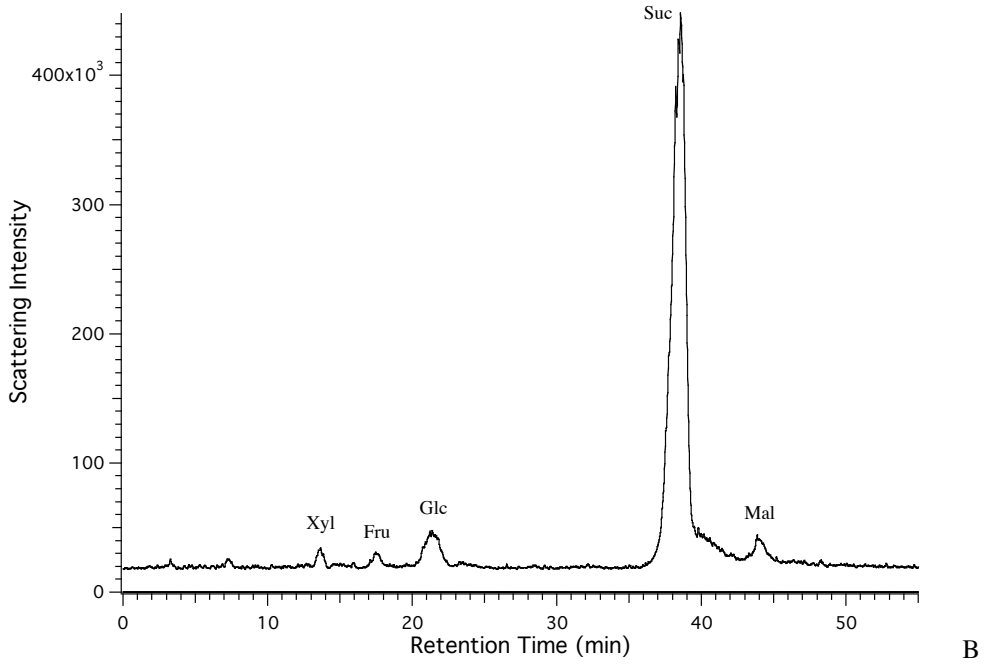

Figure 4.1 Analysis of monosaccharide and disaccharide content of the fresh roots by HPLC.

A. The chromatogram of standard sugars. Mobile phase: acetonitrile, ethyl acetate and deionized water (60:25:15, v/v). Flow rate: 1.0 mL/min. Injection: 10 μL. L-rhamnose, D-xylose, L-arabinose, D-fructose, D-mannose, D-glucose, D-galactose, sucrose and maltose were used as standard sugars, and are listed here in the sequence of their chromatographic peaks. **B.** The chromatogram of monosaccharides and disaccharides from the roots. Mobile phase: acetonitrile, ethyl acetate and deionized water (60:25:15, v/v). Flow rate: 1.0 mL/min. Injection: 10 μL. D-xylose, D-fructose, D-glucose, sucrose and maltose were identified and quantified, D-xylose: 0.17 mg/mL, D-fructose: 0.12 mg/mL, Dglucose: 0.21 mg/mL, sucrose: 1.40 mg/mL, maltose: 0.23 mg/mL, respectively. The retention times of these five sugars were: 13.66 min, 17.65 min, 21.77 min, 38.55 min and 43.86 min, respectively.

Table 4.5 Starch content of the fresh roots.*

Dilution Times	Mean of $A620_{nm}$	Starch Content (mg/mL)	Starch Content (%, w/w)*	Average (%)
200	0.54	313.92	31.4	31.1±1.0
400	0.26	308.5	30.8	

* The weight of fresh roots was used in the calculation. Experiment design and data analysis were performed by Lijing Ke; data was collected by Ms. Huiqin Wang.

4.2.2.5. Full-wavelength scanning of Arg-Glc MRPs

MRPs derived from the reaction between arginine and glucose was prepared as described in Section 4.2.1.9, and used in this study to simulate the functions of low molecular weight MRPs derived from RIE.

The full-wavelength (190 nm to 1000 nm) absorbance scanning was performed with Arg-Glc MRPs at serial concentrations. The solution of Arg-Glc MRPs at the maximum concentration of 600 mM presented a dark brownish colour, with the strongest absorbance at a wide range of wavelength, ranging from 190 nm to 900 nm. As the concentration reduced, the absorbance intensity decreased dramatically, particularly in the range of visible lights. At wavelength around 300 nm, MRPs at the low concentrations (1.9 mM and 0.5 mM) presented a single absorbance peak, which implies the double bonds of C=O (Fig 4.2).

As shown in Fig 4.3, the intensity of absorbance is proportional to the concentration of Arg-Glc MRPs at all the wavelengths and concentrations tested. Taking the intensities at 500, 600, 700 and 800 nm as examples, the concentration of MRPs is linear to the intensities. In Fig 4.4, absorbance spectra were compared between Arg-Glc MRPs and RIE MRPs. They look rather similar within the wavelength range of visible lights, in terms of intensity and curvature. This indicates that it is possible to determine the concentrations of MRPs derived from other sources with a concentration-absorbance standard curve of Arg-Glc MRPs. Among the 4 wavelengths above, 500 nm falls in the range of red-brown light, which is close to the colour of MRPs, with a fairly strong intensity. It was therefore chosen to estimate the concentration of MRPs derived from other resources, for example RIE and MCE.

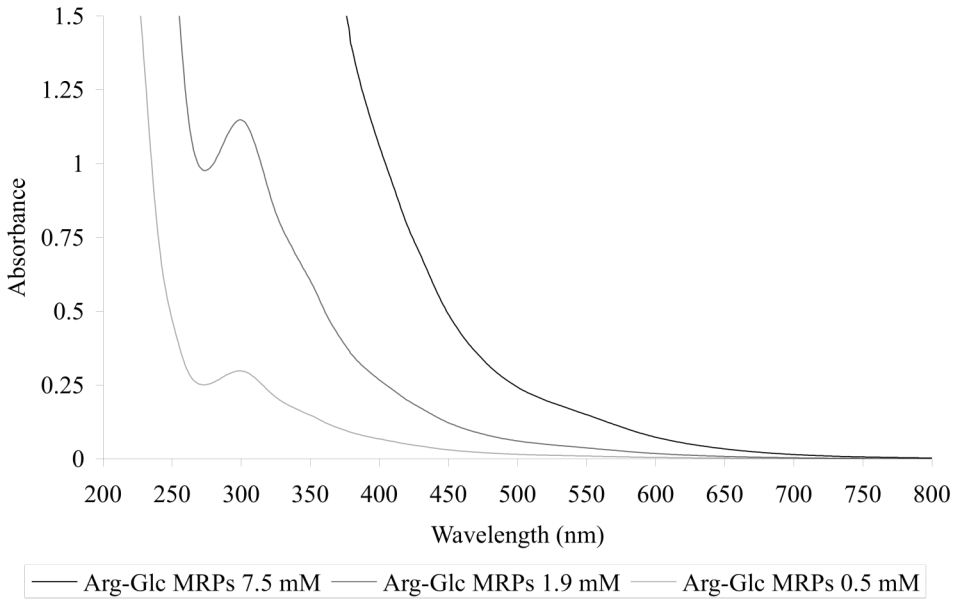

Figure 4.2 Full wavelength absorbance scan of Arg-Glc MRPs at 3 concentrations.

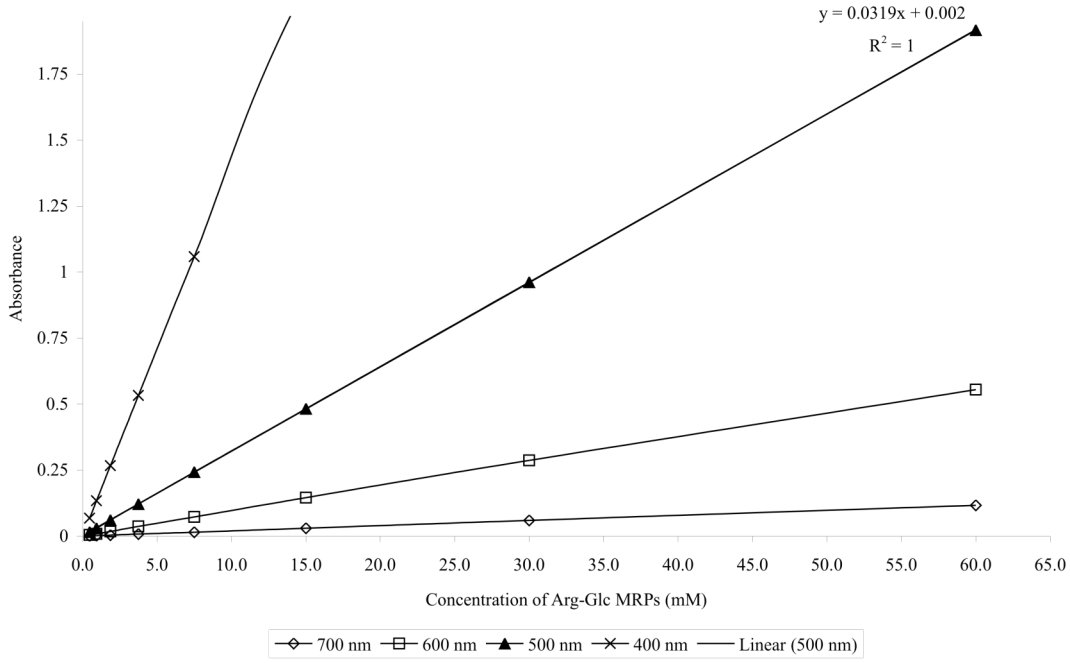

Figure 4.3 The concentration-response absorbance curves of Arg-Glc MRPs at 4 different wavelengths.

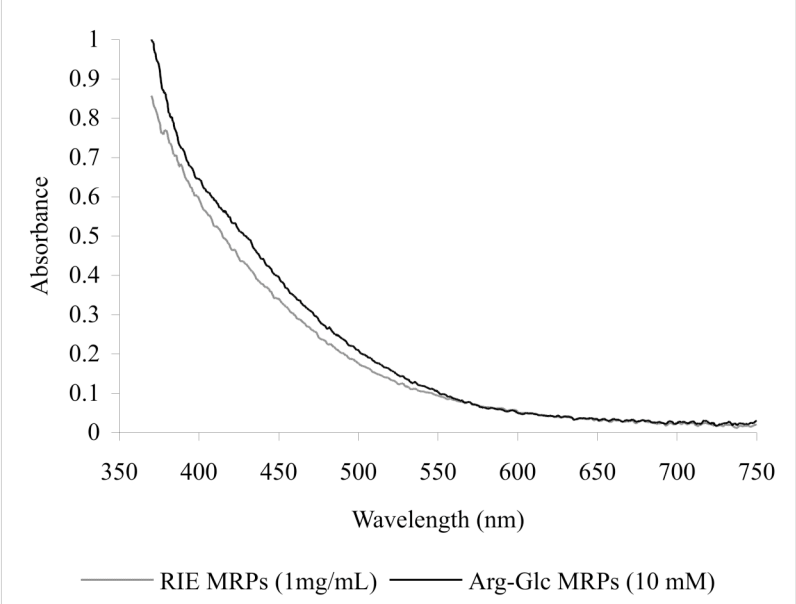

Figure 4.4 The absorbance curves of Arg-Glc MRPs and RIE in the wavelength range of visible light.

4.2.2.6. Determination of the un-reacted reactants in Arg-Glc MRPs

The Maillard reaction has to go through a highly complex reaction pathway until its end product, melanoidin, was formed. The rates of reaction could be managed by adjusting temperature, time, accessibility of water, pH, etc. It is possible to slow down the reaction by using reactants in powder form and reacting them in a controlled humidity. As described in the methods, Arg-Glc MRPs is prepared with arginine and glucose powder, with equal molar amount of them at 80% RH, 40°C, for 7 d. A part of the reactants might not have been consumed, and needs to be determined.

As shown in Table 4.6, 30.8% of arginine remained un-reacted after being incubated with equal molar amount of glucose. Two independent Arg-Glc MRPs samples were prepared under the same conditions, to ensure the accuracy of arginine quantification.

As shown in Table 4.7, 39.0% of glucose remained un-reacted in the Arg-Glc MRPs after the incubation. This is consistent with the remaining of arginine in Arg-Glc MRPs. To ensure the accuracy of measure, 10 mg/mL glucose was added as an internal standard into Arg-Glc MRPs solution. 38.5% of glucose was identified to remain un-reacted.

By summarying the data above, about two third of arginine and glucose actually reacted for generating Arg-Glc MRPs. The remaining arginine and glucose in Arg-Glc MRPs must be considered when the effects of Arg-Glc MRPs on lipid bilayer or cells are investigated. Argininen and glucose were used as controls in the neutron diffraction, X-ray diffraction and cell pathological studies.

Table 4.6 Content of arginine in Arg-Glc MRPs

	Original Arginine (mg/100mL)	Arg Remains (mg/100mL)	Percentage of Remains (%)
Arg-Glc MRPs 1	3484	1136.14	32.6
Arg-Glc MRPs 2	3484	1007.59	28.9
Average	3484	1071.87	30.8

Table 4.7 Content of glucose in Arg-Glc MRPs

	Arg-Glc MRPs 1	Arg-Glc MRPs 2	Arg-Glc MRPs+Glc 1	Arg-Glc MRPs+Glc 2
Concentration (mg/mL)	14.03	14.10	24.14	23.61
Average (mg/mL)	14.07		23.88	
Percentage of Remains	39.0%		38.5%*	

The content of glucose was measured by anthrone sulphuric acid assay.

* Calculated by subtracting 10 mg/mL from the measured mean value of Arg-Glc MRPs+Glc.

4.2.2.7. Purification of glycation-related proteins from the fresh roots

Water-soluble proteins were extracted with two types of solvent: pure water at the natural pH of roots, and PBS buffer (pH7.2). The protein compositions of both solution are identical, as shown in Fig 4.5. However, some significant differences were observed between fresh roots and sun-dried roots. As revealed by SDS-PAGE gel electrophoresis, protein bands of sun-dried roots are generally blurred and widened when comparing with those of fresh roots, which reflects the common occurrence of protein glycation (Eble, Thorpe & Baynes 1983). The widened bar of protein indicates the changes in molecular weight, possibly caused by cross-link between proteins and other reaction derivates. Proteins with molecular weights about 25 kDa, were targeted for purification due to their particularly high content in the roots and the significant degree of glycation. Since PBS buffer extract was slightly more concentrated than pure water extract, it was used for isolating the precursors of glycated proteins from the fresh roots.

Firstly, proteins were separated from the crude extracts of fresh roots by precipitation in 60% $(NH_4)_2SO_4$ solution. Protein precipitants were then dialysed to remove sulphate residues before applied to ion-exchange liquid chromatography. The dominant proteins were found in the second elution fraction of chromatographic separation, named as SP-P2, using SP-650M cation-exchange resin (Fig 4.6, Fig 4.8). SP-P2 was then separated to 8 elution fractions with reverse-phase liquid chromatograpy (RPLC) using C18 column. Among these fractions, three proteins were subsequently purified to electrophoretic homogeneity. They were named as *radix Isatidis* trypsin inhibitor proteins (RITIP) (Fig 4.7), because their amino acid sequences shared a high similarity with the trypsin inhibitor family from plants. As shown in Figures 4.8 and 4.9, their molecular weights are 26.8 kDa, 25.5 kDa and 24.6 kDa, respectively, which were calculated based on the R_f values of standards. They were named RITIP-1, RITIP-2 and RITIP-3 in order of decreasing molecular weight. Their purities were above 98.0%, as measured by high-performance size-exclusive liquid chromatography (TSK-GEL G3000SWXL) (data not shown, but available on request).

For tracking the Maillard reaction occurred during sun-drying, the glycoproteins in the roots extracts, the SP-P2 proteins and three purified glycation-relevant proteins RITIP1/2/3 were stained with PAS method firstly (Fig 4.10A), and then with Coomassie Blue (Fig 4.10B). The proteins of sun-dried roots were more intensively stained by PAS than those of fresh roots, which indicated a higher degree of glycation in sun-dried roots. Three purified proteins were also glycosylated or glycated to varying degrees.

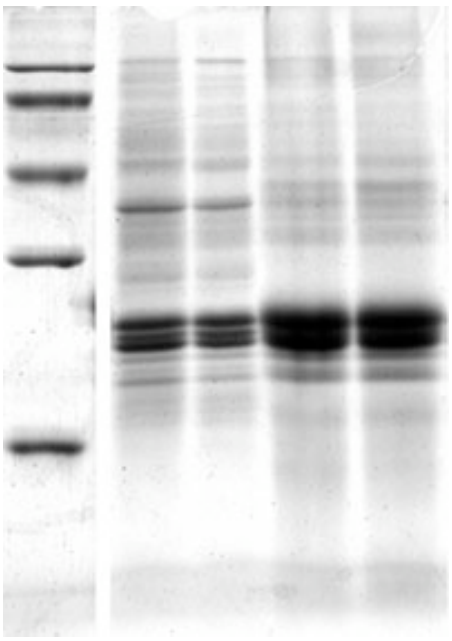

Figure 4.5 SDS-PAGE electrophoresis (12.5%) graphs of extracts and fractions of the roots.

M, markers; 1, PBS buffer extract of fresh roots (0.02M PSB+0.1M NaCl pH7.2); 2, water extract of fresh roots; 3, water extract of sun-dried roots; 4, PBS buffer extract of sun-dried roots (0.02M PSB+0.1M NaCl pH7.2).

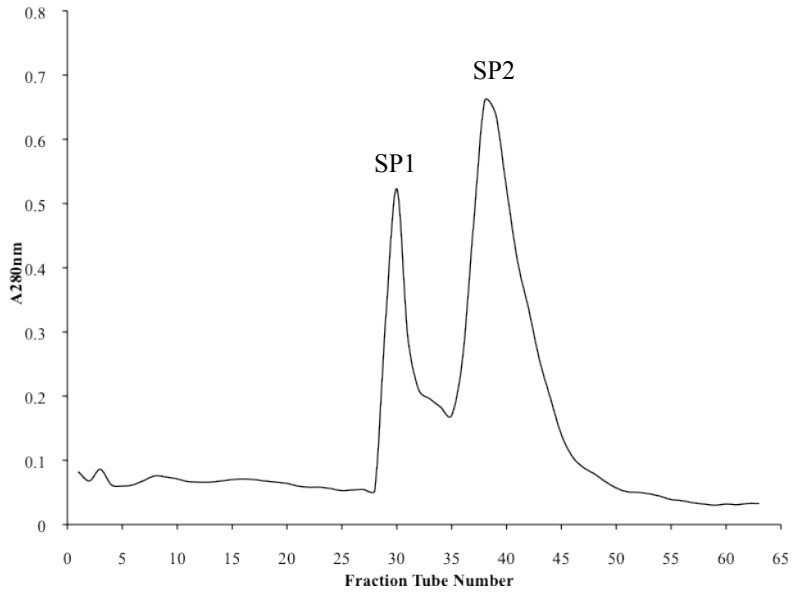

Figure 4.6 SP-650M cation exchange liquid chromatography of fresh roots extract.

Flow rate: 1 mL/min. Buffer: 0.02 M, pH3.0 Citric acid-sodium citrate buffer. Elution gradient: 0.5~1.0 M NaCl. Detector wavelength: 280 nm. Column: SP-650M 16 mm×100 mm. Fraction collector: 5 mL/tube.

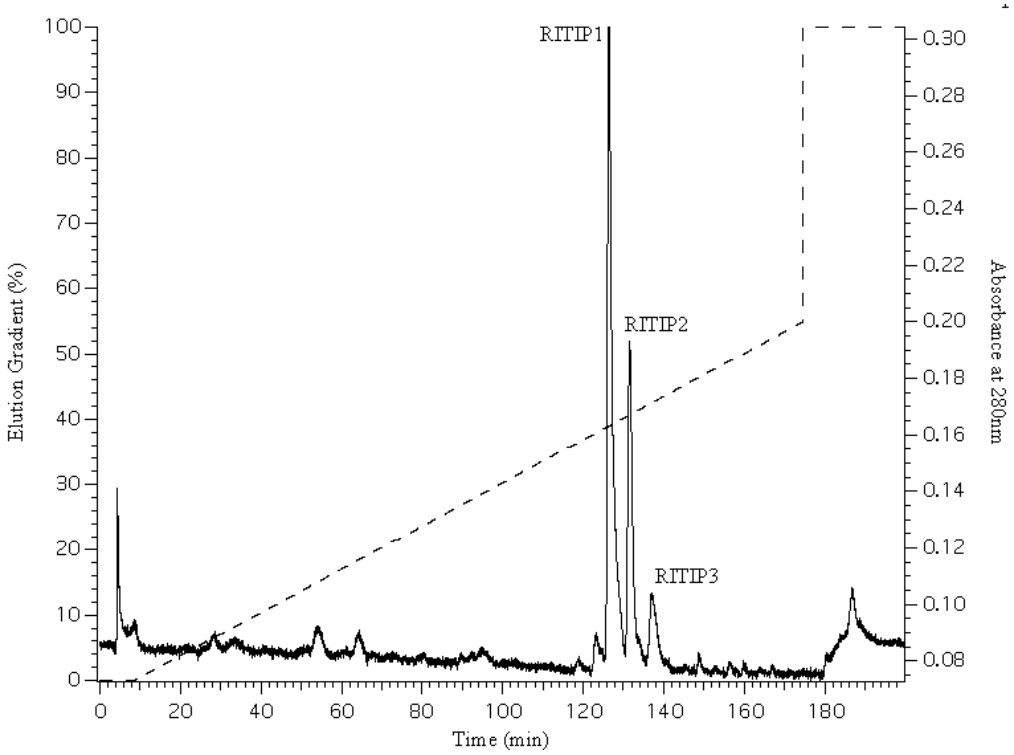

Figure 4.7 POROS R3 C18 reverse phase liquid chromatography of fresh roots extract.

Flow rate: 1 ml/min. Buffer: 0.1% TFA, 0~55% acetonitrile gradient. Detector wavelength: 280 nm; Column: POROS Oligo-R3 C18 4.6 mm×250 mm.

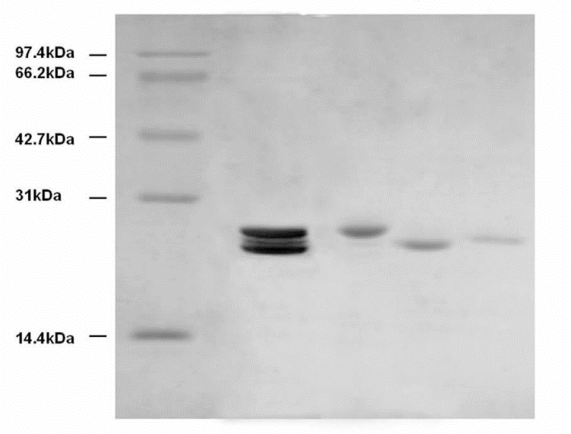

Figure 4.8 SDS-PAGE electrophoresis of purified proteins from roots.

Running Voltage: 120 V; Running gel: 12.5%; Coomassie blue staining. Marker: standard proteins. SP2: the SP2 fraction from cation-exchange chromatography.

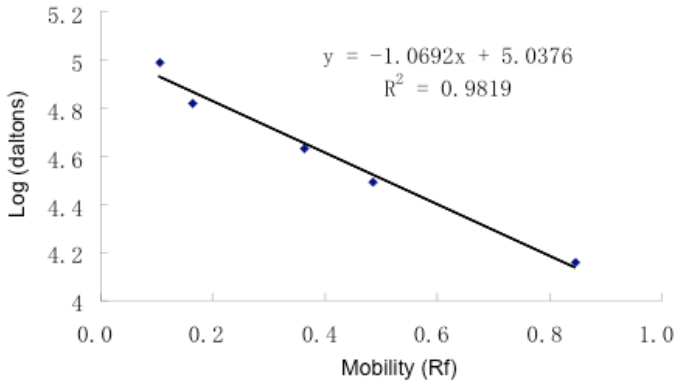

Figure 4.9 Standard curve for molecular weight calculation of proteins from the fresh roots

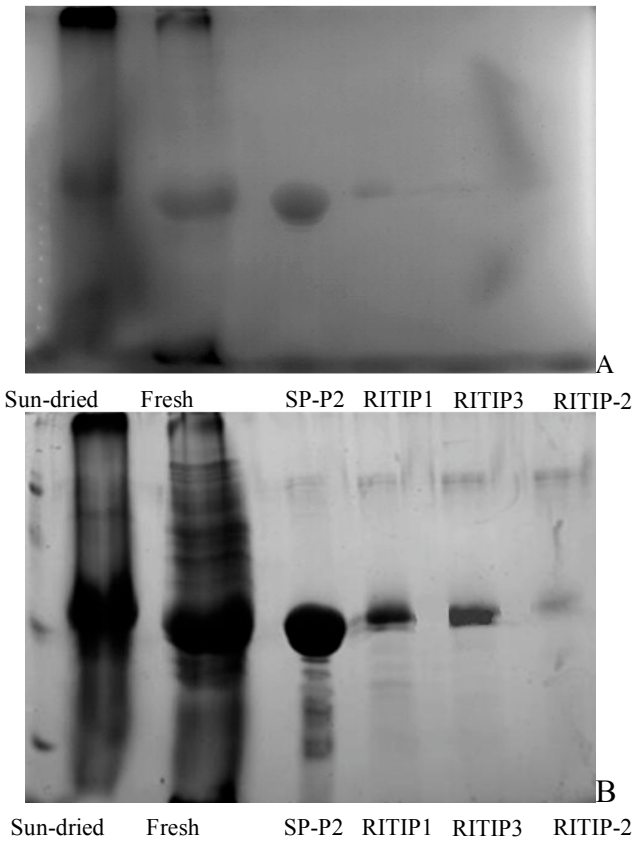

Figure 4.10 SDS-PAGE eletrophoresis of purified proteins from the fresh roots.

A. Periodic acid-Schiff (PAS) Staining. Running Voltage: 120 V. Running gel: 12.5%.
B. Coomassie blue staining. Running Voltage: 120 V. Running gel: 12.5%.

4.2.2.8. Purification of glycated proteins from sun-dried roots

In the previous section, three glycated RITIP proteins have been identified from the fresh roots extracts. To locate the chemically modified amino acids of these proteins caused by the Maillard reaction, their counterparts in sun-dried roots are required to be purified and identified. The purified proteins were used for the analysis on the glycation sites and types in Section 4.2.2.11.

The purification was following a similar protocol with purification of RITIP proteins. After $(NH_4)_2SO_4$ precipitation, soluble proteins from sun-dried roots were then separated by cation-exchange HPLC (Toyopearl SP-5PW). The target proteins were obtained in fraction P2, namely 5PW-P2 (Fig 4.11), which was further separated by RPLC method (POROS Oligo R3 C18). Two finely isolated fractions were obtained (Fig 4.12), and were identified as electrophoretic homogeneity (Fig 4.13). They were named GRITIP1 and GRITIP3 according to their molecular weights, which were 25.1 kDa and 22.5 kDa, respectively. Glycation of these proteins, including 5PW-P2, GRITIP1 and GRITIP2, was examined with PAS staining by SDS-PAGE electrophoresis. The results are shown in Fig 4.14. The bands of GRITIP proteins were blurred and expanded when stained with Coomassie blue. PAS staining presented a notable amount of carbohydrates on the proteins, indicating the progress in glycation or glycosylation of protein during the drying process.

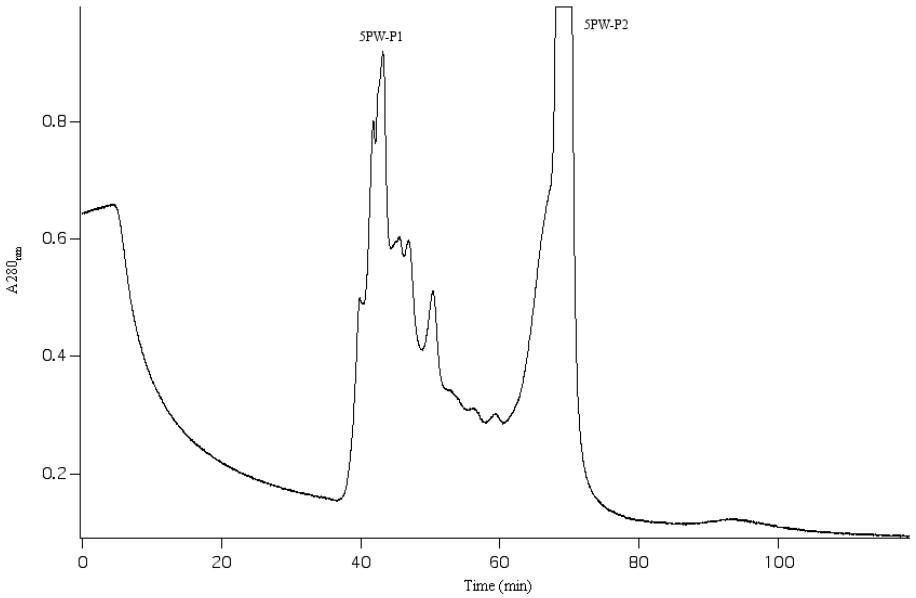

Figure 4.11 Cation-exchange liquid chromatographic separation of proteins from sun-dried roots.

Toyopearl SP-5PW cation-exchange column (4.6 mm × 250 mm). Sample loaded: 5 mL. Mobile phase 0.02M citrate buffer (pH4.0), elution gradient 0.02M citrate buffer (pH4.0) + 1 M NaCl, 60 min; flow rate= 1 mL/min.

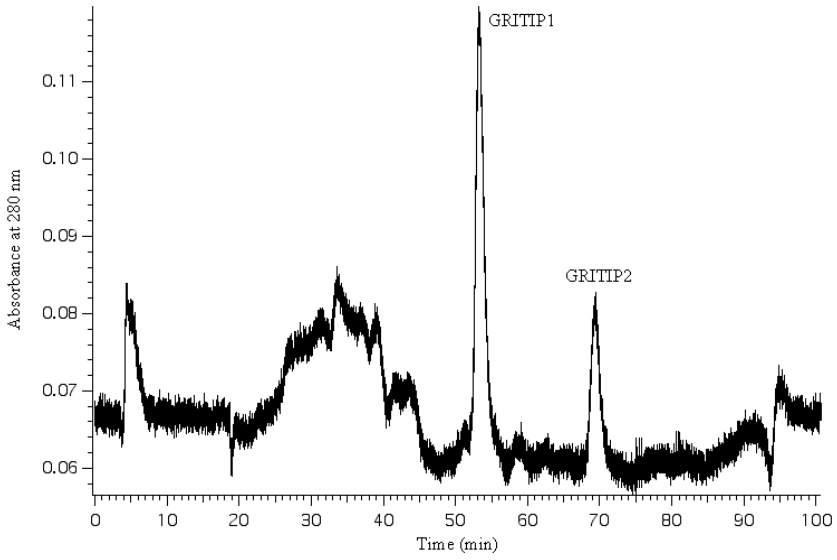

Figure 4.12 Reverse-phase liquid chromatographic separation of 5PW-P2 from sun-dried roots.

POROS Oligo R3 C18 reversed-phase column (4.6 mm × 150 mm); Mobile phase: solution A, 0.1% TFA; solution B, 0.1% TFA+ 80% CH_3CN; flow rate= 1 mL/min; detector, 280_{nm}; sample upload 5 mL; elution gradient, 0~100% in 120 min.

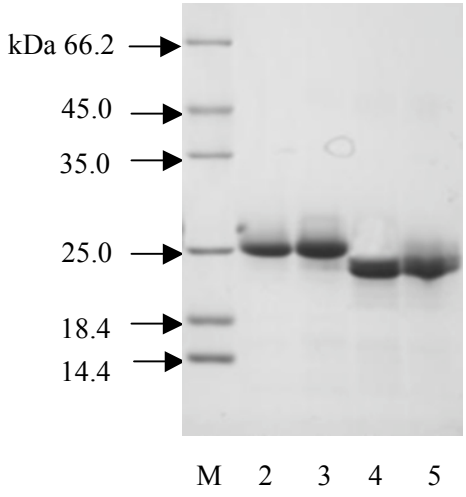

Figure 4.13 SDS-PAGE of glycated proteins purified from sun-dried roots.

M. Marker; 2. RITIP1; 3. GRITIP1; 4. RITIP3; 5. GRITIP3. Running Voltage: 120 V; Running gel: 12.5%; Coomassie blue staining.

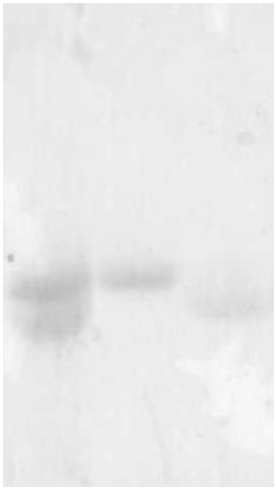

5PW-P2 GRITIP1 GRITIP3

Figure 4.14 SDS-PAGE of isolated glycated proteins from sun-dried roots stained with PAS assay.

Running Voltage: 120 V; Running gel: 12.5%; Periodic acid-Schiff staining.

4.2.2.8. Biochemical properties of purified proteins

Mass Spectroscopy

The precise molecular weight of RITIP1 was 22430 Da determined by Q-TOF MS, as shown in Fig 4.15. The molecular weight of RITIP1 determined by gel-electrophoresis was 26.8 kDa, which is about 4000 Da bigger than that from MS. The secondary structure and glycosylation of protein might contribute to the false result in gel electrophoresis. It also provides an example of differences in the molecular weights of proteins when determined by different methods.

Isoelectric Point of purified proteins

The isoelectric point (pI) of RITIP1 has previously been determined, by isoelectric focusing electrophoresis (IEF), to be 5.4. The pI of RITIP2 is 5.3 and that for RITIP3 is 5.4. In contrast, pI of GRITIP1 and GRITIP3 was 6.7 and 6.6. The pI of proteins from sun-dried roots was significantly higher than that of proteins from fresh roots. This implies that glycation decreases the electric charges on the surface of proteins.

4.2.2.9. Sequencing of purified proteins

The N-terminal sequences of two proteins, RITIP1 and RITIP3, were determined by Edman degradation (Table 4.8). In RITIP1, the first 9 amino acids were identified., while 19 amino acids in RITIP3.

The two proteins showed a high similarity in their amino acid sequences. Among the first 9 amino acids of both sequences, only the second amino acid is different, which is tryptophan in RITIP1 but valine in RITIP3. Valine, instead of arginine, took the highest proportion among amino acids of the proteins (Fig 4.17). This indicates that these RITIPs proteins do not make a major contribution to the high content of arginine, even as the dominant proteins in the roots. The N-terminal sequence of RITIP3 was used to design the primer for cloning gene of RITIP3, as reported in the next section.

4.2.2.10. Gene cloning and sequencing of purified proteins

This work was conducted under the collaboration with Dr. Jianwu Zhou and Mr. Guanzhen Gao from Institute of Biotechnology Fuzhou University. The gene cloning was conducted by

Dr. Jianwu Zhou and Mr.Guanzhen Gao. The sequence analysis was performed by the author.

According to analogous analysis of RITIP proteins with proteins from *Arabidopsis thaliana*, RITIP1 and RITIP3 are similar to proteins from a trypsin inhibitor family and were predicted to have antifungi activity (Table 4.9). Some proteins contain a similar sequence were listed here as reference.

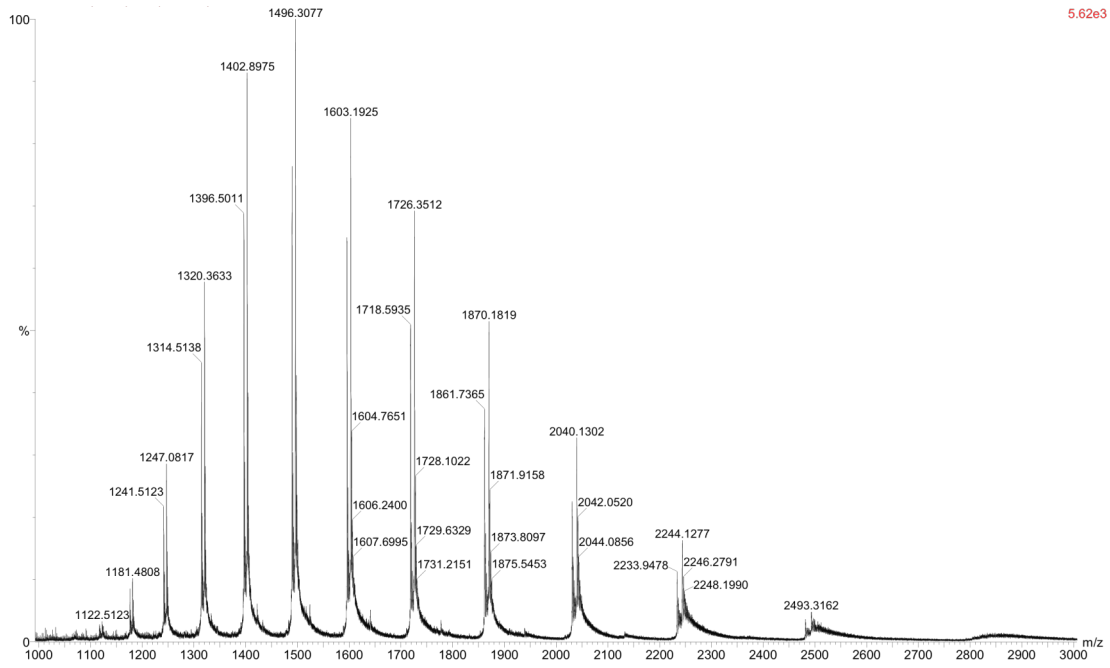

Figure 4.15 Q-TOF Mass Spectrum of RITIP1.

The MS measurement was performed by Dr. Chunteng Guo at Ulster University, North Ireland. Data analysis was conducted by the author.

Table 4.8 The N-terminal amino acids sequence of two purified proteins

Purified Protein	N-terminal amino acids sequence
RITIP1	VWREVVKDI
RITIP3	VVREVVKDIAGAVQTNEQY

The sequence of RITIP-3 was used to design the primer for gene cloning and obtained two cDNA sequences. There were only a few differences between these two sequences. One of these two sequences is presented here as an example, as shown in Fig 4.16. The full-length protein sequence (199 aa) of RITIP-3 was translated from the cDNA sequence (Fig 4.17).

The analogous analysis of RITIP-3 with proteins of *Arabidopsis thaliana* was conducted with BLAST programs, using default value. The results are presented below (Fig 4.18, Table 4.10). RITIP-3 is similar to the proteins from a family of Kunitz-type trypsin protease inhibitors in plants. RITIP-3 was anticipated to have protease inhibitory activity and used in the further enzymological studies, as shown in section 4.3. The potential function of RITIP-3 was predicted by BLAST and FASTA using EMBL and GENBANK databases (Last accessed on 10th June, 2007).

```
1                                                                   50
ATCGCCGGGG CCGTTCAAAC TAATGAACAA TACTTCATCC AACCGGTCAA
ATCTAACGGA GGTGGTCTTA TCCCACTCCC AGTTAAAGTT CCCCTTTGTC
CACTTGGCAT CAACCAAGTC TTCCGACGAG ATGTACCAGG CCTACCGGTT
AGCTTCGTAA ATCCATACCG GCCGTCGGTC GTGCACAACG TTTACACGAC
GGAGTTTGTA AACATCGAGC TCAAGCCGTC GTCCGACAAC GACTGGCCGG
TCTGCAAAGG GTTTTCCAAT TTATGGACAG TCGCTGGATC CTCATCCGCT
TCTGATGAGC CTCCGATTCT CGTCGGTGAT AAACAAGGAC ACAGCTATTT
TAAAATTGAG AGAGATGAAC ATTTTGTTGG AGGAAACGTT TACAAGTTGA
GCACCATCTT TGACGGAATC ATTGGAACCG TCCAAGGGCC GTTGTTAGGT
CTACCACAAC TAGTTCTCAC CACTGATACG GCAAAGACCT TACTCGTCAA
ATTCATCAAG GTTGAGAATG CTACTACTAC TTCTCGTGCT GGGAAGTTAG
GTCTAAGGAT GTTCCCACTC TACTAGTCAA CAAGCCAAAA ATCATGTAAC
GTAAAGCCTG AGACTCGTGA CTCGTCCATG GCCAAAATAA ATAATGGGTT
GAGATAATAT CTGCATGCAT GTACTTGAGC TTCCACAAAT AAAATCAAAT
TATGTTTTAC CAAAAAAAAA AAAAAAAAAA AAAAAAA
```

Figure 4.16 Full DNA sequence of RITIP3. (1 bp – 737 bp, direct) 737 bp

```
1                                                                   50
VVREVVKDIA GAVQTNEQYF IQPVKSNGGG LIPLPVKVPL CPLGINQVFR
RDVPGLPVSF VNPYRPSVVH NVYTTEFVNI ELKPSSDNDW PVCKGFSNLW
TVAGSSSASD EPPILVGDKQ GHSYFKIERD EHFVGGNVYK LSTIFDGIIG
TVQGPLLGLP QLVLTTDTAK TLLVKFIKVE NATTTSRAGK LGLRMFPLY
```

Figure 4.17 Full amino acid sequence of RITIP3. (1 aa – 191 aa) 199 aa

```
Query  4    EVVKDIAG-AVQTNEQYFIQPVKS---NGGGLIPLPVKV-PLCPLGINQVFRRDVPGLPV  58
            E VKD AG  + T EQYFIQPVK+   NGGGL+P  + V P CPLGI Q      PGLPV
Sbjct  25   EPVKDTAGNPLNTREQYFIQPVKTESKNGGGLVPAAITVLPFCPLGITQTLLPYQPGLPV  84

Query  59   SFVNPYRPSVVHNVYTTEFVNIELKPSSDNDWPVCKGFSNLWTVAGSSSASDEPPILVGD  118
            SFV      V   V T+  VNIE K    N WP CK FS  W V  SSSA  EP IL+G
Sbjct  85   SFVLAL--GVGSTVMTSSAVNIEFK---SNIWPFCKEFSKFWEVDDSSSAPKEPSILIGG  139

Query  119  KQG--HSYFKIERDEHFVGGNVYKLSTIFDGIIGTVQGPLLGLPQLVLTTDTAKTLLVKF  176
            K G  +S FKIE+       NVYKL+T F G +G + G  L  PQL++T DTAKTLLVKF
Sbjct  140  KMGDRNSSFKIEKAGEGARANVYKLTT-FYGTVGAIPGVWLSAPQLIITKDTAKTLLVKF  198

Query  177  IKVENATTTS  186
            KV++ATT +
Sbjct  199  KKVDDATTAT  208
```

Figure 4.18 Sequence comparison of RITIP3 with a trypsin/protease inhibitor from *Arabidopsis thaliana*.

4.2.2.11. Analysis of glycation sites of glycated proteins

This work was carried out in cooperation with Dr. Jianwu Zhou, Mr. Guanzhen Gao from Institute of Biotechnology Fuzhou University.

As previously described，three glycation-related proteins were isolated from the fresh roots. The full-length cDNA sequences of these two proteins were also obtained. Two glycated derivates of these proteins, namely GRITIP1 and GRITIP3 in the sun-dried roots were purified to electrophoretic homogeneity. The glycated proteins were subsequently digested by pepsin. The hydrolysates were analysed with RPLC-ESI/MS, for characterisation of glycated polypeptide segments. An online database searching tool, 'Peptidemap', was employed to simulate pepsin hydrolysis on RITIP3 and subtract the molecular weight of Maillard reaction products from the molecular weight of glycated proteins determined by MS.

The sequences of hydrolysed polypeptides from GRITIP3 were anticipated based on the full-length sequence of RITIP3, with the help of computer simulation of enzymatic hydrolysis. The results were manually matched to reveal the glycation sites and types of GRITIP3. Glycation sites on GRITIP1 were identified with the same method. In case of RITIP3 and GRITIP3, there were 37 peptides sequences finely matched. The coverage of these peptides on the full-length protein sequence was over 92% (Fig 4.19).

Glycation on arginine and lysine side chains of GRITIP1 and GRITIP3 was characterised with this method. In case of GRITIP3, K7 was modified to N_{ε}-carboxyethyl-lysine (CEL) or pyrraline (Pyr), K38 was modified to pyrraline (Pyr) or Fructosyl-lysine -1H_2O (FL-1H_2O), K171 was modified to Fructosyl-lysine -2H_2O (FL-2H_2O), R195 was modified to 1-Alkyl-2-formyl-3,4-glycosyl-pyrrloe(AFGP). In case of GRITIP1, R3 was modified to AFGP.

```
  1    VVREVVKDTA GNAVQTYEQY FIQPVKSNGG GLIPLPVKVP
 41    LCPLGINQVL RRDVPGLPVS FGNPYRPSVV HNVYTTEFVN
 81    IELKPSSDND WPVCKGFSNL WTVDGHSSAS DEPPILVGGK
121    PGHSYFKIER DEHFVGGNVY KLSTIFDGII GTVQGPLLGL
161    PQLVLTNDTA KTLLVKFIKV ENATTTSRAG KLALRMFPLY
```

Figure 4.19 The coverage of peptides hydrolysed from GRITIP3 on the full-length sequence of RITIP3.

Table 4.9 An analogy analysis of RITIPs with proteins from *Arabidopsis thaliana*

Protein	Amino acids sequence	Function
RITIP1	VWREVVKDI	Trypsin inhibitor/antifungi
RITIP3	VVREVVKDIAGAVQTNEQY	Trypsin inhibitor/antifungi
NP_565062/ AAG30988	QVVLDIAGHPVQSNVQY	endopeptidase inhibitor/tumor-related protein
AAC39370	REVVKDVA	trehalose-6-phosphate phosphatase
NP_001053370/AAG52092/ AAO22625/AAO42342	REVVKDVA	trehalose-6-phosphate phosphatase
NP_188110/BBA97055	REVVVSLDGDIAGAV	unknown protein
AAM61395	VREAVDDTAGA	chorismate mutase/ prephenate dehydratase
NP_187420/NP_974249/AAF13081/AAK92748/AAM45015	VREAVDDTAGA	chorismate mutase/ prephenate dehydratase
NP_180535/AAC35238/AAO42176/AAO63909	EIVKADEIAGAV	putative flavonol 3-O-glucosyltransferase
NP_850363/BAC43551	REVVRDI------KEQF	unknown protein
AAL87333	REVVKEI	unknown protein
AAF87852	REVVKEVA	unknown protein
NP_173640	REVVKEVA	catalytic/ trehalose-phosphatase
NP-173593/AAD41429	REVVKEI	unknown protein
NP_177874/AAG51662/AAN86155	REVVKEI	unknown protein

Table 4.10 The analogous analysis of full sequence of RITIP3 with proteins from *Brassica* and *Arabidopsis thaliana*.

Proteins	Organism	Sequence Length	Score (bits)
heat stress-induced protein	Brassica oleracea var. capitata	218 aa	165
water-soluble chlorophyll protein	Brassica oleracea var. acephala	212 aa	164
Kunitz-type cysteine protease inhibitor	Brassica oleracea var. botrytis	226 aa	162
BnD22 drought induced protein	Brassica napus	218 aa	159
Trypsin and protease inhibitor family protein / Kunitz family protein / drought-induced protein	Arabidopsis thaliana	215 aa	155

4.3. BIOACTIVITIES OF COMPOSITIONS OF THE ROOTS

4.3.1. Materials and Methods

4.3.1.1. Cell reparative activity

The 'cell reparative rate' was determined with Eq 4.1. The methods are described in Section 3.2.1.4 and 3.2.1.5. H1N1 influenza A viruses were used to infect MDCK cells.

$$Cells\ reparative\ rate\ (\%) = (O.D._{repair} - O.D._{virus})/(O.D._{normal} - O.D._{virus}) \times 100\%$$

Equation 4.1

4.3.1.2. Determination of cell proliferation rate

The 'cell proliferation rate' of Arg-Glc MRPs MDCK cells was determined with MTT assay (Mosmann 1983), as described in Section 2.2.2.3.

4.3.1.3. Trypsin inhibitor activity

As described in Section 2.2.2.9, the trypsin inhibitory activities of RITIP1/2/3 were determined by an improved BNPNA assay (Baker *et al.* 2009).

4.3.1.4. Haemagglutination inhibition activity

As described in Section 2.2.2.6 and Section 3.3.1.6, the anti-haemagglutination activities of Arg-Glc MRPs, RITIP proteins and GRITIP proteins were measured with chick erythrocytes. The concentration of stock solutions of RITIP and GRITIP proteins was 1 mg/mL. 9 dilutions of each sample were measured. The conventional anti-influenza virus medicines Ribavirin (50 mg/mL) and Amantadine (1 mg/mL) were used as a control.

4.3.2. Results

4.3.2.1. Inhibitory effects of Arg-Glc MRPs on virus-induced cell death

The effects of MRPs derived from amino acid compositions and protein compositions of the roots were determined respectively, to illuminate whether they are responsible for the

antiviral effects of RIE. The results of MRPs derived from amino acids, being represented by Arg-Glc MRPs, were presented here.

Arg-Glc MRPs was tested with MDCK cells after the attachment of virus to cells, by a modified method which was used in the previous chapter (Section 3.2.1.5). MRPs was added into the cell culture medium after the virus infection, and incubated with cells for 48-72 h. The results are shown in Fig 4.20. Arg-Glc MRPs inhibited the growth of influenza virus in MDCK cells. The maximum reparative rate was about 80% at 50 mM Arg-Glc MRPs. Along the concentration gradient, the activities of Arg-Glc MRPs declined quickly. There was no activity being observed at 6.25 mM and the lower concentrations.

Apart from the protection effects, Arg-Glc MRPs promoted the proliferation of MDCK cells (Fig 4.20). At the same concentration, where Arg-Glc MRPs inhibited virus the most, Arg-Glc MRPs boosted the growth of cells by nearly 50%. But this proliferation promoting activity declined along the dilutions of MRPs, and disappeared at 12.5 mM and the lower concentrations.

4.3.2.2. The trypsin inhibitory activities of RITIP proteins

As shown in Table 4.11, four different kinds of extracts were prepared and determined for the trypsin inhibitory activities. Cold-water extracts of fresh roots had the highest inhibitor activities, 41.5 TIU/mg in term of protein concentration. Sun-drying decreased the activity of cold-water extracts when increase the activity of boiling-water extracts. Boiling-water extraction decreased the activity of fresh roots, but increased that of sun-dried roots. The inhibitor activities, which were calculated as a function of protein or sugar concentration, are listed for comparison.

The trypsin inhibitory activities of RITIP proteins, and their heat stability and pH stability were studied by BNPNA assay (Fig 4.21, 4.22 & 4.23). The IC_{50} values of RITIP1, RITIP2 and RITIP3 were rather similar, and were 0.97 mg/mL, 1.07 mg/mL and 1.04 mg/mL, respectively. RITIP proteins gradually lost their inhibitory activities when temperature increased from 30°C to 70°C. The activities were stable under acidic conditions.

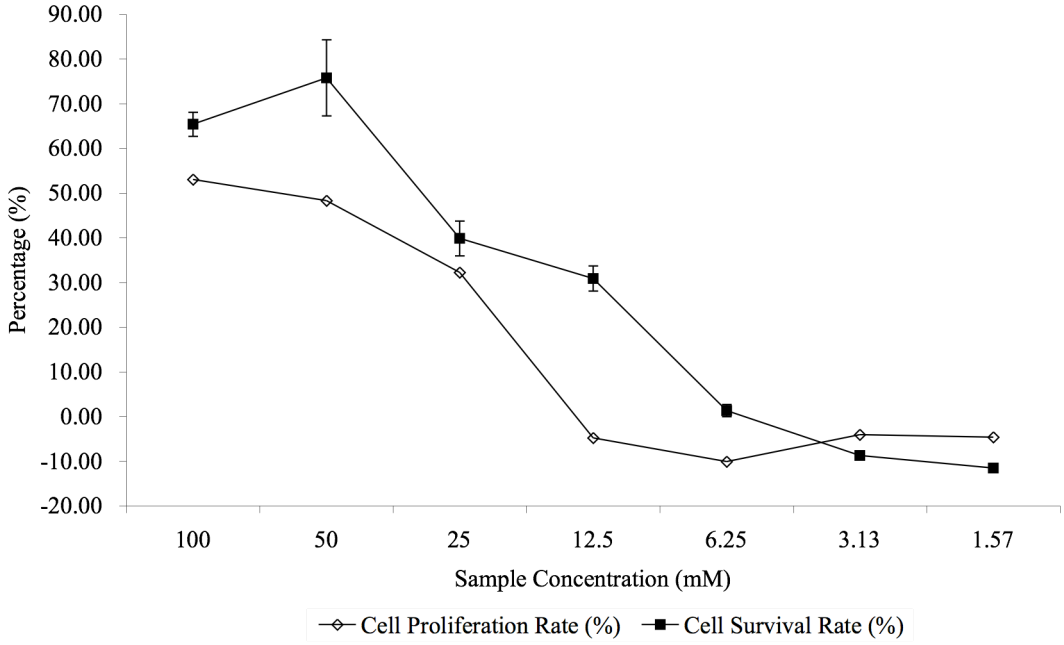

Figure 4.20 Effects of Arg-Glc MRPs on the proliferation rates of normal MDCK cells and cell survival rates infected by H1N1 virus. (n=4, P<0.01)

Table 4.11 Trypsin inhibitory activities of different extracts of the roots. *

	Trypsin Inhibitor Unit (TIU)	Inhibitor Activity (TIU/mg proteins)	Inhibitor Activity (TIU/mg sugars)
Cold-water extracts of fresh roots	82	41.5	9.9
Boiling-water extracts of fresh roots	11.9	14.3	3.2
Cold-water extracts of sun-dried roots	89	12.6	3.1
Boiling-water extracts of sun-dried roots	60.5	23.1	5.5

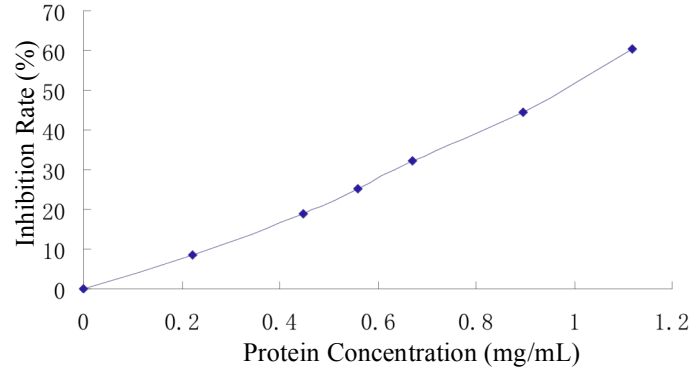

Figure 4.21 Dose-response curve of the trypsin inhibition activity of RITIP1*.

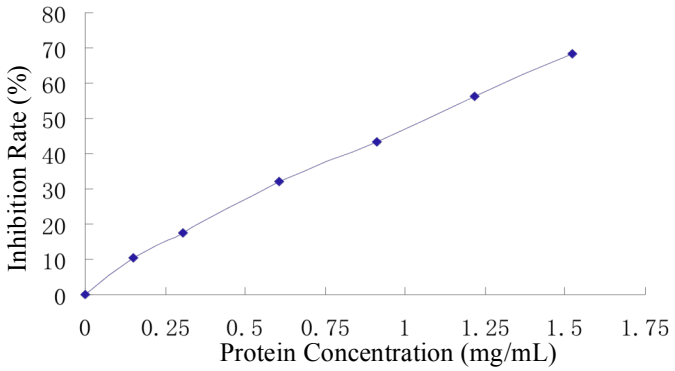

Figure 4.22 Dose-response curve of the trypsin inhibition activity of RITIP2*.

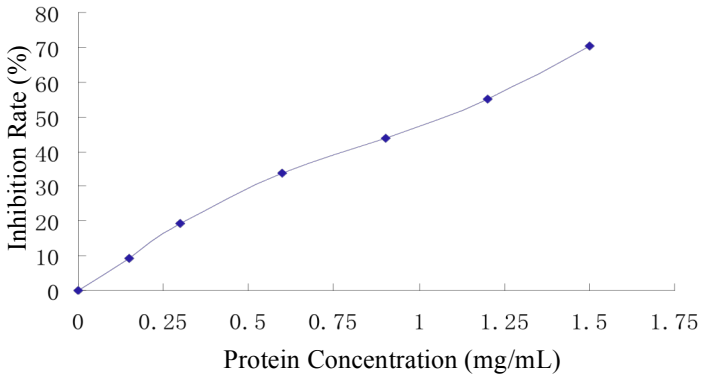

Figure 4.23 Dose-response curve of the trypsin inhibition activity of RITIP3*.

* This work was conducted under a cooperation with Mr.Huangzhao Xu from Institute of Biotechnology Fuzhou University. The data were collected by Mr.Huangzhao Xu; sample preparation and data analysis was carried out by the author.

4.3.2.3. Anti-haemagglutination activities of isolated proteins

The haemagglutination inhibition activity of RITIP proteins was also investigated with the same method decribed in Section 3.3.1.6. Arg-Glc MRPs did not inhibit the haemagglutination induced by influenza A virus H1N1, but inhibit that of H3N2 at a titre of 16.

RITIP proteins, as a mixture of three proteins RITIP1/2/3, slightly inhibited the haemagglutination induced by influenza A virus H1N1 and H3N2. The lowest effective concentration was 250 μg/mL. The titre of RITIP's haemagglutinin inhibitory activity was 4 on H1N1, 2~4 on H3N2. GRITIP proteins were weaker than RITIP in inhibitory effects.

Table 4.12 Inhibition of haemagglutination induced by influenza A virus (H1N1)

Samples	2	4	8	2^4	2^5	2^6	2^7	2^8	2^9	Titre
Arg-Glc MRPs	4+	4+	4+	4+	4+	4+	4+	4+	4+	< 2
RITIP proteins[1]	-	±	4+	4+	4+	4+	4+	4+	4+	4
GRITIP proteins[2]	1+	4+	4+	4+	4+	4+	4+	4+	4+	< 4
Ribavirin	-	4+	4+	4+	4+	4+	4+	4+	4+	2
Amantadine	1+	2+	4+	4+	4+	4+	4+	4+	4+	< 4

1: 'RITIP proteins' refers to SP-P2 chromatographic fraction of fresh roots extracts, can be considered as a mixture of RITIP1/2/3. The concentration of 'RITIP proteins' is 1 mg/mL.
2: 'GRITIP proteins' refers to 5PW-P2 chromatographic fraction of sun-dried roots extracts, can be considered as a mixture of GRITIP1/3. The concentration of 'GRITIP proteins' is 1 mg/mL.

Table 4.13 Inhibition of haemagglutination induced by Influenza virus A (H3N2)

Dilutions / Samples	2	2^2	2^3	2^4	2^5	2^6	2^7	2^8	2^9	Titre
Arg-Glc MRPs	—	—	—	—	4+	4+	4+	4+	4+	16
RITIP proteins[1]	1+	1+	4+	4+	4+	4+	4+	4+	4+	2~4
GRITIP proteins[2]	4+	4+	4+	4+	4+	4+	4+	4+	4+	2
Ribavirin	1+	4+	4+	4+	4+	4+	4+	4+	4+	< 2
Amantadine	—	—	—	4+	4+	4+	4+	4+	4+	8

1: 'RITIP proteins' refers to SP-P2 chromatographic fraction of fresh roots extracts, can be considered as a mixture of RITIP1/2/3. The concentration of 'RITIP proteins' is 1 mg/mL.
2: 'GRITIP proteins' refers to 5PW-P2 chromatographic fraction of sun-dried roots extracts, can be considered as a mixture of GRITIP1/3. The concentration of 'GRITIP proteins' is 1 mg/mL.

4.4. CONCLUSIONS AND DISCUSSION

In the roots of *Isatis indigotica Fort.*, proteins and saccharides are the major components. By adding them together, they contribute 80% of the dry weight. This figure does not change much in sun-dried roots. The water content of fresh roots and sun-dried roots are 59.6% and 12.2%, determined by Wang (Wang 2008). The soluble proteins concentration of cold water extracts of fresh roots and sun-dried roots are 2.6 mg/mL and 10.6 mg/mL, which are equal to 1.9% (w/w) and 2.2% (w/w) in dry weight of roots. As Wang reported, while the roots was incubated at 60°C for serial of time, the proportion of soluble proteins increased accordingly. This indicates an increase in the solubility of proteins, induced by Maillard reaction occurred during the heat incorporated process.

Arginine is dominant in the free amino acids, and an active reactant of Maillard reaction. Its concentration dropped dramatically after sun-drying and boiling, while the absorbance constantly increased at the range of visible lights wavelength, indicating the occurrence of an intense Maillard reaction (Hofmann & Heuberger 1999) (Morales & Jiménez-Pérez 2001).

As determined by an HPLC method, glucose is the major reducing monosaccharide in the roots, participating in the formation of amino-acid-MRPs and glycated proteins. The high content of sucrose and starch in the roots may help to aid the rapid consumption of reducing sugars in Maillard reaction. These saccharides can be degraded to reducing monosaccharides by enzymatic or acidic hydrolysis at a physiological temperature, or at the higher temperature employed in heat processing of roots (Echeverria 1990) (Echeverria & Burns 1989). Glucose is engaged as a representative of reducing sugars from the roots in this study.

Arginine and glucose were therefore chosen for a model MRPs for further studies, namely Arg-Glc MRPs. The concentration of Arg-Glc MRPs is linear with the visible lights absorbance at 500 nm. The wavelength is used for estimating the concentration of unknown MRPs. However, about 31% of arginine and 39% of glucose remained not reacted in Arg-Glc MRPs, even after a long time of reaction (7 d) or at a high reaction temperature (100 °C). The influence of arginine and glucose remained in Arg-Glc MRPs need to be cancelled out for revealing the real biological impacts of MRPs. In the later biophysical studies of MRPs, including analysis of phase transition energy consumption and positioning of MRPs on phospholipids bilayers, the influences of arginine and glucose were examined and subtracted.

Arg-Glc MRPs prevented the death of 80% of MDCK cells by inhibiting the replication of H1N1 viruses and promoting cell proliferation in due course, at a high concentration (50 mM). Arg-Glc MRPs shared similarity in chemical origin with RIE MRPs, and improve cell survival rates against virus infection. However, RIE MRPs remained highly effective to MDCK cells at a relative low concentratioin of 1 mg/mL (dry weight of roots), when the concentration of Arg-Glc MRPs is about 15 mg/mL (an estimated value based on 50 mM arginine and 50 mM glucose). Although it requires a much higher concentration for its efficacy, Arg-Glc MRPs still fairly represent some physiological functions of MRPs derived from the roots. Its cell membrane protective effects need a further study with other experimental methods. The effective compositions of Arg-Glc MRPs have not been isolated and identified.

Besides the MRPs derived from amino acids and reducing sugars, glycated proteins form another class of MRPs that need to be investigated. Three glycation protein precursors, namely RITIP1/2/3, were isolated from the fresh roots. Two genes of these proteins were cloned, and the full-length cDNA was sequenced by using N-terminal amino acid sequence of RITIP3 as template for primer design. RITIP protein sequences are homologous with a trypsin inhibitor family.

The trypsin inhibitory activity of RITIP proteins was determined at different concentrations of protein, temperature and pH, as a mixture and as a purified single compound. The heat-involved process generally decreased the activities, with an exceptional increase in the boiling-water extract of sun-dried roots. Heat processing, either in a dry (sun-drying) or aqueous substance (boiling-water extraction) can denature the proteins and cause the decline in protease inhibitory activity (DiPietro & Liener 1989) (Jiao *et al.* 1992). The glycation, in which glucose is incorporated, has been reported to decrease the protease inhibitor's activity in several trypsin inhibitor families (Kato & Matsuda 1997), and in the plasma protease inhibitor, i.e. heparin-cofactor II (Ceriello *et al.* 1990). My measures on the glycation caused by sun-drying were consistent with the finding above, whereas the glycation of boiling-water extraction caused an opposite consequence: an increase in the inhibitory activity. The mechanism behind this remains unclear.

The IC_{50} values of RITIP1/2/3 were almost the same, about 1 mg/mL. The proteins were tolerant to acidic environment. The similarity in inhibitory activities of RITIP proteins is consistent with their homogeneous amino acid sequences. The trypsin inhibitors have also been known as potential antifungal agents (Cowan 1999). The antifungal activities of RITIP

proteins were examined by Gao *et al.* (Gao *et al.* 2008). RITIP proteins showed significant antifungal activity on 3 out of 20 strains of addressed fungus. These experimental results supported the assumption that RITIP proteins are members of the trypsin inhibitors / antifungal proteins family. The proteins may play a role in the defending system of the plant against microorganisms.

The protease inhibitors have been massively studied as an antiviral or anti-influenza virus agent (Lamarre *et al.* 2003) (Patick & Potts 1998) (Serkedjieva 2009). RITIP proteins are about 25 kDa, and will easily be denatured by the heat-involved process, i.e. boiling water extraction. These inhibitors, at least their active core domains, would have to be resistant to pepsin hydrolysis to reserve the integrity of the secondary structure which is obligated for delivering the inhibitory effects. Furthermore, these protease inhibitors have to be absorbable to human digestive system. These two properties would be vital for RITIP proteins to deliver their clinical efficacy, if there is any. Therefore, it is difficult to anticipate antiviral effects of RITIP proteins in their native form.

The anti-haemagglutination activities of RITIP proteins and GRITIP proteins were determined with erythrocytes by measuring the virus titres. RITIP proteins inhibited the haemagglutination at 250 μg/mL or higher concentrations while the glycated counterpart, GRITIP proteins, conducted the weaker inhibitory effects. The anti-influenza virus activities of RITIP proteins and GRITIP proteins were determined with cultured MDCK cells by Wang *et al* (data not shown, but available on request). Both samples inhibited H1N1 viruses infection or replication at the much lower concentrations than those of haemagglutination inhibition, ranged from 2.0 μg/mL to 12.5 μg/mL, when they were introduced to the viruses attached cells. RITIP presented a stronger inhibitory effect than GRITIP, which is in an agreement with the anti-haemagglutination activity. These proteins are different from RIE in the way of conducting the antiviral effects. RIE conducts the cell protective effects while RITIP and GRITIP proteins performing cell reparative effects. The anti-influenza virus activities of these proteins need further investigations on the individual purified protein, by measuring the proliferation rates interfering with viral infection, and by plaque reduction assay.

Since none of these proteins was directly from RIE, which is the boiling-water extracts of sun-dried roots, they are hardly the representative of RIE MRPs for the biophysical studies. In contrast, being prepared through an intensive heating process with two pure active reactants, Arg-Glc MRPs represent the much more advanced products of Maillard reaction

than GRITIP proteins. It was used in the studies later due to its chemical similarity with RIE MRPs.

Two glycated proteins, GRITIP1 and GRITIP3 were purified from the sun-dried roots. The molecular weights of these two glycated proteins were approximately 25.1 kDa and 22.4 kDa. Their pI values were 6.58 and 6.68. They are very similar in terms of molecular size, amino acids seuqence and electric charge. Revealing by PAS staining, these two proteins presented the higher degree of glycosylation than their native forms, indicating that they had reacted with reducing sugar to generate non-enzymatic glycosylation (glycation) residues on the surface of proteins. Several lysine and arginine residues were identified as glycation sites on both of proteins. However, it would be totally different situation when it comes to the glycated proteins in RIE, which is highly glycated by a violent heating process. By doing the analysis on GRITIP proteins, the method of locating and identifying glycation sites and residuals was established and ready to be applied on the analysis of other glycated proteins from Chinese medicine.

CHAPTER 5

STABILISING EFFECTS OF MRPS ON ERYTHROCYTES PLASMA MEMBRANE

5.1. AIMS AND INTRODUCTION

The anti-influenza virus activities and cell protective effects of MRPs have been examined in the previous chapters, in terms of for their biochemistry. The interaction between MRPs and cell membranes is thought to be the preliminary mechanism of these activities. Various membrane components, such as proteins, lipids, polysaccharides, could be the targets of MRPs' actions.

As discussed in the last chapter, Arg-Glc MRPs inhibited haemagglutination by binding to erythrocytes, thereby improved the viability of MDCK cells against influenza viruses. Does the interaction between Arg-Glc MRPs and cells enhance the mechanical strength of phospholipid bilayer, or that of the plasma membrane of living cells? To address this question, the effects of Arg-Glc MRPs on the integrity and mechanical strength of cell membrane need to be tested. Two haemolysis models were introduced here for this purpose, to observe the influence of Arg-Glc MRPs on the stability and elasticity of erythrocyte membranes.

5.1.1. Hypotonic haemolysis

The semipermeable lipid membrane separates the red blood cells from the aqueous environment, but allow some solutes (usually small molecule like sodium chloride) to pass through driven by osmosis. This allows the adjusting of the solutes concentration gradient between intercellular solution and intracellular plasma. The behaviour of erythrocytes varies in the hypotonic, isotonic and hypertonic solutions (Tatsumi, 1981). 1) Erythrocytes remain in their normal size and biconcave shape in an isotonic solution, 0.9% NaCl solution for example. 2) In a hypertonic solution, the increased osmolarity (400 mOs or higher) forces water to flow out of the cells, and causes the cells to collapse or form the spiky appearance. 3) In a hypotonic solution, i.e. at 200 mOs or lower, water flows into the erythrocytes and causes the cells to undergo swelling and bursting (Saari & Beck, 1975). The cell contents, including haemoglobin (red coloured) and lactate dehydrogenase, are then released to the solution. The degree of haemolysis therefore can be monitored by measuring the content of these cellular proteins in the supernatant.

The possible stabilisation effects of Arg-Glc MRPs on lipids bilayers can be evaluated by measuring the resistance of erythrocytes to hypotonic pressure in the presence of Arg-Glc MRPs. In this approach, the erythrocytes are suspended in saline at various concentrations. Low osmotic pressure is introduced with diluted saline. The leakage of cell plasma was measured by two methods: lactate dehydrogenase assay and the absorbance at 540 nm.

5.1.2. Temperature dependence of haemolysis

Mammalian blood, from human or rodent sources suffers from spontaneous haemolysis when it is heated above the normal body temperature, even by a small temperature rise, such as that caused by fever (Gershfeld & Murayama, 1988). Various mechanisms have been proposed for the thermally-induced haemolysis, including: 1) denaturation of vital enzymes and proteins; 2) formation of haemolytic agents in cell plasma; 3) structural transition of plasma membrane lipids, i.e. gel-liquid crystal transition or lamellar-to-nonlamellar structure transition.

The former two mechanisms, however, are irrelevant to the haemolysis induced by the modest heating of fever. Enzymes and structural proteins are rather stable at a few degrees higher than the physiologically preferable temperature of 37°C. Enzymes like ATPase even present their optimal activities at temperature of 42°C (Brandts *et al.* 1978). The severe loss or irreversible changes in enzyme activity or protein structure only occurred if more extreme temperatures were applied, i.e. temperature > 60°C, for a prolonged time. Even if the potential denaturalisation at the lower temperature occurred, their negative effects on the cell function can also be minimized by the heat shock proteins/chaperonins (Sigal 2002). At the experimental conditions of this study, erythrocytes were exposed to supraphysiological temperature (56°C) only for a short period (30 min). Loss of enzyme activity or denaturalization of protein was unlikely to make a major contribution to haemolysis. Thus, structural transformation of membrane lipids may play an important role in heat-induced haemolysis.

Furthermore, the structural transformation can include gel-liquid crystalline phase transition and lamellar-nonlamellar phase transition. Since the transition temperature of the gel-liquid crystalline phase for erythrocytes membrane lipids is far below 37°C (Gershfeld & Murayama 1988) (Gottlieb 1974), the melting of the lipid bilayer cannot be responsible for inducing haemolysis at temperatures above 37°C. On the other hand, the formation of nonlamellar structure of membrane lipids could account for the haemolysis induced by mild heating.

The non-lamellar structures of lipid vesicles, including inverted cubic phase (Q_{II}) or inverted hexagonal phase (H_{II}), are the key intermediates of some important biological processes like endocytosis and virus-induced membrane fusion. Membrane lipids with small head-groups and unsaturated fatty-acid tails, e.g. DOPE, are readily form non-lamellar structures. As

revealed by studies using lipid vesicles composed of more than one species of synthetic phospholipids, the accumulation of unsaturated lipids (i.e. DOPE) in microdomains, resulted in an uneven distribution of lipids across the lipid bilayer. This reassortment of lipid can assist the formation of non-lamellar structures (Morein *et al.* 1996); Rietveld & Simons, 1998). A similar process would occur in the lipid membrane of living cells, like erythrocytes, if the environmental temperature of cells exceeded the lamellar to non-lamellar phase transition temperature of their major lipid components.

The major lipid components of human erythrocyte membranes are cholesterol (45 mol%), phosphatidylcholine (17 mol%), sphingomyelin (17 mol%), phosphatidylethanolamine (16 mol%) and phosphatidylserine (6 mol%) (Yeagle 1993). The phospholipids are asymmetrically distributed across the bilayer. Sphingomyelin and phosphatidylcholine are located primarily in the outer leaflet while phosphatidylethanolamine and phosphatidylserine are located in the inner leaflet (Schrier *et al.* 1983).

The non-lamellar phase transition temperature, above which the lamellar structure of cell membrane starts transforming to non-lamellar structure, is usually higher than the gel-liquid crystal transition temperature (Gershfeld 1993). The plasma membrane of human and chicken erythrocytes is optimally stable below this temperature, which is around 37°C. Although the erythrocyte's lipid bilayers can accommodate a minor rise in temperature with the aid of their cytoskeletons, and change their shapes, there is limit. When the temperature exceeds this limit, the lipid bilayers would be destablised and cells would undergo haemolysis. This response occurs as a function of time and temperature (Gershfeld & Murayama 1988). At temperature lower than 45°C, it took 5-10 h to see a significant haemolysis, whereas it only took 20 min to trigger a haemolysis at 54.5°C (Abe *et al.* 1981). Therefore, incubation of erythrocytes at a temperature higher than 37°C, in case of human or chicken, will cause a thermally induced destabilisation of the membrane and haemolysis. The degree of haemolysis can be used as an indirect parameter for evaluating the lipid bilayer stabilising activities of haemolysis inhibitory agents.

5.2. Methods and Materials

5.2.1. Inhibition of hypotonic haemolysis

The hypotonic haemolysis was performed with Seeman's protocol (Seeman 1967). 154 mM NaCl (equal to 0.9%, w/w) was dissolved in distilled water to make the isotonic solution, or 'normal saline'. Blood was donated by healthy volunteers and the erythrocytes extracted. EDTA was used as anticoagulant. Erythrocytes were separated from blood by centrifuging at 350 g for 5min, and washing with normal saline three times. Cells were re-suspended in isotonic normal saline to make a 1% suspension for all the tests. 1mL of 1% erythrocyte suspension was centrifuged at 350 g for 5 min, and the supernatant was removed. Cells were re-suspended evenly in 1mL normal saline containing Arg-Glc MRPs and Arg+Glc at various concentrations.

Arg-Glc MRPs was tested for their inhibition effects on hypotonic haemolysis, at serial concentrations of 0.24, 0.47, 0.94, 1.88, 3.75, 7.50, 15.0, 30.0 mM. Mixed solutions of arginine and glucose at the same concentrations were used for control. The hypotonic environment was created by diluting normal saline to 0% and 0.45% NaCl. Serial concentrations of NaCl have been used to impose differential hypotonic pressure on cells. 0.45% NaCl efficiently induced haemolysis and was chosen as the working concentration for measuring the inhibitory effects of the MPRs.

In order to measure the inhibition of hypotonic haemolysis, erythrocytes were incubated with samples for 2.5 h at 37°C, prior to exposure to low osmotic pressure. The cell suspension was stirred every 15 min to maintain an even distribution of cells. The cells were collected by centrifuge and washed with normal saline three times after incubation with samples. Cells were then re-suspended in hypotonic 0.45% NaCl saline for 1 h at 37°C, before the supernatant was tested for lactate dehydrogenase (LDH) activity and absorbance at 540 nm, which relates to haemoglobin concentration (Souri *et al.* 1996).

The inhibition rate of each material on hypotonic haemolysis was calculated according to the Eq 5.1.

$$Inhibition\ rate\ (\%) = \{1 - \left[\frac{A_1 - A_2}{B_1 - B_2}\right]\} \times 100 \qquad \textbf{Equation 5.1}$$

A_1: $OD540_{nm}$ or LDH activity of the sample in hypotonic solution

A_2: $OD540_{nm}$ or LDH activity of the sample in isotonic solution

B_1: $OD540_{nm}$ or LDH activity of the control in hypotonic solution

B_2: $OD540_{nm}$ or LDH activity of the control in isotonic solution

5.2.2. Lactate dehydrogenase (LDH) assay

As an abundant component of erythrocytes, LDH has been regularly used as a bio-marker of cell breakdown (Kraus, 1964 Science; Xue & Yeung, 1994). The haemolysis induced by hypotonic stress leads to a dramatic increase in LDH levels in the supernatant of the erythrocyte suspension, which can be quantified measurment of LDH activity.

The reagents were added and mixed evenly at room temperature for 3 min, as described in Table 5.1. The absorbance of each tube was measured with 1 cm diameter cuvettes at 440 nm, using distilled water as the background control. The LDH activities were calculated from absorbance readings according to the Eq 5.2.

$$LDH\ Activity\ (U/L) = \frac{\left(O.D._{Sample} - O.D._{Sample\ Blank}\right)}{\left(O.D._{standard} - O.D._{standard\ Blank}\right)} \times standard\ (2\ mmol/mL) \times 1000\ mL$$

Equation 5.2

Table 5.1 Protocal of LDH activity measurement

	Standard	Blank Control of Standard	Sample	Blank Control of Sample
2 μmol/mL Pyruvic Acid (mL)	0.02	—	—	—
Water (mL)	0.13	0.15	—	0.05
Sample (mL)	—	—	0.1	0.1
Matrix Buffer (mL)	0.25	0.25	0.25	0.25
NAD+(mL)	—	—	0.05	—
	Mixed evenly, 37°C, 15 min			
2,4-Dinitrophenylhydrazine (mL)	0.25	0.25	0.25	0.25
	Mixed evenly, 37°C, 15 min			
0.4 M NaOH (mL)	2.5	2.5	2.5	2.5

5.2.3. Inhibition of heat-induced haemolysis

The inhibition of heat-induced haemolysis by Arg-Glc MPRs was measured according to reported methods (Abe *et al.* 1981) with modifications. Chick whole blood was collected from healthy roosters. EDTA was used to prevent blood coagulation. Erythrocytes were separated from blood by centrifuging at 350 g for 5min, and washed with isotonic normal saline (0.9% NaCl) three times. The volume of erythrocytes was measured and restored to 1% (v/v) suspension with normal saline. The suspension was prepared before each of the tests and was used fresh.

Arg-Glc MRPs was dissolved in normal saline at various concentrations and incubated with red blood cells at a ratio of 1:1 (v/v) at 37°C for 2 h and washed with normal saline three times at room temperature. The cells were re-suspended and incubated at 56.5°C for 30 min to ensure high levels of cell lysis. Normal cells were incubated at 37°C for 2 h and used as control. The working concentration of Arg-Glc MRPs for each sample was 7.50, 3.75, 1.88, 0.94, 0.47, 0.24, 0.12 mg/mL. The supernatant of lytic cells was collected by centrifuging at 3000 g for 3 min, and measured at 540 nm for absorbance. The protection rate against heat-induced haemolysis was calculated according to the following equation Eq 5.3.

$$Protection\ Rate\ (\%) = 100 - \left[\frac{\left(O.D._{Sample\ heated} - O.D._{Sample\ Unheated}\right)}{\left(O.D._{Control\ sample\ heated} - O.D._{Control\ sample\ unheated}\right)} \times 100 \right]$$

Equation 5.3

5.3. RESULTS

5.3.1. Inhibitory effects of Arg-Glc MRPs on hypotonic haemolysis

Inhibition of Arg-Glc MRPs on hypotonic haemolysis was investigated in three solvents: distilled water, 0.45% NaCl saline and normal saline (0.9% NaCl), respectively. As shown in Section 4.2.2.6, 31% of arginine and 39% of glucose remained uncombined as Arg-Glc MRPs. To examine the potential interference of arginine and glucose on haemolysis, a mixture of arginine and glucose was prepared immediately before the experiments in the same ratio and concentration as Arg-Glc MRPs, and was used as a control.

As shown in Fig 5.1, more than 85% of erythrocytes were broken down in 0.45% saline, whereas less than 8% of cells broke down in the same saline following incubation with Arg-Glc MRPs for 2.5 h. However, in pure water, referred to '0% NaCl' in Fig 5.1, Arg-Glc MRPs failed to prevent haemolysis from occurring. The low osmotic pressure created by pure water was too severe for MRPs to cope with. Therefore, 0.45% NaCl was used in all further tests of MRPs' anti-haemolytic effects.

As a control, a mixture of arginine and glucose was examined for potential interference on hypotonic haemolysis but showed no effects. This implies that the inhibitory effect of Arg-Glc MRPs was not attributed to the glucose or arginine left over from the Maillard reaction. The Maillard reaction products were the effective components, although their effective molecules remained unknown.

A dose-response curve was drawn to evaluate whether the protection of Arg-Glc MRPs to erythrocytes was dependent to its concentration. As shown in Fig 5.2, Arg-Glc MRPs inhibited leakage of LDH or haemoglobin at all the concentrations tested, from 0.24 mM to 15.0 mM. The optimum protection was achieved at 7.5 mM, which produced an inhibition rate of 96%. The haemolysis inhibition rate remained at a high level at concentrations that ranged from 3.75 mM to 15.0 mM, while the inhibitory effects became less efficient at lower concentrations. At 0.24 mM, the lowest effective concentration, the haemolysis inhibition rate dropped to 32% measured by LDH assay. Once again, the mixture of arginine and glucose did not affect hypotonic haemolysis at any of the concentrations tested.

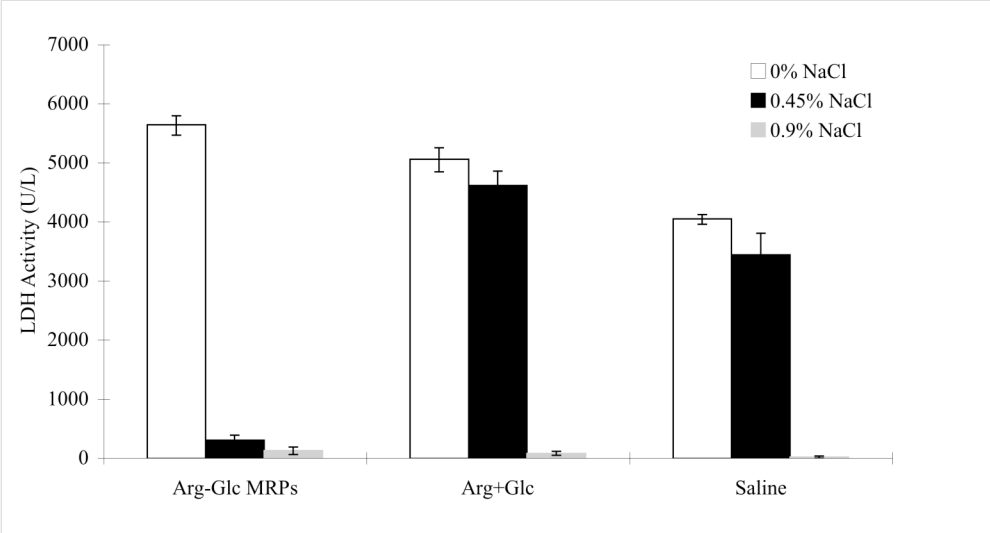

Figure 5.1 Inhibition effects of Arg-Glc MRPs on hypotonic haemolysis induced by different salt concentration in solution.

0%, 0.45%, 0.90% NaCl refers to the saline concentration of erythrocytes in suspension. The concentrations of Arg-Glc MRPs, arginine and glucose were the same, 30 mM, in the measurement. **: the differences between Arg-Glc MRPs and normal Saline, or Arg+Glc and Arg-Glc MRPs, were highly significant (n=3, P<0.01).

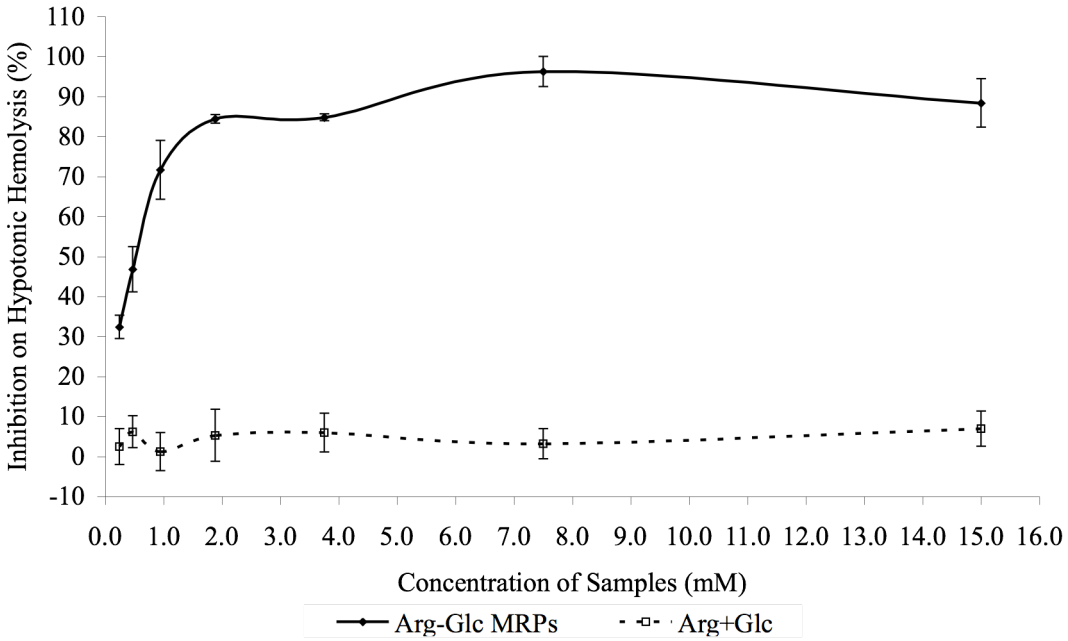

Figure 5.2 Inhibition of hypotonic haemolysis of Arg-Glc MRPs measured by LDH assay.

Note: the inhibition rates on hypotonic haemolysis were calculated with LDH activity in supernatant of erythrocytes suspension. (◆) haemolysis in the cells incubated with Arg-Glc MRPs; (□) haemolysis in the cells incubated with a mixture of arginine and glucose. Erythrocytes were suspended in 0.45% NaCl saline. (n=3, P<0.01)

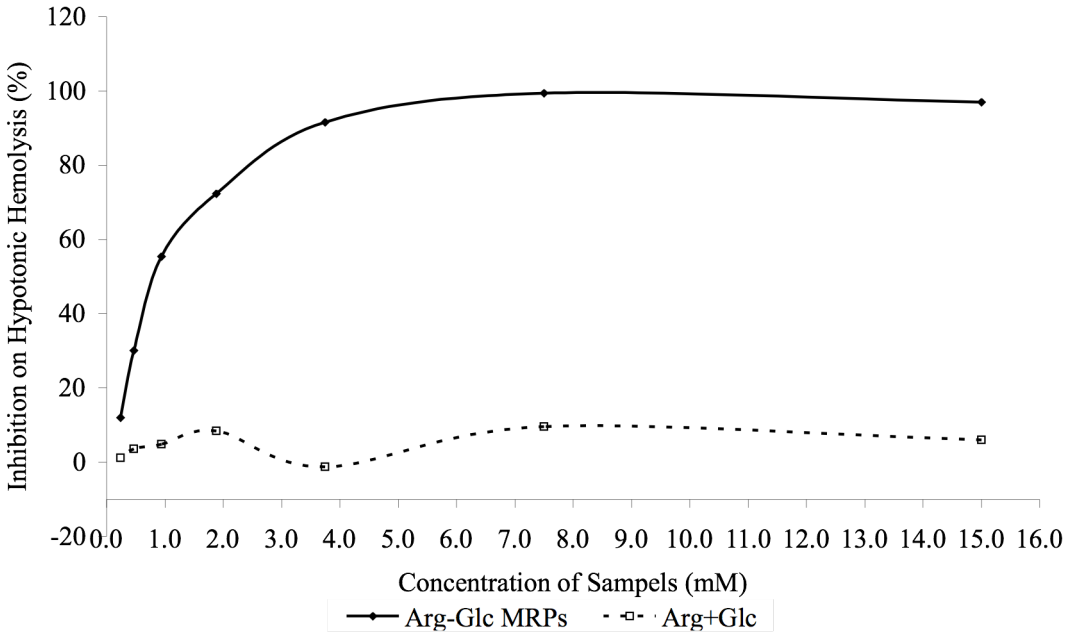

Figure 5.3 Inhibition of hypotonic haemolysis of Arg-Glc MRPs measured by absorbance.

Note: percent inhibition was calculated with OD_{540nm} of supernatant of erythrocytes suspension. (◆) haemolysis in the cells incubated with Arg-Glc MRPs; (□) haemolysis in the cells incubated with a mixture of arginine and glucose. Erythrocytes were suspended in 0.45% NaCl saline. (n=3, P<0.01)

5.3.2. Inhibitory effects of Arg-Glc MRPs on heat-induced haemolysis

As shown in Fig 5.4, Arg-Glc MRPs protected erythrocytes from heat-induced haemolysis at concentrations ranged from 0.12 to 1.88 mg/mL. The maximum protection rate was 76% at 0.47 mg/mL but decreased at either higher or lower concentrations. No inhibition effect was observed at the concentration of 3.75 mg/mL and 7.50 mg/mL. In reverse, Arg-Glc MRPs at these two concentrations might slightly promote haemolysis, although the figures were not statisticly significant.

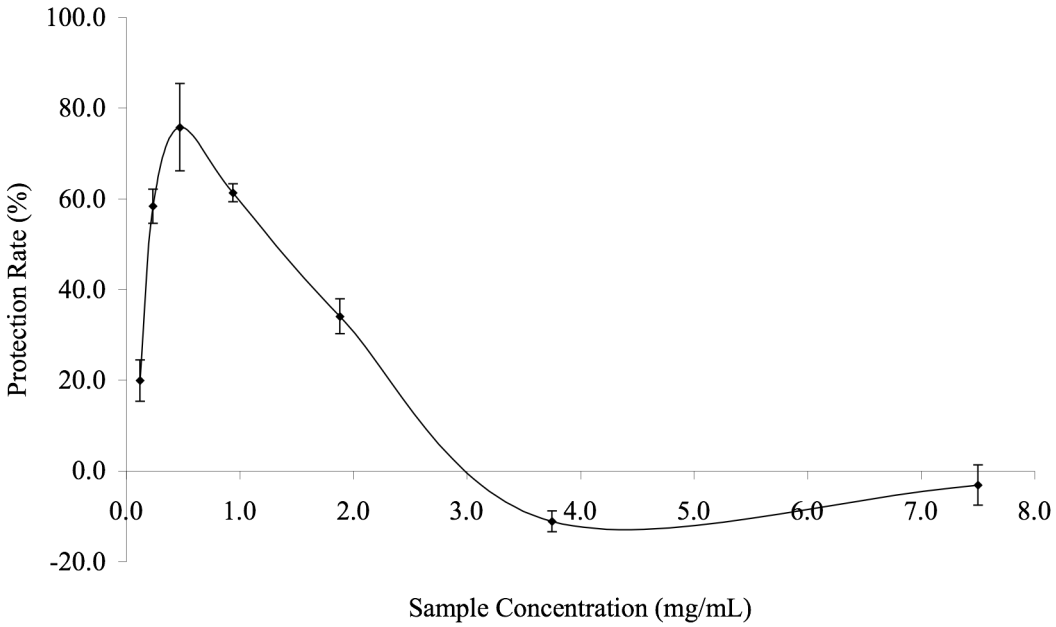

Figure 5.4 Inhibition of heat-induced haemolysis of Arg-Glc MRPs measured by absorbance.

Concentration for each sample was 7.50, 3.75, 1.88, 0.94, 0.47, 0.24, 0.12 mg/mL. (n=3, P<0.01)

This work was conducted under the collaboration with Mr. Wei Lu from Institute of Biotechnology Fuzhou University. The haemolysis was measured by Lu. The data analysis was performed by the author.

5.4. DISCUSSION AND CONCLUSIONS

Lowering the external concentration of saline will create a significant osmotic pressure gradient across the plasma membrane of a cell, and may induce a leakage of cell contents if the membrane fails to maintain its integrity against the growing pressure. Haemolysis can also occur when the environmental temperature is higher than the critical growth temperature of cells, usually 37°C. Lactate dehydrogenase assays and O.D. 540_{nm} of haemoglobin are the indices of this leakage. The more the enzyme or haemoglobin appeared in supernatant, the more serious the leakage would be.

Arg-Glc MRPs displayed cell-protective effects by inhibiting both hypotonic and heat-induced haemolysis. According to the way the measurements were performed, this haemolysis inhibition activity is more likely to be a cyto-protective effect rather than other means of interference, such as a cell-reparative effect for example. Since the anti-haemolysis effects were achieved by incubating the MRPs with erythrocytes for 2 to 2.5 h in isotonic solutions and at physiological temperature, prior to exposing the cells to hypotonic or hyperthermic circumstance, Arg-Glc MRPs would only prevent erythrocytes from haemolysis, but not be able to reverse the haemolytic process once it starts.

Furthermore, these experiments indicate that the cell membrane is the major site of the cyto-protective action of MRPs. After incubation, the cells were washed with isotonic saline to remove the free Arg-Glc MRPs from the cell suspension. Only the MRPs that were bound to cells, or those who were absorbed by endocytosis, would remain in the suspension to prevent cells from hypotonic or thermally induced haemolysis. However, if Arg-Glc MRPs were taken into the cells, they would only increase the osmotic pressure between intracellular plasma and intercellular medium. This increase would certainly increase the risk of haemolysis, particularly when the intercellular medium was in hypotonic conditions. On the contrary, administration of Arg-Glc MRPs inhibited haemolysis. Therefore, the cell membrane becomes the most likely site for Arg-Glc MRPs to perform their cell protection activity.

However, Arg-Glc MRPs acted differently on these two types of haemolysis. In hypotonic haemolysis, the degree of inhibition initially grew along the increase in concentration, but remained at the same level for concentrations ranged from 3.75 mM to 15.0 mM. In contrast, the effects of Arg-Glc MRPs on thermally induced haemolysis showed a biphasic protection-concentration curve: (1) an increasing inhibitory effect at low concentration ranged from

0.12 to 0.47 mg/mL, and (2) a decreasing inhibitory effect at high concentrations ranged from 0.94 to 7.5 mg/mL.

As shown in reported studies, some agents containing sugar moieties, i.e. plant saponins (Abe, 1981), cyclodextrins (Irie, 1982), inhibited both hypotonic and heat-induced haemolysis, and show biphasic stabilisation-lytic effects on haemolysis. At relatively low concentrations, these agents inhibit haemolysis, while the effects are reversed at higher concentrations. My results from Arg-Glc MRPs were consistent with those reports, indicating that sugar moieties or derivatives might be responsible for MRPs' haemolytic inhibition activities.

In adults, the number of erythrocytes is about 5 million per microliter. The optimum ratio between Arg-Glc MRPs and cells for protection against hypotonic haemolysis, was approximately 1.5 μmol to 10^7 cells.

How does Arg-Glc MRPs inhibit haemolysis and enhance the mechanical strength of cell membranes against osmotic stress and hyperthermal stress? There are several possible mechanisms which can be attributed to the effects of MRPs: (1) chemical modification to endogenous components of membranes; (2) preventing denaturation of vital proteins in membranes; (3) membrane disruption induced by lamellar to non-lamellar phase transition in lipid bilayers.

Firstly, chemical reactions, which might have occurred during the experiments, would result in modification of membrane components or the generation of membrane stabilising agents. However, the erythrocytes were incubated in mild conditions (2-2.5 h at 37°C) that were unlikely to allow extensive chemical reaction between MRPs and plasma membrane components.

Secondly, inactivation of vital enzymes or denaturalization of structural proteins may contribute to heat-induce haemolysis at the experimental conditions, but not to hypotonic haemolysis. And as described in Section 5.1.2, at the mild thermal conditions of this study, a severe and irreversible denaturalization of proteins is doubtable. More importantly, Arg-Glc MRPs were efficient in inhibiting both types of haemolysis, implying its protective effects do not necessarily depend on preventing proteins/enzymes from denaturation.

Thirdly, transformation of the membrane lipid bilayer from unilamellar to non-lamellar structures is directly relevant to haemolysis. Bilayer stabilisers can prevent the

transformation and subsequently prevent haemolysis, at a critical range of stabiliser-lipid ratios. When the concentration of stabiliser exceeds the upper limit of the range, the stabiliser can destabilise the bilayer by interfering with the general packing of lipids. The stabilisation of lipids bilayers becomes a reasonable mechanism whereby Arg-Glc MRPs impose an inhibitory activity on haemolysis.

To sum up, Arg-Glc MRPs stabilised the plasma membrane of red blood cells and prevented both hypotonic and heat-induced haemolysis in a dose-response manner. This assumption will be examined by the following biophysical means of study, including differential scanning calorimetry, anisotropic fluorescence spectrometry, X-ray diffraction and neutron scattering.

CHAPTER 6

EFFECTS OF MRPS ON PHYSICAL PROPERTIES OF LIPIDS BILAYERS

6.1. AIMS AND INTRODUCTION

In the previous chapters, it has been proposed that MRPs act on the surface of the cell plasma membrane, and protect cells from virus infection and hypotonic or heat-induce membrane leakage. Here in this chapter, the interactions of the MRPs with phospholipid membranes and their effects on the molecular structure of lipid assemblies were investigated with three biophysical methods, namely surface pressure measurements, fluorescence spectra and differential scanning calorimetry (DSC). The studies on the fundamental structural transformations of lipid monolayers and bilayers were carried out in the hope of discovering the primary mechanism of MRPs' cyto-protective and antiviral activities.

6.1.1. Langmuir monolayers of phospholipids

Phospholipids form lamellar monolayers at the air-water interface, and serve as models for biological membranes. Since they resemble half a bilayer, with the hydrophilic head groups pointing down towards the aqueous sub-phase (Fig 6.1 and 6.2), they are most suitable to mimic the interactions occurred on the membrane surface. The effects of MRPs on the stability of lipid monolayers provide valuable information to predict their effects on the lipid bilayers (Brezesinski & Mohwald 2003).

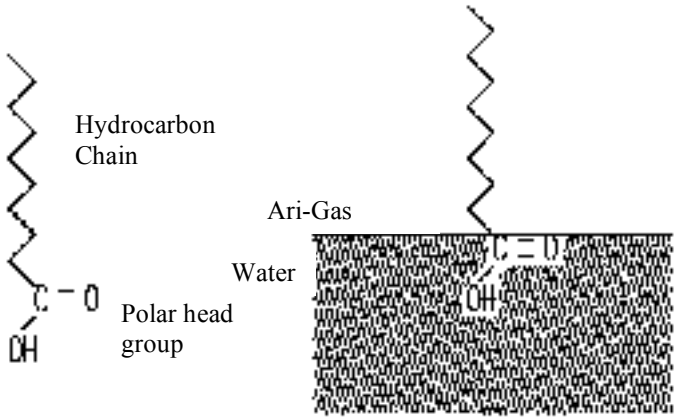

Figure 6.1 A schematic illustration showing the components of an amphiphile (left), and the orientation of an amphiphile adopted at an interface (right).

Phospholipids form lamellar or non-lamellar structures at the corresponding conditions. The main factors, which are dominant in the formation of phospholipids assemblies, are (1) the types of head/tail groups of lipids, (2) the temperature and pH of subphase in which the lipids are dispersed through, and (3) the compounds interacting with lipids and thereby adjust the molecular packing of lipids, such as electrolytes, water, detergents and membrane fusion peptides.

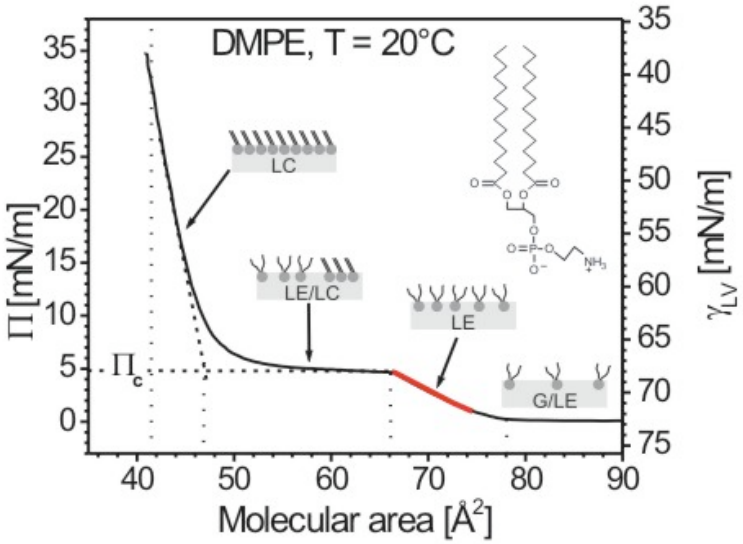

Figure 6.2 Schematic illustration of the states associated with lipid in monolayer.

Isotherm of DMPE at 20°C, quoted from Graf's diagram (Graf, 1998) and (http://www.mpip-mainz.mpg.de/~grafk/Monolayer_LB.html).

The appropriate phospholipids have to be chosen to accomplish the mission of revealing biophysical impacts of MRPs on the cell membranes by the methods mentioned above. For example, DOPG has a negatively charged head group at physiological pH values and a double bond in its fatty acid tails. A monolayer resembled by DOPG will give a better representation on mimicking the negative charged cell membrane, than the monolayers composed by zwitterrionic lipids such as PC lipids. The double bond in the tails will create a bigger free volume between lipid molecules than the saturated phospholipids, and thereby allow the exogenous amphipathic compounds to cooperate with lipids more easily.

6.1.2. Molecular packing of lipid bilayers sensed by fluorescent probes

The effects of MRPs on the stability and fluidity of lipid bilayers were studied to elucidate their stabilising activities on the plasma membrane of erythrocytes. Two lipophilic fluorescent dyes, Laurdan and Merocyanine 540 (MC540) were employed to investigate the effects of MRPs on the molecular packing and orientation in the lipid bilayers.

6.1.2.1. Steady-state spectra of Laurdan

As a hydrophobic fluorescent probe, Laurdan (2-dimethylamino-6-lauroylnaphthalene) has been widely used in natural and artificial lipid membrane systems, such as erythrocytes (Vest *et al.* 2004) and phospholipid liposomes (Parasassi *et al.* 1990), to study phase coexistence and membrane fluctuation in lipid bilayers. As shown in Fig 6.3 and 6.4 , Laurdan anchors in the phospholipid bilayers with its 12-carbon aliphatic tail while its fluorescent naphthalene moiety locates at the bilayer surface. Two possible sites have been indicated for the fluorescent moiety to reside: at the level of the glycerol backbone of the DOPC lipids (Zhang *et al.* 2006); (Sanchez *et al.* 2007) or somewhere around the choline group of the DLPC lipids (Vequi-Suplicy, Benatti & Lamy 2006). As the head groups of lipids normally bend down towards the interface between heads and tails, either site would mean that Laurdan mainly locates at the hydrophilic bilayer surface.

Laurdan is known to be sensitive to the polarity of its micro-environment. A substantial red-shift in emission wavelength results in polar solvents, compared to non-polar solvents (Parasassi *et al.* 1990). Thus, Laurdan is highly sensitive to the phases of phospholipid vesicles, as a result of the microenvironment polarity and viscosity of the system. Since the packing of membrane lipids defines the rigidity of water molecules around the fluorophore at the lipid bilayer surface, the intensity and λ_{max} of Laurdan fluorescence emission is highly sensitive to the molecular packing of the lipid bilayer, both in the gel and liquid crystalline phases. The λ_{max} of Laurdan centres at 440 nm in the gel phase, and at 490 nm in the liquid-crystalline phase. This is also supported by measurements of the fluorescence anisotropy and spin labels of Laurdan that was incorporated at different positions in the L_α phase of DLPC and DPPG bilayers (Vequi-Suplicy, Benatti & Lamy 2006).

Polarity changes appear as shifts in the Laurdan emission spectrum, between a short-wavelength band centered at around 440 nm and a long-wavelength band at 490 nm. These

may be quantified by calculating the generalized polarization (*GP*) with the equation (Eq 6.6) (Sanchez *et al.* 2007). The λ_{max} of Laurdan displays a red shift of ~50 nm when the phase of bilayers goes from L_β to L_α along with a rise in temperature (Parasassi *et al.* 1991). Long-wavelength emission predominates in the liquid crystalline phase, whereas short-wavelength emission predominates in the gel phase.

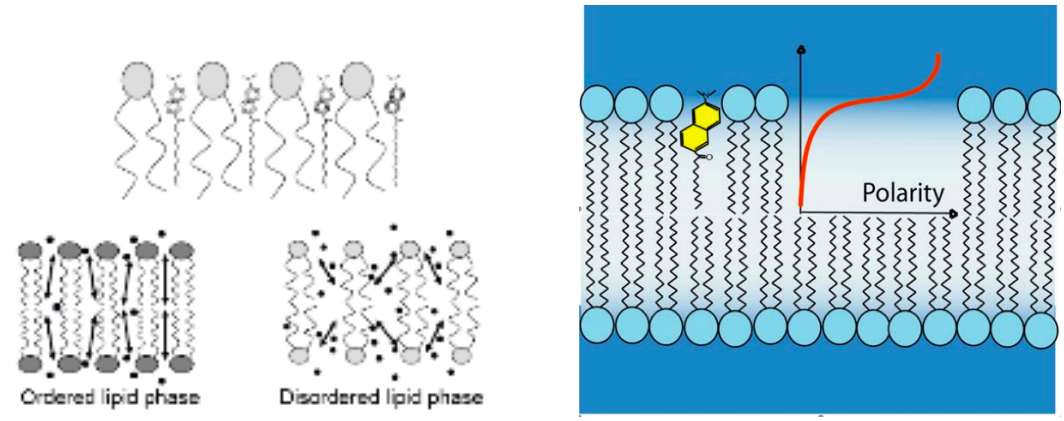

A B

Figure 6.3 Schematic representation of Laurdan fluorophore location.

In (A) the phosphocholine bilayer (Zhang *et al.* 2006) and (B) the naphthalene moiety of Laurdan sits in the DOPC membrane at the level of the glycerol backbone, while the 12-C hydrocarbon chain inserts between the lipid tails. The water molecules (black dots) relocalised around the Laurdan dipole (arrows) are responsible for the 440-to-490 nm red-shift observed during the gel-to-fluid phases transition at melting temperature. (Sanchez *et al.* 2007)

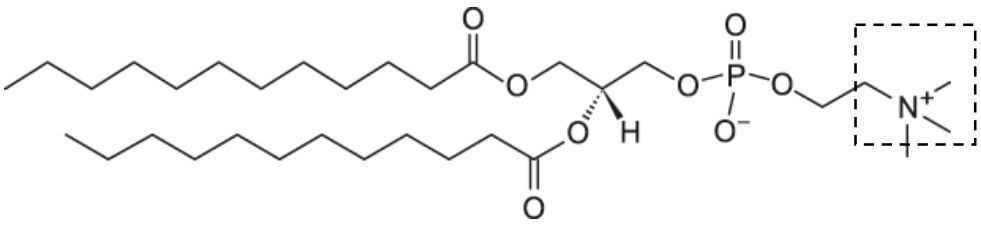

Figure 6.4 Laurdan may locate near the choline residue (dash line) of DLPC molecules (Vequi-Suplicy, Benatti & Lamy 2006).

6.1.2.2. Merocyanine 540

In contrast to Laurdan, merocyanine 540 (MC540) lies parallel to the surface of bilayers in their L_α phase, at the interface of hydrophilic and hydrophobic regions of outer leaflet, with the butyl residues penetrating into the hydrocarbon chains and the sulfate protruding to the level of amine. In L_α phase, the amphiphilic dye mainly exists as the monomer at the level slightly above the glycerol backbone of zwitterionic or negative charged lipids, whereas it is expelled from the bilayers in L_β phase but still in contact with the polar head-groups of lipids (Lelkes & Miller 1980). The schematic representation of MC540 location in lipid bilayers is shown in Fig 6.5.

The fluorescence of MC540 is enhanced when the lipophilic dye binds to artificial bilayers and enters the hydrophobic region of the membrane. Much more dye binds to multilamellar or unilamellar vesicles in the liquid-crystalline phase than the gel phase. MC540 senses the degree of lipid packing in bilayers and inserts preferentially into the bilayers with greater free space between lipids (Williamson, Mattocks & Schlegel 1983). MC540 detects the subtle differences in molecular packing of bilayers revealed by a 20-nm red-shift in emission λ_{max} as lipids become less tightly packed (Langner & Hui 1999) (Stillwell *et al.* 1993) (Krumova *et al.* 2008).

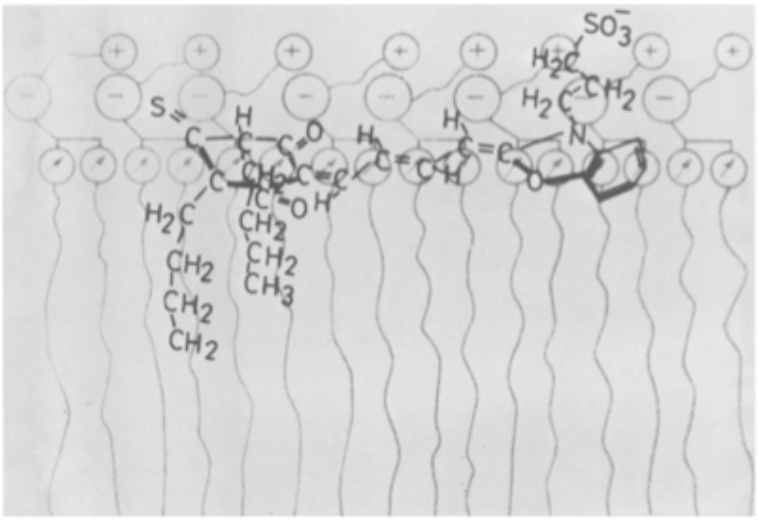

Figure 6.5 A schematic diagram presenting the location of MC540 in the lipid bilayers.

MC540 lies parallel to the hydrophilic-hydrophobic interface of bilayer (Lelkes & Miller 1980).

6.2. MATERIALS AND METHODS

6.2.1. Materials

1,2-dioleoyl-sn-glycero-3-phosphoglycerol (DOPG) sodium salt, 1,2-dioleoyl-sn-glycero-3-phosphocholine (DOPC), 1,2-dimyristoyl-sn-glycero-3-phosphocholine (DMPC) and 1,2-dioleoyl-sn-glycero-3-phosphoethanolamine-N-methyl (MeDOPE) were purchased from Avanti Polar Lipids Inc., USA, and used without further purification. Chloroform, methanol and buffers are all graded AR and purchased from Sigma-Aldrich (Irvine, UK). Laurdan was purchased from Molecular Probes (Eugene, OR). Merocyanine 540 was purchased from Sigma-Aldrich.

6.2.2. Langmuir Balance

Lipid monolayers were assembled using a Langmuir film balance (NIMA Technology, Coventry, UK). The experiments were carried out at 293K. The lipid spreading solutions were prepared with chloroform at 200 μg/mL. 24 μg of lipid (120 μL spreading solution) was used for the assembly of monolayers in each of the measurements. MRP samples were dissolved in phosphate sodium buffer (pH7.4, 0.1 M). To form the monolayer, the stock chloroform solution of DOPG was dispersed on the surface of aqueous subphase (pH7.4, 0.1 M PSB) by gently dropping with a micro-cylinder (Hamilton), followed by a wait of 10 mins to allow evaporation of the solvent. After each measurement, the trough was cleaned with chloroform, methanol and deionised water sequentially.

The surface pressure of DOPG Langmuir monolayer was controlled in two ways: (1) an isotherm scan in which the surface pressure was gradually increased by reducing the surface area; (2) a scan in which the area of monolayer was adjusted to maintain a fixed surface pressure. In the first method, the surface pressure (π) – area (A) isotherms were recorded at a barrier speed of 200 cm^2/min to measure the surface pressure change.

In the second method, the stability of the lipid monolayers was studied by measuring the mean molecular area as a function of time at a constant surface pressure of 20 mN/m. Samples were added to the subphase by pipetting the solution underneath the trough barrier. The barrier was programmed to maintain the desired surface pressure, and the surface area

was recorded. The surface area of each lipid monolayer was measured for 25 min prior to the injection of MRP samples. After injection, the surface area was recorded for 35 min. In the first 5 min immediately following injection, a change in the slope of the curve was observed as a magnetic stirrer dispersed the MRPs evenly throughout the subphase. Equation 6.1 was used for calculating of the mean molecular area of DOPG monolayer. Equation 6.2 was used for calculating of the mean molecular area of DOPG monolayer in the presence of Arg-Glc MRPs. Eq 6.3 was used for calculating of the collapse rate of monolayer.

$$mma\ (Å^2) = 86.298 - 0.0029 \times t,\quad R^2 = 0.999 \qquad \textbf{Equation 6.1}$$

$$mma\ (Å^2) = 80.291 - 0.0007 \times t,\quad R^2 = 0.976 \qquad \textbf{Equation 6.2}$$

$$Collapse\ Rate\ (Å^2/min) = (mma_{start} - mma_{end}) / (t_{start} - t_{end}) \qquad \textbf{Equation 6.3}$$

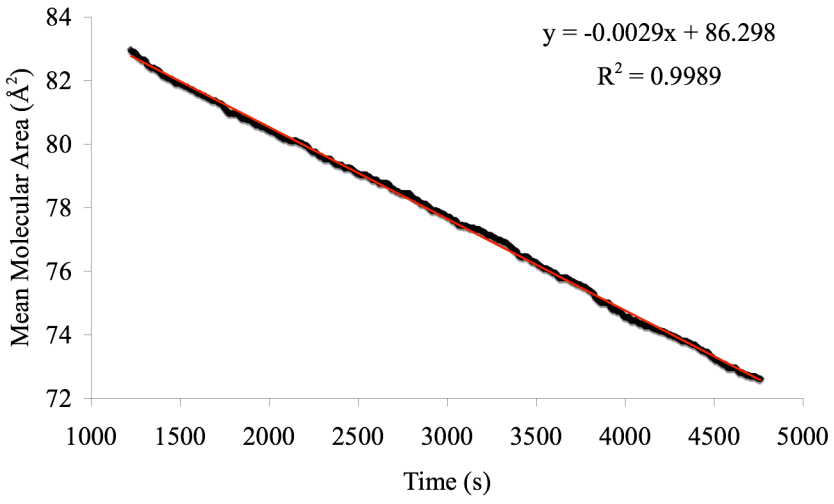

Figure 6.6 Breakdown of a DOPG monolayer under 20 mN/m surface pressure.

The *mma* was measured constantly for 60 min and used for the calculation of collapse rate. The results represent the general profile of monolayer breakdown during the test.

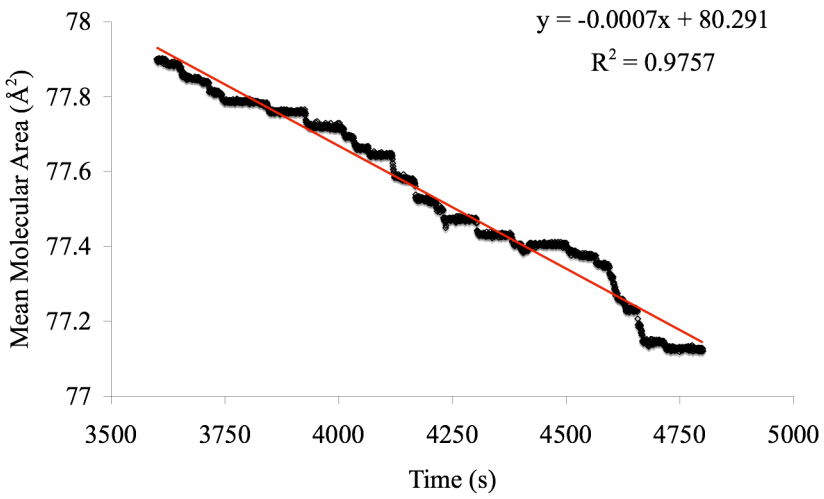

Figure 6.7 Breakdown of a DOPG monolayer under 20 mN/m surface pressure in the presence of Arg-Glc MRPs.

The *mma* was measured for 20 min at the second half of monitoring and used for the calculation of collapse rate. The second half of the monitoring represented the monolayer incorporated with Arg-Glc MRPs. The results thereby represent the general effects of the MRPs on the monolayer breakdown.

6.2.3. Fluorescence spectrum of dye-labeled lipid vesicles

6.2.3.1. Anisotropic Fluorescence Spetrum probed by Merocyanine 540

Steady-state merocyanine 540 (MC540) anisotropic emission and excitation spectrums were obtained at temperatures of 10˚C, 24˚C and 37˚C with a fluorospectrometer (Xe-900, Edinburgh Analytical Instrument) equipped with polarizers and two detectors aligned 90° to each other. Fluorescence intensity was measured with excitation and emission polarizers parallel to each other and repeated with the polarizers perpendicular to each other. The emission spectrums were measured with $\lambda_{excitation}$ = 540 nm at the range of emission wavelength $\lambda_{emission}$ = 550 ~ 700 nm with 1-nm steps. The laser light slit was set at 2 mm, the excitation slits was 2 mm and the emission slits was set at 5-6 mm in order to receive enough emission counts for calculation.

MLVs of DMPC and DOPC were prepared as reported previously (Harroun *et al.* 2003) with modifications. Lipids, MRPs and MC540 were mixed thoroughly by vortex, and dried by nitrogen stream in the test tube and left in vacuum overnight to remove trace of solvent. A serial concentrations of Arg-Glc MRPs, at the lipid/MRPs molar ratios ranged from 100:1 to 100:625, were introduced to the lipids. The lipids were re-hydrated at 37°C with phosphate

sodium buffer (pH7.4, 0.1M) and diluted to proposed concentration prior to being applied to fluorospectrometer. Samples were kept in the dark during the preparation and measurement. The measurements were carried out at 37°C. Each sample was calibrated in the cuvette for 5 min to equilibrate the temperature. The fluorescent emission intensities at both 90° and 0° were used for calculating the correction factor G and the anisotropey constant '*r*', with Eq 6.4 and 6.5.

$G=I_{HV}/I_{HH}$ **Equation 6.4**

Notes: H: horizontal, 90°; V: vertical, 0°. I_{HV}, fluorescence intensity of polarizers perpendicular to each other. I_{HH}, fluorescence intensity of both polarizers oriented at 90°.

$r = (I_0 - G \times I_{90})/(I_0 + 2 \times G \times I_{90})$ **Equation 6.5**

Notes: I_0, fluorescence intensity of polarizers parallel to each other and both oriented at 0°; I_{90}, fluorescence intensity of polarizers parallel to each other and both oriented at 90°.

6.2.3.2. Steady-state spectra of Laurdan

Multilamellar vesicles (MLVs) (10 mM) were prepared as previously described in Section 6.2.3.1, with phosphate sodium buffer (0.1M, pH7.4) at 37°C. Small unilamellar vesicles (SUVs) were prepared by sonicating MLVs for 15-30 mins at the temperature higher than the gel-liquid phase transition temperature, e.g. 37°C. Laurdan was dissolved in DMSO and added into the suspension of vesicles (50 μM) at the concentration of 5 mol%. MRP samples were then mixed evenly with vesicles. After equilibrated at 37°C for 30-60 min, measurements were carried out by a FLUOROMAX-3 spectrofluorophotometer (JOBIN YVON, Horiba, Japan). The emission spectrums of Ex=350nm and Ex=410nm were recorded with 1-nm steps in the wavelength range of 370~600 nm and 420~600 nm, respectively. The excitation spectrum of Em=440nm was recorded with 1-nm steps in the range of 200~420 nm. The lipid-alone base line in the absence of MC540 was subtracted from all spectra. The excitation generalized polarization (ex*GP*) at 350 nm and 410 nm, and the emission generalized polarization (em*GP*) at 440 nm were calculated by the formula below.

$GP_{ex} = (I_g - I_{lc})/(I_g + I_{lc})$ **Equation 6.6A**

Notes: I_g and I_{lc} are the steady-state emission intensities at 435 nm and 500 nm, respectively (Ashley *et al.* 2006); (Harris, Best & Bell 2002)(Parasassi *et al.* 1990).

$GP_{em} = (I_g - I_{lc})/(I_g + I_{lc})$ **Equation 6.6B**

Notes: I_g and I_{lc} are the steady-state emission intensities at 410 nm and 340 nm, respectively (Krasnowska, Gratton & Parasassi 1998)(Parasassi *et al.* 1990).

6.2.4. Differential scanning calorimetry

The lipid MLVs were prepared as described in Section 6.2.3, but with an additional freeze-thaw process. After the lipids were dissolved in chloroform, the samples were added and mixed thoroughly by vortex and sonication. The lipid/sample suspensions were then dried up with nitrogen stream and left in vacuum over night. Lipid concentration in the corresponding vesicle suspension was 100 mM for all the samples. MRPs were dissolved in PIPES buffer (pH7.4, 20 mM, 150 mM NaCl) added as a serial molar ratios of 0, 1, 5, 10, 20, 30, 40, 50 to 100 lipid molecules. The SIV peptide was dissolved in methanol and added to the lipid solution at 1 mol% and 2 mol%.

The dried lipid film was rehydrated with PIPES buffer at a temperature higher than T_M and vortexed to make 100 mM vesicle suspension. The suspension was sonicated for 1-2 min and soaked in liquid nitrogen (-180°C). The suspension was then defrosted at the temperature at least 20°C above the T_M. The freeze-thaw cycle was repeated for 6 times to obtain an unified lipid packing by wiping off the memory of lipids on their thermal history. The vesicles were mixed thoroughly prior to being injected and sealed into the aluminum sample pan. The pans were weighted as both empty and sealed, thereby the actual amount of lipids sealed in the pan was calculated. A Pyris 1 Differential Scanning Calorimeter (Perkin Elmer, US) was employed, at a scan rate of 40 °C/min. The sample chamber held 30 µL vesicle suspension. Continuous heating scans were run from 0°C through to 55°C for DMPC MLVs, and from -30°C through to 85°C for MeDOPE MLVs (Sykora *et al.* 2005). For the measurements on DOPC MLVs, it was heated from -30°C to -5°C at 20 °C/min.

The transition peak was analysis with the curve-fitting program (Pyris) based on nonlinear least-squares minimization. The onset phase transition temperature (T_M, T_Q *and* T_H for melting transition, transition to cubic phase and transition to hexagonal phase, respectively), energy consumption (ΔH_f), transition peak height (h) and peak area (A) were calculated automatically by the software. The transition peak height and peak area were then used to calculate the transition temperature range ΔT (Eq 6.7), presenting the homogeneous degree of phases existing in the phase transition.

$$\Delta T = \frac{2 \times A \times T}{h \times t} \qquad \textbf{Equation 6.7}$$

T, temperature from the scan rate (°C); t, time from the scan rate (s).

6.3. RESULTS

6.3.1. Effects of MRPs on surface tension and molecular area of lipid monolayer

The surface pressure and molecular area of DOPG Langmuir monolayer were measured by isotherm scan with Langmuir Balance. As shown in Fig 6.9, the mean molecular area (*mma*) of DOPG at 20 mN/m is 88 $Å^2$, which is consistent with the reported *mma* (90 $Å^2$) for DOPG (Backov *et al.* 2000). MRPs derived from RIE, *Momordica charantia* extracts (MCE) and Arg-Glc were dissolved in the subphase (pH 7.4, PB buffer), respectively. Arg-Glc MRPs (0.5 mg/mL) were demonstrated to increase the stability of DOPG monolayer by raising the *mma* to 91 $Å^2$ at 20 mN/m (Fig 6.9A), while RIE MRPs and MCE MRPs at the same concentration decreased the *mma* to 82 $Å^2$ and 84 $Å^2$ (Fig 6.9B). The maximum surface pressure of DOPG monolayer was 44 mN/m. RIE MRPs and MCE MRPs decreased the maximum surface pressure to 33 mN/m while Arg-Glc MRPs had no impacts on this figure. However, Arg-Glc MRPs increased the molecular area of DOPG monolayer from 124 $Å^2$ to 137 $Å^2$ at the low surface pressure (2 mN/m). Furthermore, in the presence of RIE MRPs and MCE MRPs, the maximum surface pressure of monolayer was reached at 70 $Å^2$ and remained the same when the *mma* was decreased to 60 $Å^2$.

The effects of Arg-Glc MRPs on the stability of DOPG monolayers were determined by measuring the collapse rate of monolayer in pressure-control tests. As shown in Fig 6.8, the mean collapse rate of DOPG monolayer was 0.17 $Å^2$/min under a surface pressure of 20 mN/m, during 60 min. Arg-Glc MRPs (1.2 mg/mL) was injected into the buffer underneath the monolayer (indicated with arrow in Fig 6.8), after which the collapse rate of the monolayer was reduced to 0.04 $Å^2$/min.

The amphipathic properties of the MRPs were examined by measuring the surface tension of their solutions. As shown in the 'surface pressure' versus 'mean molecular area' isotherms of RIE MRPs and MCE MRPs (Fig 6.10), surface pressure was gradually increased as the surface area decreased at high concentration (5 mg/mL) and in the absence of lipids. The *mma* of RIE MRPs and MCE MRPs were 18 $Å^2$ and 19 $Å^2$ at 20 mN/m, respectively. The maximum surface pressure observed on RIE MRPs and MCE MRPs was very close, 21.4 mN/m and 21.6 mN/m respectively. An increase in the surface pressure was not generally

observed on Arg-Glc MRPs, even at a higher concentration (10 mg/mL), except a minor surface pressure of 1.5 mN/m observed at the minimum molecular area (15 $Å^2$).

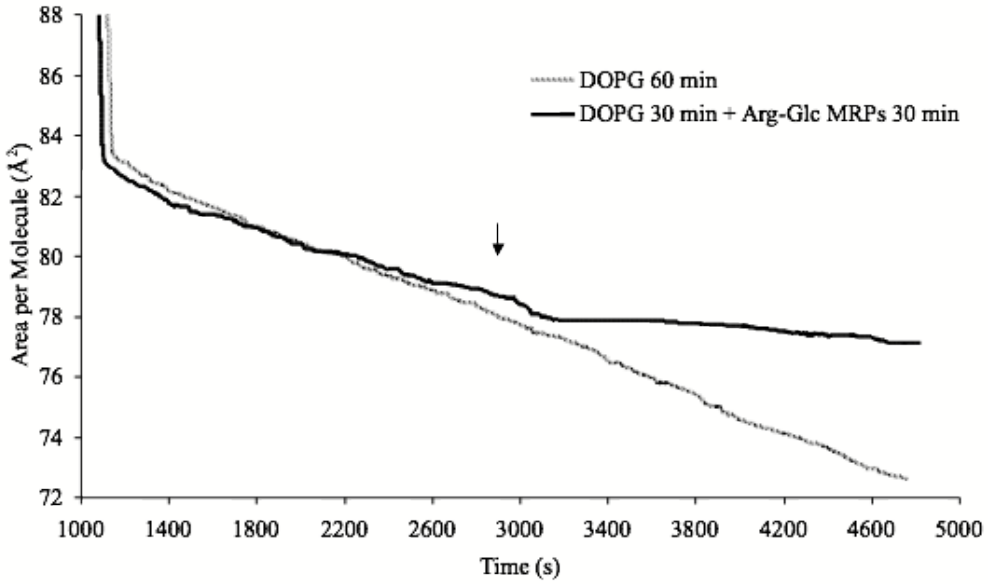

Figure 6.8 The effects of Arg-Glc MRPs on the stability of a DOPG monolayer examined by pressure-control surface pressure measurements.

Target surface pressure: 20 mN/m, Barrier speed: 200 cm^2/min; Temperature: 293K. DOPG M.W. 786.1, 0.2 mg/mL, 120 μL, DOPG was settled down on the surface of PBS (170 mL) for 10 min. MRPs (100 mg/mL, 2 mL) were injected underneath the DOPG monolayer at 25 min after the surface tension reached the target surface pressure, and the area of monolayer was measured for further 30 min.

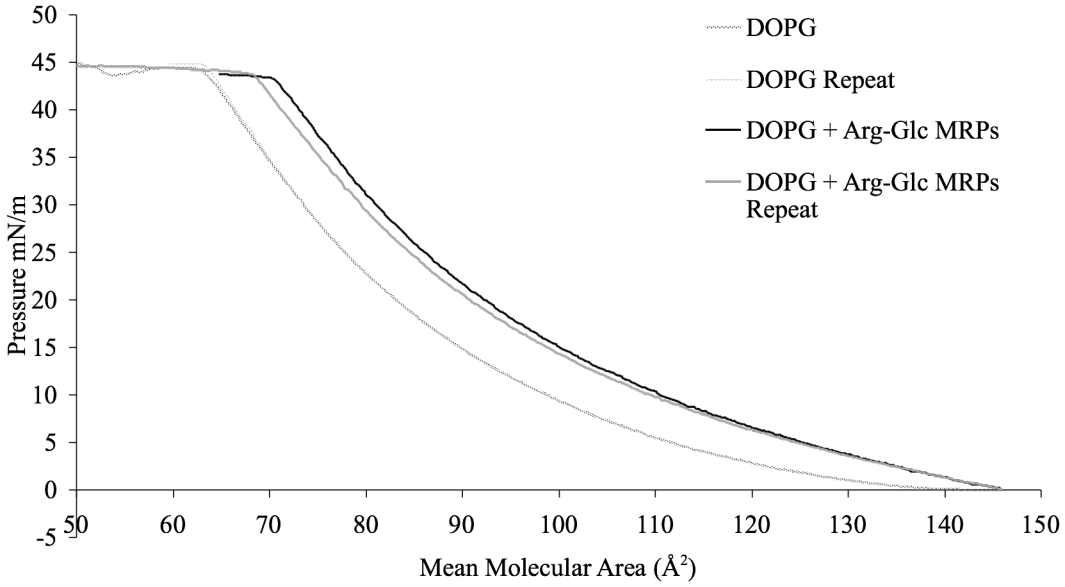

A

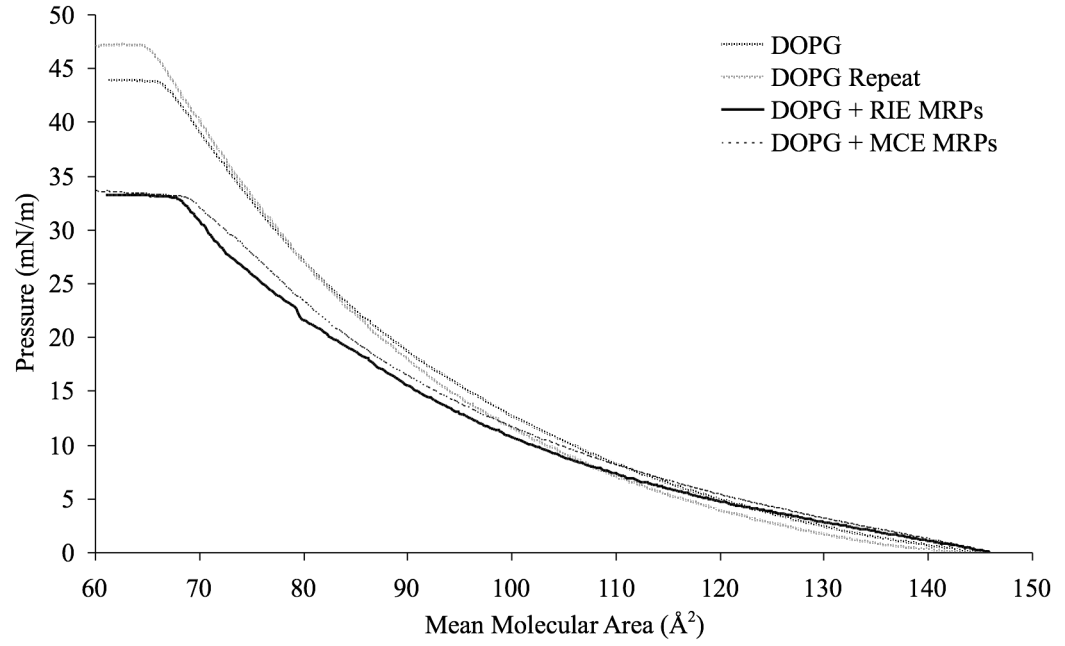

B

Figure 6.9 The surface pressure-mean molecular area isotherm measurement of the effects of MRPs derived from MCE, RIE and Arg-Glc on DOPG by Langmuir Balance.

Barrier speed: 200 cm^2/min; Temperature: 293K. DOPG M.W. 786.1, 0.2 mg/mL, 120 µL, DOPG was settled down on the surface of PBS (170 mL) for 10 min. MCE MRPs and RIE MRPs, 100 mg/mL, 850 µL. A: RIE MRPs & MCE MRPs; B: Arg-Glc MRPs.

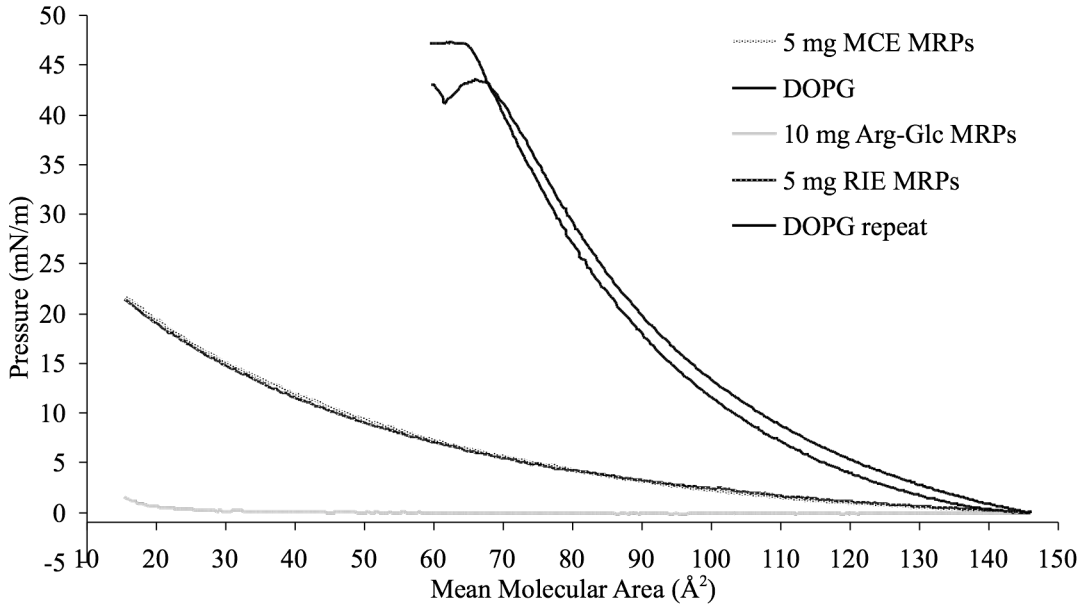

Figure 6.10 Surface pressure-mean molecular area isotherm measurements of DOPG and MRPs derived from RIE, MCE, Arg-Glc.

Barrier Speed: 200 cm^2/min; Maximum Area: 265 cm^2; Minimum Area: 30 cm^2; Temperature: 293K. DOPG concentration: 0.2 mg/mL, 120 μL; MCE MRPs concentration: 100 mg/mL, 50 μL; RIE concentration: 100 mg/mL, 50 μL; Arg-Glc MRPs: 200 mg/mL, 50 μL.

6.3.2. Effects of MRPs on the molecular packing of phospholipid bilayers: the fluorescence studies

6.3.2.1. Effects of Arg-Glc MRPs on phospholipids molecular packing sensed by MC540

As shown in Table 6.1, Figure 6.11, the anisotropy constant (*r*) of MC540 in DMPC vesicles varied along the different concentrations of Arg-Glc MRPs, and also across the gel to liquid-crystalline phase transition of DMPC bilayers.

As shown in Table 6.1 and Fig 6.11, at 10°C, DMPC vesicles are in the gel phase, where the *r* did not change or only increased slightly. When the temperature was raised up to 37°C, the presence of Arg-Glc MRPs increased *r* and thereby stabilised DMPC bilayers in their liquid crystal phase at a low concentration, ranging from 100:1 to 100:25. The *r* decreased as the bilayers destabilised at the higher concentrations (100:125 and 100:625). At 23.5°C, which is

close to the gel-to-liquid phase transition temperature (Taly 2002), *r* fluctuated between the values of *r* in gel phase and those in liquid-crystalline phase.

6.3.2.2. Effects of MRPs on lipid order determined by fluorescence probe Laurdan

Emission and excitation spectra were obtained in multilamellar vesicles (MLVs) and small unilamellar vesicles (SUVs) of three phospholipids, DOPC, DOPG, DMPC, respectively. The three lipids assayed are composed of the neutral or negatively charged head groups, and the saturated or unsaturated fatty acyl chains. The excitation and emission Generalized Polarization (*GP*) was calculated from the fluorescence spectra by Eq 6.6, to evaluate the influence of RIE MRPs on the environmental polarity in the DOPC, DOPG and DMPC liposomes, particularly at the interface of hydrophilic and hydrophobic regions of bilayer. The polarity between the head groups of bilayers reflects the spacing of lipids, and thereby infers the order of lipids.

As shown in Fig 6.12~6.17, the λ_{max} of steady-state emission spectra was around 470 nm ~ 490 nm in all the three lipids. In the presence of RIE MRPs, the λ_{max} obtained both with excitation wavelength 350 nm and 410 nm, shifts towards the longer wavelength (490 nm) by 5-8 nm in DOPG and DMPC SUVs, as well as MLVs. However, the λ_{max} shifted neither in the emission spectra nor in the excitation spectra of DOPC. The intensities of emission were altered among the three lipids, with the intensive changes observed in DOPG and DMPC, which is constant with the shift in λ_{max}. For DOPC vesicles, the low concentration of RIE MRPs (16.6 μg/mL) did not cause significant changes in the intensities, whereas the high concentration (166 μg/mL) decreased the intensity by about 25% in MLVs (Fig 6.13). For DOPG vesicles, RIE MRPs produced the opposite effects on MLVs and SUVs: concentration-dependent decreases the intensity in MLVs (Fig 6.15); and ~70% increases were observed in SUVs (Fig 6.14). For DMPC vesicles, RIE MRPs increased the intensity of emission spectra of the MLVs whereas the intensities were decreased in all the spectra of SUVs (Fig 6.16) and in the excitation spectra of MLVs (Fig 6.17).

As shown in Table 6.2, the GP_{ex} of Laurdan in all the three lipids, obtained at excitation wavelength of 350 nm, decreased in the presence of RIE MRPs in a concentration-response manner. The GP_{ex} of Laurdan in pure lipids is correspondent to the polarities in the bilayers and can be directly related to lipid order (Harris, Best & Bell 2002) (Ashley *et al.* 2006). The melting temperatures of DOPC, DOPG and DMPC are -20°C, -18°C, 23°C, respectively.

Although they were all in the liquid-crystalline phase at the assayed temperature (37°C), the GP_{ex} for DOPC, DOPG and DMPC was -0.210, -0.187 and -0.009, respectively, which showed a gradual increase. The higher polarity in DOPG and DMPC suggests the more rigid packing in DOPG and DMPC MLVs than in DOPC, which is consistent with the melting temperatures of these three lipids.

When the excitation wavelength of emission spectra was increased from 350 nm to 410 nm, the GP_{ex} of Laurdan decreased in all the lipid vesicles (Table 6.3). For SUVs, RIE MRPs decreased the GP_{ex}, which is consistent with the decline observed in the GP_{ex} (Ex=350nm).

The concentration-dependent decreases of GP_{ex} were also observed in the DMPC MLVs, whereas the concentration-dependent increases were obtained in DOPG MLVs. For DOPC, RIE MRPs at 16.6 μg/mL did alter the GP_{ex}, but increased it at 166 μg/mL.

In contrast, instead of decreasing, the emission generalized polarization (GP_{em}) of Laurdan in all the lipids vesicles increased in the presence of RIE MRPs, as shown in Table 6.4, which indicates an opposite effect on the polarization of microenvironment to the one obtained from the GP_{ex}.

Table 6.1 Anisotropy constant (*r*) of DMPC MLVs in the presence of Arg-Glc MRPs (lipid/MRPs= 100:0 ~ 100:625) at 10˚C, 23˚C and 37˚C.

Lipid/MRPs molar ratio	100:0	100:1	100:5	100:25	100:125	100:625
10°C	0.148	0.139	0.139	0.148	0.150	0.156
23°C	0.136	0.142	0.126	0.157	0.139	0.115
37°C	0.104	0.105	0.109	0.127	0.122	0.112

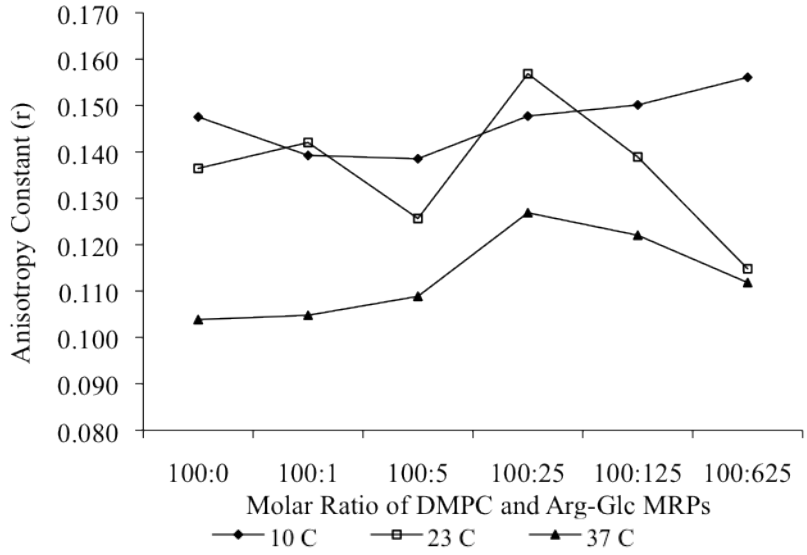

Figure 6.11 Effects of Arg-Glc MRPs on the molecular packing of DMPC MLVs across the gel to liquid-crystalline phase transition.

Examined with anisotropy factor (*r*) of MC540 at 10˚C, 23˚C and 37˚C.

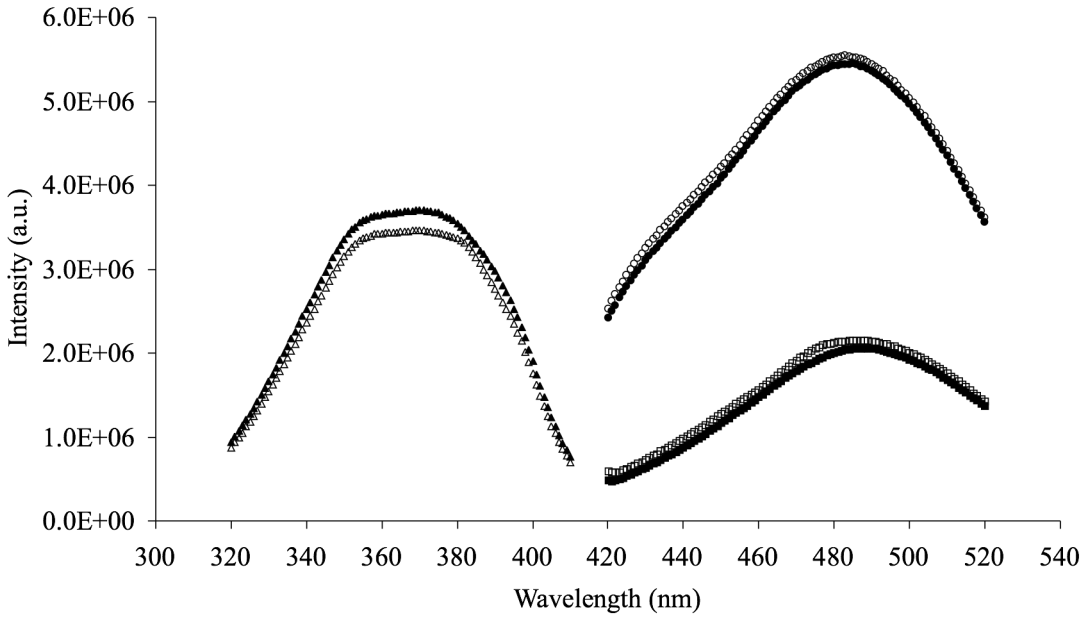

Figure 6.12 Normalized Laurdan emission and excitation spectra obtained in small unilamellar DOPC vesicles.

DOPC SUVs liquid-crystalline phase at 37°C, at the absence and presence of RIE MRPs. Lipid, 50 μM, SUVs was prepared by ultrasonic; Laurdan, 2.5 μM; RIE MRPs, 16.6 μg/mL. The excitation wavelength was at 350 ± 4 nm and 410 ± 4 nm for two emission spectra. The emission wavelength was at 440 ± 4 nm for excitation spectra. These parameters are applied for DOPG SUVs and DMPC SUVs.

(△) Em440nm DOPC SUVs; (▲) Em440nm DOPC SUVs + RIE MRPs at 16.6 μg/mL.
(○) Ex350nm DOPC SUVs; (●) Ex350nm DOPC SUVs + RIE MRPs at 16.6 μg/mL.
(□) Ex410nm DOPC SUVs; (■) Ex410nm DOPC SUVs + RIE MRPs at 16.6 μg/mL.

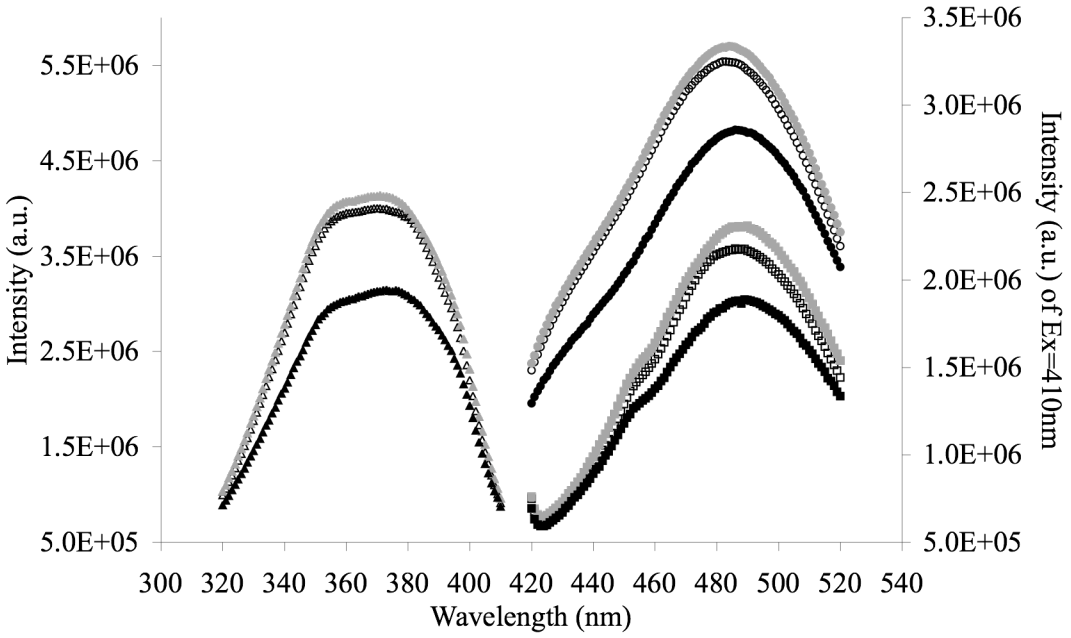

Figure 6.13 Normalized Laurdan emission and excitation spectra obtained in multilamellar DOPC vesicles.

DOPC MLVs liquid-crystalline phase at 37°C, at the absence and presence of RIE MRPs. DOPC, 50 μM, MLVs was prepared by re-hydration and vortex; Laurdan, 2.5 μM; RIE MRPs, 16.6 μg/mL and 166 μg/mL. The excitation wavelength was at 350 ± 4 nm and 410 ± 4 nm for two emission spectra. The emission wavelength was at 440 ± 4 nm for excitation spectra. These parameters are applied for DOPG MLVs and DMPC MLVs.

(△) Em440nm DOPC MLVs; (▲) Em440nm DOPC MLVs + RIE MRPs at 16.6 μg/mL; (▲) Em440nm DOPC MLVs + RIE MRPs at 166 μg/mL.
(○) Ex350nm DOPC MLVs; (●) Ex350nm DOPC MLVs + RIE MRPs at 16.6 μg/mL; (●) Ex350nm DOPC MLVs + RIE MRPs at 166 μg/mL.
(□) Ex410nm DOPC MLVs; (■) Ex410nm DOPC MLVs + RIE MRPs at 16.6 μg/mL; (■) Ex410nm DOPC MLVs + RIE MRPs at 166 μg/mL.

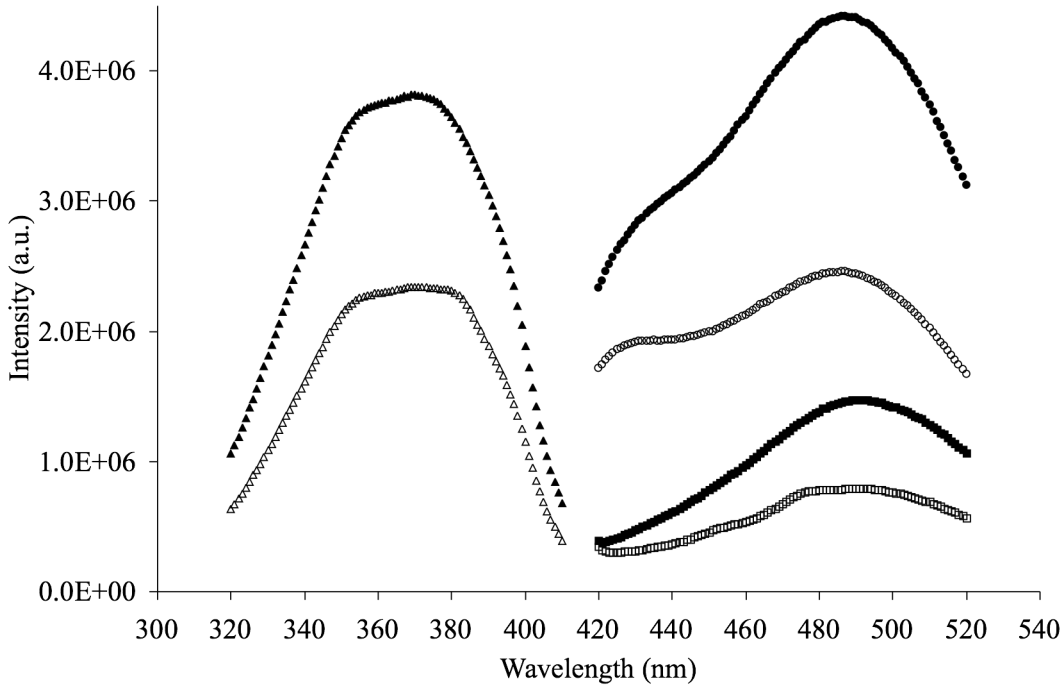

Figure 6.14 Normalized Laurdan emission and excitation spectra obtained in small unilamellar DOPG vesicles.

DOPG SUVs liquid-crystalline phase at 37°C, at the absence and presence of RIE MRPs.

(△) Em440nm DOPG SUVs; (▲) Em440nm DOPG SUVs + RIE MRPs at 16.6 μg/mL.
(○) Ex350nm DOPG SUVs; (●) Ex350nm DOPG SUVs + RIE MRPs at 16.6 μg/mL.
(□) Ex410nm DOPG SUVs; (■) Ex410nm DOPG SUVs + RIE MRPs at 16.6 μg/mL.

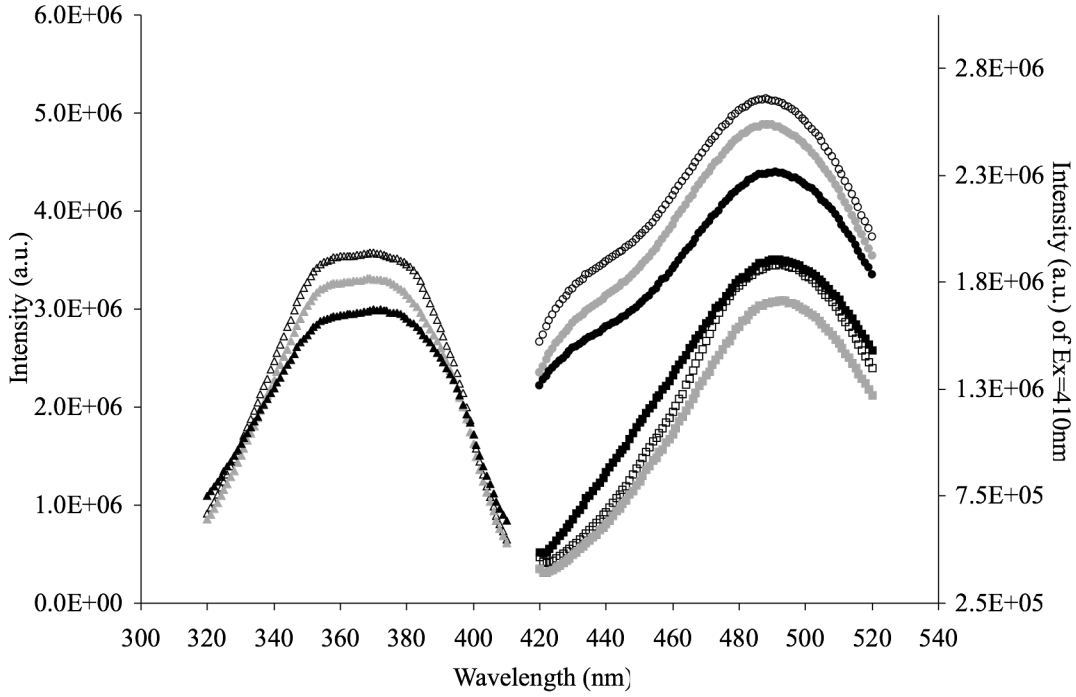

Figure 6.15 Normalized Laurdan emission and excitation spectra obtained in multilamellar DOPG vesicles.

DOPG MLVs composed of liquid-crystalline phase at 37°C, at the absence and presence of RIE MRPs.

(△) Em440nm DOPG MLVs; (▲) Em440nm DOPG MLVs + RIE MRPs at 16.6 μg/mL; (▲) Em440nm DOPG MLVs + RIE MRPs at 166 μg/mL.
(○) Ex350nm DOPG MLVs; (●) Ex350nm DOPG MLVs + RIE MRPs at 16.6 μg/mL; (●) Ex350nm DOPG MLVs + RIE MRPs at 166 μg/mL.
(□) Ex410nm DOPG MLVs; (■) Ex410nm DOPG MLVs + RIE MRPs at 16.6 μg/mL; (■) Ex410nm DOPG MLVs + RIE MRPs at 166 μg/mL.

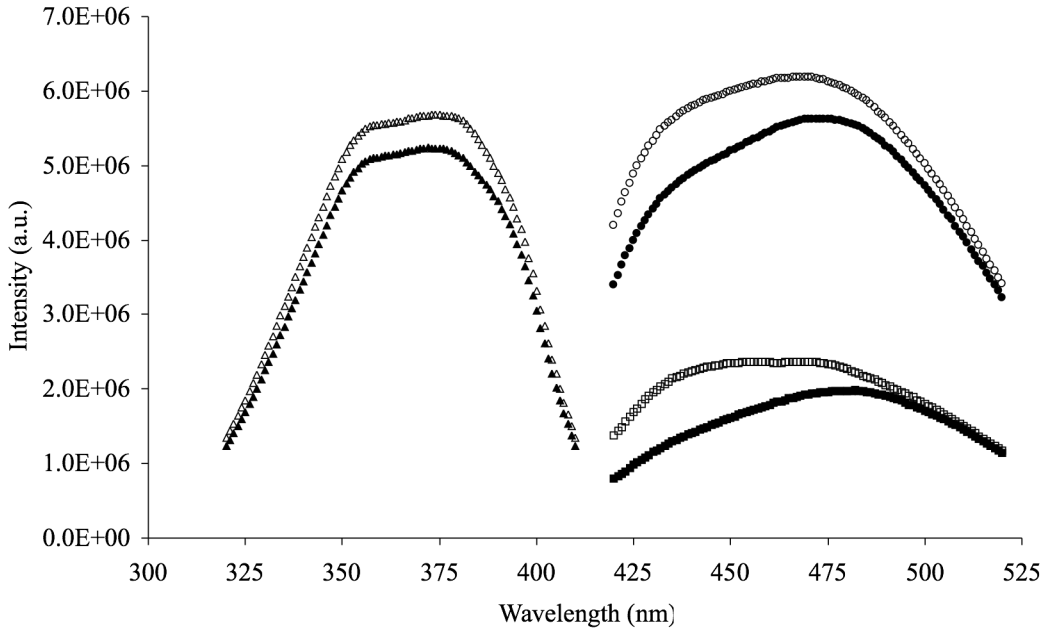

Figure 6.16 Normalized Laurdan emission and excitation spectra obtained in small unilamellar DMPC vesicles.

DMPC SUVs liquid-crystalline phase at 37°C, at the absence and presence of RIE MRPs.

(△) Em440nm DMPC SUVs; (▲) Em440nm DMPC SUVs + RIE MRPs at 16.6 μg/mL.
(○) Ex350nm DMPC SUVs; (●) Ex350nm DMPC SUVs + RIE MRPs at 16.6 μg/mL.
(□) Ex410nm DMPC SUVs; (■) Ex410nm DMPC SUVs + RIE MRPs at 16.6 μg/mL.

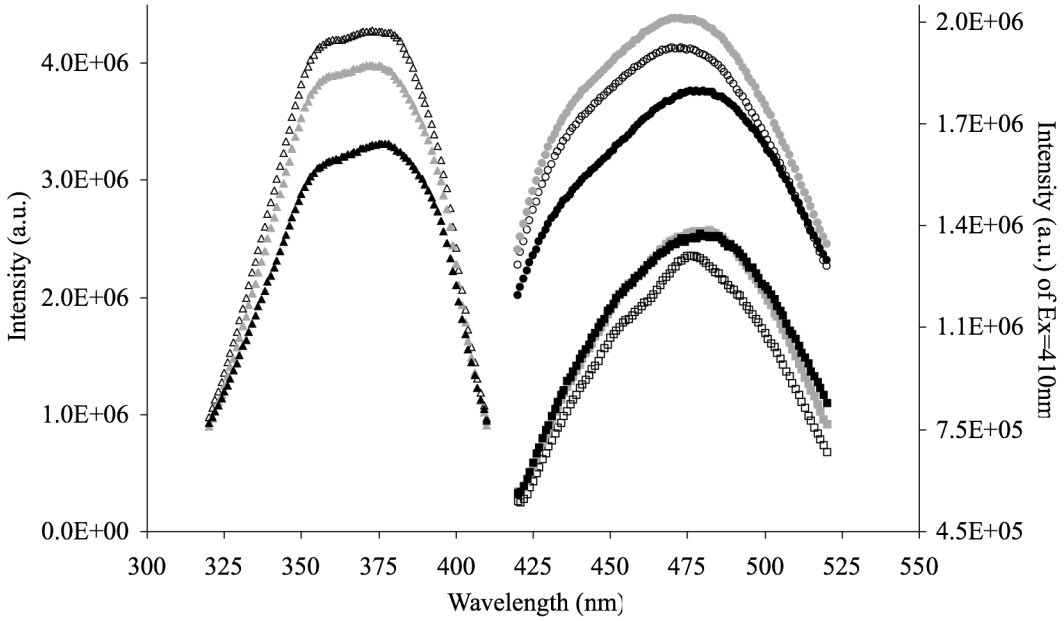

Figure 6.17 Normalized Laurdan emission and excitation spectra obtained in multilamellar DMPC vesicles.

DMPC MLVs composed of liquid-crystalline phase at 37°C, at the absence and presence of RIE MRPs.

(△) Em440nm DMPC MLVs; (▲) Em440nm DMPC MLVs + RIE MRPs at 16.6 μg/mL; (▲) Em440nm DMPC MLVs + RIE MRPs at 166 μg/mL.
(○) Ex350nm DMPC MLVs; (●) Ex350nm DMPC MLVs + RIE MRPs at 16.6 μg/mL; (●) Ex350nm DMPC MLVs + RIE MRPs at 166 μg/mL.
(□) Ex410nm DMPC MLVs; (■) Ex410nm DMPC MLVs + RIE MRPs at 16.6 μg/mL; (■) Ex410nm DMPC MLVs + RIE MRPs at 166 μg/mL.

Table 6.2 Laurdan excitation Gerenalized Polarization (GP_{ex}) of Ex=350 nm obtained in multilamellar and unilamellar phospholipids vesicles composed of liquid-crystalline phase at 37°C.

	SUVs+Laurdan		MLVs+Laurdan		
	Lipids (50 μM)	Lipids+RIE (16.6 μg/mL)	Lipids (50 μM)	Lipids+RIE (16.6 μg/mL)	Lipids+RIE (166 μg/mL)
DOPC	-0.178	-0.194 ↓	-0.210	-0.215 ↓	-0.258 ↓
DOPG	-0.084	-0.172 ↓	-0.187	-0.217 ↓	-0.223 ↓
DMPC	0.056	-0.004 ↓	-0.009	-0.015 ↓	-0.078 ↓

The GP_{ex} was calculated from the emission spectra excited at 350 nm by Eq 6.6A.

Table 6.3 Laurdan excitation Gerenalized Polarization (GP_{ex}) of Ex=410 nm obtained in multilamellar and unilamellar phospholipids vesicles composed of liquid-crystalline phase at 37°C.

	SUVs+Laurdan		MLVs+Laurdan		
	Lipids (50 μM)	Lipids+RIE (16.6 μg/mL)	Lipids (50 μM)	Lipids+RIE (16.6 μg/mL)	Lipids+RIE (166 μg/mL)
DOPC	-0.405	-0.439 ↓	-0.439	-0.438 --	-0.399 ↑
DOPG	-0.391	-0.454 ↓	-0.502	-0.498 ↑	-0.413 ↑
DMPC	0.086	-0.140 ↓	-0.133	-0.143 ↓	-0.151 ↓

The GP_{ex} was calculated from the emission spectra excited at 410 nm by Eq 6.6A.

Table 6.4 Laurdan emission Gerenalized Polarization (GP_{em}) of Em=440nm obtained in multilamellar and unilamellar phospholipids vesicles composed of liquid-crystalline phase at 37°C.

	SUVs+Laurdan		MLVs+Laurdan		
	Lipids (50 μM)	Lipids+RIE (16.6 μg/mL)	Lipids (50 μM)	Lipids+RIE (16.6 μg/mL)	Lipids+RIE (166 μg/mL)
DOPC	-0.541	-0.534 ↑	-0.494	-0.487 ↑	-0.415 ↑
DOPG	-0.607	-0.593 ↑	-0.581	-0.572 ↑	-0.445 ↑
DMPC	-0.474	-0.470 ↑	-0.488	-0.479 ↑	-0.395 ↑

The GP_{em} was calculated from the excitation spectra at the emission of 440 nm by Eq 6.6B.

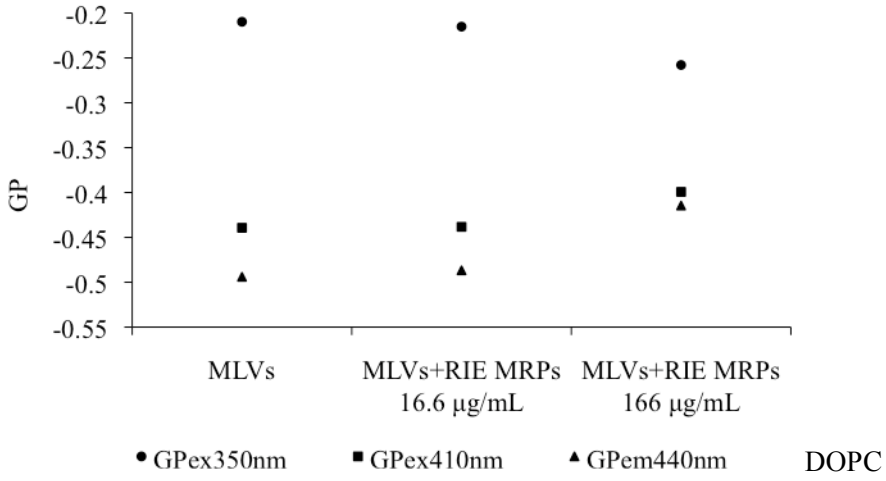

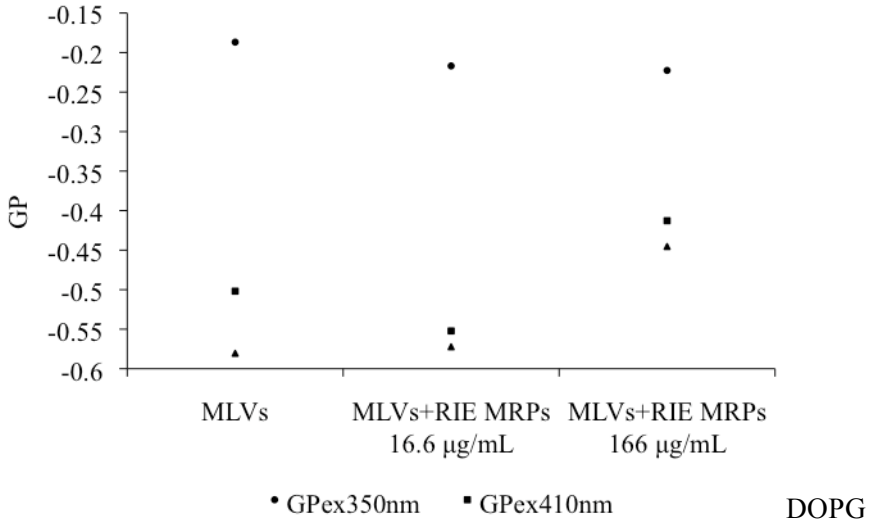

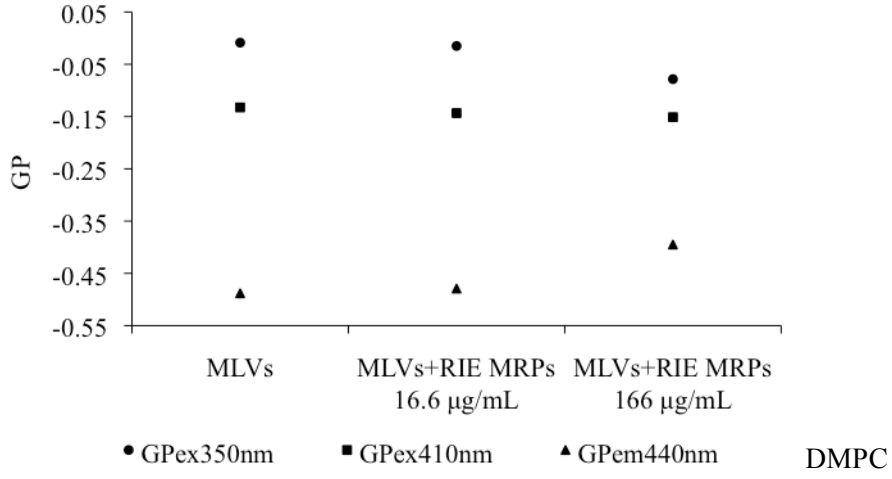

Figure 6.18 The effects of RIE MRPs on the general polarization of the MLVs of DOPC, DOPG and DMPC.

6.3.3. Effects of MRPs on phase transition of lipids

The thermodynamic properties of phase transitions in phospholipids liposome were examined by differential scanning calorimetry, a technique that measures the heat consumption of transitions as a function of temperature, in multilamellar vesicles of DMPC and N-methyl-DOPE (MeDOPE). DOPC was tested for the lamellar phase transition, but is not well-suited to this type of study, due to its low phase transition temperature (-20°C) and poor reproducibility of T_M. Therefore, vesicles composed of DMPC or MeDOPE were incorporated with different concentration of MRPs. The MLVs were prepared by six cycles of vortex-freeze-thaw, in order to erase the thermal memory of the lipids.

6.3.3.1. Phase transitions of phosphatidylcholine lipids in multilamellar vesicles

In Fig 6.19, two diagrams of DSC scanning are given as examples of measuring transition temperatures and heat consumptions (ΔH_f) of the gel (L_β) to liquid crystalline (L_α) phase transition. The SIV peptide (lipid/peptide=100:2) decreased both of the transition temperatures and heat consumption of pre-transition and main transition. As shown in Fig 6.20, during the L_β-L_α phase transition of DMPC MLVs, Arg-Glc MRPs affected the thermodynamic properties of the lipids in a concentration-dependent way. T_M, determined by

the initial temperature of the main gel-liquid crystalline transition, fluctuated as a function of MRP concentrations. However, in general, the differences were minor. The maximum difference was 1.25°C. It showed a "*W*" shape curve along the increase of concentration. T_M dropped to ~24.4°C when the molar ratio of lipid versus MRPs was 100:3, whereas T_M rose back to about the same as pure lipid (25.4°C) rapidly when the ratio was 100:5, 10:2 and 10:3. At the concentrations higher than 10:3, T_M gradually dropped again.

In contrast to its effects on T_M, the effects of MRPs on ΔH_f displayed a rather regular concentration-response curve. The value increased with the first two concentrations then decreased continuously with the higher concentrations. MRPs significantly increased ΔH_f by 5 kJ/mol at a molar concentration of 100:1, and achieved a maximum increase of 12 kJ/mol at 100:3 (P<0.01). However, ΔH_f steadily decreased with higher concentration of MRPs, ranging from 100:5 to 10:5. At 10:4 and 10:5, the heat consumption of transition dropped back to the same level as pure DMPC lipid, but with larger errors (P>0.05).

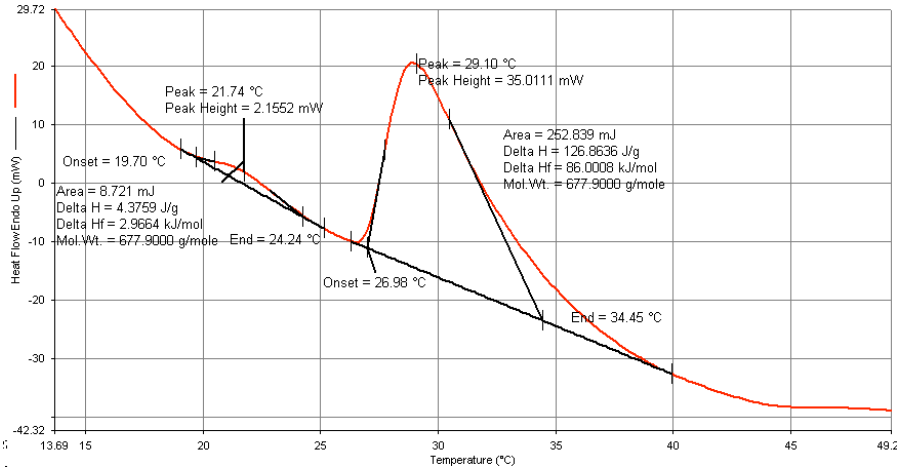

A. DMPC MLVs

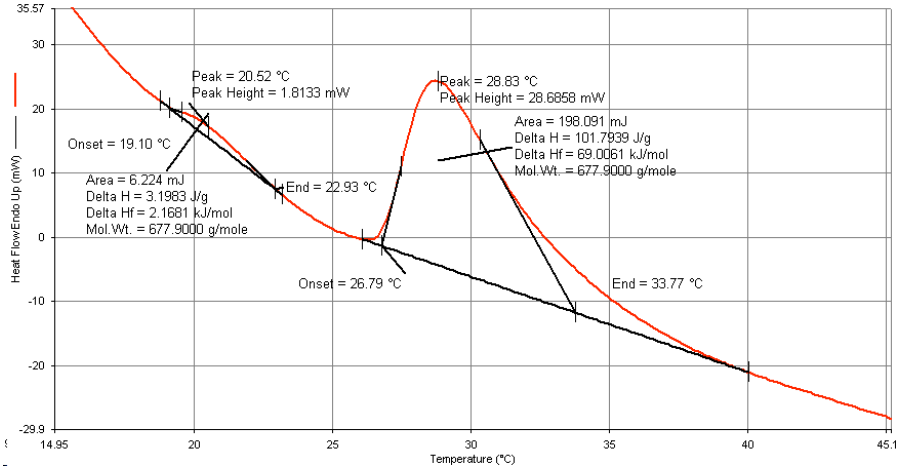

B. DMPC MLVs in the presence of 100:2 (lipid/peptide molar ratio) SIV peptide

Figure 6.19 Examples of phase transition peaks of DMPC MLVs in the presence of SIV peptide measured by DSC.

A pre-transition peak (at ~19°C) and the main transition peak (at ~26°C) are presented in the diagrams. The continuous heating scans were performed from 0°C to 55°C at a scan rate of 40 °C/min, and repeated for at least 5 times for each sample. The MLVs were prepared with PIPES buffer (pH7.4, 20 mM, 150 mM NaCl) at 100 mM. 30 µL MLVs was sealed in the sample pan for each measurement. The transition peaks were fit by Pyris DSC data-analysis software (Perkin Elmer, US).

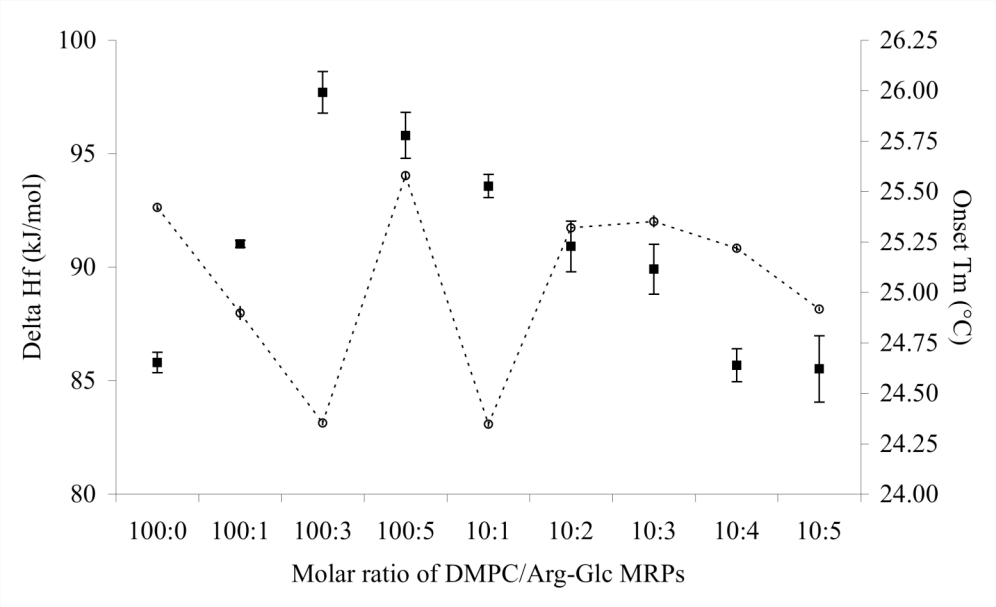

Figure 6.20 Effects of Arg-Glc MRPs on the thermodynamic properties of gel-liquid crystalline transition obtained in DMPC MLVs.

The continuous heating scans were performed from 0°C to 55°C at a scan rate of 40 °C/min, and repeated for at least 5 times for each sample. The T_M (○) and ΔH_f (■) of DMPC MLVs were presented in the diagram (n=4; P<0.01).

6.3.3.2. Effects of Arg-Glc MRPs on the phase transitions of MeDOPE MLVs

In Fig 6.21, three examples of DSC scans are given as examples of the measurement of transition temperature and heat consumption. The diagrams of L_β-L_α and L_α-H_{II} phase transitions of pure MeDOPE are shown in Fig 6.21A&B, and those of L_α-Q_{II} and L_α-H_{II} phase transitions of Arg-Glc MRPs integrated MeDOPE MLVs are shown in Fig 6.21C.

There were three phase transitions observed in MeDOPE MLVs. In general, as shown in Fig 6.22, Arg-Glc MRPs exhibited the concentration-dependent effects on the phase transitions of MLVs composed of unsaturated phosphatidylethonalamine, MeDOPE. Three phase transitions were measured: L_β-L_α, L_α-Q_{II} and L_α-H_{II}. Although the transition temperatures of all three phases were fluctuated with MRPs concentration, MRPs increased the transition temperatures at moderate concentrations (10:1 by molar ratio), but decreased them at higher concentrations, particularly at the highest concentration of 10:5 by molar ratio. The influence of Arg-Glc MRPs on ΔH_f varied between the three different phase transitions. When the L_β-L_α transition took the highest heat consumption of 30~50 kJ/mol, the L_α-Q_{II} took the least,

which was mostly below 2 kJ/mol. The heat consumption of the L_α-H_{II} transition was higher than that of L_α-Q_{II}, but mostly below 5 kJ/mol.

As shown in Fig 6.22A, the initial phase transition temperature (T_M) was ~ -7.5°C. Arg-Glc MRPs decreased this temperature gradually along the increase in the molar ratio to ~ -8.2°C, with an exceptional but significant increase of 1.0°C at the molar ratio 10:1. Although both the decrease and increase were small by numbers, but were highly significant in statistics (n=4; P<0.01). The presence of 1 mol% MRPs didn't affect the T_M significantly, but remarkably increase the standard errors of measurements. The ΔH_f was decreased by the low concentrations of MRPs and reached the bottom of ~30 kJ/mol at 5% of MRPs. It was increased with higher concentrations of MRPs and became stable at ~50 kJ/mol.

As shown in Fig 6.22B, the T_M of L_α-Q_{II} was about 62°C. MRPs increased the initial temperature of transition (T_Q) significantly to a maximum value of 68°C at a molar ratio of 10:1. At both lower and higher ratios, MRPs decreased the T_Q with greater standard errors (P<0.05). No L_α-Q_{II} phase transition was observed at molar ratios of 100:5 or 10:5. The ΔH_f of pure MeDOPE was about 4 kJ/mol, which dropped to ~ 1 kJ/mol in the presence of just 1% Arg-Glc MRPs. The ΔH_f values fluctuated at higher concentrations.

As shown in Fig 6.22C, the profiles of the L_α-H_{II} phase transition were rather similar across the pure lipids and different concentrations of Arg-Glc MRPs. The presence of MRPs did not have a significant impact on the phase transition at several concentrations. However, there were two exceptions: MRPs at 100:5 and 10:5. At the former concentration, Arg-Glc MRPs decreased the L_α-H_{II} phase transition temperature (T_H) from 73.6°C of pure MeDOPE to 69.9°C. This figure was further lowered down to 68.3°C in the presence of 10:5 molar ratio of the MRPs. In contrast, the ΔH_f did not change significantly at most of concentrations, and remained at around 3 kJ/mol. It was dramatically increased to 19 kJ/mol only when 10:5 molar ratio of Arg-Glc MRPs was added.

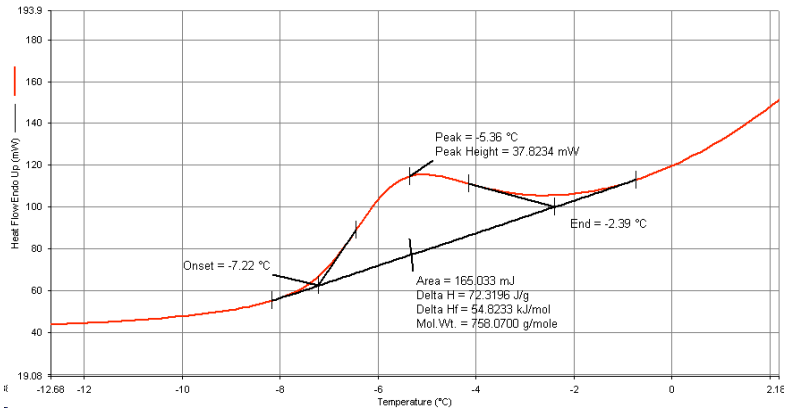

A. The gel-liquid crystalline phase transition of MeDOPE MLVs.

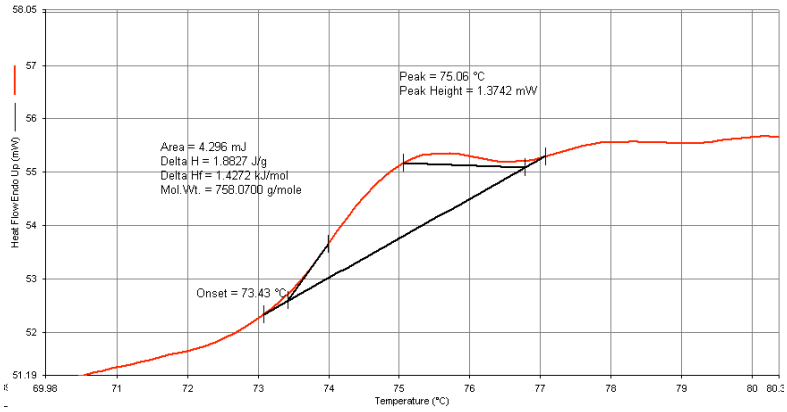

B. The lamellar-hexagonal phase transition of MeDOPE MLVs.

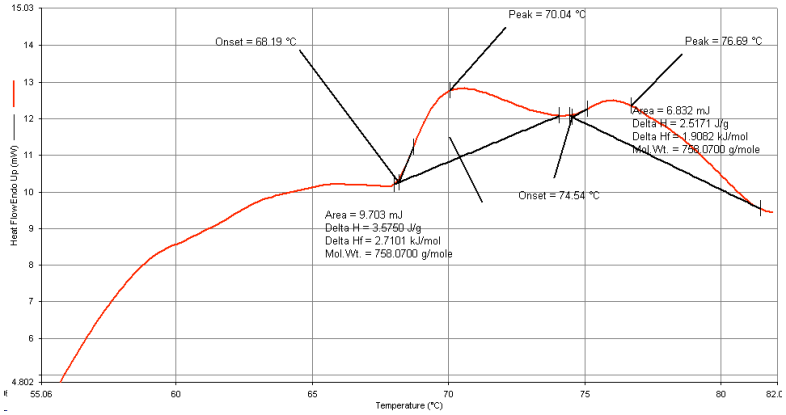

C. The lamellar to non-lamellar transitions of MeDOPE MLVs in the presence of Arg-Glc MRPs at 10:1 molar ratio.

Figure 6.21 Differential Scanning Calorimetric diagrams of MeDOPE MLVs with and without Arg-Glc MRPs at the scan rate of 40 °C/min.

The continuous heating scans were performed from -30°C to 85°C, and repeated for at least 5 times for each sample to obtain the reproducible data. The MLVs were prepared with PIPES buffer (pH7.4, 20 mM, 150 mM NaCl) at 100 mM. 30 µL MLVs was sealed in the sample pan for each measurement. The transition peaks were fit by Pyris DSC data-analysis software (Perkin Elmer, US).

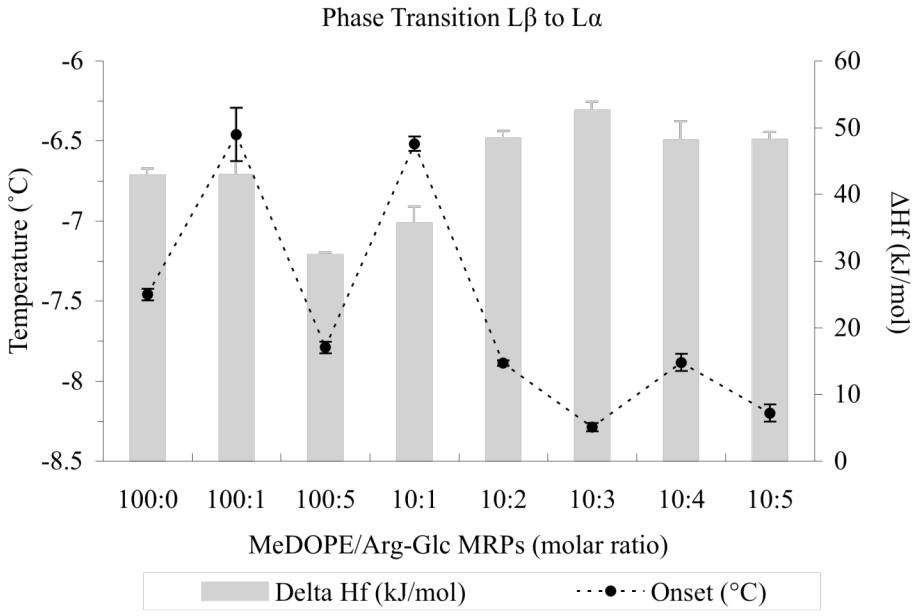

A. L_{β}-L_{α} phase transtition

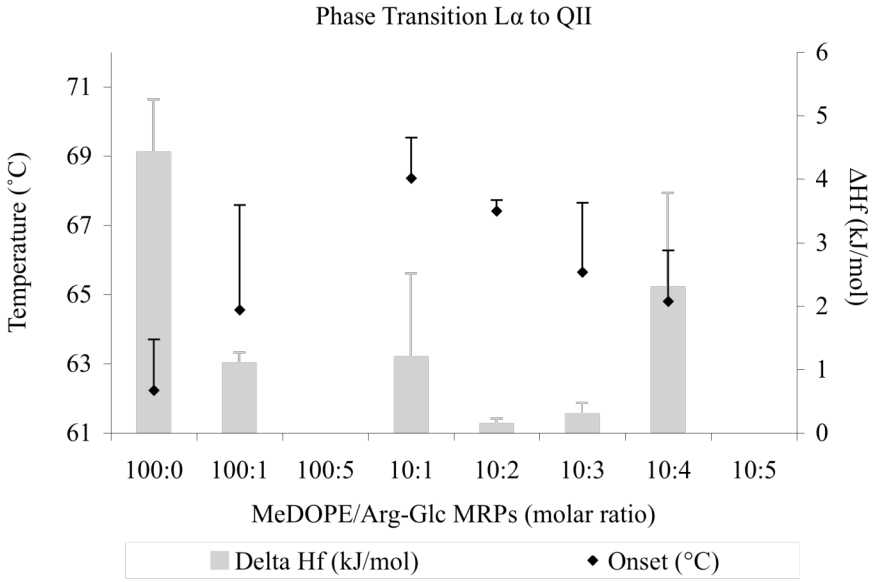

B. L_{α}-Q_{II} phase transition

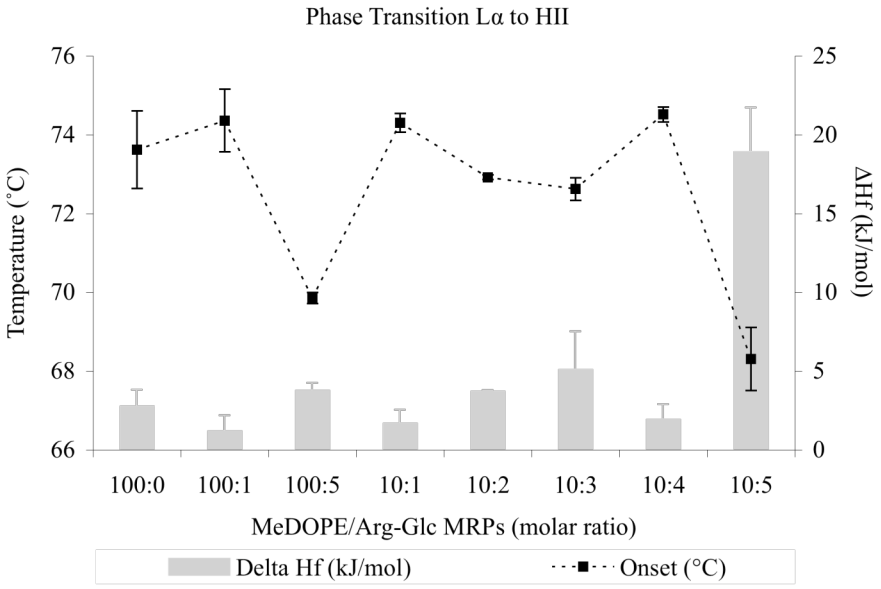

C. L_α - H_{II} phase transition

Figure 6.22 Thermodynamic effects of Arg-Glc MRPs on lipid phase transitions of MeDOPE MLVs.

Examined by differential scanning calorimeter at the scan rate of 40 °C/min. The continuous heating scans were performed from -30°C to 85°C, and repeated for at least 5 times for each sample.

(A). Lamellar-lamellar (L_β-L_α) phase transtition. ●: T_M; ■ : ΔH_f (n=4; P<0.01).

(B). Lamellar-inverted cubic (L_α-Q_{II}) phase transition. ◆: T_Q; ■ : ΔH_f (n=4; P<0.05).

(C). Lamellar-inverted hexagonal (L_α - H_{II}) phase transition. ■: T_H; ■ : ΔH_f (n=4; P<0.01).

6.3.3.3. Effects of SIV fusion peptide on phase transitions of phospholipid MLVs

As shown in Fig 6.23, SIV peptide decreased the T_M and heat consumption ΔH_f of L_β-L_α phase transition in DMPC MLVs (P<0.01), when the temperature range of the transition (ΔT_M) remained the same (P>0.05). However, the temperature range of the pre-transition was decreased significantly by 0.7°C at 100:1 SIV (lipid/peptide ratio, P<0.01) and 1.2°C at 100:2 SIV (P<0.05).

SIV peptide slightly decreased the T_M of MeDOPE MLVs (P<0.05 at 100:2) but increased

T_H by 4°C (P<0.01, Fig 6.24). In terms of transition temperatures and heat consumptions, the higher SIV concentration (100:2) was eventually not more effective than 100:1, although it

did resulte in the greater standard errors. The heat consumptions of both transitions were reduced by SIV (P<0.01). The peptide decreased the temperature range of lamellar/non-lamellar phase transition by 2°C, but slightly increased that of gel-liquid crystalline phase transition by about 0.3°C (P<0.01 for 100:1 SIV).

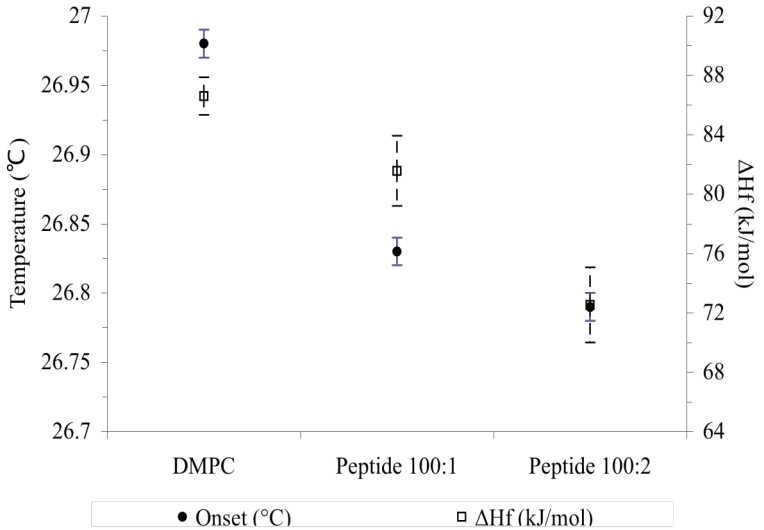

A. Effects of SIV on T_M (● ; n=5, P<0.01) and ΔH_f (□ ; n=5, P<0.01).

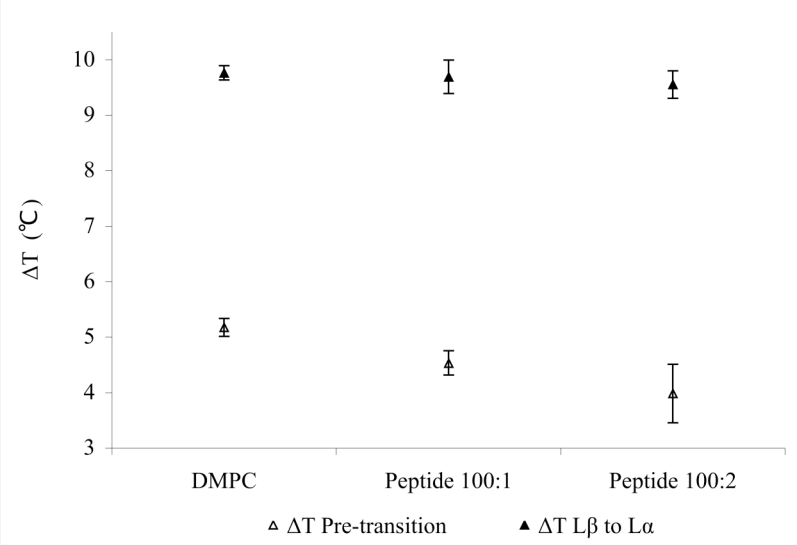

B. Effects of SIV on ΔT_M (n=5, P>0.05).

Figure 6.23 Effects of SIV peptide on phase behaviour of DMPC MLVs by DSC.

Scan rate: 40 °C/min. Temperature range of scanning: 0~55°C. Lipid concentration: 100 mM.

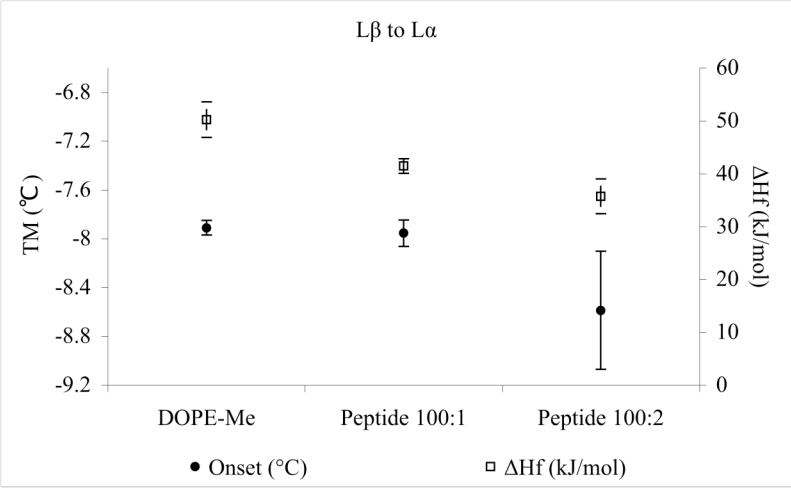

A. Effects of SIV on T_M (●) and ΔH_f of L_β-L_α transition (□).

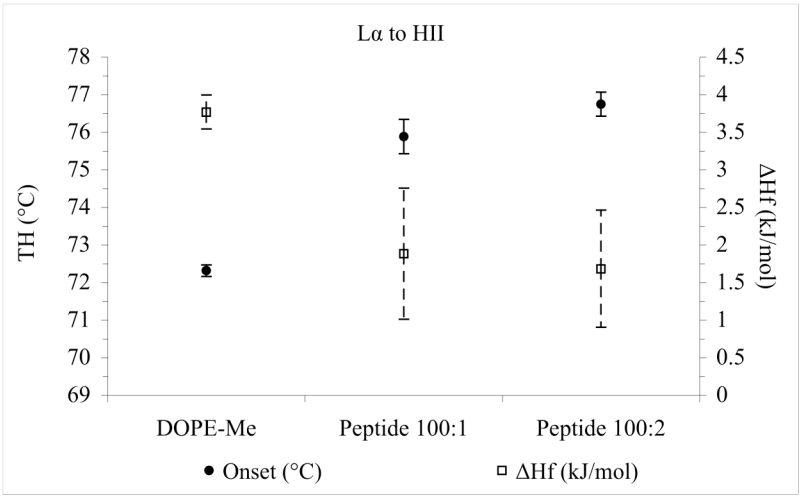

B. Effects of SIV on T_H (●) and ΔH_f of L_α-H_{II} transition (□).

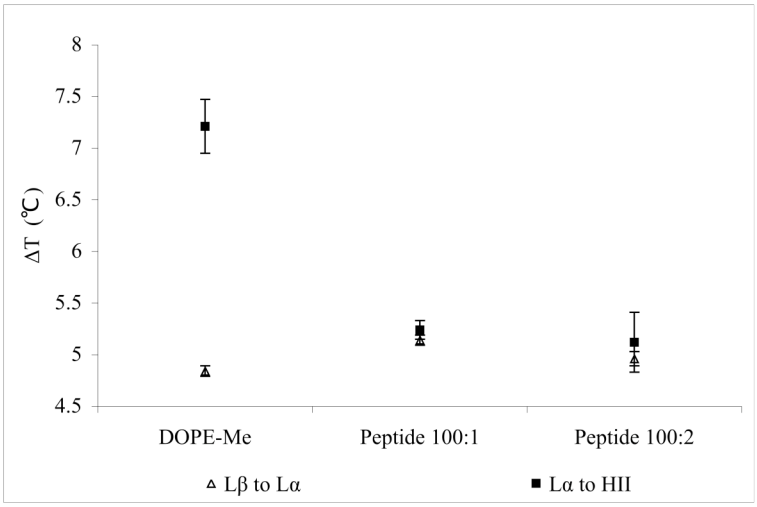

C. Effects of SIV on ΔT_M (△) and ΔT_H (■).

Figure 6.24 Effects of SIV peptide on phase behaviour obtained in MeDOPE MLVs with DSC.

Scan rate: 40 °C/min. Temperature range of scanning: -30~85°C. Lipid concentration: 100 mM. (n=5; P<0.01)

6.3.3.4. Effects of Arg-Glc MRPs on the phase transitions of MeDOPE with SIV fusion peptide

The impacts of Arg-Glc MRPs and SIV fusion peptide on the phase transition of MeDOPE are described in section 6.3.3.2 and 6.3.3.3, respectively. The influences of Arg-Glc MRPs on the membrane fusion effects of peptide were then observed in the MeDOPE MLVs in the presence of SIV fusion peptide. The results are shown in Fig 6.25. The effects of Arg-Glc MRPs on lipids in the absence of the peptide are included in the figures for comparison. Different effects of Arg-Glc MRPs on the phase transition profiles were observed in the MeDOPE vesicles in the presence or absence of SIV fusion peptide.

In the L_β-L_α phase transition (as shown in Fig 6.25A), the MRPs promoted the transition at 100:5 (lipid/MRPs molar ratio), but inhibited the transition at the lower (100:2) or higher concentrations (10:1) in vesicles with or without SIV peptide. The T_M of pure lipid was -7.5±0.05°C, which was decreased by SIV peptide to -8.0°C. The MRPs increased the T_M of MeDOPE vesicles containing 100:1 SIV peptide by 0.8°C at 100:2 (P<0.01), but decreased the T_M to -8.2°C at 100:5 (P<0.05) and increased T_M back to -7.5°C, the same number as that of pure lipid, at 10:1 (P<0.01). SIV peptide decreased the temperature range (ΔT) of this phase transition in MeDOPE vesicles to 5.1°C when Arg-Glc MRPs increased it to 5.7°C at 10:1 (P<0.01). However, in the presence of 100:1 SIV, the MRPs increased the temperature range of L_β-L_α phase transition by 0.4°C at 100:5 (P<0.05), then decreased it by 0.3°C at 10:1 (P<0.01).

In the L_α-H_{II} phase transition (as shown in Fig 6.25B), the effects of Arg-Glc MRPs were different from those in the L_β-L_α transition. The MRPs promoted the transition at 100:5, but inhibited the transition at the lower (100:2) or higher concentrations (10:1) in vesicles in the absence of SIV. For 100:1 SIV, the effects of Arg-Glc MRPs became much milder. T_H of pure lipid was 72.6±0.4°C, which was elevated to 75.9±0.5°C by the presence of 100:1 peptide (P<0.01). It was even 1.6°C higher than the T_H of vesicles containing 10:1 MRPs.

Furthermore, in the presence of 100:1 SIV, the T_H was decreased to 74.1±0.1°C by 100:5 Arg-Glc MRPs (P<0.01), whereas 10:1 Arg-Glc MRPs raised the T_H back to 75.1±0.1°C (P<0.01). Furthermore, the ΔT_H of L_α-H_{II} phase transition was significantly affected by Arg-Glc MRPs, but only at 100:2. The opposite effects were observed in the presence or absence of SIV. The MRPs decreased the ΔT_H by 3°C in the absence of SIV, but increased the ΔT_H by 2.8°C in the presence of SIV (P<0.01). At the higher concentrations of the MRPs, 100:5 and 100:10, the MRPs did not affect ΔT_H as potent as it was at 100:2.

6.3.3.5. Effects of Arg and Glc on the phase transitions of MeDOPE MLVs

As described above, Arg-Glc MRPs affected the phase transitions of MeDOPE MLVs in a concentration-dependent manner. As described in Section 4.2.2.6, there are 39% Glc and 31% Arg remaining un-reacted in the Arg-Glc MRPs. Glc and Arg were examined respectively in MeDOPE MLVs to reveal the possible contribution of these un-reacted reactants to the MRPs' effects on lipid phase transitions. The tests were conducted at the concentrations corresponding to 100:5 and 10:5 Arg-Glc MRPs. The concentrations are 100:1.95 and 100:19.5 for Glc, 100:1.67 and 100:16.7 for Arg.

As shown in Fig 6.26A, glucose, arginine and Arg-Glc MRPs decreased the T_M and ΔT_M, especially at the high concentration (10:5). However, the effects of these samples on the T_H and ΔT_H of MeDOPE MLVs were opposite between the reactants (glucose and arginine) and reaction products (Arg-Glc MRPs), responding to their concentrations (Fig 6.26B). The T_H was increased by the reactants whereas decreased by Arg-Glc MRPs. The ΔT_H was slightly decreased by the reactants whereas increased by the MRPs. The effects of these samples were stronger at the higher concentration (10:5) than at the lower concentration (100:5).

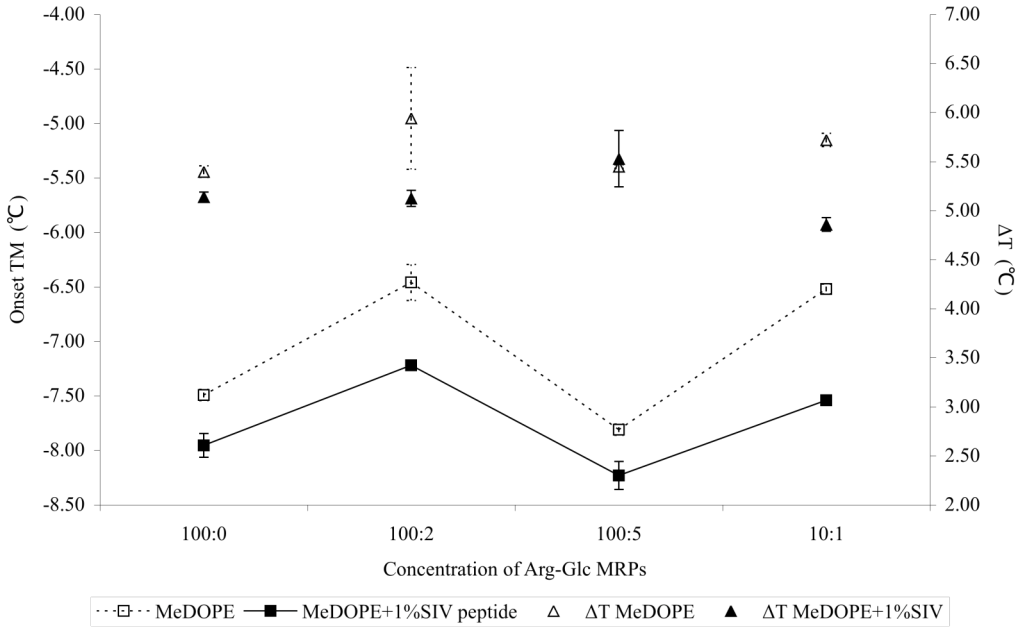

A. Effects of Arg-Glc MRPs on T_M (□ / ■) and ΔT_M (△/▲) of MeDOPE MLVs.

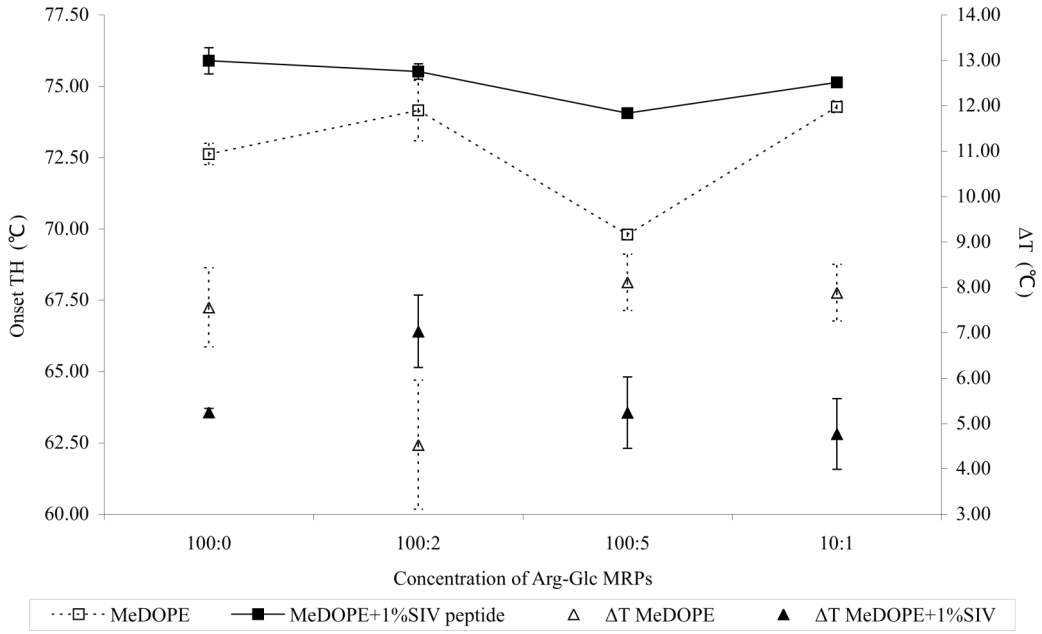

B. Effects of Arg-Glc MRPs on T_H (□ / ■) and ΔT_H (△/▲) of MeDOPE MLVs.

Figure 6.25 Effects of Arg-Glc MRPs on the phase transition behavior of MeDOPE MLVs obtained in the presence of 100:1 SIV peptide by DSC.

Scan rate: 40 °C/min. Scanning temperature range: -30~85°C. Lipid concentration: 100 mM. Data of 100:1 SIV on MeDOPE vesicles (labeled "100:0") was included for comparison (n=4; P<0.01).

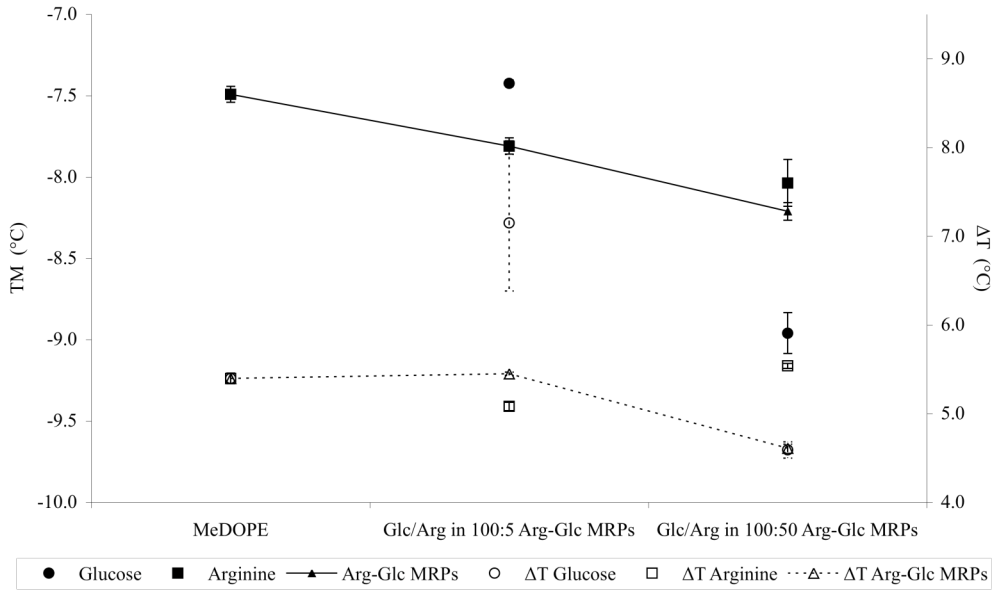

A. Effects of glucose or arginine on the T_M and ΔT_M of MeDOPE MLVs

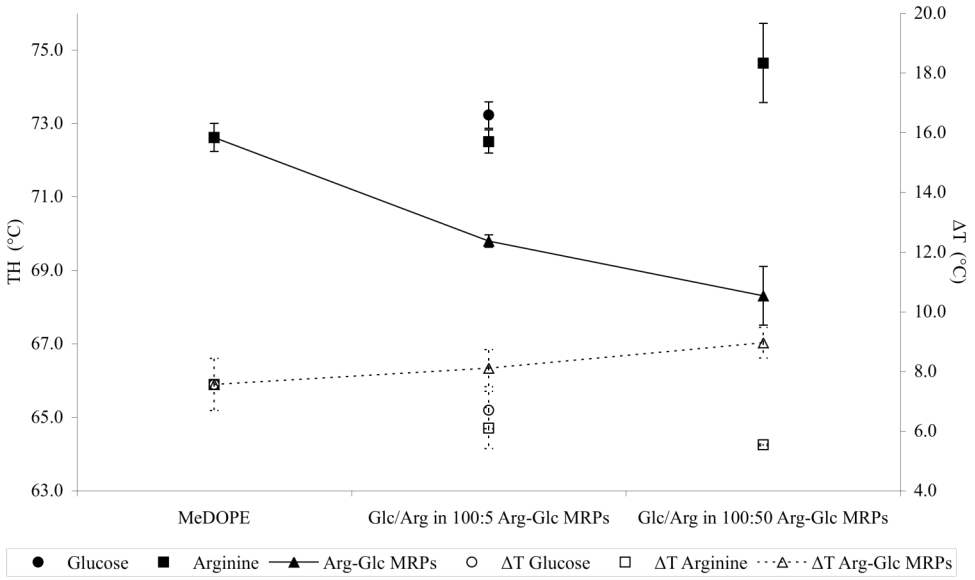

B. Effects of glucose or arginine on the T_H and ΔT_H of MeDOPE MLVs

Figure 6.26 Effects of arginine and glucose on phase transitions of MeDOPE MLVs.

Scan rate: 40 °C/min. Scanning temperature range: -30~85°C. Lipid concentration: 100 mM. The effects of Glc (at 100:1.95 and 100:19.5) and Arg (at 100:1.67 and 100:16.7) were measured to estimate the effects of Glc and Arg remained in Arg-Glc MRPs (100:5 and 100:50). The significant different T_M and T_H were observed in the presence of Glc, Arg and the MRPs, particularly in high concentration 100:50 (n=4; P<0.01).

6.4. DISCUSSIONS AND CONCLUSIONS

Lipids with a cylindrical shape and saturated fatty acid chains, e.g. DMPC, have a single, gel-liquid crystalline, transition around 24°C (Taly 2002). Other lipids with smaller head-groups and bigger tail groups present a cone-shape, such as MeDOPE. This type of lipids forms non-lamellar phases and allows us to monitor the influence of MRPs molecules on phase transition between lamellar and non-lamellar phases and, because the bigger space between the head groups of MeDOPE than those of DMPC, MRPs could also process the different impacts even in the gel-liquid crystalline phase transition of MeDOPE vesicles.

N-methyl-DOPE (MeDOPE) MLVs form different structures depending on three vital factors: temperature, concentration and thermal history of the sample. The polyphasic structural transformation of this lipid has been extensively studied with a variety of techniques (Kusube *et al.* 2006) (Harroun *et al.* 2003) (Colotto *et al.* 1996) (Siegel, Green & Talmont 1994) (Ellens, Bentz & Szoka 1986). Primarily, the MeDOPE forms three types of structure in its aqueous dispersions: lamellar, cubic and hexagonal. The cubic structure is observed as a metastable phase when the vesicles are transferring from lamellar phase to hexagonal phase. This depends on the temperature scan rate across the lamellar-to-hexagonal phase transition (Van Gorkom, Nie & Epand 1992).

6.4.1. Stability and fluidity of lipid monolayer

Despite the similarity in their chemical origin, three kinds of MRPs, referred to as RIE MRPs, MCE MRPs and Arg-Glc MRPs, produced different effects on DOPG monolayers. Under the experimental conditions of this study, each DOPG monolayer was in Liquid Expanded (LE) phase, which resembles liquid crystal phase (L_α) of the corresponding phospholipid bilayer.

Arg-Glc MRPs increased the mean molecular area (*mma*) of DOPG in LE phase, which indicates an expanding of the monolayer and probably an increase in the rigidity of the molecular packing introduced by insertion of Arg-Glc MRPs into the hydrophilic head groups of lipid. This is in good agreement with other results, in which Arg-Glc MRPs decreased the collapse rate of the monolayer and thereby enhance its stability. In contrast, RIE MRPs and MCE MRPs decreased the *mma* and the maximum surface pressure, which indicates two possible effects. The MRPs could either induce a more rigid packing of lipids by filling up the free space between lipids and squeezing the fatty acyl chains, or cause a decrease in molecular order, and therefore a less rigid packing. If the former assumption is true, a stabilised monolayer would have been demonstrated by observing a constant increase in surface pressure until it reached the maximum value as much as 44 mN/m of the homogeneous DOPG monolayer. But the surface pressure of monolayer, in the presence of RIE MRPs and MCE MRPs, reached 33 mN/m at around *mma* 70 $Å^2$ and remained at the same level while the *mma* was constantly compressed to 60 $Å^2$ (Fig 6.9). Therefore, the decreased maximum surface pressure indicates RIE MRPs and MCE MRPs are more likely to induce the less rigid packing and a shrinking in the monolayer, and thereby destabilise the monolayers but probably improve the fluidity.

Electrolytes, containing ions such as Ca^{2+} and Na^+, can significantly decrease the surface tension of phosphatidylglycerol monolayer (Marra 1986). A phosphate sodium buffer (100 mM) was used for all the measurement to give a constant electrolytic background in the subphase and monolayers. The effects of any endogenous electrolytes in the MRPs would have been swamped by the standardised Na^+ background.

Furthermore, the rising surface pressure in the π–A isotherms of RIE MRPs and MCE MRPs (Fig 6.10) indicates the amphipathic compounds from these MRPs may form a MRPs monolayer on the surface of buffer. In the presence of a lipid monolayer, these amphipathic molecules could possibly insert to the hydrophobic acryl chains of lipids and cause the

destabilisation of lipid monolayers. In contrast, the surface pressure of Arg-Glc MRPs merely rose, implying that MRPs do not form a monolayer at the air-water interface. The amphipathic components of Arg-Glc MRPs, if there are any, presumably do not contain strong hydrophobic groups. Arg-Glc MRPs prefer hydrophilic environments and could cooperate with the negative-charged phosphate head groups of DOPG and thereby stabilise the lipid monolayers.

The opposing effects of the amphipathic characteristics of these three MRPs reflect the remarkable differences in their chemical compositions. RIE MRPs and MCE MRPs are generally bigger than Arg-Glc MPRs in terms of molecular weight, including some protein-derived MRPs (see Chapter 4). The hydrophobic segments from proteins may enhance the interaction of the corresponding MRPs with lipids, particularly the hydrocarbon tails. This assumption is supported by the grafting copolymer *casein-g-dextran*, which is prepared by the Maillard reaction, and is capable of forming micelles and encapsulation of hydrophobic compounds (Pan *et al.* 2005). The micellisation of dairy proteins and their MRPs has been extensively studied in food science and colloid chemistry (Mu *et al.* 2006) (Pan *et al.* 2005) (Pellegrino *et al.* 1999).

In Fig 6.10, *mma* was used to describe the response of RIE MRPs or MCE MRPs monolayers as a function of surface pressure. However, it has to be noted that the '*mma*' values do not represent the real mean area of the MRP molecules of any single kind, due to the nature of MRPs being a mixture of products derived from the non-enzymatic glycosylation. The real mma will only be achieved by testing the purified amphipathic molecule from the MRPs.

In conclusion, Arg-Glc MRPs stabilised monolayers of phospholipids by improving the rigidity of molecular packing, whereas RIE MRPs and MCE MRPs destabilised the monolayers and improved the fluidity. The different impacts of these MRPs are largely attributed to the different hydrophobic strength of their amphipathic compositions. Arg-Glc MRPs presumably cooperate with the negative-charged head groups of DOPG lipids, while the amphipathic compounds from RIE MRPs and MCE MRPs integrate deep into the hydrophobic fatty acid tails of the monolayers.

6.4.2. Effects of MRPs on lipid order and molecular packing of lipid bilayers

The effects of Arg-Glc MRPs on lipid order and molecular packing of bilayers were examined on phosphatidylcholine and phosphatidylglycerol lamellar vesicles, with the aids of two kinds of fluorescence probes, MC540 and Laurdan. The effects of RIE MRPs were examined with Laurdan for comparison.

6.4.2.1. Effects of Arg-Glc MRPs on the fluidity of phosphatidylcholine lipids MLVs

Arg-Glc MRPs contributed a clear influence on the molecular packing of DMPC MLVs, across the melting temperature. The *r* values measured at 10°C (◆, Fig 6.11) were the highest and most stable, which are corresponding to the stable and rigid structure of bilayers in gel phase. The fluctuation of *r* measured at 23.5°C (□, Fig 6.11) is consistent with the coexistence of two phases in the bilayers across the transition temperature. The lowest values of *r*, measured at 37°C (▲, Fig 6.11), indicating the crystalline phase of DMPC MLVs, and the concentration-dependant effects of Arg-Glc MRPs on the molecular packing of the bilayers. For DMPC, the free space between the head groups is limited due to the rigid packing of the tails. The MC540 will possibly locate parallel to the bilayer surface, right above the glycerol backbone of the lipid, while Arg-Glc MPRs might fill up the space left over. The increase of *r* at lipid/MRPs ratio of 100:5/25/125 indicates the MRPs might help to hold the lipids together and encourage the more rigid molecular packing. As a result, the bilayers would become less fluid. This is constant with the fact that the bilayers in their gel phase have a generally higher *r* than in fluid phase. Furthermore, the correspondence of anisotropy constant to the MRPs concentration became clear when the lipids transferred to liquid-crystalline phase, implying the bilayers in the fluid phase are easier for the MRPs to incorporate with.

Compare to the DSC measurements, the proportion of MRPs used in this fluorospectrometric study was much higher in terms of lipid/MRPs molar ratios, while the difference in the lipid concentration of the vesicle suspension was also remarkable. For example, the lipid concentration of MLVs was 10 μM for MC540 labeled measurements, 50 μM for Laurdan, but 100 mM for DSC. The highest lipid/MRPs molar ratio was 100:625 in MC540, while it was only 100:50 in DSC. At such a high proportion as 100:625, the profiles of MLVs should have been covered up by the profiles of MRPs. However, the typical spectrum profile of

lipid MLVs was obtained even at such a high proportion, indicating the molar ratio of lipid/MRPs in MLVs suspension does not necessarily reflect the real ratio between lipid and MRPs molecules on bilayers. A number of MRPs molecules may remain in the aqueous solution. Apart from the amount of MRPs applied to the lipid system, the true ratio is also depending on the water content of the vesicle system, and the reversible binding of MRPs to lipids bilayers. For example, in DMPC MLVs, the water content is ~93% (w/w) in DSC samples, while merely 100% (w/w) in fluorospectrometric measurements. The remarkable less amount of water in DSC samples provide a much higher possibility for the amphipathic MRPs molecules to interact with lipids rather than surrounding by water. Therefore, the ratio 100:50 in 100 mM MLVs might allow much more contacts between MRPs and lipids than what the ratio 100:625 in 10 μM MLVs might conduct, and thereby is more close to the true lipid/MRPs ratio in bilayers. This can also explain the differences in the effective concentrations of the MRPs among the different types of measurements.

However, the uncertainty remains in the measurements involved a high proportion of MRPs and a low concentration of lipids. The other biophysical methods like neutron diffraction and X-ray diffraction provide the better models to monitor the ratio between lipids and the MRPs in bilayers in the more accurate way.

6.4.2.2. Effect of RIE MRPs on the polarization and order of DOPC, DOPG and DMPC vesicles

The emission wavelength and intensity of Laurdan are highly sensitive to the dipole relaxation and polarization of the environment, in case of lipid bilayer, the water penetration and polarity of the glycerol backbone region in lipid bilayer (Parasassi *et al.* 1990). As reported by Vequi-Suplicy, Laurdan in DPPG and DLPC bilayers has a maximum emission wavelength of ~440 nm in gel phase, whereas in the fluid phase the maximum emission wavelength showed a red-shifts to 490 nm. There are two average positions for Laurdan. Firstly, it sits inside the gel-phase bilayers with less mobility and less water relaxibility, mainly emitting at 440 nm. Secondly, it locates at the water/lipid interface of fluid-phase bilayers, rather mobile, mainly emitting at 490 nm (Vequi-Suplicy, Benatti & Lamy 2006). The 440-to-490 nm red-shift has been attributed to an increase in the accessibility of Laurdan to water molecules around the lipid head groups (Parasassi *et al.* 1991). In my studies, the three lipids assayed, DOPC, DOPG and DMPC, are all in the liquid-crystalline phase at 37˚C. Their λ_{max} varied from 470 nm to 490 nm, which is close to the reported wavelength

range of liquid-crystalline phase for PC and PG lipids. In the presence of RIE MRPs, the 5-8 nm red-shifts were observed in DOPG and DMPC vesicles, accompanied by the increases in the emission intensity at the λ_{max}. These results indicate RIE MRPs induce a higher fluidity in both of DOPG and DMPC bilayers, in which Laurdan gets access to more water molecules between the head groups of lipids.

The fluidity-increasing effects of RIE MRPs are dominantly supported by the decreases in GP_{ex} induced by the MRPs. When the lipids transit from gel phase to liquid-crystalline phase in a homogeneous bilayer, the *GP* decreases dramatically, implying a much higher level of water penetration and a much lower lipid order. RIE MRPs caused the decreases in the GP_{ex} of Laurdan, which implies the less ordered lipid packing of the bilayers. RIE MRPs therefore disorder the bilayers of DOPC, DOPG and DMPC, improve the fluidity of bilayer. In DOPG monolayer (as described in Section 6.3.1), the decrease in the molecular area of lipids in the presence of RIE MRPs indicates two possible assumptions: RIE MRPs occupy part of the surface and squeeze the lipids to pack more rigid; or alternatively, RIE MRPs disorder the monolayer and accelerate the forming of micelles and the break-down of monolayer. The decrease in GP_{ex} at the excitation wavelength of 350 nm finely supports the later assumption, in which a bilayer disordering effect of RIE MRPs is suggested. The GP_{ex} at Ex350nm has been widely used to determine the polarity of bilayers in various lipids (Harris, Best & Bell 2002) (Ashley *et al*. 2006).

However, some unexpected increases were observed in the GP_{ex} at Ex410nm and in GP_{em} at Em440nm, which is in opposite to the decreases on the GP_{ex} at Ex350nm. A full understanding of this increased *GP* remains unknown, although the *GP* has been suggested to depend on the homogeneity of the membrane as well as the phase of lipids. *GP* become independent to the emission wavelength only when it is measured in the single-phase membrane (Parasassi *et al.* 1990). In single-phase vesicles, the *GP* is independent to the excitation wavelength, whereas in the multi-phase vesicles, a lower energy of excitation wavelength (i.e. 410-nm) selected populations with higher polarization (smaller GP), with respect to the 350-nm excitation. In the presence of RIE MRPs, a second phase of lipids might be formed in the vesicles apart from their native phase, which can be sensed by Laurdan at the longer or shorter excitation wavelengths. In my studies, among the three lipids observed, DOPG or DOPC vesicles are more mobile than DMPC vesicle (Table 6.2&6.3), and have the higher polarization, which can be sensed by GP_{ex} at Ex410nm critically. The increase in the GP_{ex} at Ex410nm may suggest a second phase, relatively more rigid than the first phase, was created by incorporating of RIE MRPs to the bilayer, and

represented as lower polarization and higher rigidity. But in case of DMPC vesicle, RIE MRPs elevated the polarity and disorder the lipid packing.

Another change in the GP_{ex} requires an attention is the opposite results observed in SUVs and MLVs of DOPG at Ex410nm. For SUVs, the MRPs decreased the GP_{ex}, whereas an increase was observed for MLVs. Although both types of vesicles are composed by lamellar bilayers, only 10% or less of the total phospholipid is found on the outer leaflet of MLVs, while around 60 to 75% of totoal phospholipid distributes on the outside surface of SUVs (Yeagle 1993). The enormous difference in the amount of phospholipids exposing to the membrane interactive agents may have affected the general polarity profiles of bilayers reported by Laurdan in this two types of liposomes.

As mentioned above, the *GP* does not completely separate the contributions of the two excited states, which may refer to two phases of lipids. The areas of the two guassian peaks, which were fit to the emission spectra or excitation spectra of Laurdan in liposomes, are the better parameter than *GP* for analysing the structural changes occurred during the phase transition or the sub-phase transformation of lipid bilayers. For example, the gel-to-liquid crystalline transition of DPPG can be finely monitored by a dramatic decrease in the short-wavelength peak area, which is paralleled by a dramatic rise in the long-wavelength peak area (Vequi-Suplicy, Benatti & Lamy 2006). This could be a better way of studying MRPs' effects on the polarity of lipid membrane than the *GP*, for further studies.

To sum up, Arg-Glc MRPs decrease the fluidity of unsaturated phospholipids bilayers when increase that of saturated phospholipids bilayers, implying a stabilising effect on the fluid phase of lipid. RIE MRPs enhance the polarity of hydrophilic region of lipid bilayer, which infers a disorder effect on the lipid packing in the fluid phase. However, an opposite effects from the same MRPs should be take into account, by which the RIE MRPs seems to improve the lipid order of highly mobile bilayers, e.g. the liposomes composed with DOPG or DOPC, without changing the phase of lipids. These assumptions are in a good agreement with the previous observations on lipid monolayer, in which Arg-Glc MRPs stabilised the DOPG monolayer while RIE MRPs presumably destabilised the monolayer. In conclusion, MRPs generally conduct a stabilisation effects on the liquid-crystalline phase of lipids, meaning the lipid bilayer tends to remain in lamellar fluid phase in the presence of MRPs, with a respect to the destabilisation effects of MRPs to the lamellar gel-phase.

6.4.3. Stabilisation and destabilisation effects of Arg-Glc MRPs on phospholipids MLVs

6.4.3.1. DMPC MLVs

During phase transitions, the stabilisation of lipid bilayers may result in an elevated onset temperature of transition, while a destabilisation may reduce the transition temperature. On the other hand, it is not sure that a less ordered molecular packing of lipids will cause an increase or decrease of general heat consumption. This depends on two factors: when the transition started, and how long does the transition last for.

In DMPC MLVs, Arg-Glc MRPs have minor effects on T_M but significant impacts on ΔH_f. MRPs destabilised the rigid structure of DMPC vesicles by insert between the DMPC molecules. Since DMPC molecules have a cylindrical shape with almost equal sizes of head groups and tail groups, they pack in such a rigid way that even the insertion of a small amount of MRPs molecules can significantly disrupt the rigidity of a leaflet. The loss of rigidity leads to the drop in transition temperature. However, at the same time, the Arg-Glc MRPs molecules in the leaflet may act as a 'connector' to imobilise lipids around MRP molecules. This may create a subphase besides the gel phase. The heat consumption of transition would then be elevated to cope with the extra energy requirements for melting this new structure. However, when the concentration kept rising, a growing amount of MRPs inserted to the lipid bilayers and finally broke down part of the lamellar structure in gel phase, which caused the decrease in heat consumption.

6.4.3.2. MeDOPE MLVs

As shown in Fig 6.22, the T_M of MeDOPE is -7.5°C, which is the same as that previously reported (Kusube *et al.* 2006). A wide range of temperature has been reported for the inverse hexagonal phase transition. As revealed in an X-ray diffraction study reported by Cherezov, the Q_{II} phase appears at 59.1°C while the H_{II} phase appears at 63.5°C, at a scan rate of 1.5 °C/h. The T_H increased by 2°C when the scan rate was raised to 6 °C/h (Cherezov *et al.*, 2003). However, Harroun *et al.* reported the T_H at 64°C, and the T_Q at about 75°C at the scan rate of 30 K/h (Harroun *et al.*, 2003). In my measurements, there is a main phase transition at 72.6°C at the scan rate of 40 K/min which is presumably T_H since hexagonal phase is the major structure visible at the high temperature for MeDOPE. My T_H is much higher than the reported value. A remarkable difference among these measurements is the

scan rate. It is 40 °C/min in my DSC measurement compared to 1.5~30 °C/h in the X-ray diffraction measurements. There is also another phase transition at a lower temperature (~62°C), presumably the T_Q, which did not appear in every single isothermal scan of DSC. Data is given in Fig 6.22B for reference.

At a concentration of 100:5, Arg-Glc MRPs destabilised the lipid bilayers of MeDOPE in the lamellar phase, both in gel and liquid crystalline phases, and accordingly lowered the T_M and T_H (Fig 6.22A&C). However, when the ratio went up to 10:1, the MRPs stabilised the bilayer in the lamellar phase and elevated the T_M, T_Q and T_H. At ratios higher than 10:1, the MRPs destabilised the bilayers again. But T_H was constantly going down, like what occurred to T_M and T_Q. T_H rose back to about the same temperature as that of pure MeDOPE, at ratio of 10:4, indicating another stabilisation in the lipids structure before it transfers to inverted hexagonal phase. At the highest ratio, a bilayer broke down was implied by the acute drop in T_H and rise in ΔH_f.

The glucose and arginine remaining among the Arg-Glc MRPs increased T_H but decreased the ΔT_H, indicating a stabilising effect on bilayers and a shorter intermediate status during the phase transition. In contrast, at the corresponding concentrations, the Arg-Glc MRPs destabilised the lamellar phase and induced a longer intermediate status from lamellar phase to hexagonal phase. Therefore, the effects of Arg-Glc MRPs are not correlative to the glucose or arginine remaining in the MRPs. For the gel-to-liquid crystalline phase transition, the effects of Arg-Glc MRPs were similar to those of arginine, whereas were much weaker than those of glucose. Glucose has been predicted by a molecular dynamic simulation study, to interact directly with the headgroups of phospholipids through hydrogen bonds, thereby replace water bound to the bilayers. Glucose was also suggested to prevent the thermal disruption of lipid bilayers at a high temperature (Pereira, Hünenberger, 2006). The interaction of glucose with the headgroups of lipids may attribute to its effects on the phase transitions of MeDOPE MLVs.

Taking together the effects of Arg-Glc MRPs across all three phase-transitions, a general pattern of MRPs' effects emerges. The stabilisation actions of the MRPs are split into two stages. Firstly, the MRPs fill up the spaces in the head group region of leaflet and keep the hydrophilic heads away from each other. This prevents the development of negative curvature strain in the bilayers, and subsequently inhibits the lamellar/non-lamellar transition. The bilayers prefer to remain in gel or liquid crystal phase. MRPs at molar ratio of 10:1 performed the strongest stabilisation effects of this kind. Secondly, when more MRPs

molecules accumulate in the bilayers, they start to destabilise the lamellar structure of lipids and favor the lamellar-inverted cubic transition. Once the lipids transfer to non-lamellar structure, the lipids prefer to stay in cubic phase rather than hexagonal phase. The best example for this kind is bilayers contain Arg-Glc MRPs at molar ratio of 10:4. MRPs decreased the T_M and T_Q, but raised the T_H. At concentration beyond this point, the bilayer was further destabilised and became easier to transfer to inverted hexagonal phase.

A drop in transition temperature can correlate with a rise in heat consumption, such as that observed in MeDOPE MLVs in the presence of Arg-Glc MRPs. For example, Arg-Glc MRPs, at the molar ratio of 10:5 in lipid bilayers, decreased the transition temperature of lamellar-inverted hexagonal and increased the heat consumption. Similar outputs were observed in the gel-liquid crystalline phase transition at higher molar ratios than 10:1. This implies that Arg-Glc MPRs destabilise the lipid bilayers at the high concentrations and promote the phase transition from an ordered status to a less ordered status. At the meanwhile, due to the possible coexistence of several sub-phases induced by interference of MRPs, the amount of energy, in terms of heat as a function of time, was increased to overcome the overall energy barrier and encourage the formation of a regular structure.

In comparison with DMPC, Arg-Glc MRPs have almost the opposite effects on MeDOPE. At lipid/MRPs molar ratios ranging from 100:1 to 10:4, the MRPs have opposite effects on the stabilities of the two lipids. For example, MRPs stabilise DMPC bilayers at 100:5, but destabilise MeDOPE bilayers at the same concentration. At the molar ratio of 10:5, both lipids vesicles are destabilised. A similar trend is found in the heat consumption of the phase transitions. This difference could be considered as a result of different free volume between the lipid molecules.

6.4.4. Effects of SIV fusion peptide and Arg-Glc MRPs on phase behavior of lipid vesicles

SIV fusion peptide raises the T_H of MeDOPE by 4°C but decreases T_M at 40 K/min. This is in agreement with X-ray diffraction data from Harroun (Harroun *et al.* 2003), in which the SIV peptide (lipid/peptide=100:1) raises T_H by 10°C (to about 74°C) at the temperature scan rate of 30 °C/h, while at 100:2 SIV, the hexagonal phase is eliminated. In contrast, at 100:1 SIV raises T_H to about 76°C at the scan rate of 40 °C/min in my DSC studies. And at 100:2 SIV, the hexagonal phase is still observed as T_H is about 77°C. It has been described for T_H

to be scan-rate-dependent (Colotto *et al.* 1996), which is presumably to be varied along the different temperature scan rate. This might explain why the T_H of MeDOPE MLVs obtained in my DSC study is higher by 2°C than that of X-ray data at 60 °C/h. However, one can also attribute this variation to the differences in the sensitivity of the two methods. By analysing the Gaussian peaks, a minor change in structure of bilayers can be detected and examined with X-ray scattering. DSC is capable of examining main phase transition events like lamellar-to-hexagonal phase transition, but has a limited capacity to track transient structures of intermediates, e.g. cubic phase, at the relatively high scan rate employed in this study.

SIV promotes the breakdown of lamellar structure and the formation of cubic phase (Harroun *et al.* 2003). Some effects of SIV on lamellar-to-cubic phase transition, such as lowering the T_Q, are not readily to be measured by DSC as shown in Fig 6.22B, since the transient phases are in the continuous change. However, the fusogenic nature of the peptide is still implied by the drop in ΔT_H and heat consumption of L_α-H_{II} phase transition. The 2°C decline in the temperature range of this transition, in the presence of 100:1 SIV, possibly suggests a relatively uniform lipid packing is installed in the transient structure prior to the occurring of L_α-H_{II} transition. Furthermore, in terms of its effect upon T_M, T_H, ΔH_f and ΔT_H, 100:2 SIV peptide is more potent than 100:1 SIV, but not much. It is also consistent with previous X-ray diffraction data reported by Harroun *et al.*.

Arg-Glc MRPs partly offset the effects of SIV peptide on MeDOPE phase transition, in a concentration-dependent manner. In the presence of 100:1 SIV, the MRPs at 100:2 and 10:1 stabilise the gel phase when 100:5 MRPs destabilises the gel phase and liquid crystal phase. However, due to the lack of reproducible data upon cubic phase, no assumption can be drawn from DSC data to explain the effects of Arg-Glc MRPs.

In conclusion, Arg-Glc MRPs expand and stabilise the DOPG monolayer, reinforce the rigidity of molecular packing in DMPC bilayers and stabilise the lamellar phase of MeDOPE MLVs at a suitable concentration (100:2 or 10:1 for example). RIE MRPs destabilise the DOPG monolayer, increase the polarization and fluidity of phospholipids bilayers. The MRPs reversed the destabilising effects of SIV fusion peptide on the lamellar phase of liposome, to potentially inhibit membrane fusion induced by SIV.

CHAPTER 7

DISTRIBUTION OF MRPS IN LIPID BILAYERS

7.1. AIMS OF THIS CHAPTER

In the previous chapters, the interactions of Arg-Glc MRPs, RIE MRPs and MCE MRPs with lipid bilayers have been investigated with various methods that have evaluated their effects on the molecular packing, polarization, stability, fluidity and phase transition of phospholipid monolayers and bilayers. In this chapter, the insertion and positioning of MRPs in the lipid bilayers was studied by neutron diffraction to reveal the distribution pattern of the MRPs in DOPC and DMPC bilayers. The position of MRPs in bilayer provides fundamental structure information on the mechanism of the interaction of MRPs with phospholipids.

Arginine has been shown to be a major component of the roots, as described in Chapter 4, and in published studies (Xiang *et al.* 2007) (Dong & Liu 2001), and is a promising molecule for generating MRPs. The disappearance of three quarters of the free arginine after boiling water extraction adds weight to this argument. Therefore, together with RIE MRPs, the Arg-Glc MRPs prepared by the Maillard reaction between equal molar amount of arginine and glucose was used as a modelled material in this study.

7.2. METHODS AND MATERIALS

7.2.1. Sample Preparation

Lipids were purchased from Avanti Polar Lipids or Sigma. 20 mg samples were dissolved in chloroform and deposit onto quartz microscope slides by a nitrogen propelled artist's airbrush. The slides were then placed in a vacuum for 2 h in order to remove all traces of the solvent. Samples were hydrated in a humid atmosphere with water containing 8.06% or 25% ^2H_2O. The samples were protected from light and oxygen whenever possible in order to reduce the chance of lipid peroxidation.

7.2.2. Neutron data collection

Neutron-diffraction measurements were carried out on the D16 membrane diffractometer at the Institut Laue et Langevin, Grenoble, France, or the V1 membrane diffractometer at the BENSC, Helmholtz Zentrum Berlin, Germany. Humidity control was achieved by changing the temperature of the sample can (at ILL) or changing the saturated salts solutions in the sample can (at BENSC). At ILL, the difference between the ambient temperature in the sample can and the temperature of water slots at the bottom of the sample can was adjusted individually with water baths.

Each sample was quickly transferred straight from a humid tube into the sample can. After a minimum 6 h equilibration, a series of continuous θ-2θ scans were initiated (from θ= 1.5° to 20.0° for DOPC, 1.8° to 16.0° for DMPC). The samples were run at 298 ~ 303 K for DOPC, and at 310K for DMPC.

7.2.3. Data analysis

The two-dimensional array of detector counts for each frame of data was corrected for variations in pixel response. The complete set of frames from each scan were then collapsed into a linear spectrum and combined to generate a pseudo θ-2θ scan. All of the analysis to this stage was carried out by the software LAMP on D16 or CARESS on V1. The background around each peak was fitted and subtracted using PeakFit (Systat Software Inc., USA) or Igor Pro (Version 6.0, WaveMetrics Inc., Oregon, USA). Gaussian distributions were then fitted to the Bragg reflections and the angular position, width and area of each

peak recorded. Absorption and Lorentz corrections were applied and the square-root of the intensities taken to produce the structure factor amplitudes.

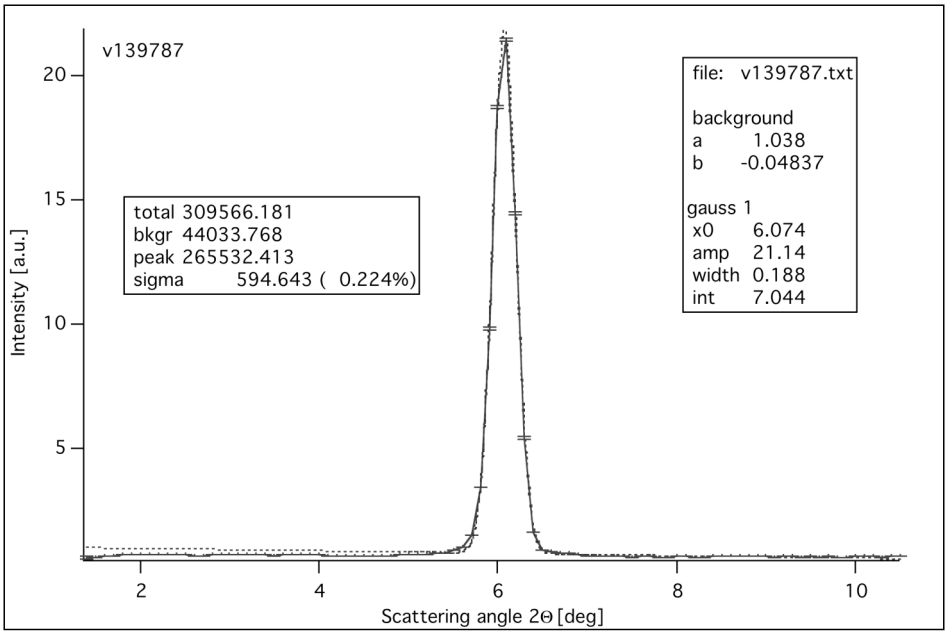

Figure 7.1 Gaussian-fitting of a lamellar diffraction peak (1st order) of DMPC bilayers at 96% RH in the presence of 8% $^{2}H_2O$.

7.3. RESULTS AND DISCUSSIONS

7.3.1. Distribution of Arg-Glc MRPs, RIE MRPs and MCE MRPs across the DOPC bilayers

Neutron scattering length density profiles were calculated from the structure factors in Table 7.1. Difference profiles were calculated by subtracting the profile of DOPC bilayers from each of the DOPC+MRPs profiles in turn. The results are shown in Fig 7.2. Since any profile constructed from an incomplete set of structure factors will contain termination error – artefactual structure resulting from the abrupt termination of the Fourier series of structure factors – models of the MRP distributions were constructed and fitted in reciprocal space, to avoid this problem. The models consisted of calculated diffraction patterns of pairs of Gaussian distributions, which were fitted to the difference structure factors by least-squares refinement. Each Gaussian fitting profile represents the distribution of one population of the sample. The results of this model fitting are shown in Fig 7.2, Fig 7.3 and Table 7.2. Termination error often manifests itself in the form of small peaks or "ripples", such as those seen in the DOPC+MCE MRPs plots. The criterion for determining whether the features are real or artefacts is to see if Gaussian peaks can be fitted to them in reciprocal space.

Possibly the most important observation is that the three products have significantly different interactions with DOPC. One criticism that has been leveled against MRPs as pharmaceutical agents is that the preparation produces a spectrum of products, so any interaction with cellular components is expected to be vague and ill defined. These results clearly refute this argument; the different products have different distributions across the phospholipid bilayer system. It is worth noting that biological membranes tend to comprise a mixture of molecular species, yet membranes from different sources (e.g. mitochondria, bacteria, nerve axon) have well defined, but very different molecular composition and physico-chemical properties.

The RIE MRPs results reveal that the principal site of interaction is a well-defined peak 19.5 Å from the centre of the bilayer. This position lies in the interface region of the bilayer, close to the glycerol backbone of the phospholipids (in neutron scattering profiles of phospholipids, the maxima are caused by relatively low hydrogen content of the glycerol and the phosphates). The peak accounts for 65% of the total scattering density; the other 35% lies deeper, at 10.4 Å from the bilayer centre. Of the three products studied, RIE MRPs is the one that inserts deepest into the bilayer.

The difference profiles for MCE MRPs display some similarity to the RIE MRPs profiles, but in this case, all of the MRPs lie in the interface region, a bit closer to the centre of bilayer (18.1 Å). Gaussian fitting reveals that the small ripples observed at around 6.5 Å from the bilayer centre are actually artefacts caused by Fourier series truncation, indicating that none of the MCE MRPs penetrates into the fatty-acyl region of the bilayer, in contrast to the RIE MRPs, in which 35% of the total is found deep within the bilayer core.

Although the synthetic MRPs (Arg-Glc MRPs) and RIE MRPs distributions are not the same, there are also some similarities between the two. In the Arg-Glc MRPs profiles, there is a major peak at 14.9 Å from the bilayer centre. This lies much closer to the fatty-acyl region than the MCE MRPs peak, indicating that the Arg-Glc MRPs is able to penetrate deep into the core of the bilayer, similar to the RIE MRPs. This is very interesting, because the presence of arginine in the reaction mixture would lead us to expect the resulting charged MRPs to interact with the polar environment of the water layer and the surface of the bilayer.

Table 7.1 Neutron structure factors for bilayers composed of DOPC and of DOPC with each of the three types of MRPs.

	$F^*(1)$	$F^*(2)$	$F^*(3)$	$F^*(4)$	$F^*(5)$
DOPC	7.13	-5.35	-3.20	-1.09	1.04
	±0.26	±0.22	±0.16	±0.11	±0.11
DOPC+RIE MRPs	8.57	-5.98	-3.56	-1.25	1.16
	±0.31	±0.25	±0.19	±0.14	±0.14
DOPC+Arg-Glc MRPs	8.44	-5.35	-3.01	-0.83	1.11
	±0.29	±0.21	±0.16	±0.11	±0.11
DOPC+MCE MRPs	8.12	-5.73	-3.54	-1.19	1.17
	±0.28	±0.22	±0.17	±0.12	±0.12

The bilayers were hydrated with 8% ^2H_2O, since water of this isotopic composition has a net neutron scattering length density of zero.

Table 7.2 Gaussian models of bilayer distributions of (a) MRPs and (b) water.

(a) MRP distribution		DOPC	DOPC+Arg-Glc MRPs	DOPC+RIE MRPs	DOPC+MCE MRPs
Gaussian 1	Position*	-	26.0 Å	19.5 Å	18.1 Å
	Width#	-	6.0 Å	6.6 Å	6.9 Å
	Occupancy	-	35%	65%	100%
Gaussian 2	Position*	-	14.9 Å	10.4 Å	-
	Width#	-	7.6 Å	7.3 Å	-
	Occupancy	-	65%	35%	-

(b) Water distribution		DOPC	DOPC+Arg-Glc MRPs	DOPC+RIE MRPs	DOPC+MCE MRPs
Gaussian 1	Position*	24.5 Å	23.2 Å	23.4 Å	22.9 Å
	Width#	5.7 Å	6.7 Å	6.2 Å	5.5 Å
	Occupancy	100%	77%	73%	74%
Gaussian 2	Position*	-	14.7 Å	15.6 Å	15.3 Å
	Width#	-	5.6 Å	5.3 Å	4.9 Å
	Occupancy	-	23%	27%	26%

The position, width and size of Gaussian distributions were fitted, in reciprocal space, to difference neutron structure factors. Five orders of diffraction were used in the fitting procedure. * The position of each label site is expressed as distance from the centre of the bilayer; # the width is the half width at 1/e height.

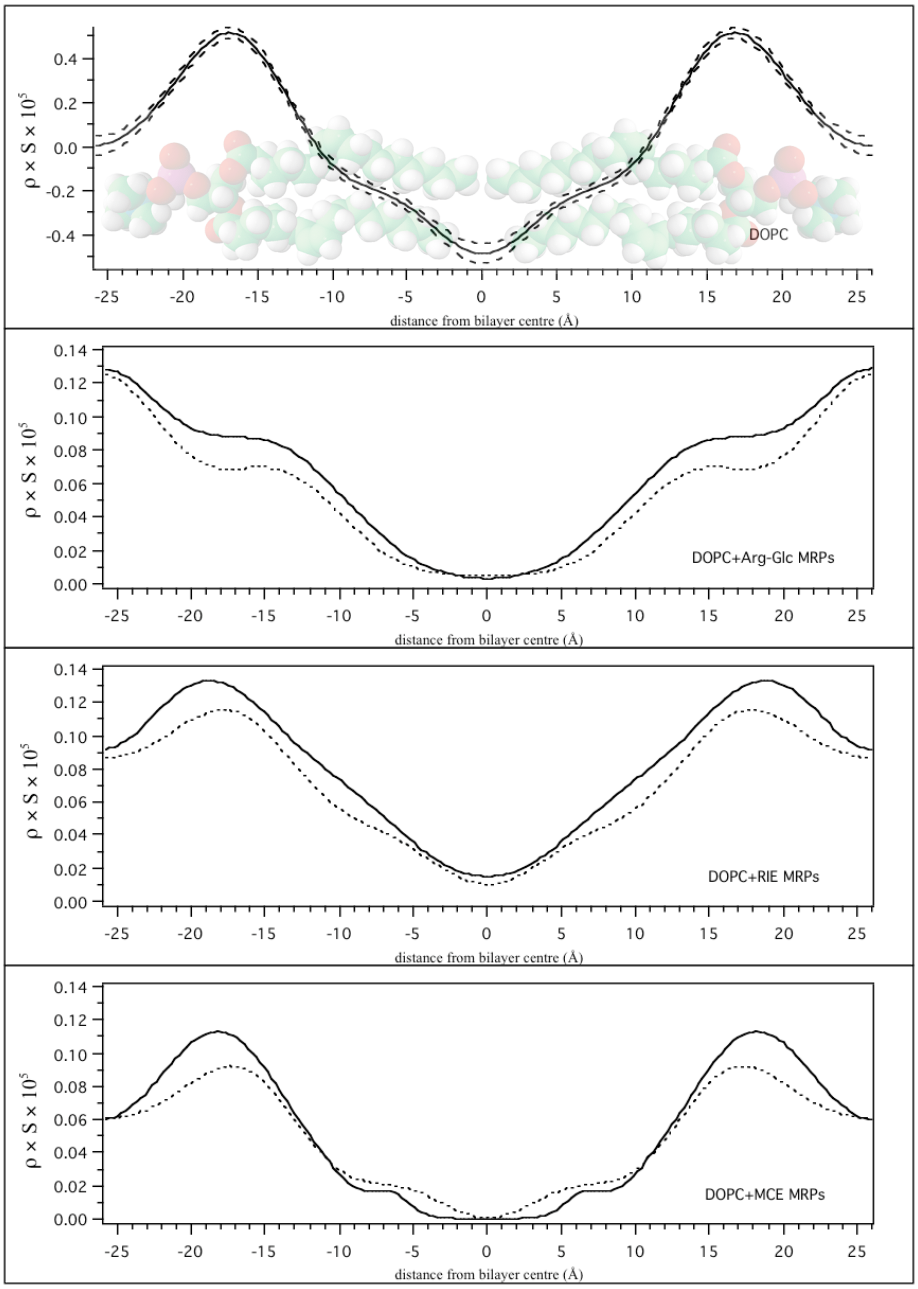

Figure 7.2 Neutron scattering length density profiles of the distribution of each of the three different types of MRP across DOPC bilayer.

The profiles were reconstructed from difference structure factors and therefore only show changes in neutron scattering length density brought about by the introduction of MRPs. The top panel shows a bilayer profile of DOPC, for comparison and orientation. In each case, the structure factors for bilayers hydrated with 8% ^2H_2O were used to calculate the profiles (Table 7.1), since water of this isotopic composition has a net neutron scattering length density of zero. The top panel also gives an indication of the errors. The dashed lines represent the maximum and minimum neutron scattering length density at each point, based on reconstructions using all possible combinations of structure factors within the range defined by the calculated errors shown in Table 7.1. The three panels below give the profiles of three MRPs across DOPC bilayers. The dashed lines are the difference profiles (minus DOPC), and the solid lines are the corresponding best-fit Gaussian distributions for these difference profiles.

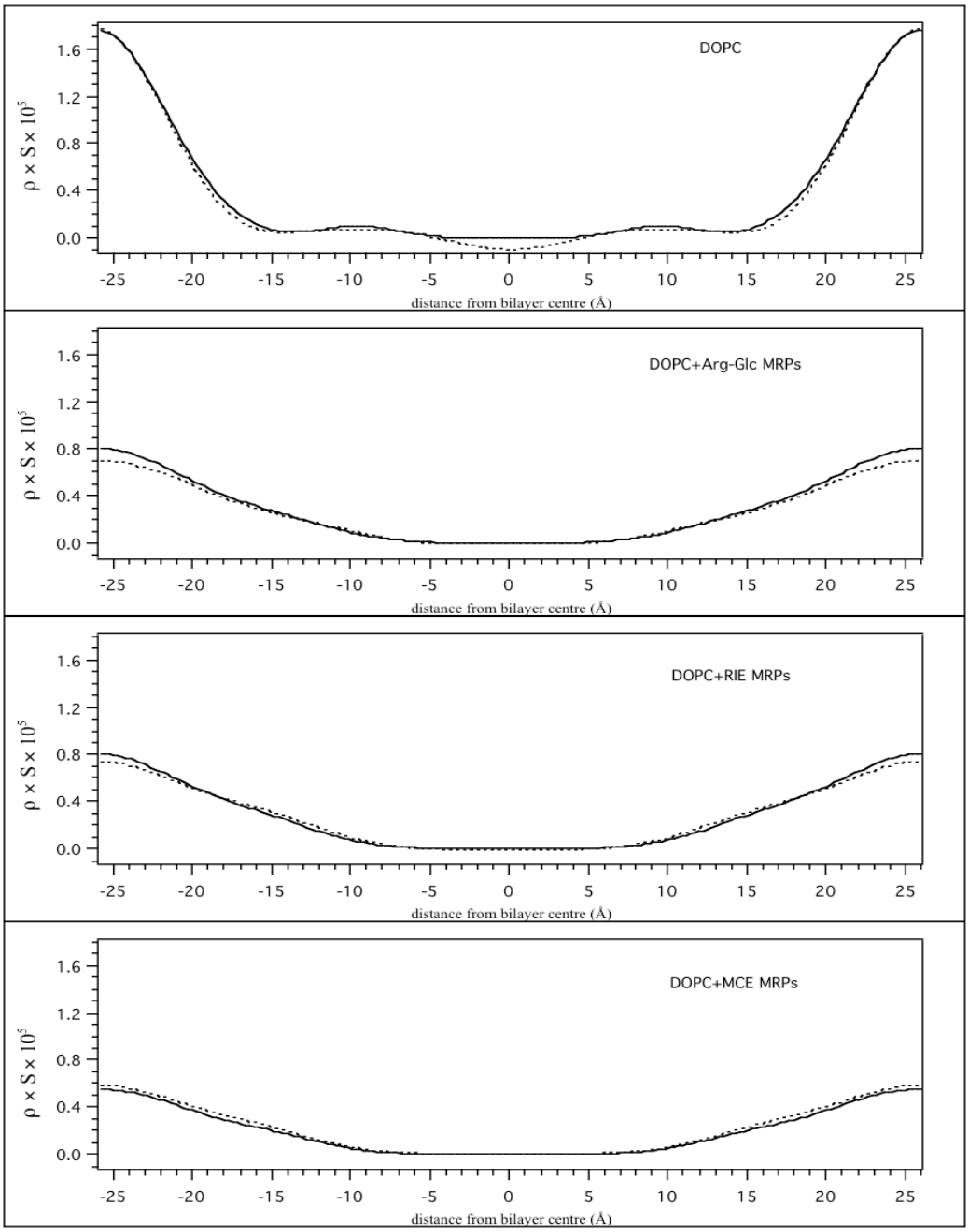

Figure 7.3 Difference profiles of the neutron scattering length density of water (^2H_2O) in stacked phospholipid bilayers of DOPC and DOPC with each of the three types of MRPs.

The dashed lines are the difference profiles, and the solid lines are the corresponding best-fit Gaussian distributions for these difference profiles. Structure factors for bilayers hydrated in 8.1% H_2O were subtracted from corresponding 25% ^2H_2O structure factors and the result used to calculate the profiles shown.

However, 65% of the Arg-Glc MRPs are actually lying below the level of phosphates, indicating that the interaction is not simply based on charge. The minor peak (35%) in the bilayer distribution of Arg-Glc MRPs is centred at 26.0 Å, in the water layer, very close to the phosphate headgroups of the lipid molecules, which lie at 25.5 Å (Fig 7.2). This may have something to do with amino groups left after the Maillard reaction. About 31% of arginine and 39% of glucose remain in the Arg-Glc MRPs. The overall pattern of interaction of the Arg-Glc MRPs is similar to that of the RIE: there are two peaks in the distribution (though the relative heights of the peaks differ between the two types of MRPs, suggesting that the simple arginine-glucose preparation does not fully replicate the complexity of the RIE MRPs); and one of the peaks penetrates deep into the hydrophobic core of the bilayers.

The two populations of density observed in the Arg-Glc MRPs and the RIE MRPs may result from saturation of preferred membrane locations, with the excess material forced to occupy a second, less-favourable location, or it could simply reflect different populations of MRPs. Given the relatively unregulated nature of the Maillard reaction, the second suggestion is a strong possibility. The *d*-repeats, which refer to the thickness of each repeating unit, comprising one bilayer and one water layer of the lipid stack, are about 52.0 Å, which is consistent with the lamellar spacing values of DOPC bilayer measured by X-ray diffraction at 30°C and 98% RH (Hung *et al.*, 2008). The introduction of RIE MRPs and Arg-Glc MRPs slightly expanded the *d*-repeat of the system, when MCE MRPs decreased the *d*-repeat slightly (*d*-repeats at 25°C, 97% RH: DOPC 51.74 Å; DOPC + RIE MRPs 51.96 Å; DOPC + Arg-Glc MRPs 52.06 Å; DOPC + MCE MRPs 51.57 Å). However, these differences in *d*-repeat are very small and probably not significant.

Fig 7.3 shows water difference profiles, calculated by subtraction of an 8.1% $^{2}H_2O$ profile from the corresponding 25.0% $^{2}H_2O$ profile. The results reveal the distribution of water across the unit cell, because everything cancels out in the subtraction except for the different neutron scattering length density of the 25% $^{2}H_2O$ water. As with the MRPs distributions (Fig 7.2), Gaussian distributions were fitted to the water distributions, using the structure factors rather than the profiles themselves, in order to avoid Fourier series truncation errors. The results are shown in Table 7.2(b). One complication with the MRPs' distribution-difference profiles, as described above, is that the profiles report all changes to the bilayer structure caused by the introduction of the MRPs. This means that any phospholipid rearrangements will also contribute to the difference profile, as long as there is a net shift of scattering density along the bilayer normal. For this reason, the water-difference profiles can be particularly informative, since all other contributions are cancelled out.

The water profile for pure lipid bilayers (Fig 7.3 top panel) was entirely consistent with previous neutron studies of phospholipid membranes (Harroun *et al.* 2005). The peak (split between the two ends of the profile in the figure) represents a block of water confined between adjacent bilayers in the multi-bilayer stack. Although the peak was fitted (in reciprocal space) to a pair of Gaussians, centred at 24.5 Å from the middle of the bilayer and 5.7 Å wide (full width at 1/e height). These Gaussians represent the hydration shells around the phosphate-containing headgroups of the lipids and describe a typical water distribution profile across a DOPC system. The minor fluctuations between 10 Å and 40 Å are caused by termination error, due to the finite number of Bragg peaks used in the reconstructions.

As shown in Table 7.2(b), water penetrated deep into the lipid bilayers in the presence of MRPs. Consistent with the observation (above) that the RIE MRPs has the deepest penetration into the bilayer, the main peak of water boundary went from 24.5 Å of pure DOPC to 23.4 Å of RIE MRPs and occupied 73% of total, while reducing the width of the first peak by 0.4 Å. The second peak appeared at 15.6 Å, but not as deep as the RIE MRPs 10.4 Å. Similar to this, insertion of Arg-Glc MRPs mainly lied at 23.2 Å, when the width was expanded by 1.0 Å. The second peak appears at 14.7 Å, and comprised 23% of total water, consistent with the observation of Arg-Glc MRPs above.

In the water profiles of DOPC and MCE MRPs, there are two Gaussian peaks, one at 22.9 Å and another at 15.3 Å. The former one accounts for 74% of the total, when the latter one lies deeper than the 18.1 Å subsidiary peak of MCE MRPs distribution. This implies that insertion of MCE MRPs brought water closer to the hydrophobic centre of bilayer, and demonstrated again the different modes of influence of MRPs on phospholipid bilayers.

It is possible to calculate the location of the water boundary for each sample from the data in Table 7.2(b). Subtracting the half-width values from the Gaussian centre for each sample reveals that the edge of the water peak lies at 24.5 Å in the pure-lipid bilayers and slightly closer to the bilayer centre in all of the samples containing MRPs (DOPC + RIE MRPs 23.4 Å; DOPC + MCE MRPs 22.9 Å; DOPC + Arg-Glc MRPs 23.2 Å). Thus, although there are some variations in the location and width of the water peaks in the samples containing MRPs from different sources, the width of the bilayer from water boundary to water boundary changes only very slightly. This is significant since it implies that none of the products disrupt the bilayer (disturb the side-by-side packing of the phospholipid molecules in such a way that water is allowed to penetrate between them), consistent with a model in which the MRPs repairs or protects the bilayer.

Our results support the earlier observation that RIE MRPs changes the membrane properties of erythrocytes membranes (Chen *et al.*, 2006), by demonstrating a direct molecular interaction between RIE MRPs and phospholipid molecules. Intercalation of the MRPs molecules between the phospholipids would be expected to modify the biophysical properties of cell membranes and may also indicate a mechanism by which RIE MRPs could prevent influenza virus induced haemagglutination, as previously observed by Chen and co-workers (Chen *et al.*, 2006). It is interesting to note that the other TCM preparation used in our study, MCE MRPs, also interacts with phospholipid membranes, though in a subtly different way. Since both reagents are MRPs, the similarities are not surprising; it is more remarkable that the two are not identical. The interaction of MCE MRPs with membrane phospholipids warrants further investigation, as it may form the basis of the anti-diabetic properties of this TCM by indicating how MCE MRPs helps to maintain the integrity of cell membranes against damage by free radicals or other molecular species (Xiang, Huang, *et al.* 2007).

7.3.2. Distributions of MRPs and their reactants in DMPC bilayers

7.3.2.1. Distributions of RIE MRPs, Arg-Glc MRPs and MCE MRPs in the DMPC bilayers

The influence of presence of Arg-Glc MRPs in DMPC bilayers was firstly investigated in D16 of ILL (Grenoble, France), by measuring the neutron scattering length density around the phase transition temperature of DMPC. Arg-Glc MRPs had significant different distribution across DMPC bilayers at gel phase and liquid crystal phase, but didn't change the *d*-repeats of systems, which were about 55 Å as measured, in both gel and liquid crystal phase. The Gaussians distribution of water in pure lipid bilayer represented not only a hydration shells around the phosphate headgroups of the lipids, but also a small block of water penetrated towards the hydrophobic area of lipid tails. However, water shouldn't appear at the hydrophobic area in the absence of another molecule that breaks the strong hydrophobic force between the lipid tails.

This abnormal observation may be attributed to the sample temperature. As described in Section 7.2.2, the relative humidity of sample slide was controlled by adjusting the temperature of the sample can. However, the sample temperatures used in ILL measurement were so close to the L_β -L_α transition temperature (~24°C) of DMPC. This may result in the

coexistence of gel and liquid crystalline structure, thereafter affect the accuracy and reliability of measurements. Thus, a new set of neutron diffraction measurements on the DMPC and different types of MRPs have been conducted on instrument V1 (BENSC, Helmholtz Zentrum Berlin, Germany). In order to illuminate the distribution of Arg-Glc MRPs across DMPC bilayer in L_α phase, the neutron scattering was measured at 37 °C, which is 13 °C higher than the transition temperature, and at various humidity created by saturated salts solutions.

Table 7.3 The difference structure factors and estimated maximum overall errors.

	*F**(1)	*F**(2)	*F**(3)	*F**(4)	*F**(5)
DMPC	24.37	-15.28	-10.66	-2.20	2.05
	±1.47	±1.02	±0.79	±0.37	±0.36
DMPC+Arg-Glc MRPs 100:5	27.98	-15.08	-10.87	-1.80	2.43
	±1.61	±0.96	±0.75	±0.30	±0.33
DMPC+Arg	28.65	-15.88	-11.52	-2.05	2.49
	±1.69	±1.06	±0.84	±0.37	±0.39
DMPC+Glc	33.76	-18.82	-16.58	-4.63	3.88
	±1.99	±1.24	±1.13	±0.53	±0.49
DMPC+RIE MRPs	23.71	-15.92	-9.34	-1.95	2.04
	±1.44	±1.05	±0.73	±0.36	±0.36
DMPC+MCE MRPs	26.71	-12.02	-9.38	-2.40	2.29
	±1.63	±0.90	±0.76	±0.42	±0.41
DMPC+Arg-Glc MRPs 100:2	27.92	-12.26	-10.04	-3.04	2.06
	±1.69	±0.91	±0.78	±0.45	±0.40
DMPC+Arg-Glc MRPs 100:10	25.68	-13.97	-8.78	-2.18	2.24
	±1.56	±0.98	±0.72	±0.39	±0.39

$$\text{Error}_{F(n)} = 0.0499 \times F(n) + 0.2014$$

Neutron structure factors for bilayers composed of DMPC and of DMPC in the presence of MRPs, arginine, glucose and Arg-Glc MRPs on three lipid/MRPs ratios. The bilayers were hydrated with 8% ^2H_2O thoroughly before each angular scan, since water of this isotopic composition has a net neutron scattering length density of zero.

Similar to the previously measurements on DOPC, the neutron scattering length density profiles of bilayers were calculated from the structure factors in Table 7.3. Difference profiles were calculated by subtracting the profile of DMPC bilayers from each of the DMPC+MRPs profiles in turn. The models of the MRPs distributions were constructed and fitted in reciprocal space to avoid the termination error. The results of model-fitting are shown in Figure 7.4 and Table 7.4(a). The *d*-repeat of DMPC bilayer in L_α phase was 49 Å, which is about 3 Å thinner than the DOPC bilayer. This is consistent with the fact that DMPC has a shorter acryl chain (14 carbons) than DOPC (18 carbons).

A profile diagram together with errors is shown in the top panel of Figure 7.4 to give an image of estimated maximum errors and tend (Table 7.3). The most accurate profiles are ranged from 10 Å to 20 Å. Figure 7.5 shows water difference profiles, calculated by subtraction of an 8.1% ^2H_2O profile from the corresponding 25.0% ^2H_2O profile. The result reveals the Gaussian distribution of water across the unit cell of DMPC. The results are shown in Table 7.4(b).

Generally, all the three types of MRPs have two-Gaussian distribution profiles in DMPC bilayers. RIE MRPs and Arg-Glc MRPs share the similar distributions in both of hydrophobic and hydrophilic regions, whereas MCE MRPs lie mainly in the hydrophilic region and present the strongest scattering density, as shown in Fig 7.6. Arg-Glc MRPs slightly increased the *d*-repeat of unit cell when RIE MRPs and MCE MRPs had little effects on the *d*-repeat. Arg-Glc MRPs have the least scattering density. In water distributions, Arg-Glc MRPs associated with the greatest amount of water whereas MCE MRPs attracted the least amount of water.

The distribution of Arg-Glc MRPs on DMPC was different to that on DOPC bilayer, although the proportions of MRPs population lies in the hydrophilic and hydrophobic region were rather similar. It reflects a truth that the two lipids share the same headgroup but different length of acryl chains. DOPC bilayer has a *d*-repeat of about 52.0 Å at 25 °C (96% RH), which is 3~4 Å thicker than DMPC's 48.6 Å at 37 °C (96% RH), both in L_α phase. The thickness of one leaflet is 26.0 Å and 24.3 Å for DOPC and DMPC, respectively. The distances of Arg-Glc MRPs to the bilayer center are different between these two kinds of phosphatidylcholine, centering at 14.9 Å in DOPC bilayers versus 12.7 Å in DMPC bilayers. Apparently, Arg-Glc MRPs lied about 2.0 Å closer to the hydrophobic region in DMPC bilayer than in DOPC bilayer. However, as shown in Table 7.4(b), a deeper water penetration was not observed in the DMPC bilayers. On the contrary, in the presence of Arg-

Glc MRPs, the distribution of water centered at 14.7 Å in the DOPC bilayers, which is 2.3 Å closer to the hydrophobic core than that in the DMPC bilayers. If the length difference of lipid tails (1.5~2.0 Å) were taken into account, Arg-Glc MRPs distribute at the same level of hydrophobic tails in lipid leaflet, and the water lie about 4 Å deeper in DOPC bilayer than that in DMPC bilayer. Therefore, the presence of Arg-Glc MRPs causes a stronger water penetration in DOPC bilayers than in DMPC bilayers. The unsaturated fatty acid tails of DOPC tilt and cause a bigger head-to-head space than that of DMPC bilayers, which allow a deeper water penetration. The shorter distance of the MRPs to the DMPC bilayer center is attributed to the shorter myristoyl chains (14 carbons) of DMPC than the oleoyl chain (18 carbons) of DOPC.

As shown in Table 7.2 & 7.4, the major population (68%) of RIE MRPs lays in the hydrophobic region of the DMPC bilayers, right below the level of glycerol back bone, whereas a minor population (32%) was observed in hydrophilic bilayer surface. Although the majority of RIE MRPs (65%) was located at the headgroup region in DOPC bilayers, but the minority of the MRPs was 2 Å further into the hydrophobic tails of DOPC than those of DMPC. Despite the differences described above, the water distributions on the lipid bilayers in the presence of RIE MRPs were rather similar in DOPC and DMPC: about 70% of water remains at the surface of bilayers (at ~23 Å) while about 30% of water penetrates into the bilayers at ~16.0 Å. RIE MRPs help to attract more water to the lipid head groups and thereby enhance the hydration of bilayer, which is in a good agreement with the increasing polarization of lipid bilayers by the MRPs detected with Laurdan fluorescent spectra.

Unlike their location in DOPC bilayers, MCE MRPs mainly lie on the surface of DMPC bilayer, whereas 17% of the MRPs appear at the hydrophobic core of the bilayer, at 5.3 Å from the center. However, the water distribution profile did not agree with the penetration of MCE MRPs, since the water only sit on the top of bilayer, at 22.2 Å. This indicates the MCE MRPs perform a partial insertion to the bilayer without introducing any water into the hydrophobic site. A similar phenomenon has been observed in the MD simulation study with a myristoylated decapeptide in DMPC bilayers (Khandelia, Ipsen, & Mouritsen, 2008). As described in Section 6.3.1, the strong hydrophobic compositions from MCE MRPs formed monolayer at the air/water interface. The water was associated to the hydrophilic part of the MRPs, and was kept away from the hydrophobic core of the bilayer. In DOPC bilayers, there was 26% of water penetrate to the acyl group, at 15.3 Å. The double-bond containing acyl chains allow the DOPC to pack less rigid than the DMPC, which consequently results in the penetration of water.

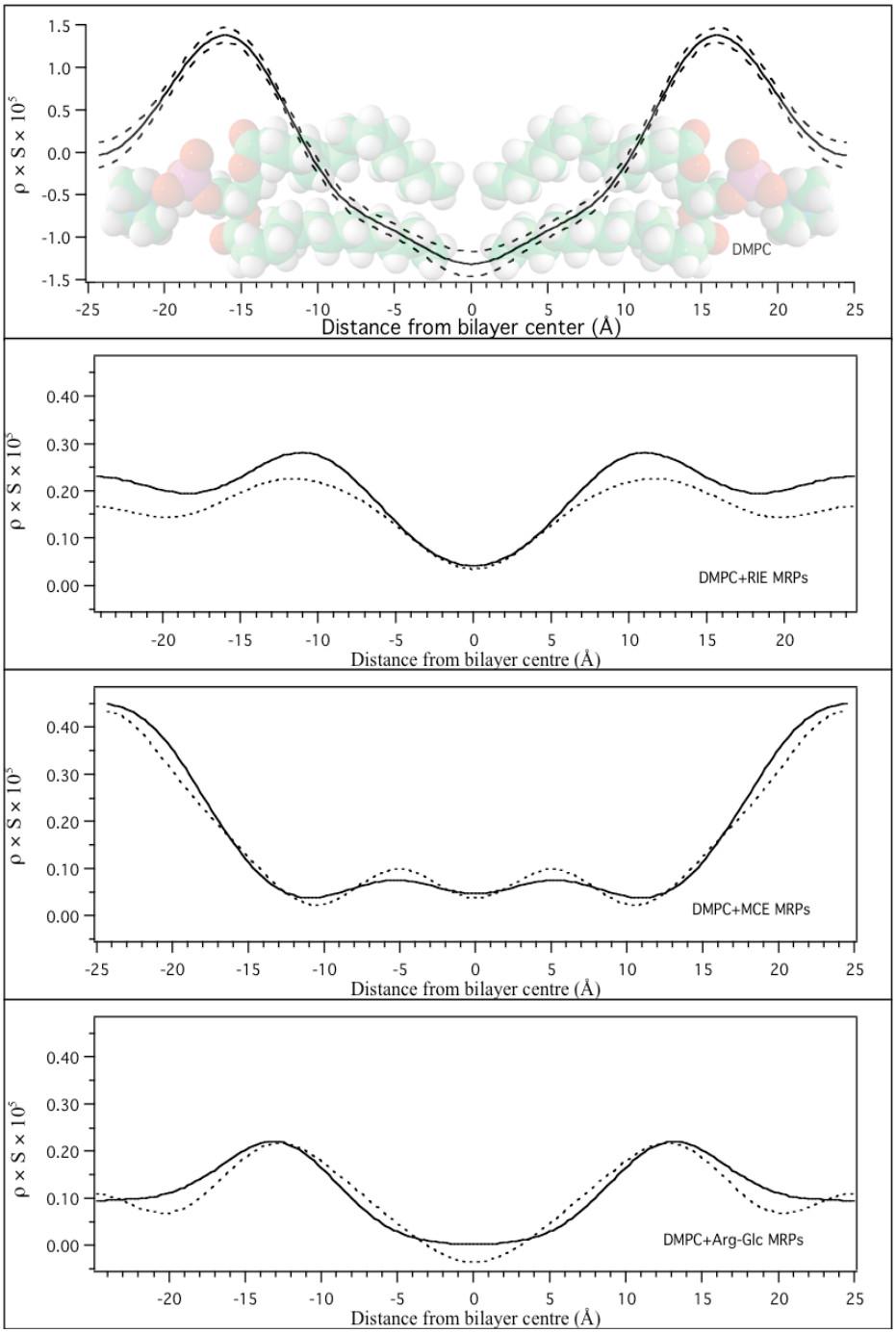

Figure 7.4 Neutron scattering length density profiles of the distribution of the three types of MRPs in DMPC bilayers.

The top panel shows a bilayer profile of DMPC, for comparison and orientation. The dashed lines represent the maximum and minimum neutron scattering length density at each point, based on reconstructions using all possible combinations of structure factors within the range defined by the calculated errors shown in Table 7.3. The three panels below give the profiles of three types of MRPs in DMPC bilayers. Dot line: the difference profiles, represents the measured distribution profiles of sampling substance (minus DMPC). Solid line: model of profiles, represents the corresponding best theoretically fitted Gaussian distributions for these different profiles. In each case, the structure factors for bilayers hydrated with 8.1% $^{2}H_2O$ were used to calculate the profiles (Table 7.3).

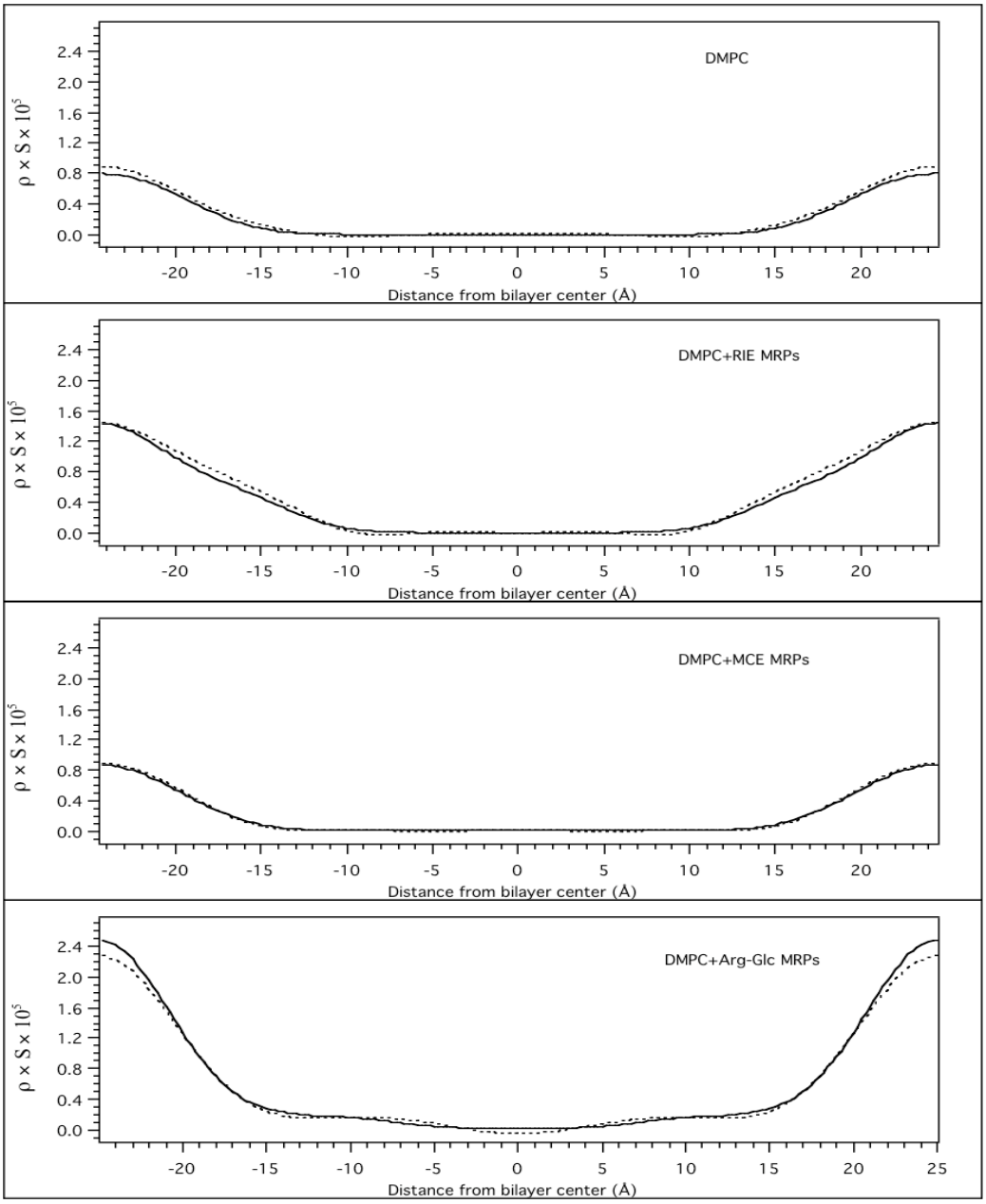

Figure 7.5 Difference profiles of the neutron scattering length density of water (^2H_2O) in stacked phospholipid bilayers of DMPC and DMPC with each of the three types of MRPs.

The dashed lines are the difference profiles, and the solid lines are the corresponding best-fit Gaussian distributions for these difference profiles. Structure factors for bilayers hydrated in 8.1% H_2O were subtracted from corresponding 25% ^2H_2O structure factors and the result used to calculate the profiles shown.

Table 7.4 Gaussian models of bilayer distributions.

(a) MRPs distribution		DMPC	DMPC+Arg-Glc MRPs	DMPC+RIE MRPs	DMPC+MCE MRPs
Gaussian 1	Position*	-	20.6 Å	22.1 Å	21.1 Å
	Width[#]	-	7.9 Å	7.4 Å	6.0 Å
	Occupancy	-	32%	32%	83%
Gaussian 2	Position*	-	12.7 Å	10.5 Å	5.3 Å
	Width[#]	-	5.5 Å	6.8 Å	5.0 Å
	Occupancy	-	68%	68%	17%

(b) Water distribution		DMPC	DMPC+Arg-Glc MRPs	DMPC+RIE MRPs	DMPC+MCE MRPs
Gaussian 1	Position*	21.8 Å	22.4 Å	22.9 Å	22.2 Å
	Width[#]	5.0 Å	5.9 Å	5.3 Å	5.3 Å
	Occupancy	100%	86%	69 %	100%
Gaussian 2	Position*	-	17.0 Å	16.3 Å	-
	Width[#]	-	7.0 Å	4.6 Å	-
	Occupancy	-	14%	31%	-

Gaussian models of bilayer distributions of (a) the three types of MRPs at lipid/MRPs molar ratio 100:5 and (b) water. The position, width and size of Gaussian distributions were fitted, in reciprocal space, to difference neutron structure factors. Five orders of diffraction were used in the fitting procedure. *, the position of each label site is expressed as distance from the centre of the bilayer; [#], the width is the half width at 1/e height.

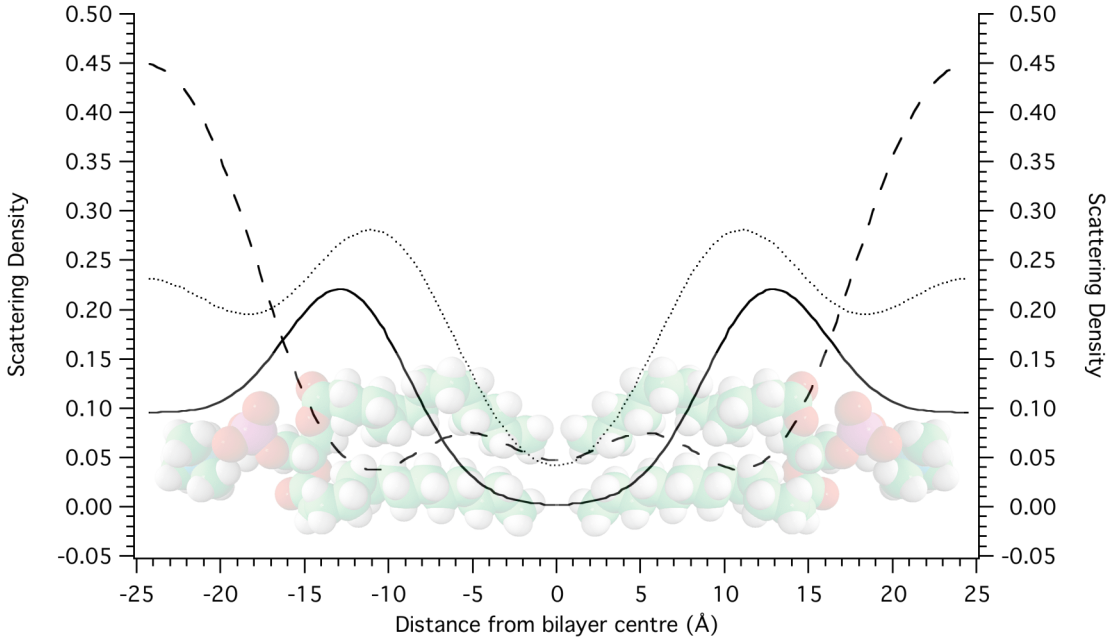

Figure 7.6 The neutron scattering length density profiles of three types of MRPs distributing across the DMPC bilayer.

The profiles of the MRPs are overlapped for comparison: Arg-Glc MRPs (solid line); RIE MRPs (dot line); MCE MRPs (dash line).

7.3.2.2. Concentration-response in the distributions of Arg-Glc MRPs in the DMPC bilayers

As shown in Table 7.5 & Fig 7.7, the Gaussian models of Arg-Glc MRPs' distributions in DMPC bilayers varied corresponding to the lipid/MRPs ratios. At the lowest concentration of MRPs (100:2), most of the MRPs located at the hydrophilic region (Fig 7.7, dot line) and decreased the *d*-repeat by 0.5 Å. At the middle concentration (100:5), the majority of Arg-Glc MRPs inserted into the hydrophobic tails of lipids at a position (12.7 Å) close to the hydrophobic-hydrophilic interface, right next to the glycerol back bone of lipids. The MRPs had a mild effect on the *d*-repeat. At the high concentration (10:1), the majority of the MRPs stayed with the hydrophilic head groups whereas about one fifth of which partially inserted deep into the hydrophobic site at 8.5 Å, and increased the *d*-repeat by 1.0 Å.

The water distributions in the presence of Arg-Glc MRPs were consistent with the observations described above. The majority of water remained on the surface of DMPC bilayers while a small amount of which associated with the phosphate group, at about 17.0 Å

(Table 7.5(b)). At the low concentration (100:2), only 5% of water associated with the phosphate group, which is usually not considered as a significant distribution. With the rise of concentration, 14% of water sat around the phosphate group, indicating that Arg-Glc MRPs attract water and increase the hydration degree of lipid head groups at lipid/MRPs molar ratio 100:5. At the higher concentration (10:1), the water remained at the level of phosphates with a slightly less proportion, 11%. The partial insertion of high-concentration Arg-Glc MRPs did not induce a deeper water penetration in the bilayers. This shares a similarity with the insertion of RIE MRPs in DMPC bilayers, described in Section 7.3.2.1.

Table 7.5 The Gaussian models of bilayer distributions

(a) MRPs distribution		DMPC	100:2 Arg-Glc MRPs	100:5 Arg-Glc MRPs	10:1 Arg-Glc MRPs
Gaussian 1	Position*	-	21.1 Å	20.6 Å	22.0 Å
	Width[#]	-	5.9 Å	7.9 Å	8.2 Å
	Occupancy	-	96%	32%	78%
Gaussian 2	Position*	-	18.0	12.7 Å	8.5 Å
	Width	-	3.9	5.5 Å	4.9 Å
	Occupancy	-	4%	68%	22%

(b) Water distribution		DMPC	100:2 Arg-Glc MRPs	100:5 Arg-Glc MRPs	10:1 Arg-Glc MRPs
Gaussian 1	Position*	21.8 Å	22.0 Å	22.4 Å	22.1 Å
	Width[#]	5.0 Å	5.4 Å	5.9 Å	5.0 Å
	Occupancy	100%	95%	86%	89%
Gaussian 2	Position*	-	17.4 Å	17.0 Å	17.3 Å
	Width[#]	-	10.8 Å	7.0 Å	4.3 Å
	Occupancy	-	5%	14%	11%

Gaussian models of bilayer distributions of (a) Arg-Glc MRPs at 100:2, 100:5, 10:1 lipid/MRPs molar ratio and (b) water. The position, width and size of Gaussian distributions were fitted, in reciprocal space, to difference neutron structure factors. Five orders of diffraction were used in the fitting procedure. *, the position of each label site is expressed as distance from the centre of the bilayer; [#], the width is the half width at 1/e height.

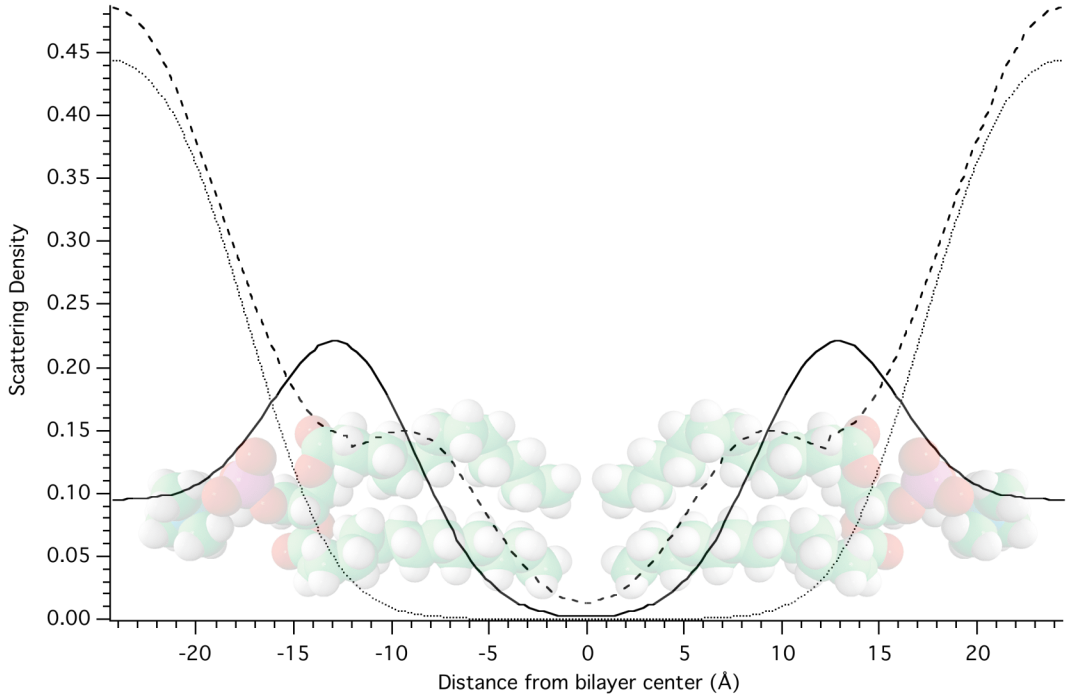

Figure 7.7 The scattering density length profiles of the distribution of Arg-Glc MRPs at three different concentrations on DMPC bilayers.

The molar ratio (lipid/MRPs) concentrations of the MRPs were 100:2 (dot line), 100:5 (solid line) and 10:1 (dash line).

7.3.2.3. The distributions of arginine and glucose in the DMPC bilayers

As described in Chapter 4, there were about 31% of arginine and 39% of glucose remained un-reacted in Arg-Glc MRPs. The distributions profiles of arginine (100:1.65) and glucose (100:1.95) in DMPC bilayers were measured to estimate the possible influences of these two reactants remained in Arg-Glc MRPs (100:5). The molar ratios of arginine and glucose chosen in the measurement were mimicking their amounts remaining in the 5% Arg-Glc MRPs.

As shown in Table 7.6(a), two Gaussian profiles were identified for arginine, on the surface of DMPC bilayer (at 22.8 Å) and in the interface region of bilayer (at 14.0 Å). Most of the arginine (94%) settled in the interface region, which is around the glycerol backbone of the lipid. However, observed in the water distribution profiles, all the water lied on the surface of bilayer in the presence of arginine. Arginine did not introduce any water to the glycerol groups, and did not affect the *d*-repeat of the bilayer.

In case of glucose, its distribution fitted a single Gaussian profile that centered at 17.2 Å, around the phosphate group. D-glucose can interact with the phosphate group of lipid, probably with its hydroxyl groups by hydrogen bonding (Crowe *et al.* 1987). It would not cause a profile change deeper than where the phosphate group lies. There is a small 'ripple' at about 6.5 Å, which occupied less than 5% of glucose population and is considered as an experimental false. Glucose introduced one forth of water to the level of phosphate while the rest of water remained on the surface, promoting a stronger hydration effect on the lipid head groups than the Arg-Glc MRPs. No water penetration was observed in the acyl chain region, thereby glucose did not change the thickness of the bilayers.

The majority of Arg-Glc MRPs were found at the deepest insertion to the bilayer and a minor distribution at the headgroups, compared with arginine and glucose (Fig 7.8). The distribution profile of the MRPs does not equate to the combined profile of arginine and glucose, indicating the MRPs have their own membrane interactive properties. The Gaussian profiles of Arg-Glc MRPs observed in lipid bilayers mainly represent the distributions of the reaction products, but not those of the reactants.

In aqueous environments, arginine tends to be positively charged with a pKa of ~13 (Li *et al.* 2008), due to its guanidinium side chain. The positive charge stops arginine from moving into the hydrophobic core of bilayer with a large free energy barrier (Dorairaj & Allen 2007), but associate arginine with the negative charged phosphate group. This explains well why the location of arginine in the lipid bilayer is near the phosphates. Furthermore, the Maillard reaction between the guanidinium of arginine and aldehyde of glucose can neutralise the positive charge of guanidinium residue and allow the MRPs to insert deeply.

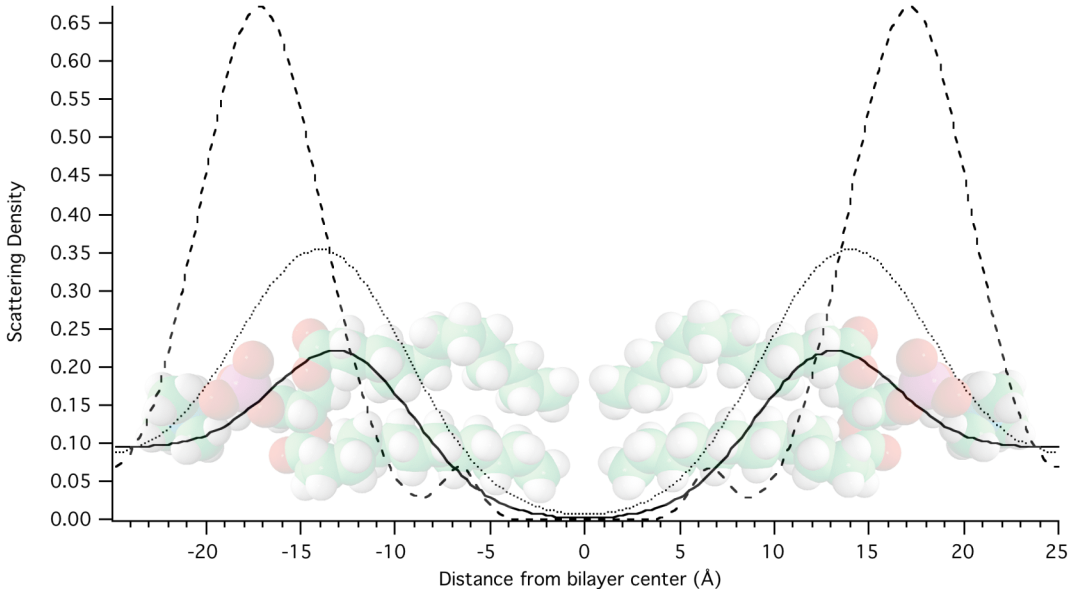

Figure 7.8 Bilayer profiles of the distribution of Arg-Glc MRPs (solid line), arginine (dot line) and glucose (dash line) across the DMPC bilayers were presented with the best-fit model curve.

Table 7.6 Gaussian models of bilayer distributions of Arg-Glc MRPs, arginine and glucose.

(a) MRPs distribution		100:5 Arg-Glc MRPs	100:1.65 Arg	10:1.95 Glc
Gaussian 1	Position*	20.6 Å	22.8 Å	-
	Width[#]	7.9 Å	5.1 Å	-
	Occupancy	32%	6%	-
Gaussian 2	Position*	12.7 Å	14.0 Å	17.2 Å
	Width	5.5 Å	6.5 Å	4.6 Å
	Occupancy	68%	94%	100%

(b) Water distribution		100:5 Arg-Glc MRPs	100:1.65 Arg	10:1.95 Glc
Gaussian 1	Position*	22.4 Å	22.2 Å	22.9 Å
	Width[#]	5.9 Å	6.2 Å	6.1 Å
	Occupancy	86%	100%	75%
Gaussian 2	Position*	17.0 Å	-	16.9 Å
	Width[#]	7.0 Å	-	5.8 Å
	Occupancy	14%	-	25%

Gaussian models of bilayer distributions of (a) Arg-Glc MRPs, arginine, glucose and their deuterated counterparts and (b) water. The position, width and size of Gaussian distributions were fitted, in reciprocal space, to difference neutron structure factors. Five orders of diffraction were used in the fitting procedure. *, The position of each label site is expressed as distance from the centre of the bilayer; [#], the width is the half width at 1/e height.

7.4. CONCLUSIONS

The three types of MRPs, referring to Arg-Glc MRPs, RIE MRPs and MCE MRPs, present different distribution pattern across the two types of PC lipid bilayers. RIE showed the most potent interaction with DOPC bilayers among the three candidates observed. It has a major

distribution above the phosphate group and a minor distribution among the hydrocarbon chains of bilayer, near to ester carbonyls. The overall distribution pattern of Arg-Glc MRPs in DOPC bilayer is similar to that of the RIE: there are two Gaussian peaks with differed relative heights, while one of which penetrates deep into the hydrophobic region of the bilayers. MCE MRPs appeared only above the phosphate and induced an enhanced hydration in the hydrophilic section of bilayer. The water distribution of bilayer, incorporated with MRPs, is correlated to the MRPs' distribution.

The introduction of RIE and Arg-Glc MRPs (at 100:5) slightly expanded the *d*-repeats of the DOPC and DMPC bilayers, when MCE MRPs decreased it, but not significantly. Arg-Glc MRPs at 10:1 expanded the *d*-repeat of DMPC by 1.0 Å. The arginine and glucose do not affect the thickness of DMPC bilayer. It implies that none of the products disrupt the bilayer, consistent with a model in which the MRPs repairs or protects the membrane bilayers, or stabilises the DOPG monolayer.

Arg-Glc MRPs expanded the *d*-repeat of DMPC bilayers by 1.0 Å at high concentration (lipid/MRPs molar ratio 10:1), when it decreased the thickness of unit cell by 0.5 Å at low concentration. In agreement with DOPC, MCE MRPs decreased *d*-repeat of DMPC slightly. The insertion of Arg-Glc MRPs to DMPC bilayer was described in a concentration-dependent mode, in which MRPs at its highest concentration achieves a deepest insertion to the hydrophobic core of bilayer.

Arginine and glucose each distribute across the hydrophilic region of bilayer, from the phosphate, to the ester carbonyls. The distribution profiles are very different from that of Arg-Glc MRPs, in terms of either the Gaussian distribution center or the scattering density. Although they could possibly be accounted for a small part of the scattering intensity of Arg-Glc MRPs at the regions of hydrophilic region of lipid bilayer, the influences of these two reactants on the distribution profiles of Arg-Glc MRPs are minor. Neither the arginine nor the glucose penetrated into the hydrophobic hydrocarbon chains of lipids, which is in agreement with the hydrophilic nature of arginine and glucose. The water distribution profiles finely support the observation above: water appears mainly at the surface of bilayers when remains a significant amount around the phosphates.

CHAPTER 8

INHIBITION OF MRPS ON MEMBRANE FUSION

8.1. INTRODUCTION & AIMS OF CHAPTER

8.1.1. Introduction

8.1.1.1. Viral infection and membrane fusion

In order to infect the host cell, both enveloped and nonenveloped viruses have to penetrate the barrier of a cellular membrane. For enveloped viruses, influenza virus A for example, penetration involves membrane fusion. For nonenveloped viruses, picornaviruses for instance, penetration involves membrane lysis or pore formation (Marsh & Helenius 2006). Non-lamellar structures have been discovered either at the sites of membrane fusion or membrane pore formation. Peptides or proteins, which promote membrane fusion or lyse membrane, facilitate the formation of non-lamellar phases, either micelles, cubic phases or hexagonal phases (Epand 1998).

Membrane fusion is critical early event for an influenza virus to transfer its genetic information to human epithelial cells and complete its replication. From there, the new virus particles are formed and released to infect other cells. Nevertheless, membrane fusion is also involved in the budding of newly formed virus particles before they are released from the host-cells.

A framework is given as Fig 8.1 showing the life cycle of influenza viruses and the occurrence of membrane fusion. Increased understanding of membrane fusion has the potential to reveal new targets for attacking enveloped viruses before they can attach to and enter the host-cells for replication.

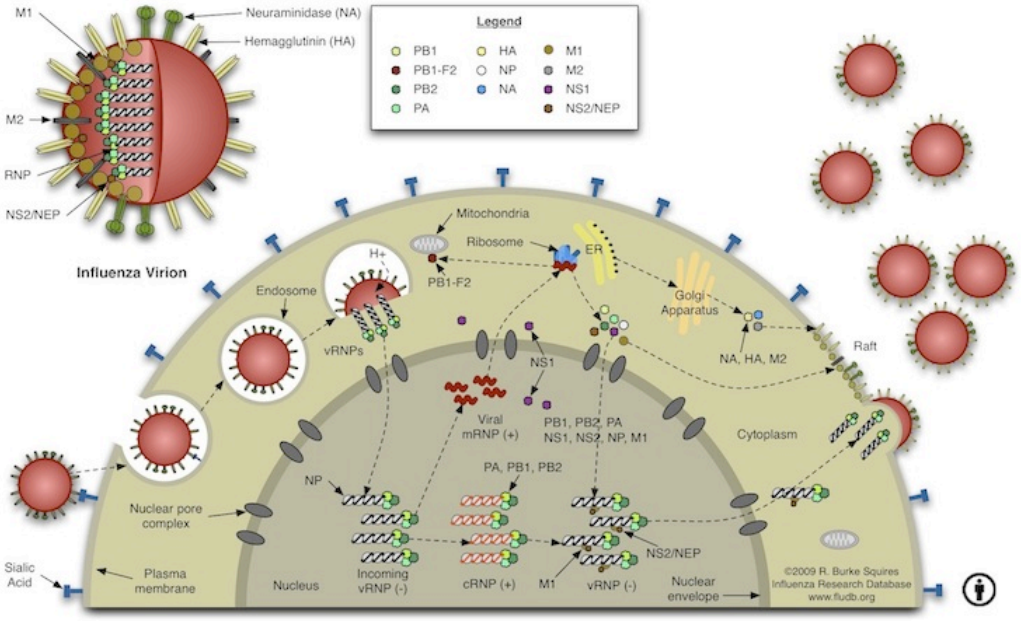

Figure 8.1 A schematic diagram of influenza virus life cycle and membrane fusion.

Modified from Palese's diagram (Palese & Shaw 2001).

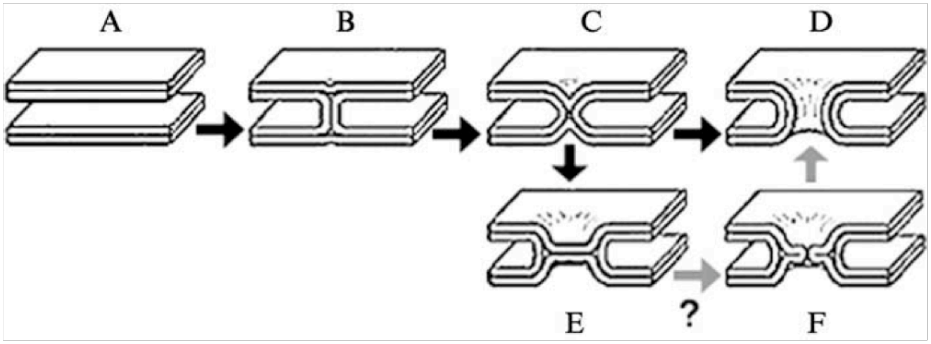

Figure 8.2 Schematic representation of the fusion of two lipid bilayers (Harrison 2005).

(A) Two parallel lipid bilayers, with a substantial barrier to close approach. (B) The semi-fusion stalk. (C) Proposed intermediate structure of transition. (D) Fusion pore formation. (E) The semi-fusion diaphragm. (F) A model includes the perforation of a semi-fusion diaphragm as the step essentially toward the fusion pore formation. The diagram was originally adapted by Harrison from the diagram of (Jahn, Lang & Südhof 2003), see also (Chen, Markosyan & Melikyan 2002).

8.1.1.2. Fusion peptide and membrane fusion

A class of hydrophobic peptides, commonly known as membrane fusion peptides, actively participate in fusion events, such as the entry of enveloped viruses into their host cells, or cell-cell fusions induced by viruses. The fusion peptide of influenza A viruses refers to the 20 NH_2-terminal amino acids of the HA2 subunit of hemagglutinin. Here is an example of amino acid sequence of this wild type fusion peptide: GLFGAIAGFIENGWEGMIDG-amide (Harrison 2005). The sequence, which varies slightly between different strains of the virus, is rich in hydrophobic residues (Lear & Degrado 1987). In an acidic environment, the binding of protons stimulates a conformational change in HA that exposes the fusion peptide, thereby triggering the fusion event. Most strains of influenza viruses have a critical pH of about 5-5.5 (Harrison 2005).

The fusion peptide (GVFVLGFLGFLA) from simian immunodeficiency virus (SIV) transmembrane glycoprotein gp32 belongs to a family of "oblique-orientated peptides", and inserts into cellular membranes at an angle of 30˚ (Lear & Degrado 1987). SIV gp120 and gp32 contain amino acid sequences share with HIV-1 gp120 and gp41. SIV fusion peptide belongs to the same family (class I fusion proteins) with that of influenza A virus (Harrison 2005). However, unlike fusion peptide from influenza HA2, SIV fusion peptide does not require a low pH to trigger the fusion-inducing conformation.

8.1.1.3. Oblique insertion of SIV fusion peptide

The oblique membrane insertion of SIV fusion peptide has been directly observed with neutron diffraction on the stacked multi-bilayers of DOPC (Bradshaw *et al.* 2000). As shown in Fig 8.3C, SIV fusion peptide associates with lipids in the bilayer at the hydrophobic and hydrophilic interface. The effects of this peptide on the phase transition of MeDOPE bilayers have been studied by a temperature-resolved X-ray diffraction (Harroun *et al.* 2003). SIV peptide raises the T_H by 10°C whereas it decreases the T_Q by 10°C, at the heating rate of 0.5 °C/min.

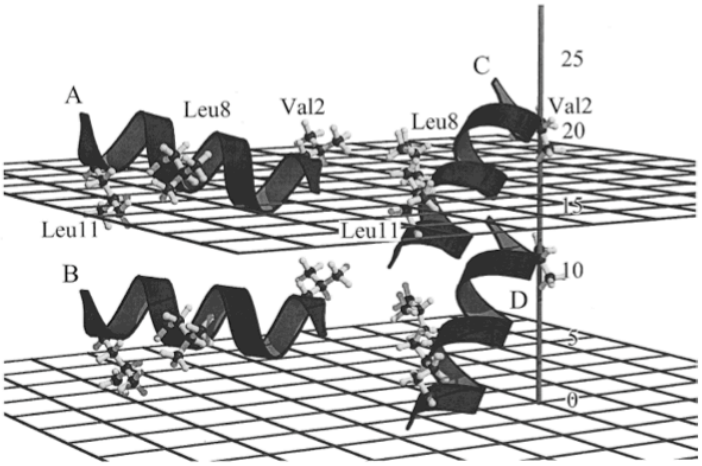

Figure 8.3 Molecular models of SIV peptide oriented in one-half of a bilayer.

The vertical line is the z-axis scale parallel to the membrane normal. The center of the bilayer is represented by the lower mesh, and the hydrophobic and/or hydrophilic interface is suggested by the upper mesh at the approximate value of 16 Å. The peptide helix is represented as a coiled ribbon. The diagram is quoted from Bradshaw's publication (Bradshaw *et al*. 2000).

8.1.1.4. Lipids and formation of non-lamellar structures

Representing typical non-lamellar structures, the inverted cubic and inverted hexagonal phases are crucial in the mechanism of membrane fusion. The chemical composition of phospholipids influences the formation of lamellar and non-lamellar phases. Lipids with a big headgroup and a pair of saturated fatty acid tails, i.e. DMPC, do not form structures with negative curvature, such as and cubic or hexagonal phases, under physiological conditions, while un-saturated lipids with small headgroups, e.g. MeDOPE, promote negative curvature and allow non-lamellar phases to form above T_H or T_Q (Fig 8.4). Membrane fusion inhibitors, such as lysophosphatidylcholine (LPC), stop the lipid bilayers from transferring to non-lamellar structures by inserting into the bilayer and occupying the spare space between the lipid headgroups, thereby prevent the negative curvature. Amphiphilic molecules like some compositions of MRPs may have the potential to inhibit membrane fusion by a similar mechanism.

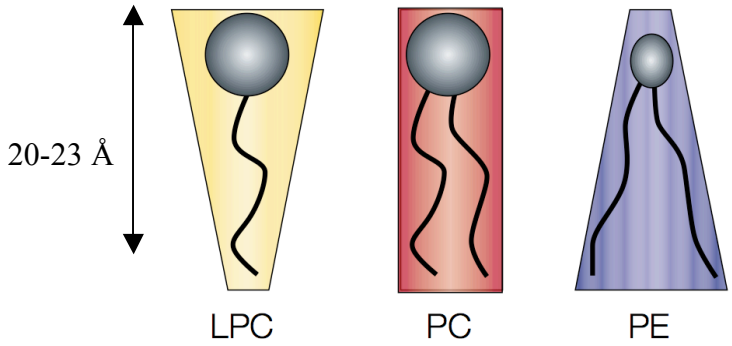

Figure 8.4 Schematic diagram of the shape of lipids composed of different types of polar headgroup and apolar tails.

The shape depends on the relative size of headgroup to tails. If the cross-sectional areas of the headgroup and acyl chains are similar, the lipid is cylindrical in shape (phosphatidylcholine (PC), i.e. DMPC), whereas the lipids with a small headgroup (phosphatidylethanolamine (PE), i.e. MeDOPE) are cone-shaped. If the tail is a single fatty acid chain, the lipid molecule has a relatively small surface area and thereby has the shape of an inverted cone (LPC). The head-to-tail length of lipid molecules varied among the different types of lipids. The diagram is adapted from Sprong's graph (Sprong *et al.* 2001).

8.1.2. Aims of this chapter

In previous studies, we have determined that a group of Maillard reaction products (MRPs) insert between the phospholipids of bilayers and affect the molecular packaging of lipid leaflet. The insertion of MRPs affects the thermal stability of bilayers in a concentration dependent manner. As revealed by the differential scanning calorimetery, the thermodynamic changes (in terms of the phase transition temperature (T) and energy flow (ΔH) during the phase transitions of lipid MLVs have been measured in the presence and absence of MRPs.

The study presented here aims to examine the possible inhibitory effects of MRPs on membrane fusion induced by the SIV fusion peptide. To characterise the structural rearrangements involved in the transition processes, small angle X-ray scattering (SAXS) was used to investigate the transitions from lamellar phase (L_α) to inverted hexagonal phase (H_{II}), and/or from L_α to inverted cubic phase (Q_{II}) with a concentration range of Arg-Glc MRPs.

8.2. METHODS

The inhibition of membrane fusion could be investigated by various methods, depending on what aspect the candidate molecule might target. Two methods, small angle X-ray scattering (SAXS) and lamellar X-ray diffraction (LXD), were employed here to investigate the effects of MRPs and/or SIV fusion peptide on the phase transition and structural transforming of lipid bilayers. N-methylated dioleoyl-phosphatidylethanolanmine (MeDOPE) adopts lamellar phase at low temperatures, and two non-lamellar phases at higher temperatures. The non-lamellar structures are believed to relate to the initiation of peptide-induced membrane fusion. The presence of non-lamellar structure in MeDOPE samples indicates a destabilisation of the lipid layers, thus MeDOPE MLVs was used as a model lipid system for evaluating the effects of MRPs on membrane fusion induced by SIV peptide.

8.2.1. Sample preparation

1,2-dioleoyl-sn-glycero-3-phosphoethanolamine-N-methyl (MeDOPE) was purchased from Avanti Polar Lipids Inc., USA (purity >99%), and used without further purification. For X-ray diffraction measurement, the MLVs were prepared by dispersing 15 wt% of MeDOPE, as described in Section 6.2.3 and 6.2.4, in PIPES buffer (pH7.4, 20 mM, 150 mM NaCl), Sigma-Aldrich (Irvine, UK). Various samples including Arg-Glc MRPs, RIE MRPs, SIV fusion peptide (GVFVLGFLGFLA, >99%), lysophosphatidylcholine (LPC), arginine and glucose, were dissolved in deionized water or methanol and mixed thoroughly with lipid MLVs by vigorous vortex for 2 min.

SIV fusion peptide, rather than influenza virus fusion peptide, was used in this study for several reasons. SIV has a shorter amino acid sequence which means it is easier to synthesise. It acts similarly as the influenza HA fusion peptide which promotes on lamellar/inverted phase transitions in dipalmitoleoylphosphatidyl-ethanolamine (DiPOPE) (Siegel & Epand 2000). The SIV peptide has been studied by a number of well-established methods, including an X-ray diffraction study on SIV's effects on the phase behaviour of MeDOPE MLVs (Harroun *et al.* 2003), which allows the comparison of the experimental data from this study with the published data.

8.2.2. Temperature-resolved SAXS

The X-ray diffraction experiments were performed on the Austrian SAXS beamline at ELETTRA, Trieste, Italy (Amenitsch *et al.* 1998) (Rappolt *et al.* 2003). Diffraction patterns of MeDOPE MLVs were recorded by a one-dimensional position sensitive detector (Petrascu, Koch & Gabriel 1998) covering the corresponding *s*-range of interest from ~1/450 $Å^{-1}$ to 1/12 $Å^{-1}$ ($s=2\pi\mathrm{Sin}(\theta)/\lambda$). As shown in Fig 8.5&8.6, the angular calibration was performed with silver-behenate ($CH_3(CH_2)_{20}$ -COOAg) for the detector: *d001*=58.378 Å, λ=1.54 Å (Huang *et al.* 1993). The specimen-to-detector length was approximately 0.75 m. The Eq 8.1 was obtained for the calculation of *s*-range (Fig 8.6) by drawing a linear curve of '*s*' as a function of detector channels. Each sample was sealed in a steel chamber with a pair of thin mica film on both the entrance and exit windows, held in a steel block which was in thermal contact with a water circuit connected to a programmable temperature control unit (Unistat CC, Huber, Offenburg, Germany). The temperature was continuously monitored with a thermocouple fixed to the sample chamber in a linear fashion at a heating rate of 60 K/h, and written into the data files automatically. Each frame of data collection lasted for 10s ~ 20s depended on the scattering intensity, and for every 0.5˚C (collecting for 10s) or 1.0˚C (collecting for 20s). The X-ray beams conduct a minimal effect of thermal radiation.

8.2.3. X-ray diffraction data analysis

The raw data were corrected for detector efficiency. The background scattering of water and the sample chamber was subtracted from the corrected raw data. The location, width and amplitude of each Bragg peak were then fitted by Lorentzian distributions (SigmaPlot, Systat Software Inc.). After the sample temperature curve was drawn as a function of frames, the transition temperature of each sample was determined by identifying the initiate point of non-lamellar phases. The square root of the peak intensity was used for determination of the form factor F of each individual reflection. The electron density maps of the phospholipid samples in the H_{II} phases were derived from the small-angle x-ray diffractograms by standard procedures (for example see (Harper *et al.* 2001); (Rappolt *et al.* 2003)).

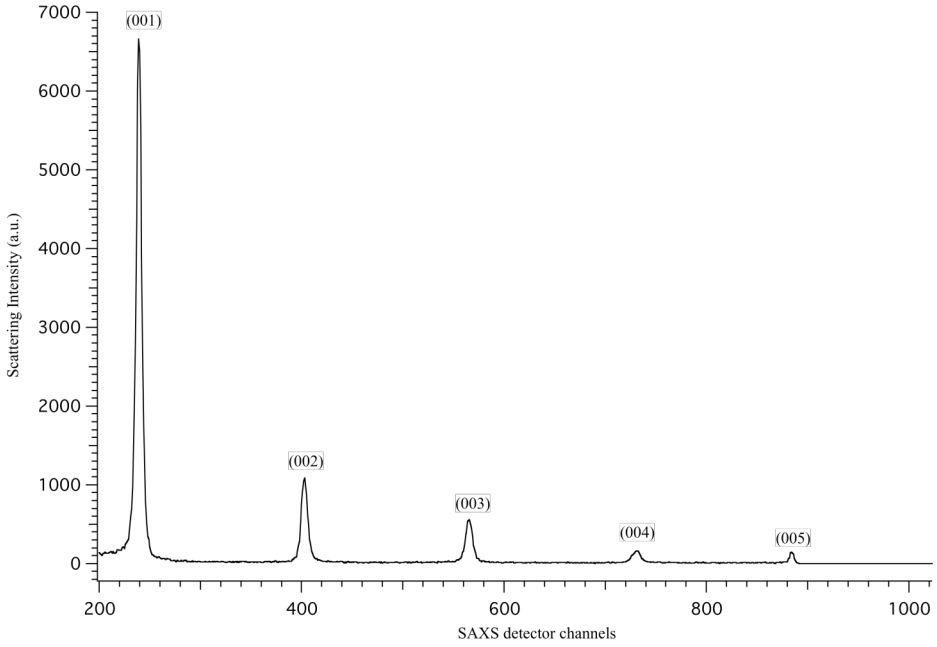

Figure 8.5 X-ray diffraction pattern of AgBE

λ=1.54 Å, detector channels=1~1024. The s-range of diffraction was calculated by Eq 8.1.

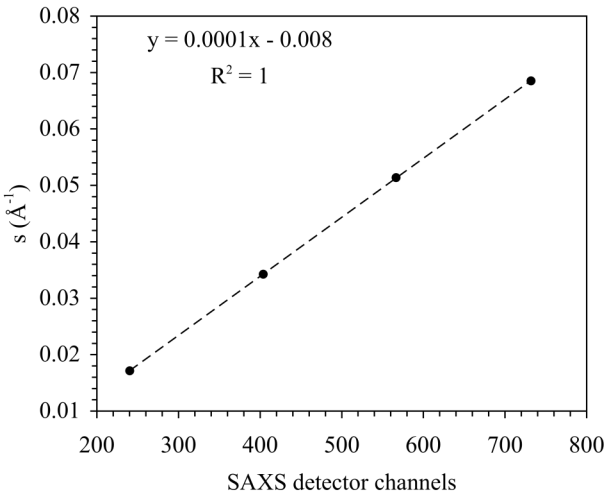

Figure 8.6 The standard curve for calculating the s-range.

The following equation was used for calculating the *s*-range of diffracton.

S (Å^{-1}) = *0.0001* × *channel* - *0.008*, R^2=1.000 (**Equation 8.1**)

8.2.4. Lamellar X-ray diffraction (LXD)

Lamellar X-ray diffraction (LXD) was used to determine the structural phase of MeDOPE, in the presence or absence of SIV fusion peptide, LPC and Arg-Glc MRPs. The measurements were carried out with synchrotron radiation at the beam line 13A1 SW6, HsinChu, Taiwan. The sample to detector distance was 906.6 mm. The X-ray wavelength λ=1.03 Å, when the beam size was 1 mm in wide and 300 μm in high. Two aluminium stripes were installed (as shown in Fig 8.12) to give a total attenuation of 1120 times (40×28=1120).

For each diffraction sample, 10 mg MeDOPE was dissolved in 200 μL methanol to make a 50 mg/mL lipid solution. The samples were dissolved in methanol (for SIV, LPC) or in deionized water (for Arg-Glc MRPs). After the sample was mixed with the lipid methanol solution thoroughly by vortext and sonication, 10 μL lipid-sample mixture were spread on a small piece of silica plate and dried out by evaporating and keeping in the vacuum for 1-2 h. The silica plate was then place in the sample chamber and installed horizontally. The sample humidity was increased gradually by decreasing the temperature difference between sample plates and water baths. The temperature of water bath was increased from 20°C to 28°C, at a rate of 1°C per step. The highest and lowest humidity in this measurement was 93% RH and 63% RH, respectively. The samples were exposed to X-ray for certain time, in order to obtain a diffraction pattern strong enough for analysing but not over-loaded. The exposure time was varied from 5 s to 180 s.

As shown in Fig 8.13, the position, intensity and width of Bragg diffraction peaks can be calculated by MATLAB (MathWorks Inc., USA). The other structure profiles, i.e. the *d* spacing of the lipid stack and the structure factors can be calculated accordingly. Further data analysis needs to be done for revealing effects of Arg-Glc MRPs and/or SIV fusion peptide.

8.3. RESULTS AND DISCUSSIONS

The lipid used in this study, N-methyl-dioleoyl-phosphatidylethanolamine (MeDOPE), exhibits two or three phases in vesicle suspensions, depending on the temperature and the heating rates of the system (Harroun *et al.* 2003). According to the results determined by DSC (Section 6.3.3.4), the T_H of MeDOPE multilamellar liposome vesicles (MLVs), from the lamellar phase (L_α) to the inverted hexagonal phase (H_{II}), was 72.0 ~ 73.0˚C, when the T_Q between lamellar phase (L_α) and the inverted cubic phase (Q_{II}) was about 62.0˚C. The heating rate in the DSC measurements was 40 ˚C/min, at the temperature ranging from -30˚C to 85˚C.

As shown in Fig 8.7, three phases, the lamellar, cubic and hexagonal phase, were observed with temperature-resolved SAXS in MeDOPE MLVs by determining the membrane structure-corresponding scattering density profiles at a heating rate of 1 ˚C/min. At least two cubic structures, possibly the diamond and primitive bicontinuous phases, were observed while two orders of diffraction peaks in lamellar and hexagonal phase each were measured. The continuous existence and coexistence of different phases makes it possible to evaluate the influence of MRPs, SIV fusion peptide, fusion inhibitor (LPC) and reactants of Maillard reaction on MeDOPE MLVs. For example, the L_α-to-H_{II} and L_α-to-Q_{II} phase transitions were also observed in the presence of Arg-Glc MRPs (100:5), as shown in Fig 8.8, though at the decreased T_H and T_Q. All the results are reported here.

8.3.1. Pure lipid and MRPs

As shown in Fig 8.7 and Fig 8.10A, the coexistence of H_{II} and Q_{II} phase was observed in pure lipid bilayers. The T_H was 69.3˚C (Fig 8.10), at where the L_α phase also ended. The inverted cubic phase started at 72.2˚C. The scattering profile indicates that lipids bilayer in the cubic phase have more than one structure, possibly the double-diamond (P_{n3m}) and primitive phase (I_{m3m}). It is finely supported by the lattice spacing (Fig 8.11) and the electron density profiles of hexagonal phase (Fig 8.10B).

The addition of 100:2 Arg-Glc MRPs to the pure lipid vesicles raised the T_H to 70.9˚C, and the T_Q to 74.3˚C (Fig 8.9). However, when the concentration of Arg-Glc MRPs was increased to 100:5, the T_Q decreased to 69.4˚C, while the T_H decreased to 66.9˚C. At this

proportion, the MRPs induced a 2˚C gap between the L_α and H_{II} phase where no structure was observed.

When the proportion of Arg-Glc MRPs reached 10:1, the T_H and T_Q were 68.0˚C and 68.5˚C, respectively, which was 1.3˚C and 3.7˚C lower than the normal vesicle. However, T_H of the MRPs at 10:1 was 1.1˚C higher than the at 100:5, when T_Q was 0.9˚C lower than that.

As shown in Fig 8.9 "RIE 5%", RIE MRPs decreased the T_H and then end of L_α phase by 0.6˚C, and decreased the T_Q by 4.0˚C. The effects are similar to those of Arg-Glc MRPs at high concentration (10:1), which indicates a destabilisation of the lamellar phase.

8.3.2. SIV fusion peptide and Arg-Glc MRPs

As described above, the SIV fusion peptide induces membrane fusion by oblique insertion into the phospholipids bilayers, promoting negative curvature, and thereby encouraging the formation of non-lamellar structures of lipid packing around the insertion site.

SIV fusion peptide (1 mol%) lowered the T_Q to 64.3˚C, but increased the T_H to 85.0˚C. SIV weakened and broadened the scattering profile of liquid crystalline phase, and extended the end of this phase to 72.7˚C (Fig 8.9, 'SIV 1%'). However, since the shape and intensity of Bragg peak were not identical to those of the normal L_α phase, a further analysis needs to be performed on the lattice spacing and electron density. Different from the pure lipid, SIV induced a coexistence of L_α and Q_{II} phase at the temperature ranged from 64.3˚C to 72.7˚C, and a coexistence of Q_{II} and H_{II} phase at the temperature ranged from 85.0˚C to the end of scan (90˚C). This indicates the dominant impacts of SIV on the lipid phase behaviour.

The low concentration of Arg-Glc MRPs (100:2) raised the T_H to 85.5˚C in the lipid bilayer with 1% SIV, which was slightly higher than the T_H of SIV, whereas the T_Q was not affected. The end of the lamellar phase was raised up by 6.9˚C, which narrowed down the gap from L_α to H_{II}. The rise in the T_H and the extension of lamellar phase both suggest a stabilising effect of Arg-Glc MRPs (100:2) on SIV containing lipid bilayers. The T_Q remains the same as that of SIV, which implies the cubic phase is more preferable than the hexagonal phase in the presence of the MRPs.

At the medium concentration, Arg-Glc MRPs lowered all of the T_H, T_Q and the end of L_α phase in the presence of SIV while induced the largest temperature gap between L_α and H_{II}

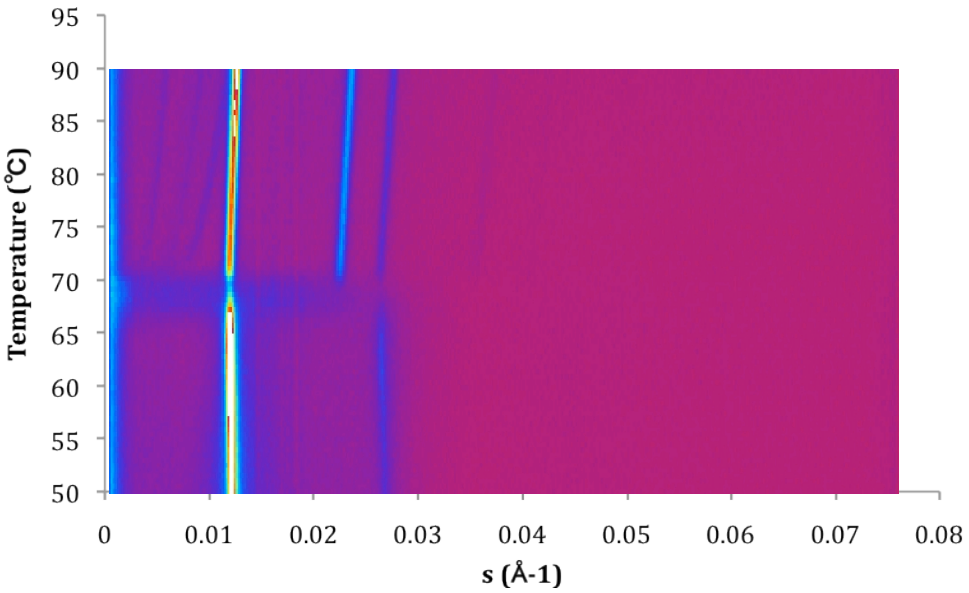

Figure 8.7 Contour plot of X-ray scattering of MeDOPE MLVs.

Temperature scan rate of 1°C/min. The figure shows a L_α to H_{II} transition around 70°C and a coexisting of H_{II} and Q_{II}.

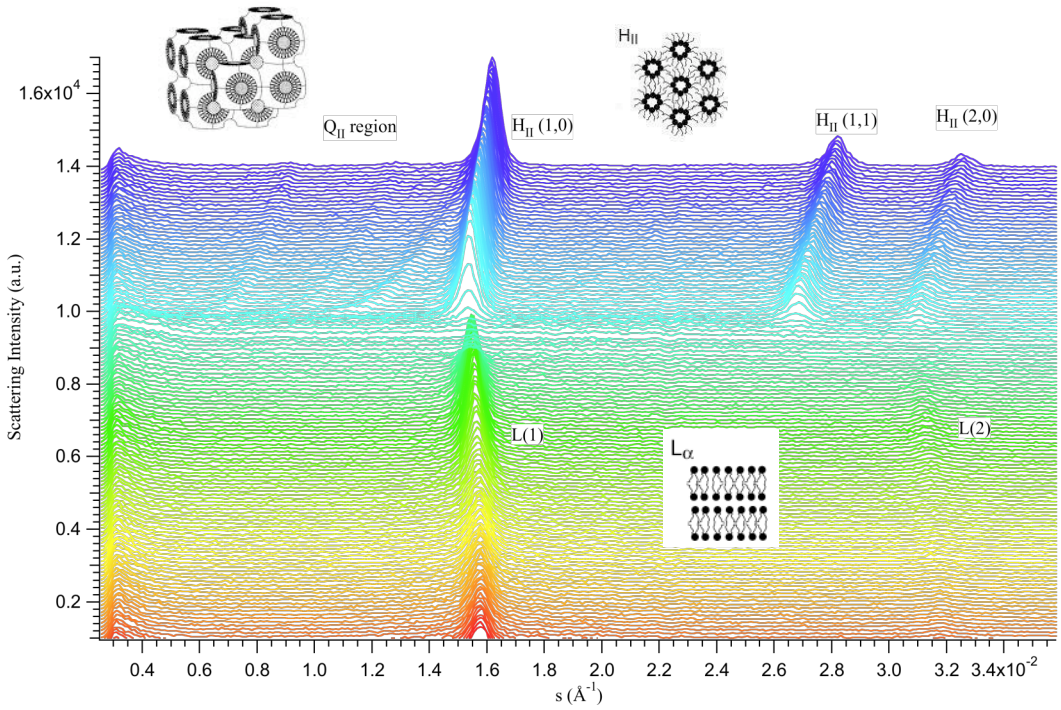

A. Temperature-resolved 3D scattering density profiles of lipid MLVs with 100:5 Arg-Glc MRPs.

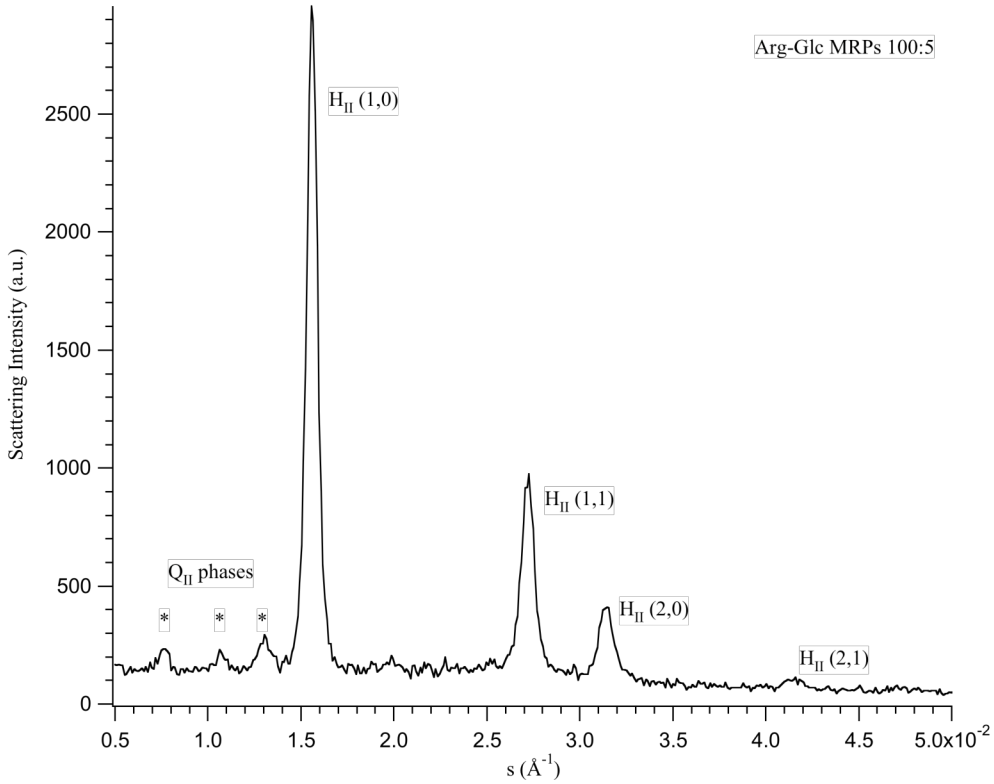

B. The scattering profiles as function of s-range at 74.4°C.

Figure 8.8 Scattering profiles of MeDOPE MLVs in the presence of Arg-Glc MRPs (100:5).

(A) Temperature-resolved 3D scattering density profiles; (B) The scattering density profiles as function of s-range at 74.4°C (T_H + 7.5°C). L(1) refers to the 1_{st} order scattering peak of L_α phase. L(2) refers to the 2_{nd} order scattering peak of L_α phase. Q_{II} refers to the inverted cubic phase, in which three diffraction peaks were observed, labelled with *. H_{II}(1,0)/(1,1)/(2,0)/(2,1) refer to the first and second order of the inverted hexagonal phase.

phase (Fig 8.9). This indicates a destabilising effect of MRPs on the lamellar structure. And the stronger scattering intensity of all the phases observed upon 100:5 MRPs may suggest a more ordered packing of lipids in each phase.

8.3.3. Arginine and glucose: effects of reactants of MRPs

The arginine (100:1.55) and glucose (100:1.95) were tested for their effects on the phase transitions, as a control of the un-reacted reactants in Arg-Glc MRPs (100:5). The cubic phase was not observed in the MeDOPE MLVs containing either arginine or glucose. The T_H for these two reactants was 68.5˚C and 69.3˚C, respectively, which was at the same level as

pure lipid. Alike the pure lipid and 5% RIE MRPs, arginine or glucose presented a continuous transfer from L_α to H_{II} phase. There is no inverted cubic phase observed in the presence of these two reagents.

8.3.4. LPC and Arg-Glc MRPs

LPC, lysophosphatidylcholine, is a potent inhibitor against SIV peptide induced membrane fusion, by strongly inhibiting the formation of negative curvature (Harroun *et al.* 2003). 2 mol% of LPC induced a broad and weak the scattering profile (data not shown, but available on request), which may indicate either a disordered lamellar phase or a mixed structures of different phases. No measurable phase transition temperature was observed since the phase transformation was not clear. The addition of Arg-Glc MRPs (at 100:5) did not show a significant influence on the phase behaviour of lipid bilayer with LPC, although a sign of increase in T_H was noted in the contour diagram of scattering pattern (data not shown, but available on request).

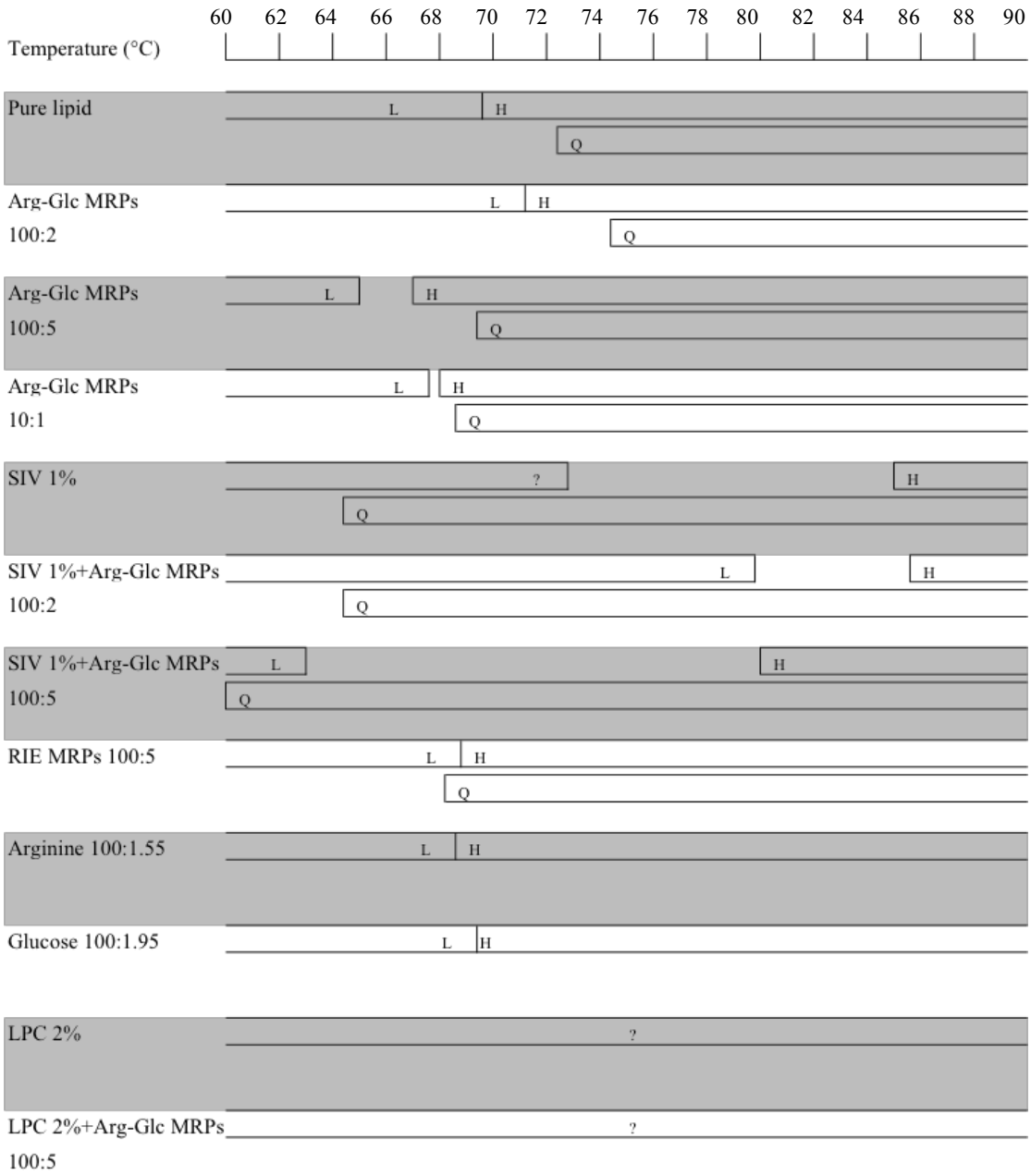

Figure 8.9 Schematic summary of the phase behaviour of MeDOPE MLVs and the MeDOPE in the presence of Arg-Glc MRPs and/or SIV fusion peptide and fusion inhibitor.

The transition temperatures were measured by a temperature scanning at 1˚C/min from 30˚C to 90˚C with the temperature-resolved X-ray diffraction.

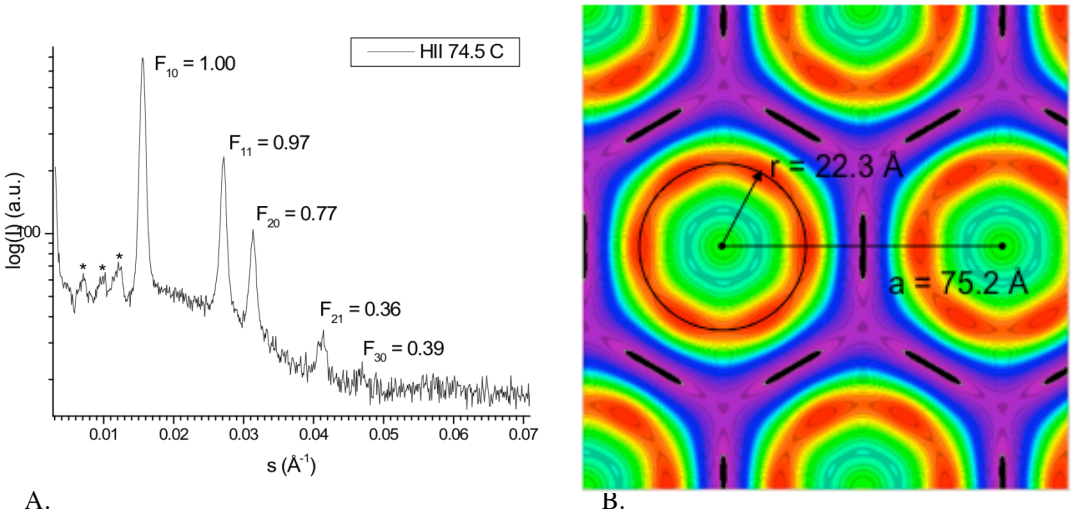

Figure 8.10 Electron density of the H_{II} phase of pure MeDOPE MLVs at 74.8°C (T_H + 5.0°C).

For calculating the electron density, the first first five peaks of the hexagonal phase were fitted by Lorentzians to deduce the form factor values F1-F5, and then a Fourier Transform was applied. The electron density diagram was reconstructed by Dr. Michael Rappolt, Elettra, Italy.

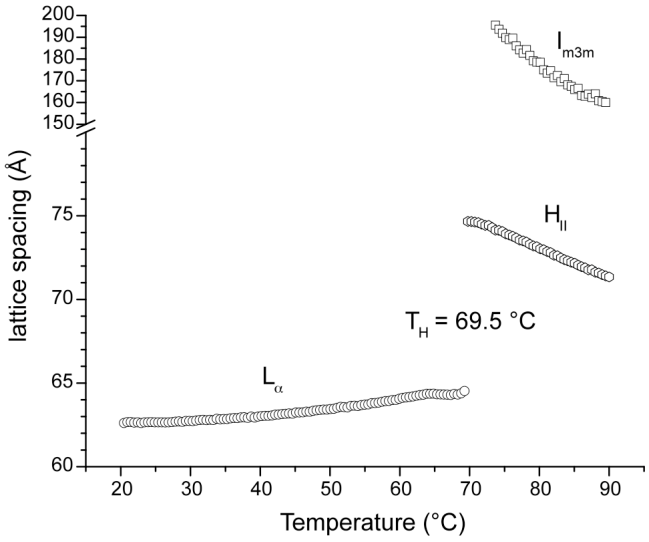

Figure 8.11 The lattice unit spacing of MeDOPE across the three phases.

The first order peak of L_α and H_{II}, and *sqrt(2)* peak of the I_{m3m} phase was fitted as a function of temperature for each scan. This diagram was reconstructed by Dr. Michael Rappolt, Elettra, Italy.

8.3.5. Humidity-resolved LXD

As shown in Fig 8.12, at the relative humidity lower than 81% RH, MeDOPE was fully in H_{II} phase, although the distance between each peak was decreasing when the humidity was raising up, which indicates the happening of phase transition from invert hexagonal phase to lamellar phase. At the humidity higher than 81% RH, the lipid bilayer was gradually transited to L_{α} phase. The proportion of lipids in L_{α} phase increased step by step until L_{α} phase became dominant at 93% RH.

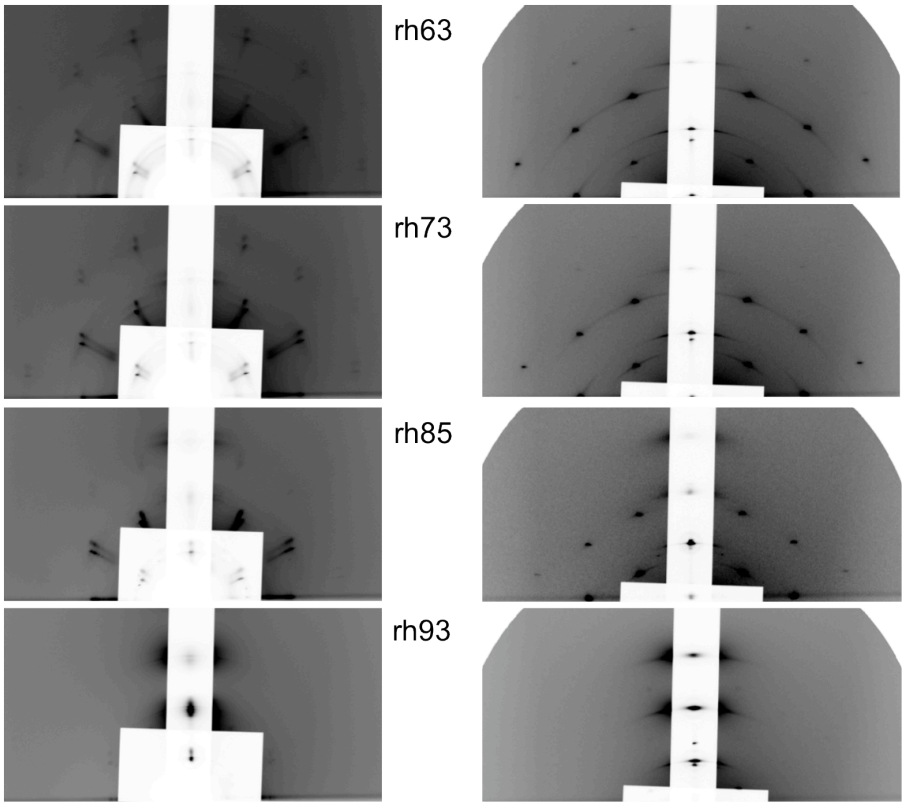

Figure 8.12 Diffraction of MeDOPE

In the presence (A) and absence (B) of Arg-Glc MRPs (100:5) at four humidities, 63% RH, 73% RH, 85% RH and 93% RH.

The addition of Arg-Glc MRPs (100:5) generally weakened the lipid diffraction signal in H_{II} phase, which resulted in a longer exposure time to X-ray for the same amount of lipids, and a smaller peak-to-peak distance (Fig 8.12). Furthermore, at the highest humidity, 93% RH, the lipid bilayers haven't been fully transited to L_{α} phase since a weak diffraction of H_{II} phase was observed in both of the figures. The appearance of L_{α} phase was at 81% RH in the

presence of Arg-Glc MRPs, the same as the pure MeDOPE. The weakening of diffraction indicates that the MRPs disorders the H_{II} phase and makes it easier for lipid bilayers to transit to L_{α} phase.

The presence of SIV fusion peptide (1 mol%) generally enhanced the diffraction signal of H_{II} phase, which indicates a stabilisation effect. This is constant with the previous studies (Harroun *et al.* 2003). Arg-Glc MRPs dramatically decreased the scattering intensity of this lipid-peptide system in H_{II} phase. Arg-Glc MRPs inhibited the effects of SIV peptide on lipid bilayer, in a concentration dependent manner.

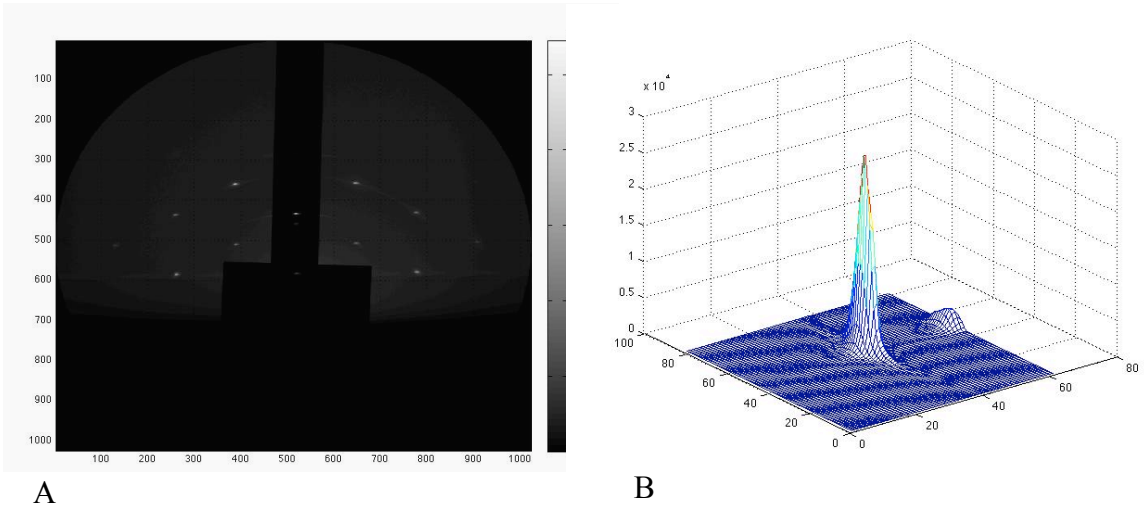

Figure 8.13 MeDOPE scattering profiles measured at 64% RH, 28°C.

(A) The diffraction pattern. (B) Diffraction peak at detector position (517, 433), (Q_x,Q_y) of the peak is (0.0032, 0.3165) where the peak area is 6.29×10^5.

8.4. CONCLUSIONS

By measuring the phase transition as a function of temperature with SAXS, the influences of Arg-Glc MRPs and RIE MRPs on the SIV peptide induced membrane fusion are revealed. The rise in the transition temperature of non-lamellar phases, induced by 100:2 Arg-Glc MRPs, implies a stabilisation of lamellar structure conducted by the MRPs. However, the effects of Arg-Glc MRPs on T_H and T_Q are reversed by increasing their proportion in lipid bilayer, to 100:5. The MRPs destabilise the lamellar bilayer and encourage the formation of non-lamellar phase. At a higher proportion of 10:1, the inverted hexagonal phase promoting effects Arg-Glc MRPs become weaker, while the T_Q is even lower than 100:5. This implies the high concentration of Arg-Glc MRPs have a mild effects on L_α-to-H_{II} transition when present a stronger promoting on L_α-to-Q_{II} transition. The effects of RIE MRPs are similar to those of Arg-Glc MRPs at 10:1. This observation is in a good agreement with the phase transition studies conducted with DSC, and the molecular packing profiles sensed by fluorescent probes.

The action of fusion peptides on the inverse hexagonal phase is separated from their ability to inducing inverse cubic phase (Darkes *et al.* 2002). It has been reported that SIV peptide dramatically delayed the inverse hexagonal phase while induced 'a gap between the phase where no structure was presented' (Harroun *et al.* 2003). In my study, SIV acts very similarly except the gap between L_α and H_{II} phases is covered up by the extension of a lamellar-like phase. SIV tends to promote the formation of inverse cubic phase when bypasses the intermediate structures leading to the hexagonal phase. 100:2 Arg-Glc MRPs stabilise the bilayer and increase the temperature range of lamellar phase by about 7°C. However, the MRPs at 100:5 destabilise the lamellar phase and promote the formation of the inverse cubic phase and inverse hexagonal phase.

Arginine and glucose show very mild effects on T_H, and inhibit the formation of cubic phase. LPC (2 mol%) releases the curvature-strain and fully inhibit the formation of non-lamellar phases. The Arg-Glc MRPs at 100:5 has no significant effects upon the LPC incorporated lipids bilayers.

As revealed by the humidity-resolved LXD study, the presence of SIV fusion peptide (1 mol%) generally enhances the diffraction signal of H_{II} phase, which indicates a stabilising function of the peptide on non-lamellar phase. Arg-Glc MRPs dramatically decrease the scattering intensity of this lipid-peptide system in H_{II} phase, implies an inhibitory effect on

SIV induced formation of negative curvature and thereby the non-lamellar structures, in a concentration dependent manner.

In summary, Arg-Glc MRPs stabilise the lamellar phase and inhibit the SIV-induced negative curvature-strain of bilayer at a low concentration (100:2), but destabilise the bilayers at the higher concentrations (100:5). The MRPs may inhibit SIV-induced membrane fusion.

CHAPTER 9

GENERAL CONCLUSIONS

This study contains two major parts. Part one, including Chapters 3, 4 and 5, focuses on biochemistry studies of the chemical composition and biological activities of MRPs. Part two, including Chapters 6, 7 and 8, describes biophysical studies of the interaction between MRPs and membrane phospholipids in several artificial model membrane systems.

In summary, significant anti-influenza viruses effects were demonstrated *in vitro* in RIE MRPs, but not in the cold water extracts of the fresh roots. The heat processing contributed to the antiviral activity of RIE MRPs. By observing the heat-induced chemical changes, the Maillard reaction was identified as the dominant chemical reaction occurring during the heat processing. It generated significant quantities of products which were conjectured as a new class of active compounds protecting cells from influenza viruses' infection. Determination of the amino acids and monosaccharides contents of the roots showed that, of all the possible reactants for Maillard, arginine and glucose were the major ones. The composition changed as the heat processing progressed. Their Maillard reaction products, Arg-Glc MRPs, possessed a similar anti-influenza viruses activity as RIE MRPs, whereas no significant antiviral effects were identified either on the native proteins from the fresh roots or on the glycated proteins from sun-dried roots. These results demonstrate the antiviral effects of RIE are related to the MRPs formed in the heat involved processes, and indicate that Arg-Glc MRPs are suitable to be used as a model MRPs for the mechanism studies of RIE's antiviral effects.

RIE and Arg-Glc MRPs bound to the cell membranes of erythrocytes and MDCK cells and, remarkably, altered the membranes' properties. With incorporation of the MRPs into their membranes, cells became less susceptible to influenza virus infection or hypotonic/hyperthermic haemolysis. Based on these observations, an antiviral mechanism was hypothesised for RIE MRPs: the MRPs bind to the cell membrane to provide cyto-protective effects against viral infection, rather than directly inactivate the viruses. To test the hypothesis, the interaction between MRPs and membrane lipids was investigated with a serial of biophysical experiments, on several artificial phospholipids monolayer and bilayer systems. Arg-Glc MRPs help lipids to pack more rigidly in monolayers or bilayers, and stabilise the liquid lamellar phase of lipids. In contrast, RIE MRPs and MCE MRPs increase the polarity of lipid bilayer and thereby improve the fluidity of membrane.

Both Arg-Glc MRPs and RIE MRPs insert into the hydrophobic region of bilayer, though at different strengths. The insertion of MRPs causes either stabilisation or destabilisation on the

lamellar structures of bilayers, in a process that is highly dependent on the concentration and overall distribution pattern of the MRPs. Arg-Glc MRPs reduce the SIV fusion peptide induced curvature-strain of bilayer at a low concentration (100:2, molar ratio) by stabilising the lamellar structures. The MRPs may thereby inhibit the SIV fusion peptide induced membrane fusion. However, an exceptional lamellar-destabilising effect was also observed for the MRPs at a higher concentration (100:5).

The mechanism of the anti-influenza virus activity of RIE is correlated to the interaction between MRPs and phospholipid bilayers, which prevents the formation of negative curvature and eventually membrane fusion. It is possible to view the interactions in terms of distinct stages. In the first stage, insertion of the MRPs into the spaces between head groups, pushes the hydrophilic heads away from each other. This would have the effect of decreasing negative curvature strain and would inhibit membrane fusion. The second stage is reached when the inter-head group spaces are filled, and MRP molecules start to accumulate in the bilayer core. This would tend to destabilise the lamellar structure of lipids. As the concentration of MRPs continues to increase, they incorporate across the whole thickness of the bilayer, and have no significant affect on monolayer curvature strain.

By combining the results from neutron diffraction, X-ray diffraction and DSC measurements, a model of the interaction between Arg-Glc MRPs and PE lipids emerges, as shown in Fig 8.1. It includes three concentration-dependent stages of interaction, described as below.

1) At low concentrations (e.g. 100:2), Arg-Glc MRPs mainly lie between the hydrophilic head groups of the lipids and relax negative curvature strain. The formation of non-lamellar structures is subsequently prevented by filling up the space between inverted-cone shaped phosphatidyethanolamine groups.

2) At a medium concentration (e.g. 100:5), the additional MRPs accumulate in the hydrophobic-hydrophilic intermediate region of bilayer, and thereby promote the formation of non-lamellar structures by pushing lipid tails away from each other.

3) At a high concentration (e.g 10:1), about 1/3 to 2/3 of the MRPs population sits close to, if not in, the hydrophobic region of bilayer, while the rest of MRPs remains in the hydrophilic head group. This results in a balanced state of the lipid bilayer under a joint influence of head group space filling and tails expelling.

This model fits well with the bilayer distribution profiles of RIE MRPs and their impacts on the formation of non-lamellar structures in liposomes. RIE MRPs interact with bilayers in a similar manner to high-concentrations (10:1) of Arg-Glc MRPs. Among the three concentrations of MRP employed in the study, the lowest one is closest to the realistic concentration of MRPs in blood or in the cell culture. Consideration of the results from this concentration be more valuable when trying to understand the effects of MRPs on the structure and function of cell membranes.

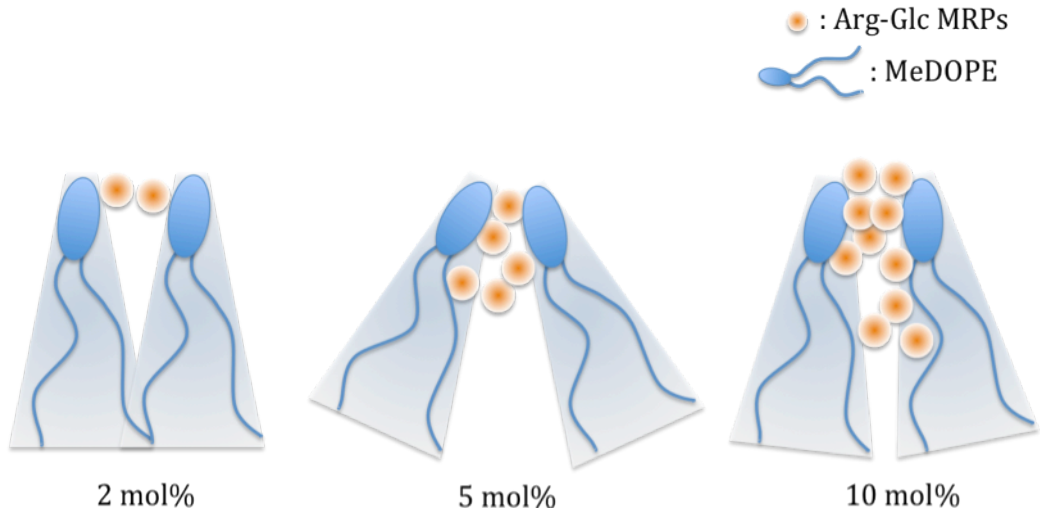

Figure 9.1 Schematic diagram of Arg-Glc MRPs' interaction with MeDOPE bilayer at 3 different concentrations.

Based on these findings, for the first time, MRPs are identified as the quantitatively predominant and biologically active compositions in RIE. A new anti-viral mechanism can be proposed for MRPs, in which MRPs bind to cell membranes and insert into phospholipid bilayers, which prevents the formation of negative curvature strain and eventually membrane fusion (as shown in Fig 9.2).

The most prominent feature of this proposed mechanism is that instead of blocking the virus infection and proliferation pathways at a specific point, virus infection is prevented by the overall strengthening the cell membrane. It is not unreasonable to speculate that these findings may form the basis of a broad spectrum antiviral agent with few adverse side effects. As an novel anti-viral mechanism, it echoes recent observations of anti-viral action through interaction with cell membranes (Wolf et al., 2010), which proposed a new antiviral molecule, belong to the rhodanine derivatives, has been demonstrated to act on a broad range of enveloped viruses by specifically intercalating into viral membranes. This paper is highly relevant to my hypothesis, though the target membranes differ between the two studies.

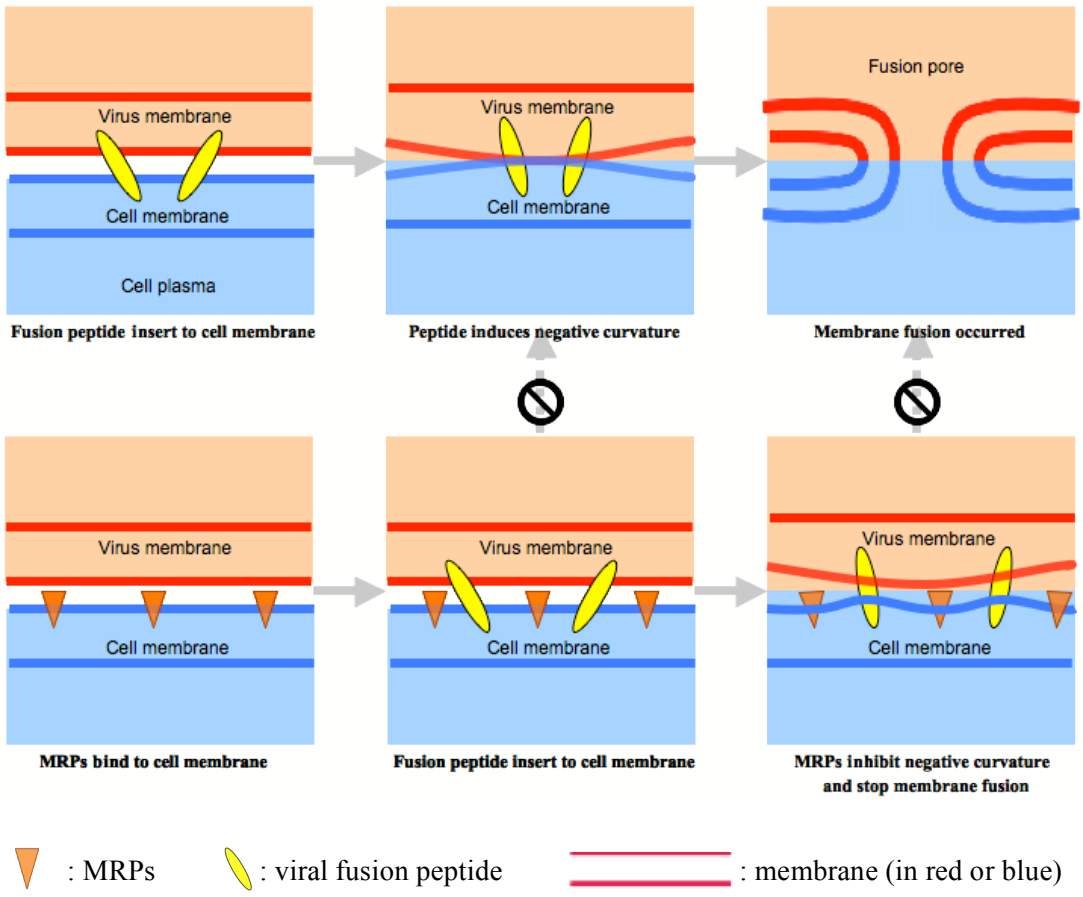

Figure 9.2 Schematic diagram showing the anti-viral mechanism of MRPs.

The upper three graphs show the fusion pore formation induced by the viral fusion peptide. The lower three graphs show that MRPs stabilise the cell membrane, inhibit the membrane negative curvature potentially induced by the insertion of fusion peptide, and eventually stop the membrane to occur.

The membrane-protection effects of MRPs provide a most plausible mechanism to the well-recorded clinical observations of preventing/treating viral infection with Chinese herbal medicine, which is mean to operate by strengthening the defending force of the patient's body. Above all, it is anticipated that the proposed mechanism will eventually lead to an effective new tool in the increasingly fierce battle against viral infections.

REFERENCES

Abe, H., Sakaguchi, M., A, M. & Arichi, S. (1981) Erythrocyte Membrane Stabilization by Plant Saponins and Sapogenins. *Archives of Pharmacology*, pp. 262-265.

Ames, J.M., 2007. Review Evidence against dietary advanced glycation endproducts being a risk to human health. *Mol Nutr Food Res, 51 (9),* pp. 1085 - 1090.

Amenitsch, H., Rappolt, M., Kriechbaum, M., Mio, H., Laggner, P. & Bernstorff S. (1998) First performance assessment of the small-angle X-ray scattering beamline at ELETTRA. *Journal of Synchrotron Radiation*, 5, pp. 506-508. Available at: http://scripts.iucr.org/cgi-bin/paper?az3042.

Anese, M., Nicoli, M.C., Massini, R. & Lerici, C.R. (1999) Eects of drying processing on the Maillard reaction in pasta. *Food Research International*, 32, pp. 193-199.

Antony, S.M., Han, I.Y., Rieck, J.R. & Dawson, P.L. (2000) Antioxidative Effect of Maillard Reaction Products Formed from Honey at Different Reaction Times †. *Journal of Agricultural and Food Chemistry*, 48 (9), pp. 3985-3989. Available at: http://dx.doi.org/10.1021/jf000305x.

Arenas, A., Carranza, J., Perea, A., Miranda, A., Maldonado, A. & Hermoso, M. (1990) Type a influenza viruses in birds in southern Spain: serological survey by enzyme-linked immunosorbent assay and haemagglutination inhibition tests. *Avian Pathology,* 19 (3), pp. 539-46. Available at: http://www.informaworld.com/10.1080/03079459008418706.

Ashley, R. H., Harroun, T. A., Hauss, T., Breen, K. C., & Bradshaw, J. P. (2006). Autoinsertion of soluble oligomers of Alzheimer's Aβ(1–42) peptide into cholesterol-containing membranes is accompanied by relocation of the sterol towards the bilayer surface. *BMC Structural Biology*, *11*, 1-11. doi: 10.1186/1472-6807-6-21.

Backov, R., Lee, C.M., Khan, S.R., Mingotaud, C., Fanucci, G.E. & Talham, D.R. (2000) Calcium Oxalate Monohydrate Precipitation at Phosphatidylglycerol Langmuir Monolayers. *Langmuir*, 16, pp. 6013-6019.

Baker, RL, Brown, RL, Chen, Z, Cleveland, TE & Fakhoury, AM 2009, "A maize trypsin inhibitor (ZmTIp) with limited activity against Aspergillus flavus.." *Journal of Food Protection*, vol. 72, no. 1, pp. 185-8. Retrieved from http://www.ncbi.nlm.nih.gov/pubmed/19205484

Bedinghaus, A.J. & Ockerman, H.W., 1995. Antioxidative Maillard Reaction Products from Reducing Sugars and Free Amino Acids in Cooked Ground Pork Patties. *Journal of Food Science*, 60(5) pp. 992-995. Available at: http://www3.interscience.wiley.com/journal/119237723/abstract.

Benjakul, S., Lertittikul, W. & Bauer, F., 2005. Antioxidant activity of Maillard reaction products from a porcine plasma protein–sugar model system. *Food Chemistry*, 93(2) pp. 189-196. Available at: http://dx.doi.org/10.1016/j.foodchem.2004.10.019.

Bensk, D., Clavey, S., Erich, S., Andrew, G. & Bensky, L.L. (2004) *Chinese Herbal Medicine: Materia Medica* 3rd., Eastland Press.

Blough, H.A., 1971. Fatty Acid Composition of Individual Phospholipids of Influenza Virus. *Journal of Biological Chemistry*, 12 pp. 317-320.

Boulan, E.R. & Sabatini, D.D., 1978. Asymmetric budding of viruses in epithelial monolayers: A model system for study of epithelial polarity. *Proc.Natl. Acad.Sci*, 75(10) pp. 5071-5075.

Bown, D., 1995. *Encyclopaedia of Herbs and their Uses*, London: Dorling Kindersley.

Bradford, M., 1976. A rapid and sensitive method for quantitation of microgram quantities of protein utilizing the principle of protein-dye-binding. *Anal Biochem*, 72 pp. 248-254.

Bradshaw, J.P., Darkes, M.J., Harroun, T.A., Katsaras, J. & Epand, R.M. (2000) Oblique membrane insertion of viral fusion peptide probed by neutron diffraction. *Biochemistry*, 39, pp. 6581-6585.

Brandts, JF, Taverna, RD, Sadasivan, E & Lysko, KA 1978, "Calorimetric studies of the structural transitions of the human erythrocyte membrane. Studies of the B and C transitions.." *Biochimica et Biophysica Acta*, vol. 512, no. 3, pp. 566-78. Retrieved from http://www.ncbi.nlm.nih.gov/pubmed/708733

Brezesinski, G. & Mohwald, H., 2003. Langmuir monolayers to study interactions at model membrane surfaces. *Advances in Colloid and Interface Science*, 102 pp. 563-584.

Briandet, R., Meylheuc, T., Maher, C. & Bellon-Fontaine, M.N. (1999) Listeria monocytogenes Scott A: Cell Surface Charge, Hydrophobicity, and Electron Donor and Acceptor Characteristics under Different Environmental Growth Conditions. *Appl. Envir. Microbiol.*, 65 (12), pp. 5328-5333. Available at: http://aem.asm.org/cgi/content/abstract /65/12/5328.

Burleson, F, Chambers, T & Wiedbrauk, D 1992, *Virology: A Laboratory Manual* F.G. Chambers & T Wiedbrauk, Academic Press, Inc., California.

Byrne, D.V., Mottram, D.S. & Martens, M., 2002. Sensory and chemical investigations on the e ect of oven cooking on warmed-over avour development in chicken meat. *Meat Science*, 61 pp. 127-139.

Cataldo, D.A., Schrader, L.E. & Youngs, V.L., 1974. Analysis by Digestion and Colourimetric Assay of Total Nitrogen in Plant Tissues High in Nitrate. *Crop Sci.*, 14(6) pp. 854-856. Available at: http://crop.scijournals.org/cgi/content/abstract/14/6/854.

Cao, G., Zheng, Y. & Xu, C., 2001. Changes of the Content of Arginine Derivatives of Red Ginseng at Different Stages of Processing. *Journal of Jilin Agricultural University (China)*, 23(3) pp. 69-71.

CDC, 2005. *Avian Influenza A Viruses*, Centers for Disease Control and Prevention. Available at: http://www.cdc.gov/flu/avian.

Ceriello, A., Marchi, E., Barbanti, M., Milani, M.R., Giugliano, D., Quatraro, A. & Lefebvre, P. (1990) Non-enzymatic glycation reduces heparin cofactor II anti-thrombin activity. *Diabetologia*, 33 (4), pp. 205-207. Available at: http://www.springerlink.com/ content/j772707w0t1305x1.

Chen, F., Lee, M., & Huang, H. W. (2003). Evidence for Membrane Thinning Effect as the Mechanism for Peptide-Induced Pore Formation. *Biophysical Journal*, *84*(6), 3751-3758. Elsevier. doi: 10.1016/S0006-3495(03)75103-0.

Chen, F.S., Markosyan, R.M. & Melikyan, G.B. (2002) The process of membrane fusion: Nipples, hemifusion, pores, and pore growth. *Current Topics in Membranes*, 52, pp. 501-529. Available at: http://dx.doi.org/10.1016/S1063-5823(02)52020-2.

Chen, Z., Wu, L., Liu, S., Cai, C., Rao, P. & Ke, L. (2006) Mechanism study of anti-influenza effects of radix Isatidis water extract by red blood cells capillary electrophoresis. *China Journal of Chinese Materia Medica*, 31 (20), pp. 1715-9. Available at: http://www.ncbi.nlm.nih.gov/pubmed/17225545.

Cherezov, V., Siegel, D.P., Shaw, W., Burgess, S.W. & Caffrey, M. (2003) The Kinetics of Non-Lamellar Phase Formation in DOPE-Me: Relevance to Biomembrane Fusion. *Journal of Membrane Biology*, 195, pp. 165-182.

Chinese Pharmacopoeia Commission, 2005. *Chinese Pharmacopoeia (Part I)* 2005 ed. Chinese Pharmacopoeia Commission, Chemical Industry Press, Beijing, China.

Cho, E.J., Piao, X.L., Jang, M.H., Baek, S.H., Kim, H.Y., S, K.K., Kwon, S.W. & Joeng, H.P. (2008) The effect of steaming on the free amino acid contents and antioxidant activity of Panax ginseng. *Food Chemistry*, 107, pp. 876-882.

Chuyen, N.V., 1998. Maillard reaction and food processing. Application aspects. *Advances in Experimental Medicine and Biology*, 434 pp. 213-35. Available at: http://www.ncbi.nlm.nih.gov/pubmed/9598202.

Chuyen, N.V., 2006. Toxicity of the AGEs generated from the Maillard reaction: on the relationship of food-AGEs and biological-AGEs. *Molecular Nutrition & Food Research*, 50(12) pp. 1140-9. Available at: http://www3.interscience.wiley.com/journal/113489010/abstract.

Colotto, A., Martin, I., Ruysschaert, J.M., Sen, A., Hui, S.W. & Epand, R.M. (1996) Structural Study of the Interaction between the SIV Fusion Peptide and Model Membranes. *Biochemistry*, 35, pp. 980-989.

Corzo-Martínez, M., Soria, A.C., Belloque, J., Villamiel, M. & Moreno, F.J. (2010) Effect of glycation on the gastrointestinal digestibility and immunoreactivity of bovine β-lactoglobulin. *International Dairy Journal*. Available at: http://dx.doi.org/10.1016/j.idairyj.2010.04.002.

Cowan, M.M., 1999. Plant Products as Antimicrobial Agents. *Clinical Microbiology Reviews*, 12(4) pp. 564-582.

Cox, N.J. & Subbarao, K., 1999. Influenza. *The Lancet*, 354 pp. 1277-1282.

Crance, J.M., Scaramozzino, N., Jouan, A. & Garin, D. (2003) Interferon , ribavirin , 6-azauridine and glycyrrhizin : antiviral compounds active against pathogenic flaviviruses. *Antiviral Research*, 58, pp. 73-79.

Crowe, JH, Crowe, LM, Carpenter, JF & Wistrom, CA 1987, "Stabilization of dry phospholipid bilayers and proteins by sugars." *Biochem. J.*, vol. 242, pp. 1-10.

Darkes, M.J., Harroun, T.A., Davies, S.M. & Bradshaw, J.P. (2002) The Effect of Fusio Inhibitors on the Phase Behaviour of N-Methylated Dioleoylphosphatidylethanolamine. *Biochemica et Biophysica Acta*, 78220, pp. 1-10.

DiPietro, C.M. & Liener, I.E., 1989. Heat inactivation of the Kunitz and Bowman-Birk soybean protease inhibitors. *Journal of Agricultural and Food Chemistry*, 37(1) pp. 39-44. Available at: http://dx.doi.org/10.1021/jf00085a010.

Dische, Z., 1967. Modifications of two colour reactions of hexoses with cysteine and sulfuric acid*1. *Analytical Biochemistry*, 21(1) pp. 119-124. Available at: http://dx.doi.org/10.1016/0003-2697(67)90090-5.

Dong, X. & Liu, W., 2001. Determination of arginine in *radix Isatidis* by TLCS. *Chinese Journal of Analysis Laboratory*, 20(4) pp. 92-3.

Dorairaj, S & Allen, TW 2007, On the thermodynamic stability of a charged arginine side chain in a transmembrane helix. *Proc. Natl. Acad. Sci. USA*, vol. 104, no. 12, pp. 4943-4948.

Duff, K., 1992. The secondary structure of influenza A M2 transmembrane domain A circular dichroism study. *FEBS Letters*, 311(3) pp. 256-258. Available at: http://dx.doi.org/10.1016/0014-5793(92)81114-2.

Duke, J.A. & Ayensu, E.S., 1985. *Medicinal Plants of China*, Reference Publications, Inc.

Eble, A., Thorpe, S. & Baynes, J., 1983. Nonenzymatic glucosylation and glucose-dependent cross-linking of protein. *J. Biol. Chem.*, 258(15) pp. 9406-9412. Available at: http://www.jbc.org/cgi/content/abstract/258/15/9406.

Echeverria, E. & Burns, J.K. (1989) Vacuolar Acid Hydrolysis as a Physiological Mechanism for Sucrose Breakdown. *Plant Physiology*, 90 (2), pp. 530-533. Available at: http://www.plantphysiol.org/cgi/content/abstract/90/2/530.

Echeverria, E. (1990) Developmental Transition from Enzymatic to Acid Hydrolysis of Sucrose in Acid Limes (Citrus aurantifolia). *Plant Physiology*, 92 (1), pp. 168-171. Available at: http://www.plantphysiol.org/cgi/content/abstract/92/1/168.

Edman, P., 1950. Method for determination of the amino acid sequence in peptides. *Acta Chemica Scandinavica*, 4 pp. 283-293.

Einarsson, H., Snygg, B.G. & Eriksson, C., 1983. Inhibition of bacterial growth by Maillard reaction products. *J. Agric. Food Chem.*, 31 pp. 1043-1047.

Epand, R. M., Rychnovsky, S. D., Belani, J. D., Epand, R. F., This, C., Mas, T. N., *et al.* (2005). Role of chirality in peptide-induced formation of cholesterol-rich domains. *Biochem. J*, *548*, 541-548. doi: 10.1042/BJ20050649.

Ellens, H., Bentz, J. & Szoka, F.C., 1986. Fusion of phosphatidylethanolamine-containing liposomes and mechanism of the L alpha-HII phase transition. *Biochemistry*, 25(14) pp. 4141-7. Available at: http://www.ncbi.nlm.nih.gov/pubmed/3741846.

Epand, R.M., 1998. Lipid polymorphism and protein-lipid interactions. *Biochimica et Biophysica Acta*, 1376(3) pp. 353-68. Available at: http://www.ncbi.nlm.nih.gov/pubmed/9804988.

Fenn, J., Mann, M., Meng, C., Wong, S. & Whitehouse, C. (1989) Electrospray ionization for mass spectrometry of large biomolecules. *Science*, 246 (4926), pp. 64-71. Available at: http://www.sciencemag.org/cgi/content/abstract/246/4926/64.

Fireman, Z., Segal, A., Kopelman, Y., Sternberg, A. & Carasso, R. (2001) Acupuncture treatment for irritable bowel syndrome. A double-blind controlled study. *Digestion*, 64 (2), pp. 100-3. Available at: http://content.karger.com/ProdukteDB/produkte.asp?Aktion=ShowAbstract&ArtikelNr=48847&Ausgabe=227606&ProduktNr=223838.

Franzke, C. & Iwainsky, H., 1954. Zur antioxydativen Wirksamveit der Melanoidine. *Deutche Lebensmittle-Rundschau*, (50) pp. 251-254.

Gallin, J.I., Durocher, J.R. & Kaplan, A.P., 1975. Interaction of leukocyte chemotactic factors with the cell surface. I. Chemotactic factor-induced changes in human granulocyte surface charge. *The Journal of Clinical Investigation*, 55(5) pp. 967-74. Available at: http://www.pubmedcentral.nih.gov/articlerender.fcgi?artid=301842&tool =pmcentrez&rendertype=abstract.

2010. Glossary. *Nature publishing Group*. Available at: http://www.nature. com/nri/journal/v4/n11/glossary/nri1486_glossary.html.

Gao, W., Li, J., Tang, Y., Zhuang, C., Li, B., Wang, S. & Huang, H. (2008) Experiment study on Ma-Xing-Shi-Gan-Tang (MXSGT) and its decomposed recipes on anti-influenza virus A. *Nature Precedings*. Available at: http://precedings.nature.com/documents/2260/ version/1.

Gaush, C.R. & Smith, T.F., 1968. Replication and plaque assay of influenza virus in an established line of canine kidney cells. *Applied Microbiology*, 16(4) pp. 588-594.

Gershfeld, N. & Murayama, M., 1988. Thermal instability of red blood cell membrane bilayers: temperature dependence of hemolysis. *Journal of Membrane Biology*, 101 pp. 67-72. Available at: http://www.springerlink.com/index/J601063K1906544M.pdf.

Gershfeld, N.L., 1993. Critical temperature for unilamellar vesicle formation in dimyristoylphosphatidylcholine dispersions from specific heat measurements. *Biophysical Journal*, 65(3) pp. 1174-1179. Available at: http://dx.doi.org/10.1016/S0006-3495(93) 81157-3.

Glatter, O., & Kratky, O. (1982). *Small Angle X-ray Scattering*. Academic Press.

Glossmann, H. & Neville, D.M., 1971. Glycoproteins of Cell Surfaces. A Comparative Study of Three Different Cell Surfaces of the Rat. *J. Biol. Chem.*, 246(20) pp. 6339-6346. Available at: http://www.jbc.org/cgi/content/abstract/246/20/6339.

Graf, K., Riegler, H., 1998. Molecular adhesion interactions between Langmuir monolayers and solid substrates. *Colloids and Surfaces A: Physicochemical and Engineering Aspects*, 131 pp. 215-224. Available at : http://linkinghub.elsevier.com/retrieve/pii/S0927775796039

234.

Gubareva, L.V., Webster, R.G. & Hayden, F.G., 2002. Detection of in uenza virus resistance to neuraminidase inhibitors by an enzyme inhibition assay. *Science*, 53 pp. 47 - 61.

Hamilton, P.B., Bogue, D.C. & Anderson, R.A., 1960. Ion exchange chromatography of amino acids.Analysis of diffusion (Mass transfer) mechanisms. *Analytical Chemistry*, 32(13) pp. 1782-1792. Available at: http://dx.doi.org/10.1021/ac50153a025.

Harper, P.E., Mannock, D.A., Lewis, R.N., Mcelhaney, R.N., Gruner, S.M. & Gruner, S.M. (2001) X-Ray Diffraction Structures of Some Phosphatidylethanolamine Lamellar and Inverted Hexagonal Phases. *Biophysical Journal*, 81, pp. 2693-2706.

Hansen, A.P. & Hemphill, P.L., 1984. Utilization of heat to increase shelf life of blended acid whey and buttermilk powder for frozen desserts. *Journal of Dairy Science* pp. 54-56.

Hauss, T. (2010). V1 Diffractometer for Cold Neutrons with Area Detector. *BENSC, HZB Berlin*.

Harris, N. & Tan, B., 1999. Effect of Maillard reaction products on microbial growth. In *The IFT Annual Meeting*. pp. 37D-31.

Harris, F.M., Best, K.B. & Bell, J.D., 2002. Use of laurdan fluorescence intensity and polarization to distinguish between changes in membrane fluidity and phospholipid order. *Biochimica et Biophysica Acta*, 1565 pp. 123 - 128.

Harrison, S., 2005. Mechanism of membrane fusion by viral envelope proteins. *Advances In Virus Research*, 64(05), 231-261.

Harroun, T.A., Balai-mood, K., Hauss, T., Otomo, T. & Bradshaw, J.P. (2005) Neutron Diffraction with an Excess-Water Cell. *Journal of Biological Physics*, 31, pp. 207-218.

Harroun, T.A., Balali-Mood, K., Gourlay, I. & Bradshaw, J.P. (2003) The fusion peptide of simian immunodeficiency virus and the phase behaviour of N-methylated dioleoylphosphatidylethanolamine. *Biochimica et Biophysica Acta*, 1617, pp. 62-68.

Hayashi, T. & Namiki, M., 1980. Formation of two-carbon sugar fragments at an early stage of the browning reaction of sugar and amine. *Agric. Biol. Chem.*, 44 pp. 2575-2580.

HidalgoI, F.J. & Zamora, R., 2006. Interplay between the Maillard Reaction and Lipid Peroxidation in Biochemical Systems. *Annals Of The New York Academy Of Sciences*, 1043(The Maillard Reaction: Chemistry at the Interface of Nutrition, Aging, and Disease) pp. 319-326.

Hill, D.W., Walters, F.H., Wilson, T.D. & Stuart, J.D. (1979) High performance liquid chromatographic determination of amino acids in the picomole range. *Analytical Chemistry*, 51 (8), pp. 1338-1341. Available at: http://dx.doi.org/10.1021/ac50044a055.

Hodge, J.E., 1953. Dehydrated Foods, Chemistry of Browning Reactions in Model Systems. *Journal of Agricultural and Food Chemistry*, 1(15) pp. 928-943. Available at: http://dx.doi.org/10.1021/jf60015a004.

Hofmann, T. & Heuberger, S., 1999. The contribution of coloured Maillard reaction products to the total colour of browned glucose/L-alanine solutions and studies on their formation. *Z Lebensm Unters Forsch A*, 208 pp. 17-26.

Hou, Z., Zhang, Z., Zhang, C. & Huang, M. (2004) Use of natural plant exudates (Sanguis Draxonis) for sustained oral insulin delivery with dramatic reduction of glycemic effects in diabetic rats. *Journal of Controlled Release*, 97 (3), pp. 467-75. Available at: http://www.ncbi.nlm.nih.gov/pubmed/15212878.

Hu, X. & Zheng, W., 2003. Resistance to Isatia indigotica Fort Lectin inhibit influenza. *Jounral of Shanghai Teachers University (Natural Sciences)*, 32(1) pp. 62-5.

Huang, T., Toraya, H., Blanton, T. & Wu, Y. (1993) X-ray Powder Diffraction Analysis of Silver Behenate, a Possible Low-Angle Diffraction Standard. *J. Appl. Cryst.*, 26, pp. 180-184.

Hung, W., & Chen, F. (2003). The Hydrophobic-Hydrophilic Interface of Phospholipid Membranes Studied by Lamellar X-Ray Diffraction. *Chinese Journal of Physics*, *41*(1), 85-91.

Hung, W., Chen, F., Lee, C., Sun, Y., Lee, M., Huang, H. W., *et al.* (2008). Membrane-Thinning Effect of Curcumin. *Biophysical Journal*, *94*(June), 4331-4338. doi: 10.1529/biophysj.107.126888.

Ilyushina, N.A., Govorkova, E.A., Russell, C.J., Hoffmann, E. & Webster, R.G. (2007) Contribution of H7 haemagglutinin to amantadine resistance and infectivity of influenza virus. *Journal of General Virology*, 88, pp. 1266-1274.

Jahn, R., Lang, T. & Südhof, T.C., 2003. Membrane Fusion. *Cell*, 112(4) pp. 519-533. Available at: http://www.cell.com/retrieve/pii/S0092867403001120.

Jakuš, V. & Rietbrock, N., 2004. Advanced Glycation End-Products and the Progress of Diabetic Vascular Complications. *Physiological Research*, (53) pp. 131-142.

Jiao, J.A., Yee, B.C., Kobrehel, K. & Buchanan, B.B. (1992) Effect of thioredoxin-linked reduction on the activity and stability of the Kunitz and Bowman-Birk soybean trypsin inhibitor proteins. *Journal of Agricultural and Food Chemistry*, 40 (12), pp. 2333-2336. Available at: http://dx.doi.org/10.1021/jf00024a002.

Jin, M., Ren, D., Meng, F. & Li, X. (2007) The Effects of *radix Isatidis* on Immunological Function and Influenza Virus (FM1) in Kunming Mice. *Lishizhen Medicine and Materia Medica Research*, 18 (2), pp. 394-396.Karlsson, G., Winge, S. & Sandberg, H., 2005. Separation of monosaccharides by hydrophilic interaction chromatography with evaporative light scattering detection. , 1092 pp. 246-249.

Kato, Y. & Matsuda, T., 1997. Glycation of Proteinous Inhibitors: Loss in Trypsin Inhibitory Activity by the Blocking of Arginine and Lysine Residues at Their Reactive Sites. *Journal of Agricultural and Food Chemistry*, 45(10) pp. 3826-3831. Available at: http://dx.doi.org/10.1021/jf970310+.

Ke, L., Lu, W., Chang, J., Yuan, F., Rao, P. & Zhou, J. (2010) Effects of Heat drying Process on Amino Acids content of Momordica charantia L. *Amino Acids and Biotic Resources*, 32 (2).

Khandelia, H., Ipsen, J. H., & Mouritsen, O. G. (2008). Review: The Impact of Peptide on Lipid Membranes. *Biochimica et Biophysica Acta The Impact of Peptides on Lipid Membranes*, *1778*, 1528-1536. doi: 10.1016/j.bbamem.2008.02.009.

Klasse, P.J. & Sattentau, Q.J., 2002. Occupancy and mechanism in antibody-mediated neutralization of animal viruses. *The Journal of General Virology*, 83(Pt 9) pp. 2091-108. Available at: http://vir.sgmjournals.org/cgi/content/full/83/9/2091.

Kobasa, D., Takada, A., Shinya, K., Hatta, M., Halfmann, P., Theriault, S., Suzuki, H., Nishimura, H., Mitamura, K., Sugaya, N., Usui, T., Murata, T., Maeda, Y., Watanabe, S., Suresh, M., Suzuki, T., Suzuki, Y., Feldmann, H. & Kawaoka, Y. (2004) Enhanced virulence of influenza A viruses with the haemagglutinin of the 1918 pandemic virus. *Nature*, 431 (7009), pp. 703-7. Available at: http://dx.doi.org/10.1038/nature02951.

Kong, W., Zhao, Y., Shan, L., Xiao, X. & Guo, W. (2008) Investigation on the spectrum-effect relationships of EtOAc extract from *Radix Isatidis* based on HPLC fingerprints and microcalorimetry. *Journal of Chromatography. B, Analytical Technologies in the Biomedical and Life Sciences*, 871 (1), pp. 109-14. Available at: http://dx.doi.org/10.1016/j.jchromb.2008.06.053.

Kong, W., Zhao, Y., Shan, L., Xiao, X. & Guo, W. (2008) Thermochemical studies on the quantity-antibacterial effect relationship of four organic acids from Radix Isatidis on Escherichia coli growth. *Biological & Pharmaceutical Bulletin*, 31 (7), pp. 1301-5. Available at: http://www.ncbi.nlm.nih.gov/pubmed/18591764.

Krasnowska, E.K., Gratton, E. & Parasassi, T., 1998. Prodan as a Membrane Surface Fluorescence Probe: Partitioning between Water and Phospholipid Phases. *Biophysical Journal*, 74(April) pp. 1984-1993.

Krumova, S.B., Koehorst, R.B., Bóta, A., Páli, T., Hoek, A.V., Garab, G. & Amerongen, H.V. (2008) Temperature dependence of the lipid packing in thylakoid membranes studied by time- and spectrally resolved fluorescence of Merocyanine 540. *Biochimica et Biophysica Acta - Biomembranes*, 1778 (12), pp. 2823-2833. Available at: http://dx.doi.org/10.1016/j.bbamem.2008.09.007.

Kundinger, M.M., 2004. Growth and virulence response of Salmonella typhimurium to soluble Maillard reaction products. , (May) pp. 78-88.

Kusube, M., Goto, M., Tamai, N., Matsuki, H. & Kaneshina, S. (2006) Bilayer phase transitions of N-methylated dioleoylphosphatidylethanolamines under high pressure. *Chemistry and Physics of Lipids*, 142, pp. 94-102.

Laemmli, U.K., 1970. Cleavage of structural proteins during the assembly of the head of bacteriophage T4. *Nature*, 227(5259) pp. 680-5. Available at: http://www.ncbi.nlm.nih.gov/pubmed/5432063.

Lamarre, D., Anderson, P.C., Bailey, M., Beaulieu, P., Bolger, G., Bonneau, P., Bös, M., Cameron, D.R., Cartier, M., Cordingley, M.G., Faucher, A., Goudreau, N., Kawai, S.H., Kukolj, G., Lagacé, L., LaPlante, S.R., Narjes, H., Poupart, M., Rancourt, J., Sentjens, R.E., St George, R., Simoneau, B., Steinmann, G., Thibeault, D., Tsantrizos, Y.S., Weldon, S.M., Yong, C. & Llinàs-Brunet, M. (2003) An NS3 protease inhibitor with antiviral effects in humans infected with hepatitis C virus. *Nature*, 426 (6963), pp. 186-9. Available at: http://dx.doi.org/10.1038/nature02099.

Langner, M. & Hui, S.W., 1999. Merocyanine 540 as a fluorescence indicator for molecular packing stress at the onset of lamellar-hexagonal transition of phosphatidylethanolamine bilayers. *Lipids*, 1415 pp. 323-330.

Lear, J.D. & Degrado, F., 1987. Membrane Binding and Conformational Properties of Peptides Representing the NH2 Terminus of Influenza HA-2. *The Journal of biological chemistry*, 262(14), 6500-6505.

Lederer, M.O. & Klaiber, R.G., 1999. Cross-Linking of Proteins by Maillard Processes: Characterisation and Detection of Lysine±Arginine Cross-Links Derived from Glyoxal and Methylglyoxal. *Bioorganic & Medicinal Chemistry*, 7 pp. 2499-2507.

Lee, K., Simpson, G. & Ortwerth, B., 1999. A systematic approach to evaluate the modifcation of lens proteins by glycation-induced crosslinking. *Science*, 1453 pp. 141-151.

Lelkes, P. & Miller, I., 1980. Perturbations of membrane structure by optical probes: I. Location and structural sensitivity of merocyanine 540 bound to phospholipid membranes. *Journal of Membrane Biology*, 15 pp. 1-15. Available at: http://www.springerlink.com/index/hu28w13v3631217w.pdf.

Lenard, J., Tsai, D.K., Compans, R.W. & Landsberger, F.R. (1976) Observations on the Membrane Organization of Standard Incomplete Influenza Grown in MDBK Cells. *Virology*, 71, pp. 389-394Levi, R., Beeor-tzahar, T. & Amon, R., 1995. Microculture virus titration - a simple colourimetric assay for influenza virus titration. *Journal of Virological Methods*, 52 pp. 55-64.

Li, H., Yan, D., Wang, J., Wang, J. & Bei, Z. (2009) Biological evaluation of Radix Isatidis based on neuraminidase activity assay. *Acta Pharmaceutica*, 44 (2), pp. 162-166.

Li, L., Vorobyov, I., Jr., A.D. & Allen, T.W. (2008) Is Arginine Charged in a Membrane? *Biophysical Journal: Biophysical Letters*, 94 (2), pp. 11-13.

Li, X., Zheng, Y., Liu, M. & Zhang, L. (1999) [A study on maillard reaction and its products during processing of red ginseng]. *China Journal of Chinese Materia Medica*, 24 (5), pp. 274-8, 318. Available at: http://www.ncbi.nlm.nih.gov/pubmed/12205883.

Li, Y., Ma, L., Gong, M. & Guan, H. (2009) Optimizing cutting process of Radix Isatidis and comparing difference of fingerprints before and after cutting. *China Journal of Chinese Materia Medica*, 34 (17), pp. 2177-80. Available at: http://www.ncbi.nlm.nih.gov/pubmed/19943479.

Lin, C. & Tsai, F., 2005. Inhibition of SARS Coronavirus 3C-Like Protease by lsatis indigotica Root and Plant-derived Phenolic Compounds *In Vitro* Antibacterial Activity Against Gram-positive and Gram-negative Pathogens in Asia - Tigecycline Evaluation Surveillance Trial, *Management* pp. 2005-2005.

Lin, W., Mo, J., Yu, R., Zhou, C. & Zhao, Y. (2005) Studies on HPLC fingerprint chromatogram of Radix Isatidis. *The Chinese Journal of Modern Applied Pharmacy* (5), pp. 27-9.

Lingnert, H. & Hall, G., 1986. Formation of antioxidative Maillard reaction products during food processing. In M. Fujimaki, M. Namiki, & E. Kato *Amino-carbonyl Reactions in Food and Biological Systems*. Tokyo: Elsevier pp. 273-279.

Lingnert, H. & Lundgren, B., 1980. Antioxidative Maillard reaction products IV. Application in sausage. *Journal of Food Processing and Preservation*, 4(4) pp. 235-246. Available at: http://www3.interscience.wiley.com/journal/119590168/abstract.

Lingnert, H. & Waller, G.R., 1983. Stability of antioxidants formed from histidine and glucose by the Maillard reaction. *Journal of Agricultural and Food Chemistry*, 31(1) pp. 27-30. Available at: http://dx.doi.org/10.1021/jf00115a007.

Link, A.J., Eng, J., Schieltz, D.M., Carmack, E., Mize, G.J., Morris, D.R., Garvik, B.M. & Yates, J.R. (1999) Direct analysis of protein complexes using mass spectrometry. *Nature Biotechnology*, 17 (7), pp. 676-82. Available at: http://dx.doi.org/10.1038/10890.

Liu, J., Li, X. & Jiang, Y., 2008. Study of Radix Isatidis extraction on mouse with influenza virus FM1 strain. M*odern Journal of Intergrated Traditional Chinese and Western Medicine*, 17(9) pp. 1303-1304.

Loo, J., Udseth, H. & Smith, R., 1989. Peptide and protein analysis by electrospray ionization-mass spectrometry and capillary electrophoresis-mass spectrometry. *Analytical Biochemistry*, 179(2) pp. 404-412. Available at: http://dx.doi.org/10.1016/0003-2697(89)90153-X.

Loosdrecht, A.V., Beelen, R., Ossenkoppele, G., Broekhoven, M. & Langenhuijsen, M. (1994) A tetrazolium-based colorimetric MTT assay to quantitate human monocyte mediated cytotoxicity against leukemic cells from cell lines and patients with acute myeloid leukemia. *Journal of Immunological Methods*, 174 (1-2), pp. 311-320. Available at: http://dx.doi.org/10.1016/0022-1759(94)90034-5.

Lowry, O., Rosebrough, N., Farr, A. & Randall, R. (1951) Protein measurement with the Folin Phenol reagent. *J Biol Chem*, 193, pp. 265-275.

Lu, W., Deng, W., Liu, S., Chen, T. & Rao, P. (2003) Capillary electrophoresis of erythrocytes. *Analytical Biochemistry*, 314, pp. 194-198.

Maillard, L.C., 1912. Action Des Acides Amine's Sur Les Sucres. Formation Des Melanoidins. *Par Voie Methodique' in Compt.*, Rend(154) pp. 66-8.

Marsh, M. & Helenius, A., 2006. Virus Entry: Open Sesame. *Cell*, 124 pp. 729-740.

Martins, S.I. & Boekel, M.A., 2005. A kinetic model for the glucose/glycine Maillard reaction pathways. *Food Chemistry*, 90 pp. 257-269.

Martins, S.I., Jongen, W.M. & Boekel, M.A., 2001. A review of Maillard reaction in food and implications to kinetic modelling. *Trends in Food Science & Technology*, 11 pp. 364-373.

Marra, J., 1986. Direct Measurement of the Interaction between Phosphatidylglycerol Bilayers. *Biophysical Journal*, 50(5) pp. 815-825. Available at: http://dx.doi.org/10.1016/S0006-3495(86)83522-6.

McManus, M., 1995. Effects of the soybean (Kunitz) trypsin inhibitor on growth and digestive proteases of larvae of Spodoptera litura. *Journal of Insect Physiology*, 41(9) pp. 731-738. Available at: http://dx.doi.org/10.1016/0022-1910(95)00043-T.

Meer, G.V. & Simons, K., 1982. Viruses budding from either the apical or the basolateral plasma membrane domain of MDCK cells have unique phospholipid compositions. *EMBO Journal*, 1(7) pp. 847-852.

Miller, C.R., Bondurant, B., McLean, S.D., McGovern, K.A. & O'Brien, D.F. (1998) Liposome-cell interactions in vitro: effect of liposome surface charge on the binding and endocytosis of conventional and sterically stabilized liposomes. *Biochemistry*, 37 (37), pp. 12875-83. Available at: http://dx.doi.org/10.1021/bi980096y.

Morein, S., Andersson, A., Rilfors, L. & Lindblom, G. (1996) Wild-type Escherichia coli cells regulate the membrane lipid composition in a "window" between gel and non-lamellar structures. *The Journal of Biological Chemistry*, 271 (12), pp. 6801-9. Available at: http://www.ncbi.nlm.nih.gov/pubmed/8636103.

Moreno, F.J., Quintanilla-López, J.E., Lebrón-Aguilar, R., Olano, A. & Sanz, M.L. (2008) Mass spectrometric characterisation of glycated beta-lactoglobulin peptides derived from galacto-oligosaccharides surviving the in vitro gastrointestinal digestion. *Journal of the American Society for Mass Spectrometry*, 19 (7), pp. 927-37. Available at: http://www.ncbi.nlm.nih.gov/pubmed/18467121.

Moscona, A., 2005. Neuraminidase Inhibitors for Influenza. *N Engl J Med,* 2005; 353 pp. 1363-1373.

Mosmann, T., 1983. Rapid colourimetric assay for cellular growth and survival: Application to proliferation and cytotoxicity assays. *Journal of Immunological Methods*, 65(1-2) pp. 55-63. Available at: http://dx.doi.org/10.1016/0022-1759(83)90303-4.

Mu, M., Pan, X., Yao, P. & Jiang, M. (2006) Acidic solution properties of beta-casein-graft-dextran copolymer prepared through Maillard reaction. *Journal of colloid and interface Science*, 301 (1), pp. 98-106. Available at: http://dx.doi.org/10.1016/j.jcis.2006.04.048.

Nagai, T., Yang, J., Sakurai, M. & Yamada, H. (1998) Anti-influenza viral glycoprotein from the roots of Isatis tinctoria L. *Antiviral Research*, 37, p. 88.

Nayak, D.P. & Reichl, U., 2004. Neuraminidase activity assays for monitoring MDCK cell culture derived influenza virus. *Journal of Virological Methods*, 122(1) pp. 9-15. Available at: http://www.ncbi.nlm.nih.gov/pubmed/15488615.

Nayak, D.P., Balogun, R.A., Yamada, H., Zhou, Z.H. & Barman, S. (2009) Influenza virus morphogenesis and budding. *Virus Research*, 143, pp. 147-161.

Nayak, D.P., Hui, E.K. & Barman, S., 2004. Assembly and budding of influenza virus. *Virus Research*, 106 pp. 147-165.

Nguyen, C.V., 2006. Toxicity of the AGEs generated from the Maillard reaction: on the relationship of food-AGEs and biological-AGEs. *Molecular Nutrition & Food Research*, 50(12) pp. 1140-1149.

Niall, H.D., 1973. Automated Edman degradation: the protein sequenator. *Methods in Enzymology*, 27 pp. 942-1010. Available at: http://www.ncbi.nlm.nih.gov/pubmed/4773306.

Niebuhr, A.D., 1970. *Herbs of Greece*, Herb Society of America.

Palese, P. & Shaw, M., 2001. Orthomyxoviridae: The Viruses and Their Replication. In D. Knipe & P. Howley *Fundamental Virology*. Lippencott Williams and Wilkins, Philadelphia.

Pan, X., Mu, M., Hu, B., Yao, P. & Jiang, M. (2005) Micellization of Casein-graft- Dextran Copolymer Prepared through Maillard Reaction. *Biopolymers*, 81, pp. 29-38.

Parasassi, T., De Stasio, G., D'Ubaldo, A. & Gratton, E. (1990) Phase fluctuation in phospholipid membranes reaveled by Laurdan fluorecence. *Biophys. J*, 57 (June), pp. 1179-1186.

Parasassi, T., Stasio, G.D., Ravagnan, G., Rusch, R.M. & Gratton, E. (1991) Quantitation of lipid phases in phospholipid vesicles by the generalized polarization of Laurdan fluorescence. *Biophysical Journal*, 60, pp. 179-189.

Patick, A.K. & Potts, K.E., 1998. Protease Inhibitors as Antiviral Agents. *Clin. Microbiol. Rev.*, 11(4) pp. 614-627. Available at: http://cmr.asm.org/cgi/content/11/4/614.

Pellegrino, L., Gruppen, H., Resmini, P. & Pagani, M.A. (1999) Heat-induced aggregation and covalent linkages in -casein model systems. *International Dairy Journal*, 9, pp. 255-260.

Pereira, C.S. & Hünenberger, P.H., 2006. Interaction of the sugars trehalose, maltose and glucose with a phospholipid bilayer: a comparative molecular dynamics study. *The Journal of Physical Chemistry. B*, 110(31) pp. 15572-81. Available at: http://www.ncbi. nlm.nih.gov/pubmed/16884281.

Perkins, D.N., Pappin, D.J., Creasy, D.M. & Cottrell, J.S. (1999) Probability-based protein identification by searching sequence databases using mass spectrometry data. *Electrophoresis*, 20 (18), pp. 3551-3567. Available at: http://www3.interscience.wiley.com /journal/68500773/abstract.

Petrascu, A.-., Koch, M.H. & Gabriel, A., 1998. A beginners' guide to gas-filled proportional detectors with delay line readout. *Journal of Macromolecular Science, Part B*, 37(4) pp. 463-483. Available at: http://www.informaworld.com/10.1080/00222349808220487.

Pinto, L.H. & Lamb, R.A., 2007. The M2 Proton Channels of Influenza A and B Viruses *. *Journal of Biological Chemistry*, 281(14) pp. 8997-9000.

Potter, C.W. & Oxford, J.S., 1979. Determinants of immunity to influenza infection in man. *British Medical Bulletin*, 35(1) pp. 69-75. Available at: http://www.ncbi.nlm.nih.gov/ pubmed/367490.

Price, R., 1996. Effects of artemisinin derivatives on malaria transmissibility. *The Lancet*, 347(9016) pp. 1654-1658. Available at: http://www.thelancet.com/journals/a/article/ PIIS0140-6736(96)91488-9/fulltext.

Price, R., van Vugt, M., Phaipun, L., Luxemburger, C., Simpson, J., McGready, R., ter Kuile, F., Kham, A., Chongsuphajaisiddhi, T., White, N.J. & Nosten, F. (1999) Adverse effects in patients with acute falciparum malaria treated with artemisinin derivatives. *The American Journal of Tropical Medicine and Hygiene*, 60 (4), pp. 547-55. Available at: http://www.ncbi.nlm.nih.gov/pubmed/10348227.

Racaniello, V., 2009. Influenza virus growth in eggs. *Virology Blog* pp. 1-9.

Rappolt, M., Hickel, A., Bringezu, F. & Lohner, K. (2003) Mechanism of the lamellar/inverse hexagonal phase transition examined by high resolution X-ray diffraction. *Biophysical Journal*, 84, pp. 3111-3122.

Rappolt, M., Laggner, P. & Pabst, G., 2004. Structure and elasticity of phospholipid bilayers in the L-alpha phase: A comparison of phosphatidylcholine and phosphatidylethanolamine membranes. *Recent Res. Devel. Biophys.*, 3 pp. 363-392.

Rappolt, M., & Pabst, G. (2008). Structure and dynamics of membranous interfaces. In K. Nag, *Structure* (pp. 54-60). John Wiley & Sons, Inc.

Reading, S.A. & Dimmock, N.J., 2007. Neutralization of animal virus infectivity by antibody. *Archives of Virology*, 152(6) pp. 1047-59. Available at: http://www.springerlink.com/content/jj0086m55p219532.

Reed, L. & Muench, H., 1938. A simple method of estimating fifty percent endpoints. *The American Journal of Hygiene*, 27 pp. 493-497.

Rogers, G., Daniels, R., Skehel, J., Wiley, D., Wang, X., Higa, H. & Paulson, J. (1985) Host-mediated selection of influenza virus receptor variants. Sialic acid-alpha 2,6Gal-specific clones of A/duck/Ukraine/1/63 revert to sialic acid-alpha 2,3Gal-specific wild type in ovo. *J. Biol. Chem.*, 260 (12), pp. 7362-7367. Available at: http://www.jbc.org/cgi/content/abstract/260/12/7362.

Rufián-Henares, J.A. & Morales, F.J., 2006. A new application of a commercial microtiter plate-based assay for assessing the antimicrobial activity of Maillard reaction products ´. *Food Research International*, 39 pp. 33-39.

Ruigrok, R.W., Wrigley, N.G., Calder, L.J., Cusack, S., Wharton, S.A., Brown, E.B. & Skehel, J.J. (1986) Electron microscopy of the low pH structure of influenza virus haemagglutinin. *The EMBO Journal*, 5 (1), pp. 41-9. Available at: http://www.pubmedcentral.nih.gov/articlerender.fcgi?artid=1166693&tool=pmcentrez&rendertype=abstract.

Saari, J.T. & Beck, J.S., 1975. Hypotonic hemolysis of human red blood cells: a two-phase process. *The Journal of Membrane Biology*, 23(1) pp. 213-226. Available at: http://www.springerlink.com/content/x28328t435m0w804.

Sanchez, S.A., Tricerri, M.A., Gunther, G. & Gratton, E. (2007) Laurdan Generalized Polarization : from cuvette to microscope. *Modern Research and Educational Topics in Microscopy*, pp. 1007-1014.

Schrier, S.L., Chiu, D.T., Yee, M., Sizer, K. & Lubin, B. (1983) Alteration of Membrane Phospholipid Bilayer Organization in Human Erythrocytes during Drug-induced Endocytosis. *Measurement*, 72 (November).

Schmidtke, M. & Bauer, K., 2006. Amantadine Resistance among Porcine H1N1 , H1N2 , and H3N2 Infl uenza A Viruses Isolated in Germany between 1981 and 2001. *Intervirology* pp. 286-293.

Scopes, R.K., 1994. *Protein Purification: Principles and Practice* 3rd., Springer Science&Business Media, LLC., USA.

Seeman, P., 1967. Transient holes in the erythrocyte membrane during hypotonic hemolysis and stable holes in the membrane after lysis by saponin and lysoleithin. *The Journal of Cell Biology*, 32(1) pp. 55-70. Available at: http://jcb.rupress.org/content/32/1/55.abstract.

Serkedjieva, J., 2009. Combined antiinfluenza virus effect of a plant preparation and a bacterial protease inhibitor. *Biotechnology and Biotechnological Equipment*, Special ed pp. 589-593. Available at: http://md1.csa.com/partners/viewrecord.php?requester=gs&collection=ENV&recid=10907628&q=&uid=789683402&setcookie=yes.

Siegel, D.P., Green, W.J. & Talmont, Y., 1994. The Mechanism of Lamellar-to-Inverted Hexagonal Phase Transitions : A Study using Temperature-Jump Cryo-Electron Microscopy. *Biophysical Journal*, 66(February) pp. 402-414.

Siegel, D.P. & Epand, R.M., 2000. Effect of influenza hemagglutinin fusion peptide on lamellar/inverted phase transitions in dipalmitoleoylphosphatidylethanolamine: implications for membrane fusion mechanisms. *Biochim. Biophys. Acta*, 1468, 87-98.

Sigal, L.H., 2002. Molecular Biology and Immunology for Clinicians 17: T-Cell Signal Transduction. *Journal of Clinical Rheumatology*, 8(2) pp. 113-116. Available at: http://journals.lww.com/jclinrheum/Abstract/2002/04000/Molecular_Biology_and_Immunology_for_Clinicians.10.aspx.

Sladowski, D., Steer, S.J., Clothier, R.H. & Balls, M. (1993) An improved MTT assay. *Journal of Immunological Methods*, 157 (1-2), pp. 203-207. Available at: http://cat.inist.fr/?aModele=afficheN&cpsidt=4568895.

Smith, C., van Megen, W., Twaalfhoven, L. & Hitchcock, C. (1980) The determination of trypsin inhibitor levels in foodstuffs. *Journal of the Science of Food and Agriculture*, 31 (4), pp. 341-350. Available at: http://www3.interscience.wiley.com/journal/113323007/abstract.

Souri, M., Aoyama, T., Orii, K., Yamaguchi, S. & Hashimoto, T. (1996) Mutation analysis of very-long-chain acyl-coenzyme A dehydrogenase (VLCAD) deficiency: identification and characterisation of mutant VLCAD cDNAs from four patients. *American Journal of Human Genetics*, 58 (1), pp. 97-106. Available at: http://www.pubmedcentral.nih.gov/articlerender.fcgi?artid=1914938&tool=pmcentrez&rendertype=abstract.

Sprong, H., Sluijs, P.V. & Meer, G.V., 2001. Review: How Proteins Move Lipids. *Nature Molecular Cell Biology*, 2(July), 504-513.

Stillwell, W., Wassall, S., Dumaua, A., Ehringer, W., Browning, C. & Jenski, L. (1993) Use of merocyanine (MC540) in quantifying lipid domains and packing in phospholipid vesicles and tumor cells. *Biochimica et Biophysica Acta (BBA) - Biomembranes*, 1146 (1), pp. 136-144. Available at: http://dx.doi.org/10.1016/0005-2736(93)90348-4.

Suzuki, Y., Choi, K., Uchida, K., Ko, S., Sohn, H. & Park, J. (2004) Arginyl-fructosyl-glucose and Arginyl-fructose, Compounds Related to Browning Reaction in the Model System of Steaming and Heat-drying Processes for the Preparation of Red Ginseng. *Journal of GInsing Research*, 28 (3), pp. 143-148.

Sykora, J., Jurkiewicz, P., Epand, R.M., Kraayenhof, R., Langner, M. & Hof, M. (2005) Influence of the curvature on the water structure in the headgroup region of phospholipid bilayer studied by the solvent relaxation technique. *Chem Phys Lipids*, 135, pp. 213-221. Available at: http://linkinghub.elsevier.com/retrieve/pii/S0009308405000605.

Taly, A., 2002. The DMPC lipid phase transition influences differently the first and the second electron transfer reactions in bacterial reaction centers. *FEBS Letters*, 532(1-2) pp. 91-96. Available at: http://dx.doi.org/10.1016/S0014-5793(02)03635-9.

Tang, J., 2006. Research priorities in traditional Chinese medicine. *BMJ (Clinical research ed.)*, 333(7564) pp. 391-4. Available at: http://www.bmj.com.

Tashiro, M. & Rott, R., 1996. The role of proteolytic cleavage of viral glycoproteins in the pathogenesis of influenza virus infections. , 7(Figure 1) pp. 237-243.

Tatsumi, N., 1981. The size of erythrocyte ghosts. *Biochimica et Biophysica Acta (BBA) - Biomembranes*, 641(1) pp. 276-280. Available at: http://dx.doi.org/10.1016/0005-2736(81)90592-7.

Tezuka, M., Koyama, N., Morisaki, N., Saito, Y., Yoshida, S., Araki, N. & Horiuchi, S. (1993) Angiogenic effects of advanced glycation end products of the Maillard reaction on cultured human umbilical cord vein endothelial cells. *Biochemical and Biophysical Research Communications*, 193 (2), pp. 674-680.

Thompson, C.I., Barclay, W.S. & Zambon, M.C., 2004. Changes in. *Chemotherapy*, 53(5) pp. 759-765.

Thorpe, S.R. & Baynes, J.W., 2003. Maillard reaction products in tissue proteins: New products and new perspective. *Amino Acids* pp. 275-281.

Ugolini, S., Mondor, I., Parren, P.W., Burton, D.R., Tilley, S.A., Klasse, P.J. & Sattentau, Q.J. (1997) Inhibition of virus attachment to CD4+ target cells is a major mechanism of T cell line-adapted HIV-1 neutralization. *The Journal of Experimental Medicine*, 186 (8), pp. 1287-98. Available at: http://www.pubmedcentral.nih.gov/articlerender.fcgi?artid=2199094&tool=pmcentrez&rendertype=abstract.

Van Gorkom, L.C., Nie, S.Q. & Epand, R.M., 1992. Hydrophobic lipid additives affect membrane stability and phase behavior of N-monomethyldioleoylphosphatidylethanolamine. *Biochemistry*, 31(3) pp. 671-677. Available at: http://dx.doi.org/10.1021/bi00118a006

Vequi-Suplicy, C.D., Benatti, C.R. & Lamy, M.T., 2006. Laurdan in Fluid Bilayers : Position and Structural Sensitivity. *Journal of Fluorescence*, 16(3) pp. 431-439.

Vest, R.S., Gonzales, L.J., Permann, S.A., Spencer, E., Hansen, L.D., Judd, A.M. & Bell, J.D. (2004) Divalent Cations Increase Lipid Order in Erythrocytes and Susceptibility to Secretory Phospholipase A2. *Biophysical Journal*, 86 (4), pp. 2251-2260.

Vlassara, H., Cai, W., Crandall, J., Goldberg, T., Oberstein, R., Dardaine, V., Peppa, M. & Rayfield, E.J. (2007) Inflammatory mediators are induced by dietary glycotoxins, a major risk factor for diabetic angiopathy. *PNAS*, 99 (24), pp. 15596-15601.

Wang, X., Jia, W., Zhao, A. & Wang, X. (2006) Anti-influenza agents from plants and traditional Chinese medicine. *Phytotherapy Research*, 20 (5), pp. 335-341.

Wang, H., 2008. Effects of Maillard reaction on the bioactivities of radix Isatidis (Banlangen). p. 32.

Wang, X., Cui, B., Wei, Z., Liu, R., XU, D. & Yang, M.F. (2009) Extraction of Indigowoad Root Polysaccharides and Its in vitro Reaction to Porcine Reproductive and Respiration Syndrome Virus (PRRSV). *Jiangsu Journal of Agricultural Science*, 25 (2), pp. 311-314.

Watanabe, K., Sato, Y. & Kato, Y. (1980) Chemical and Conformational Changes of Ovalbumin due to the Maillard Reaction. *Journal of Food Processing and Preservation*, 3 (4), pp. 263-274. Available at: http://www3.interscience.wiley.com/journal/119590143/abstract.

Watanabe, W., 1995. Use of lactate dehydrogenase to evaluate the anti-viral activity against influenza A virus. *Journal of Virological Methods*, 51(2-3) pp. 185-191. Available at: http://dx.doi.org/10.1016/0166-0934(94)00103-N.

Wautier, L. & Guillausseau, J., 2001. Advanced glycation end products, their receptors and diabetic angiopathy. *Nature*, (1) pp. 535-542.

Wharton, S.A., Calder, L.J., Ruigrok, R.W., Skehel, J.J., Steinhauer, D.A. & Wiley, D.C. (1995) Electron microscopy of antibody complexes of influenza virus haemagglutinin in the fusion pH conformation. *The EMBO Journal*, 14 (2), pp. 240-6. Available at: http://www.pubmedcentral.nih.gov/articlerender.fcgi?artid=398077&tool=pmcentrez&rendertype=abstract.

Whittaker, G.R., 2001. Intracellular trafficking of influenza virus : clinical implications. *Expert Reviews in Molecular Medicine*, (0 1) pp. 1-13.

Wiley, D.C. & Skehel, J.J., 1987. The structure and function of the hemagglutinin membrane glycoprotein of influenza virus. *Annual Review of Biochemistry*, 56 pp. 365-94. Available at: http://arjournals.annualreviews.org/doi/abs/10.1146/annurev.bi.56.070187.002053.

Williamson, P., Mattocks, K. & Schlegel, R., 1983. Merocyanine 540, a fluorescent probe sensitive to lipid packing. *Biochimica et Biophysica Acta (BBA) - Biomembranes*, 732(2) pp. 387-393. Available at: http://dx.doi.org/10.1016/0005-2736(83)90055-X.

Wikipedia. (2010). Bragg's Law. *Wikipedia website*. Retrieved from http://en.wikipedia.org/wiki/Bragg_law.

Wolf, M. C., Freiberg, A. N., Zhang, T., Akyol-Ataman, Z., Grock, A., Hong, P. W., *et al.* (2010). A broad-spectrum antiviral targeting entry of enveloped viruses. *Proceedings of the National Academy of Sciences of the United States of America*, *107*(7), 3157-62. doi: 10.1073/pnas.0909587107.

Wu, J., Daugulis, A., Faulkner, P., & Goosen, M. (1992). Correlation of LDH activity with loss of insect cell viability: an assessment of the LDH assay. *Biotechnology Techniques*, *4*(4), 335-340.

Wu, L., 2005. Research on the biochemical mechanism of radix Isatidis against influenza virus. pp. 64-68.

Xiang, L., Wang, H., Lu, H., Gao, G., Ke, L., Rao, P. & Zhou, J. (2007) Analysis of amino acids in Banlangen during heating process. *Aminoe Acids & Biotic Resources*, 29, pp. 3-5.

Xiang, L., Huang, X., Chen, L., Rao, P., & Ke, L. (2007). The reparative effects of Mormodica Charantia Linn. extract on HIT-T15 pancreatic beta-Cells. *Asia Pacific Journal of Clinical Nutrition*, *16*(Suppl 1), 249-252.

Xu, L., Huang, F., Cheng, T. & Wu, J. (2005) Antivirus constituents of radix of Isatis indigotica. *Chinese Journal of Natural Medicines*, 3 (6), pp. 359-61.

Yeagle, P.L. (1993) *The Membranes of Cells* 2nd Edition, Academic Press, Inc.

Yen, G. & Hsieh, P., 1995. Antioxidative activity and scavenging effects on active oxygen of xylose-lysine maillard reaction products. *Journal of the Science of Food and Agriculture*, 67(3) pp. 415-420. Available at: http://www3.interscience.wiley.com/journal/113320382/abstract.

Yen, G.C. & Hsieh, P.P., 1994. Possible mechanisms of antimutagenic effect of Maillard reaction products prepared from xylose and lysine. *Journal of Agricultural and Food Chemistry*, 42(1) pp. 133-137. Available at: http://dx.doi.org/10.1021/jf00037a023.

Yeung, H., 1985. *Handbook of Chinese Herbs and Formulas*, Los Angeles: Institute of Chinese Medicine.

Yoo, B., Park, G., Okuda, H., Takaku, T., Kim, S. & Hwang, W. (1999) Inhibitory effect of arginine-derivatives from ginseng extract and basic amino acids on protein-arginine N-methyltransferase. *Amino Acids*, 17, pp. 391-400.

Yoshimura, Y., Iijima, T., Watanabe, T. & Nakazawa, H. (1997) Antioxidative Effect of Maillard Reaction Products Using Glucose-Glycine Model System. *J. Agric. Food Chem*, 8561 (96), pp. 4106-4109.

Zhang, J., Stanley, R.A., Adaim, A., Melton, L.D. & Skinner, M.A. (2006) Free radical scavenging and cytoprotective activities of phenolic antioxidants. *Mol.Nutr.Food Res.*, 50, pp. 996 - 1005.

Zhang, Q., Ames, J.M., Smith, R.D., Baynes, J.W. & Metz, T.O. (2009) A perspective on the Maillard reaction and the analysis of protein glycation by mass spectrometry: probing the pathogenesis of chronic disease. *Journal of Proteome Research*, 8 (2), pp. 754-69. Available at: http://www.ncbi.nlm.nih.gov/pubmed/19093874.

Zhao, Y., Xiao, X., Liao, Q., Wang, J., Ma, Y., Yan, D. & Jin, C. (2006) [Effects of different extracts from Radix isatidis on lymphocytes of mice by biothermodynamics]. *China Journal of Chinese Materia Medica*, 31 (7), pp. 590-3. Available at: http://www.ncbi.nlm.nih.gov /pubmed/16780167.

Zou, P., Hong, Y. & Koh, H.L., 2005. Chemical ngerprinting of Isatis indigotica root by RP-HPLC and hierarchical clustering analysis. *Journal of Pharmaceutical and Biomedical Analysis*, 38 pp. 514-520.

INDEX OF FIGURES

INDEX OF TABLES

APPENDIX: RELEVANT PUBLICATIONS

氨基酸和生物资源 2007, 29(3): 57～59
Amino Acids & Biotic Resources

板蓝根热加工过程中氨基酸组分分析

项雷文[1,2],汪惠勤[1], 陆华珍[1],高观祯[1], 柯李晶[1],饶平凡[1],周建武[1*]

(1. 福州大学生物工程研究所,福建 福州 350002 2. 福建师范大学福清分校,福建 福清 350300)

摘要:利用氨基酸自动分析仪对板蓝根的新鲜植物组织和不同加工程度的板蓝根药材中的总氨基酸和游离氨基酸含量进行测定。结果表明:板蓝根的新鲜植物组织和不同加工程度的板蓝根药材氨基酸在含量上有明显差别。结论为:不同加工程度的板蓝根药材中氨基酸含量差别明显,其中碱性氨基酸含量的差别尤其显著,该差异可能是由于加工过程中发生美拉德反应造成的。

关键词:板蓝根;氨基酸;美拉德反应

中图分类号: Q517 **文献标识码**: A **文章编号**: 1006 - 8376(2007)03 - 0057 - 03

板蓝根 (Radix Isatidis)为十字花科植物菘蓝 (*Isatis indigotica* Fort)的干燥根,味苦,性寒,有清热解毒、凉血利咽功效[1]。板蓝根在中医临床上常用于治疗病毒性疾病,尤其在抗流感病毒方面疗效确切。本文通过氨基酸自动分析仪测定板蓝根的氨基酸组成及含量。

1 实验仪器及材料

1.1 样品:

板蓝根:鲜根采自安徽省阜阳市太和县阮桥镇北板蓝根药材 GAP种植基地;鲜根晒干后为生药;药材由福建中医学院杨成梓教授鉴定。

1.2 试剂:

所用试剂均为分析纯,所有溶液均用高纯水配制。

1.3 仪器:

J - 251型高速离心机,美国 Beckman公司; HHS恒温水浴锅,厦门医疗仪器厂;日立 L - 8800型全自动氨基酸分析仪,日本日立公司; FW100型高速万能粉碎机,天津泰斯特公司;DK - 8D型电热性恒温箱,上海精宏实验设备有限公司。

2 实验方法:

2.1 样品制备:

生药的制备: (1)取板蓝根的鲜根若干,利用太阳晒干后得到晒干生药; (2)取板蓝根的鲜根若干,利用恒温箱 40℃烘至衡重得到烘干生药;

称取一定数量板蓝根的鲜根和生药,分别置于液氮中冷却,然后在高速万能粉碎机中粉碎。

测定总氨基酸:精密称取 30 mg样品放入玻璃水解管中,加 6 mol·L^{-1} HCl 3 mL,抽真空下立即封管,然后在 130 ℃下水解 6 h,水解完冷却后打开水解管,用蒸馏水定容至 25 mL,取 5 mL蒸干,然后用 0.02 mol·L^{-1} HCl稀释至一定浓度, 14000 g离心 20 min,取上清液测定除色氨酸以外的氨基酸。

测定游离氨基酸: (1)分别精密称取 1 g样品 (鲜根、晒干后生药、40℃烘干生药),加 30 mL0.02 mol·L^{-1}HCl,超声波振荡 1 h, 14000 g离心 20 min,取上清液测定除色氨酸以外的氨基酸; (2)为了考察板蓝根生药在煎煮过程中其氨基酸组分的变化情况,精密称取 1 g样品烘干生药,加 30 mL0.02 mol·L^{-1}HCl,沸水浴 1 h, 14000 g离心 20 min,取上清液测定除色氨酸以外的氨基酸。

3 结果

3.1 板蓝根中氨基酸质量分数测定结果

利用日立 8350型氨基酸自动分析仪分别测定板蓝根的总氨基酸以及游离氨基酸质量分数,结果如表 1。

从表 1可以看出,板蓝根中含有除色氨酸 (酸解时被破坏)外的所有种类的氨基酸,质量分数较高的氨基酸依次为精氨酸、谷氨酸、天冬氨酸、赖氨酸、脯氨酸。

新鲜状态的板蓝根总氨基酸质量分数比晒干后的板蓝根总氨基酸质量分数高,质量分数从 9.09%降到 8.18%;总氨基酸中质量分数最高的 3种氨基酸为精氨酸、谷氨酸和天冬氨酸。

游离氨基酸质量分数随加工方式而变,加工条件越剧烈,游离氨基酸越少,新鲜板蓝根中游离氨基

收稿日期: 2007 - 05 - 15
作者简介:项雷文,男 (1975 -)讲师,博士生,生物大分子分离与表征
*通讯作者 E - mail: zhoujianwu@gmail.com

酸质量分数占 4.21%,晒干后的板蓝根中游离氨基酸质量分数为 3.87%,40 ℃烘干的板蓝根中游离氨基酸为 1.69%,经 40 ℃烘干后再水煮的板蓝根中游离氨基酸的质量分数仅占 1.16%。

在加工过程中,各种氨基酸质量分数发生变化的程度不一致,其中精氨酸质量分数下降幅度为最大。新鲜板蓝根经晒干后,总氨基酸中精氨酸从 3.59%下降到 3.12%,游离氨基酸中精氨酸从 3.07%下降到 2.65%,即总氨基酸中精氨酸的下降主要是游离的精氨酸下降所引起的。经过 40 ℃烘干后游离精氨酸质量分数进一步下降为 1.02%,烘干后再经水煮的游离精氨酸质量分数仅有 0.76%。

表 1 板蓝根中总氨基酸及游离氨基酸质量分数 /%

氨基酸	总氨基酸		游离氨基酸			
	鲜根	生药	鲜根	生药	烘干	水煮
天冬氨酸	0.65	0.57	0.08	0.07	0.04	0.03
苏氨酸	0.38	0.35	0.18	0.09	0.09	0.06
丝氨酸	0.29	0.26	0.05	0.06	0.03	0.02
谷氨酸	0.88	0.73	0.05	0.02	0.01	0.01
甘氨酸	0.26	0.26	0.01	0.01	0.00	0.00
丙氨酸	0.29	0.31	0.07	0.11	0.04	0.02
胱氨酸	0.03	0.02	0.01	0.02	0.00	0.00
缬氨酸	0.38	0.38	0.07	0.10	0.05	0.03
甲硫氨酸	0.00	0.03	0.00	0.01	0.00	0.00
异亮氨酸	0.24	0.23	0.03	0.04	0.02	0.01
亮氨酸	0.38	0.37	0.03	0.07	0.03	0.02
酪氨酸	0.12	0.12	0.01	0.02	0.01	0.00
苯丙氨酸	0.24	0.22	0.02	0.05	0.03	0.01
赖氨酸	0.56	0.47	0.13	0.16	0.08	0.04
色氨酸	-	-	-	-	-	-
组氨酸	0.26	0.22	0.11	0.09	0.05	0.03
精氨酸	3.59	3.12	3.07	2.65	1.02	0.76
脯氨酸	0.53	0.51	0.29	0.31	0.17	0.10
总量	9.09	8.18	4.21	3.87	1.69	1.16

注:氨基酸质量分数均以板蓝根干物质计算。

4 讨论

板蓝根中精氨酸质量分数较高,并且游离精氨酸占总精氨酸的比例较高,这和王明辉等[2]、乔章星[3]、崔熙等[4]测定的结果较一致,板蓝根氨基酸含量因药材产地不同而有所差异。板蓝根中质量分数较高的氨基酸还有谷氨酸、天冬氨酸、赖氨酸、脯氨酸。

本文首次跟踪了板蓝根药材加工过程中 (新鲜药用植物组织 - 晒干后的生药 - 40 ℃烘干的生药 - 40 ℃烘干后的粉末经沸水煮) 其氨基酸组分的变化情况。研究结果显示随加工温度的增加,板蓝根药材中的总氨基酸和游离氨基酸质量分数均逐渐降低,其中碱性氨基酸特别是精氨酸质量分数下降趋势最为显著。课题还对板蓝根新鲜组织中的糖组分进行了测定,发现其提取液中具有相当浓度的糖分 (结果未显示)。热加工贯穿了整个板蓝根的成药过程,提供了板蓝根成分中氨基酸和糖发生美拉德反应的条件,该反应可能是板蓝根成药过程中颜色逐步加深的主要原因。本文结果中碱性氨基酸特别是精氨酸质量分数随加工进程而显著下降的趋势,从氨基酸成分的角度提供了板蓝根成药过程中发生美拉德反应的实验证据。

板蓝根、南板蓝根与大青叶都是传统的抗病毒中药,对各种病毒性疾病具有很好的治疗效果,对其作用机理目前有多种猜测。崔熙等[2]、王明辉等[4]认为含量较高的精氨酸可能是板蓝根药效的主要成分。胡兴昌等[5]认为抑制流感病毒的效果与板蓝根凝集素血凝活性的高低相关,刘思贞等[6]发现板蓝根活性部位是亲水性的、被阳离子吸附的结合氨基酸部分。 Yamada[7]从板蓝根热水提取物中分离得到一种分子量 7 kDa左右,具有体外抗流感病毒活性的糖蛋白。刘盛等[8]则认为药材种质之间差异不大。还有许多研究是针对板蓝根、南板蓝根及大青叶中所含有的小分子物质,如生物碱、靛蓝、靛玉红等。这些研究及机理探讨多针对生药进行,而没有考虑部分中草药药材在采挖、晒干、炮制和煎制

过程中所发生的变化。在多数中草药的成药过程中,热加工都贯穿其中,药材中所含有的成分如蛋白质、多肽、氨基酸、糖分等都会发生变化,产生药材植物成分中所没有的化合物,美拉德反应产物正是其中主要部分,它给大多数中草药汤剂提供了黑褐颜色。根据中医临床上的观测,汤药颜色和其实际药效具有一定相关性,美拉德反应产物或许在板蓝根抗病毒功效中也扮演着重要的角色。

致谢:感谢福建省农业科学院钱爱萍老师对样品进行氨基酸分析,福建中医学院杨成梓教授对药材进行鉴定。

参考文献

[1] 《中国药典》[S]2005版.
[2] 王明辉,周亚敏,高华筠等.板蓝根中的氨基酸成份测定及其药用机理的探讨[J].氨基酸杂志,1989,2:45~46.
[3] 乔章星.板蓝根水醇提取液中氨基酸成份的测定[J].现代应用药学,1991,8(3):14~15.
[4] 崔熙,李松林,王建新等.南、北板蓝根的鉴别和氨基酸含量比较分析[J].中药材,1992,15(2):17~19.
[5] 胡兴昌,郑伟强.板蓝根粗提液抑制流感病毒的实验研究[J].上海师范大学学报(自然科学版),2003,32(1):62~65.
[6] 刘思贞,祝希娴,邵玉芹,马天波.板蓝根抗流感病毒有效部位的筛选[J].中草药,1999,30(9):650~651
[7] Yamada H. Anti-viral compositions containing new glycoprotein from Isatis tintoria[P]. JP1160599,1999-03~02.
[8] 刘盛,陈万生,乔传卓,郑水庆,曾明,张汉明,宋赵军.不同种质板蓝根和大青叶的抗甲型流感病毒作用[J].第二军医大学学报,2000,21(3):204~206.

Analysis of Amino Acids in Banlangen during Heating Process

XIANG Lei-wen[1,2], WANG Hui-qin[1], LU Hua-zhen[1], GAO Guan-zhen[1], KE Li-jing[1], RAO Ping-fan[1], ZHOU Jian-wu[1*]

(1. *Institute of Biotechnology Fuzhou University, Fuzhou* 350002, *China*;
2. *Fuqing Branch of Fujian Normal University, Fuqing* 350300, *China*)

Abstract: To analyze amino acid contents of Banlangen samples, which were processed under different temperatures, including sun-dried, dried under 40℃, boiled Banlangen and fresh Banlangen tissue, the total amino acid (TAA) and the free amino acid (FAA) contents were determined by amino acids analyzer. The investigated Banlangen samples varied in TAA and FAA contents. The amino acid contents of Banlangen samples were different, especially varied in basic amino acid contents, which may be due to the Maillard reaction occurred during the heating process.

key words: Banlangen; amino acid; Maillard reaction

氨基酸和生物资源 2010,32(2):14~16
Amino Acids & Biotic Resources

苦瓜干制前后氨基酸组分的变化

柯李晶,鲁 伟,常景立,袁凤英,饶平凡,周建武*

(福州大学生物工程研究所,福建 福州 350002)

摘要:经酸水解,利用氨基酸自动分析仪测定干制加工前后的苦瓜中总氨基酸和游离氨基酸含量。结果表明干制前后的苦瓜在氨基酸质量分数上有明显差别,总氨基酸质量分数分别为11.99%和10.87%,游离氨基酸分别为2.36%和0.70%。结论:干制前后的苦瓜中氨基酸质量分数差别明显,其中碱性氨基酸质量分数的变化尤其显著,总氨基酸中精氨酸质量分数下降50%,在游离氨基酸中下降78%;同时还原糖质量分数也由干制前的4.86%下降为干制后的1.86%,说明苦瓜干制过程中发生了美拉德反应,造成了氨基酸和还原糖含量的下降。

关键词:苦瓜;氨基酸;美拉德反应

中图分类号:Q5 **文献标识码**:A **文章编号**:1006-8376(2010)02-0014-03

苦瓜(*Momordica charantia* L.)为葫芦科(Cucurbitaceae)苦瓜属植物,广泛生长于亚热带地区,又名凉瓜、锦荔枝、癞瓜。《本草纲目》记载:苦瓜"苦寒、无毒、除邪热、解劳乏、清心明目、益气壮阳。"大量研究表明,苦瓜富含苦瓜甙、苦瓜素、多肽、糖类、维生素、氨基酸等多种活性成分,具有降血糖、抗癌、抗病毒、抗生育、增强免疫力等功效[1]。为了更好的开发利用苦瓜资源,本文较全面的分析了苦瓜中氨基酸的含量变化,并指出可能与干制过程中美拉德反应有一定关系。

1 材料与方法

1.1 材料

新鲜苦瓜(购自福建省福州市永辉超市),新鲜苦瓜经烘干后制成苦瓜干。

J-251型高速离心机(美国Beckman公司),HHS恒温水浴锅(厦门医疗仪器厂),8350型全自动氨基酸分析仪(日本日立公司),FW100型高速万能粉碎机(天津泰斯特公司),DK-8D型电热性恒温箱(上海精宏实验设备有限公司),所用试剂均为分析纯,所有溶液均用高纯水配制。

1.2 方法

1.2.1 苦瓜干制备

取新鲜苦瓜若干,利用恒温箱60℃烘干至干爽,即得苦瓜干,然后在高速万能粉碎机中粉碎。

收稿日期:2010-01-20
作者简介:柯李晶,男(1977-), E-mail: ke.lijing@gmail.com
基金项目:福建省科技厅重大专项2008Y0088;福建省科技厅重点项目2008Y0053
* 通讯联系人 jianwuzhou@gmail.com

1.2.2 水分测定

称取苦瓜干粉3份10 g,置于电热鼓风干燥箱中,105℃下烘0.5 h,80℃下烘干至恒重,于干燥器中冷却后称重,计算苦瓜干水分质量分数。

新鲜苦瓜制备苦瓜干过程中,根据其质量前后变化,即可得新鲜苦瓜水分质量分数。

1.2.3 蛋白质含量的测定

采用Folin-酚法测定[2],以牛血清白蛋白为标准蛋白。

1.2.4 还原糖含量测定

采用蒽酮比色法[3]测定。

1.2.5 测定总氨基酸

精密称取30 mg样品(新鲜苦瓜、苦瓜干)放入玻璃水解管中,加6 mol·L^{-1} HCl 3 mL,抽真空下立即封管,然后在130℃下水解6 h,水解完冷却后打开水解管,用蒸馏水定容至25 mL,取5 mL蒸干,然后用0.02 mol·L^{-1} HCl稀释至一定浓度,14000 g离心20 min,取上清液测定除色氨酸以外的氨基酸。

1.2.6 测定游离氨基酸

分别精密称取新鲜苦瓜、苦瓜干各1 g,加30 mL 0.02 mol·L^{-1} HCl,超声波振荡1 h,14000 g离心20 min,取上清液测定除色氨酸以外的氨基酸。

2 结果

2.1 苦瓜干制前后蛋白质和还原糖质量分数测定结果

新鲜苦瓜中蛋白质质量分数为4.17%,还原糖为4.86%;经干制后,蛋白质质量分数达到2.64%,还原糖为1.86%。干制后蛋白质和还原糖的质量分数都明显的降低。

2.2 苦瓜中氨基酸质量分数测定结果

利用日立8350型氨基酸自动分析仪分别测定苦瓜中的总氨基酸以及游离氨基酸质量分数，结果如表1所示。

从表1可以看出，苦瓜干中含有除色氨酸（酸解时被破坏）外的所有种类的氨基酸，质量分数较高的氨基酸依次为精氨酸、谷氨酸、天冬氨酸、赖氨酸。新鲜状态的苦瓜经干制后总氨基酸质量分数从11.99%降到10.87%；总氨基酸中质量分数最高的4种氨基酸为精氨酸、谷氨酸、天冬氨酸、赖氨酸。新鲜苦瓜中游离氨基酸质量分数占2.36%，干制后的苦瓜中游离氨基酸质量分数为0.70%。

在干制过程中，各种氨基酸质量分数发生变化的程度不一致：在总氨基酸和游离氨基酸的测定中，中性氨基酸、芳香族氨基酸及杂环氨基酸质量分数无明显变化。酸性氨基酸中的天冬氨酸的质量分数也无明显变化；但是谷氨酸在总氨基酸测定中的质量分数变化较大，由1.87%降低到1.43%，下降了约24%。这可能是由于谷氨酸相对较多的分布在肽链的N端，提供了游离的氨基，参加了美拉德反应。而在碱性氨基酸中，精氨酸质量分数下降幅度为最大，在总氨基酸中从2.18%下降到1.29%，下降50%；在游离氨基酸从1.40%下降到0.36%，下降78%。可见，总氨基酸中精氨酸的下降主要是游离的精氨酸下降所引起的。

表1 苦瓜中总氨基酸及游离氨基酸质量分数/%

氨基酸	总氨基酸		游离氨基酸	
	新鲜苦瓜	苦瓜干	新鲜苦瓜	苦瓜干
天冬氨酸	1.04	1.06	0.08	0.02
苏氨酸	0.58	0.55	0.00	0.05
丝氨酸	0.58	0.60	0.06	0.01
谷氨酸	1.87	1.43	0.00	0.02
甘氨酸	0.48	0.56	0.02	0.01
丙氨酸	0.57	0.66	0.05	0.03
胱氨酸	0.09	0.12	0.00	0.01
缬氨酸	0.58	0.72	0.11	0.03
甲硫氨酸	0.07	0.15	0.02	0.03
异亮氨酸	0.41	0.49	0.07	0.01
亮氨酸	0.73	0.83	0.08	0.02
酪氨酸	0.44	0.39	0.06	0.02
苯丙氨酸	0.55	0.56	0.14	0.03
赖氨酸	0.99	0.70	0.08	0.02
色氨酸	–	–	–	–
组氨酸	0.40	0.25	0.17	0.01
精氨酸	2.18	1.29	1.40	0.36
脯氨酸	0.41	0.49	0.03	0.02
总量	11.99	10.87	2.36	0.70

注：氨基酸含量均以苦瓜恒重计算。

3 讨论

苦瓜作为一种食药兼用的植物，具有较高的药用和保健价值，正日益受到人们的关注，目前对苦瓜的研究主要集中在对其种子的核糖体失活蛋白及蛋白酶抑制剂等蛋白组分，但对苦瓜加工前后氨基酸、蛋白成分的化学变化没有系统研究，而这些化学变化对苦瓜提取物的生物活性的影响也属空白。

本文首次跟踪了苦瓜加工前后其氨基酸组分的变化情况。研究结果显示苦瓜加工后的总氨基酸和游离氨酸含量均降低，其中碱性氨基酸特别是精氨酸含量下降趋势最为显著，而结合态酸性氨基酸的含量基本不变，这与苦瓜中还原糖含量减少的现象，同为美拉德反应的典型特征，从初始反应物的角度提供了苦瓜加工过程中发生美拉德反应的实验证据。

热加工贯穿了整个苦瓜的加工过程，提供了苦瓜成分中氨基酸和糖发生美拉德反应的条件，该反应可能是苦瓜加工过程中颜色逐步加深的主要原因。这和蔡长河等[4]对从糖分变化情况分析荔枝干加工后褐变原因一致。

苦瓜具有降糖作用，目前一般认为可能包括甾苷、皂苷、脑苷、生物碱及肽类物质。Jaspreet Virdi等[5]用三种不同的方法对苦瓜果实的降糖成分进行了提取，带有种子的干果实的甲醇及氯仿提取物，带有种子的未成熟鲜果的水提物，降糖实验结果表明，未成熟鲜果的水提物降糖效果最好，在饲喂剂量为20 mg/Kg时与常用药物Glibenclamide的降糖效果相当。另外苦瓜还具有抗病毒[6]、抗菌[7]、抗生育[8]等功能。综上所述，这些研究及机理探讨多分别针对新鲜苦瓜的各个部位或苦瓜干粉，而没有考虑苦瓜在采摘、晒干、煎制和精制过程中所发生的变化。

在多数药用植物的成药过程中，热加工都贯穿其中，药材中所含有的成分如蛋白质、多肽、氨基酸、糖分等都会发生变化，产生药材植物成分中所没有的化合物，美拉德反应产物正是其重要组成部分。苦瓜中氨基酸含量较高的依次为精氨酸、谷氨酸、天冬氨酸、赖氨酸，与项雷文等[9]板蓝根中测得的氨基酸有所不同。不同中药材中各种氨基酸含量不同，它们在热加工过程中进行的美拉德反应所形成的产物就不一样，这可能是它们药效各异的原因之一。

致谢：感谢福建省农业科学院钱爱萍老师对样品进行氨基酸分析。

参考文献

[1] 叶国杰，钱瑞卿，卢保元等. 苦瓜子蛋白的分离纯化及

其性质研究[J]. 化学学报, 1998, 56: 1135~1144
[2] Loery O H, Rosebrough N J, FarrA L, et a l. Protein measurementwith the Folin Phenol Reagent[J]. J Biol Chem, 1951, 193: 265~275
[3] 文赤夫,董爱文,李国章等. 葸酮比色法测定紫花地丁中总糖及还原糖含量. 现代食品科技[J], 2005, 85(3):122~124
[4] 蔡长河,郭际,曾庆孝. 荔枝干加工过程果肉糖分变化与褐变[J]. 食品科学,2006,27(9):87~90
[5] Jaspreet Virdi, S. Sivakami, S. Shahani, et al. Antihyperglycemic effects of three extracts from Momordica charantia. Journal of Ethnopharmacology, 2003, 88:107~111
[6] 陈执中. 抗艾滋病天然药物——苦瓜成分的研究Ⅰ水溶性成分的分析[J]. 中国民族民间医药杂志, 1999, 37(2): 63~65
[7] 张绪忠,陈青山,程广文. 苦瓜抑菌作用的研究[J]. 中草药,1995,26(10):556~556
[8] Chan WY, et al. Contraception, 1986, 34(5):537
[9] 项雷文,汪惠勤,陆华珍等. 板蓝根热加工过程中氨基酸组分分析[J]. 氨基酸和生物资源,2007,29(3):57~59

Effects of Heat Drying Process on Amino Acid Content of *Momordica charantia* L.

KE Li-jing, LU Wei, CHANG Jing-li, YUAN Feng-ying, RAO Ping-fan, ZHOU Jian-wu*

(*Institute of Biotechnology Fuzhou University, Fujian*, 350002, *China*)

Abstract: To analyze amino acids of *Momordica charantia* L. samples, heat drying. (60℃) was used and compared with fresh samples. Total amino acid (TAA) and the free amino acid (FAA) were determined by acid hydrolysis and amino acid analyzer. Both of the TAA and FAA decreased, from 11.99% to10.87% and from 2.36% to 0.70%, respectively. The basic amino acids declined dramatically, particularly arginine, which dropped by 50% in TAA and 78% in FAA. Together with the decrease of reducing sugars, from 4.86% to 1.86%. These concentration changes indicated the occurring of Maillard reaction during the heat drying process.

Key words: *Momordica charantia* L.; amino acid; Maillard reaction

(上接第 13 页)

Study on Collagen in *Tilapia* Skin and Its Maillard Reaction Products in the Acidolysis Solution

WU Bin[1]*, LIN Xian[2]

(1. *College of Food Science and Technology, Guangdong Ocean University, Zhanjiang* 524088;
2. *Sericulture & Farm Product Processing Research Institute, Guangdong Academy of Agricultural Science, Guangdong Open Access Laboratory of Agricultural Product Processing, Guangzhou* 510610, *China*)

Abstract: Collagen in *Tilapia* skin was used as raw material. The composition of free amino acid and main flavor components in collagen were analyzed by automatic amino acid analyzer. The flavor components of maillard reaction products were identified by GC-MS. Results showed that the collagen extraction rate was 6.61%, the composition of free amino acid in the collagen was in accordance with that in general collagen and flavor amino acid accounted for 52.57% and 20 flavor components were identified in maillard reaction products..

Key words: *Tilapia*; collagen; maillard reaction product; flavor component